COVALENT ATTACHMENT OF NANOSCALE ORGANIC FILMS TO CARBON SURFACES

A thesis submitted in partial fulfilment of the requirements for the

Degree

of Doctor of Philosophy in Chemistry

in the University of Canterbury

by Samuel (Shing Chi) Yu

University of Canterbury

2008

Acknowledgements.

I am grateful to my family and friends for their support in my life. I would like to extend a big thank you to Assoc. Prof Alison Downard for her guidance and support during my years doing chemistry. Also, thank you must go to members of our research group and staff in the MacDiarmid Institute network for all their technical help and support over the many years. I am indebted to the Tertiary Education Commission, University of Canterbury (Chemistry Department) and the Evans fund for their scholarships.

Table of Contents.

Abstract.

Modification of planar graphitic carbon surfaces by the attachment of molecular films has been investigated in this work. Molecular layers have been grafted to glassy carbon (GC) and pyrolyzed photoresist film (PPF) by employing a range of techniques, which involved electrochemically and photochemically assisted procedures. Modification methods involve the electrochemical reduction of aryldiazonium salt, electrochemical oxidation of arylcarboxylate and photolysis of alkene, alkyne and azide on carbon surfaces. For these methods, it is proposed that reactive species are generated by the procedures, which leads to the grafting of modifiers to the carbon surfaces.

A selection of molecular species was grafted to GC and PPF by these method containing different terminal R-functional groups that include –COOH, $-NO_2$, $-NH_2$, and –NCS. The grafted R-functional groups permit for further chemical reactions on the surface. Electrochemically and photochemically grafted films were examined with a combination of water contact angle measurements, cyclic voltammetry, X-ray electron spectroscopy (XPS), optical microscopy, scanning electron microscopy (SEM) and atomic force microscopy (AFM). Film properties such as surface concentration, film thickness, wettability, chemical composition and reactivity were characterized by the above mentioned techniques.

Films electrochemically prepared from aryldiazonium salts and arylcarboxylates, under the conditions applied in this work, formed loosely packed multilayers with typical film thicknesses of < 5 nm. Photochemically grafted films prepared from alkenes and azides, in general, formed loosely packed monolayers with film thicknesses of < 2 nm. Loosely packed multilayers were also prepared from alkene and alkyne by photochemical procedures.

Chemical reactions on grafted films were demonstrated and analyzed by a combination of the above mentioned characterization techniques. In particular, the reduction of nitrophenyl (NP) films, amine-coupling reactions, photoactivation of grafted films with oxalyl chloride and electrostatic assembly of anionic gold nanoparticles were investigated. Selected chemical reactions permitted identification and evaluation of the grafted layers, and demonstrated the ability to control the immobilization of chemical species. Microscale chemical patterning of two different types of modifiers on carbon surfaces was demonstrated using photolithographical techniques that utilized photochemical reactions with azides. Patterns of line-arrays with line widths of hundreds of micrometers to 10 μm were formed.

Abbreviations.

ACN	Acetonitrile
AFM	Atomic force microscopy
AP	4-Aminophenyl
APOH	4-hydroxylaminophenyl
APA	Azidoaniline
API	Azidophenylisothiocynate
BA	Benzoic acid
BSA	Bovine serum albumin
BSU	Basic structural unit
CP	Carboxyphenyl
DC	Direct current
DCM	Dichloromethane
DMF	Dimethylformamide
DOPAC	Dihydroxyphenylacetic acid
DP	Decylphenyl
EDC	1-ethyl-3-(3'-dimethylaminopropyl)carbodiimide hydrochloride
en	ethylenediamine
EtOH	Ethanol
FAD	Flavin adenine dinucleotide
Fc	Ferrocene
GC	Glassy carbon
HRP	Horseradish peroxidase
HOPG	Highly ordered pyrolytic graphite
HRTEM	High resolution transmission electron microscope
MQ	Milli-Q water
MeOB	4-Methoxyphenyl
MW	Molecular wire
NAAB	4-Nitro-4-aminoazobenzene
NB	4-Nitrophenylmethyl
NBCl	4-Nitrobenzoyl chloride
NM	Napthylmethyl
NP	Nitrophenyl
NPA	4-Nitrophenyl azide
NHS	N-hydroxysuccinimide
PBS	Phosphate buffered saline
PEG	Poly(ethylene glycol)
PDMS	Poly(dimethyl)siloxane

PPF	Pyrolyzed photoresist films
SCE	Saturated calomel electrode
SEM	Scanning electron microscope
TFAAD	Trifluoroacetic acid protected 10-aminodec-1-ene
TBA	Tetrabutylammonium
XPS	X-ray photoelectron spectroscopy

Chapter 1. Introduction

Carbon-based materials are attractive for use in device-type applications such as for molecular electronics and sensors,[1-8] since they are generally easy to synthesize, relatively inexpensive to produce, mechanically stable and electrically conducting.[9] Graphitic carbon comes in many forms such as glassy carbon (GC), pyrolyzed photoresist film (PPF), highly ordered pyrolytic graphite (HOPG), carbon nanotubes, carbon powder, and carbon composites.[9-12] Planar carbon substrates are particularly important in device fabrication as a platform for molecular construction. Stable layers of molecular species can be formed on carbon surfaces by simple modification methods. These procedures are the main focus of this thesis. The stability of planar carbon surfaces and the stable linkages that can form between a modifier layer and the surface makes modification of carbon an attractive area of research.[13, 14] The nature of the attached molecular layers can have a strong influence on the interfacial properties and reactivity of the surface. The choice of the types of layers grafted to the surface can tailor properties for specific applications. In this thesis, planar GC and PPF surfaces are chosen as substrates for surface modification. Relevant information about these surfaces and the modification of carbon *via* the reduction of aryldiazonium salt are reviewed in this chapter. Other modification methods are reviewed at the start of the relevant later chapters.

1.1 Glassy carbon (GC)

Glassy carbon is widely used as an electrode material for electrochemistry. It is usually fabricated commercially into disks, plates, crucibles and rods, from polymeric resins such as polyacrylonitrile (PAN) or phenol/formaldehyde polymers, through thermal treatment.[12] The fabrication process involves carbonizing the polymer by subjecting the material to a series of heat treatments, often under pressure, typically in excess of 1000 ^{o}C. Heat treatment can reach temperatures as high as 3000 ^{o}C in the carbonization process.[12, 15, 16] The structure of GC has been the subject of research since GC was first produced in the early 1960s. The widely accepted model for the structure of GC is that it is a disordered form of carbon containing sp^2 (> 85 %) and sp^3 bonded carbon atoms with a complex network of interwoven graphitic ribbons (fibrils) as depicted in Figure 1.1.[10-12, 15-18] The fine structure of the precursor-polymer, after heat treatments, is observed by high resolution transmission electron microscopy (HRTEM) of the resulting GC material.[10, 15] Hence, the structure of GC bears

some resemblance to the precursor-polymer. The observed structure of GC consisted of curved and twisted ribbons, which contained pores bounded by single or multilayered graphitic fragments. According to this model, the basic structural units (BSU) are made up of planar aromatic systems consisting of basal and edge planes as depicted in Figure 1.1.[18] The BSU contains a substantial proportion of graphite edge plane (zigzag and armchair) sites, which are known to be more reactive than basal plane ('in-plane') sites.[18] For example, scanning tunneling microscopy (STM) and electrochemical studies have revealed that oxides form predominantly at the edge planes while the basal planes remained unreacted after oxidation treatments of ordered graphite surfaces.[18] Also, electron-transfer is approximately 10^6 faster at edge plane than at the basal plane.[12, 19, 20] The low reactivity of graphite basal plane has been attributed to its low density of electronic states and to the lack of functional groups and adsorption sites.[12, 19-24] STM studies of GC have shown small graphite-like domains with sizes less than 5 x 5 nm^2.[18, 25, 26] Regions of large bundles of a fibrillar structure and bundle edges have also been observed at GC, which consisted of helical and cylindrical fibers of diameters of approximately 50 to 300 nm.[18, 27]

Recently, a new model for the structure of GC has been proposed. HRTEM of GC has revealed the presence of fullerene-like components, which led to the proposal of a fullerene-related model for microstructure of GC.[10, 28] This model suggest that the structure of GC consists of broken or imperfect fullerene-like fragments with curved carbon sheets, in which pentagons and heptagons are randomly dispersed throughout networks of hexagons.[10, 28] Such a model would also yield a surface that entails basal and edge plane sites in the structure of GC.

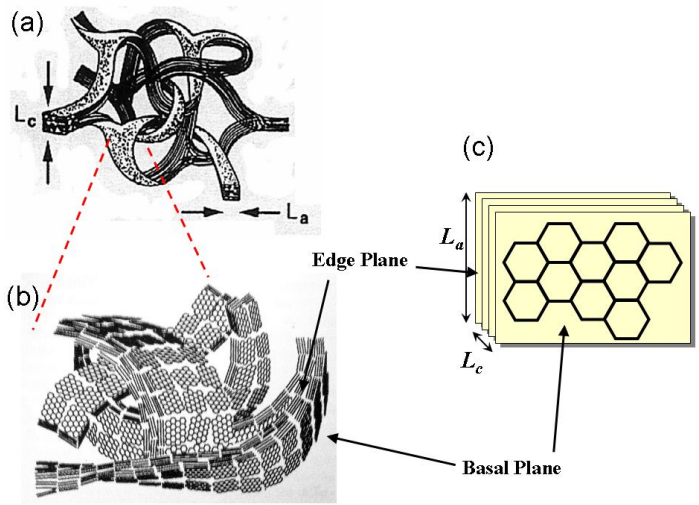

Figure 1.1. Structures of glassy carbon. L_a and L_c are the lengths of the graphitic domains. Reproduced with permission from references 15, 18.

X-ray photoelectron spectroscopy (XPS) studies of GC reveal an O/C ratio typically between 7 and 20 %; with fractured GC possessing O/C ratios at the lower end of the range and polished GC, at the higher end of the range.[21, 29, 30] Oxidation of GC surface may occur upon mechanical abrasion and exposure in air for extended periods of time for polished GC and hence may lead to higher O/C ratios. The substantial oxygen content of GC is attributed to a variety of functional groups heterogeneously distributed within regions of graphite edge plane.[21, 30-32] A general depiction is shown in Figure 1.2. XPS and electrochemical analysis have identified some of these oxygen-containing functional groups, which include phenol, ketone, lactone, carboxylic acid, quinone and other impurities.[21, 29, 31, 32] Furthermore, detailed XPS studies reveal that GC typically has approximately 2 % of atomic oxygen as carbonyl functionalities at the surface.[32] It maybe reasonable to assume that these functional groups contribute in part to the higher reactivity of edge plane sites than basal planes. These oxygen-containing domains at the edge plane may provide reactive sites for adsorption and/or chemical reaction.

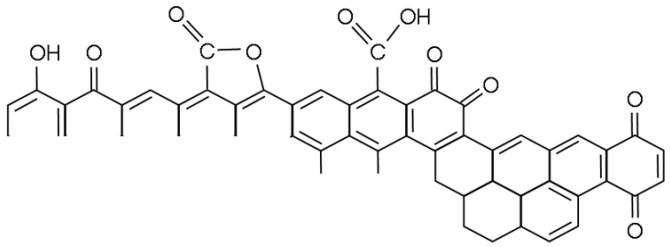

Figure 1.2. Edge plane sites showing various oxygen-containing functional groups.

The edge plane has also been commonly assumed to contain σ radicals that arise from discontinuities at graphene sheets.[33, 34] However, it is reasonable to expect that these radicals are highly reactive and hence are not likely to be present at the edge sites in ambient conditions. It has been proposed that some electrons from the π orbitals interact with broken carbon (in-plane) σ bonds at the discontinuities.[33, 34] The coupling of π and σ orbitals offer stabilization for these radical speciesπ-electrons. Recently, a new model has been proposed for the edge plane of graphitic carbon.[33] The model, depicted in Figure 1.3, proposes that the edge plane contains a substantial fraction of carbene-like and carbyne-like (*o*-benzyne-like) structures at oxygen-free zigzag and armchair sites, respectively. The presence of these structures is consistent with the chemical properties observed for graphitic carbon, in particular, the relatively higher reactivity of the edge plane than the basal plane (above). The key feature of this model is that the edge plane does not contain isolated radicals (‘dangling

bonds') but rather, carbene- and carbyne-like groups that are consistent with the reactivity of graphitic edge planes. To determine whether carbene- and carbyne-like structures can exist in ambient conditions, investigations using theoretical calculations have revealed that carbene- and carbyne-like structures conjugated within a network of graphene sheets are stable under ambient conditions.[33] The stability of these structures increases with increasing size of the graphene sheet due to greater stabilisation from extended conjugation and resonance with the carbon network. The stability of these groups in ambient conditions is reflected in the chemisorption of oxygen in which it shows the tendency for reaction of carbene sites with oxygen. Reaction of oxygen at carbene sites becomes unfavoured within a network of graphene sheets (enthalpy of reaction ~ 7 kJ mol^{-1}), contrary to spontaneous chemisorption reaction at isolated carbene sites (enthalpy of reaction ~ -40 kJ mol^{-1}).[33] Hence the graphene network stabilises the carbene site for the group to exist under ambient conditions.

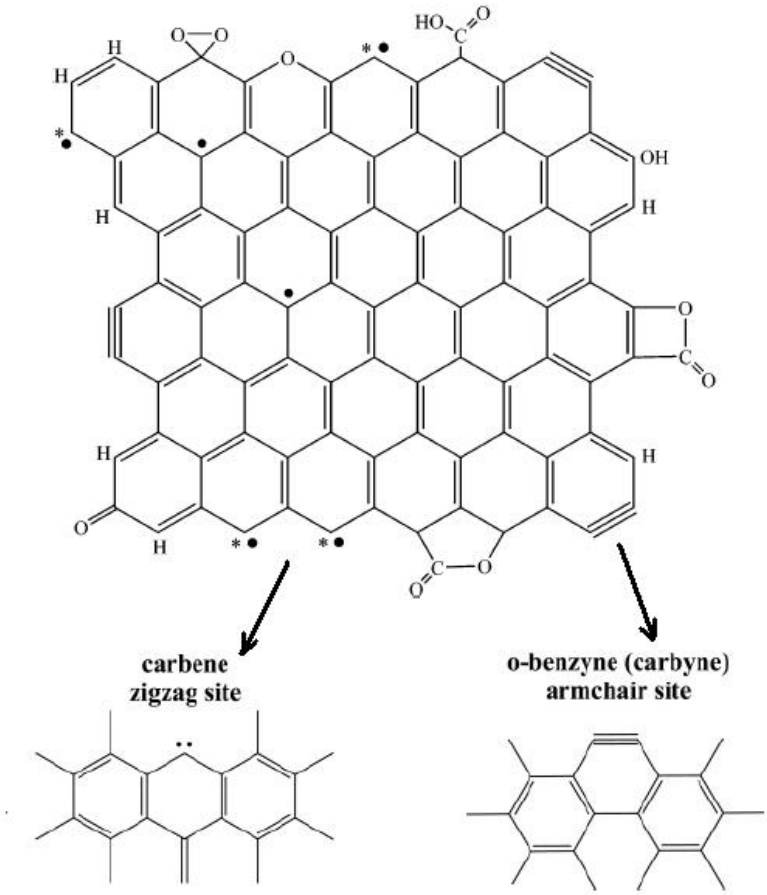

Figure 1.3. Schematic representation of the main chemical features in a graphene sheet, with its typical surface functionalities, and including the free edge sites. The pairing of carbene electrons (* and •) at the zigzag sites and the presence of triple bonds at the armchair sites is indicated. Adapted with permission from reference 33.

Pre-treatment of the GC surface is important in order to obtain a reproducible surface for use, such as for electrochemistry. Pre-treatment methods commonly used are electrochemical polarization and mechanical polishing.[18, 35-37] Microscopy studies have revealed that electrochemical pre-treatments (in aqueous solution) destroy the original fibrillar and bundle surface structures to a certain extent depending on the applied potential. The breakdown in surface has been attributed to increased oxidation of the edge plane, which creates extra pores and voids in the structure.[18, 35, 36] In contrast, mechanical polishing has been shown to maintain the original structure of the GC surface without destruction to the fibrillar network.[18, 36] This has been the method used in this thesis to treat GC surfaces prior to modification. Polished GC have typically surface roughness ranging between 1.3 and 44 nm.[27, 30, 37, 38]

1.2 Pyrolyzed photoresist film (PPF)

PPF consists of a thin carbon film on a silicon wafer. It is fabricated by pyrolyzing, in an oxygen-free environment, commercially available photoresist that has been spin-coated onto silicon wafers. Photoresist is widely used in the microelectronics industry for photolithographical applications. PPF is made from novolak-type photoresist, which is a phenol- and formaldehyde-containing polymeric resin.[39-41] Pyrolysis of this material at 1000–1100 ^{o}C carbonizes the polymeric resin into a highly conducting carbon substrate that has glassy carbon-like properties.[30, 39-42] The chemical composition of PPF is dependent on the maximum pyrolysis temperature at which the carbonaceous film is formed. The pyrolysis process is carried out in increments over several hours to the maximum temperature. During heat treatment temperatures below 350 ^{o}C, the photoresist decomposes and forms water, carbon monoxide and carbon dioxide.[39, 41] The carbonaceous gases originate from decarboxylation and decarbonylation of the products that are formed during the process.[39, 41] At temperatures above 350 ^{o}C, mixtures of aromatic fragments are formed, such as phenol, cresol and xylenol.[39, 41] Thermogravimetric analysis shows a large decrease of approximately 60 % in the weight of the photoresist-coated sample during pyrolysis temperatures up to 500 ^{o}C.[39, 41] The weight-loss is attributed to the formation of gases and aromatic products in the heat treatment. During pyrolysis at temperatures above 500 ^{o}C, the rate of weight-loss follows a monotonic decrease and a final weight of approximately 13 % of the original sample is reached at a temperature of 1000 ^{o}C.[39, 41] The thickness of the photoresist layer also

decreases significantly during pyrolysis. For example, an 8 μm photoresist layer gives an approximately 2 μm PPF carbaneous layer.[39, 41] Changes to the lateral dimension of the layer are minor.[41] PPF surfaces have very low surface roughness typically between 0.2 and 0.6 nm,[30, 40, 43] which is much lower than that for GC (1.3-44 nm, above).[27, 30, 37, 38]

HRTEM studies of PPF revealed that it contains small crystallites with an average diameter of approximately 3 nm with a graphite-like structure that are smaller than the graphitic domains of GC (above).[41] The small crystallites are distributed in a predominantly amorphous carbon film that has a lattice plane with the (002) arrangement.[39] PPF surface exhibits the characteristic sp^2 carbon bands at ~ 1360 (D band) and 1600 cm^{-1} (E_{2g} band) in Raman spectra.[40, 41] The D band, also referred to as the disorder band, is known to correspond to the density of graphitic edge planes in the carbon substrate, while E_{2g} band is related to the presence of graphitic basal plane.[12] The peak intensity ratio of the D/E_{2g} bands is directly proportional to $1/L_a$ (see Figure 1.1 for explanation of L_a) and hence relates to the relative size of the graphite crystallite.[11, 12] In general, a large D/E_{2g} ratio correlates with smaller graphite crystallite. For example, HOPG has a D/E_{2g} ratio that is less than 1,[12, 44] which is consistent with a large L_a for the basal plane. The D/E_{2g} ratio of PPF prepared from a pyrolysis temperature of 1100 ^oC is greater than 1,[40, 41] which is similar to GC and indicates relatively smaller graphitic domains, consistent to HRTEM analysis (above). The D/E_{2g} ratio also reflects a high density of edge plane sites in the structure of PPF. PPF prepared at 600 ^oC has a D/E_{2g} ratio of less than 1,[40, 41] which indicates that it contains relatively large graphite crystallites and a relatively lesser amount of edge plane domains. This may account for the lower reactivity and conductance (below) of the PPF layer due to less reactive edge plane sites present for chemical reactions.

Freshly prepared PPF surfaces have a low O/C ratio, typically around 1 %.[30, 40] The O/C ratio of PPF increases up to maximum of 6 % after four days exposure in air.[30] This compares with a typical O/C ratio of 7-20 % for GC (above). Thereafter, there is no further increase in oxygen content at the surface with air-exposure.[30] XPS studies revealed the presence of C=O or O-C-O and C-OH containing groups at the surface, similar to the groups described for GC surfaces (above).[40] However, these oxygen-containing groups would be present at lower amounts than GC as reflected in the lower O/C ratio.

The surface resistivity of PPF is largely dependent on the pyrolysis temperature at

which it was prepared. Investigations of the effects of different pyrolysis temperatures, ranging between 600 and 1100 ^{o}C, revealed that the sheet resistance of PPF decreases with increasing preparation temperature.[30, 39] PPF prepared at 700 ^{o}C had a resistance of > 400 ohms/square, decreasing to < 60 ohms/square for a prep temperature of 1000 ^{o}C was reported.[30, 39] Sheet resistance was constant for pyrolysis temperatures above 1000 ^{o}C. A PPF layer 1 mm thick prepared at 1000 ^{o}C, corresponds to a resistivity of 5.7 x 10^{-3} ohms cm, which compares very similarly to that for GC heat-treated at 1000 ^{o}C (4.5-5.0 x 10^{-3} ohms cm) and 2000 ^{o}C (4.0–4.5 x 10^{-3} ohms cm).[30]

PPF shows weaker adsorption of molecular species to its surface than GC. Methylene blue and anthraquinone-2,6-disulfonate have been shown to physisorb strongly to GC however very low amounts adsorb to PPF.[30] This is possibly due to the large amounts of pores and voids in the structure of GC for the molecular species to adsorb inside than PPF. Redox probe voltammetry on PPF have been shown to be very similar to GC for redox probe systems such as $Fe(CN)_6^{3-/4-}$ and $Ru(NH_3)_6^{3+/2+}$ with well-defined and reproducible voltammetry, which indicates that sufficient edge plane sites are available at the surface for efficient electron-transfer for electrochemistry of redox probes.[30, 39] Slower electrode kinetics for $Fe^{3+/2+}$ and dopamine redox probe systems are observed on PPF[30] however this is consistent with lower O/C ratio and adsorption properties of PPF compared to GC surfaces (above) since these redox probes are sensitive to surface-oxygen sites. The apparent rate of electron-transfer of solution redox probes (redox probe voltammetry) on bare PPF is dependent on the pyrolysis temperature that PPF was prepared from. PPF fabricated from a curing temperature of 600 ^{o}C exhibited poor electrochemistry for the $Fe(CN)_6^{3-/4-}$ redox system however dramatic improvements were observed for temperatures above 700 ^{o}C.[30, 39] The best voltammetric response was observed for temperatures above 900 ^{o}C and thereafter, very little difference was found with PPF prepared from 1100 ^{o}C.[30, 39] This is likely to be related to the size and amount of edge plane sites formed during pyrolysis as described earlier.

1.3 Surface modification of carbon

Modification *via* the attachment of molecular species (modifiers) can lead to useful changes to chemical and physical properties of the surface. This enables control over properties such as surface wettability, adhesion and resistance to damage. Introduction of

modifiers can also lead to functionalization and changes to reactivity of the surface, which allows the possibility of improving surface sensitivity and selectivity and carrying out direct chemical reactions at the interface. The advantages of carbon substrates as a material and the stable molecular layers that can be covalently attached to carbon surfaces raises the need for the identification and development of experimentally simple modification methods. Electrochemically assisted methods have been a popular route to covalently graft modifiers to carbon surfaces.[13, 14] These surface grafting techniques include the electrochemical oxidation of arylcarboxylates[45] and amines[46-48] and the electrochemical reduction of iodonium salts[49, 50], sulfonium salts[51] and aryldiazonium salts[14, 52]. Modification of carbon *via* electroreduction of aryldiazonium salts forms the focus of Chapters 3 and 4 and is reviewed in the following section. Background information on the modification of carbon *via* electrooxidation of arylacetates is presented in Chapter 5. Nonelectrochemical modification methods are also useful for grafting modifiers to carbon surfaces and forming stable layers. These methods include spontaneous reactions of aryldiazonium ions[53, 54], inorganic azide[55], and amines[56], thermal reactions of alkenes and alkynes[57, 58], and photochemical attachment of alkenes, azides and diazirines[59-64]. Background information to research in the area of modification of planar carbon surfaces *via* photochemical reactions of alkenes, alkyne and azides is presented in Chapters 6 and 7.

1.3.1 Electrochemical reduction of aryldiazonium ions

The electrochemical reduction of aryldiazonium salts has been widely used to form organic films on a variety of surfaces, which include semiconductors and metals such as silicon, iron, gold and as well as carbon.[13, 14, 65-75] The method was first used on glassy carbon (GC) and has since been applied to a large variety of carbon materials including, pyrolyzed photoresist films (PPF), highly ordered pyrolytic graphite (HOPG), diamond, carbon fibers, nanotubes and powders.[13, 14, 37, 44, 52, 76-84] The reduction of aryldiazonium ion generates reactive aryl radicals very close to the electrode *via* the loss of N_2 from the diazonium ion moiety, which leads to the formation of covalent bond with the surface (Figure 1.4).[85]

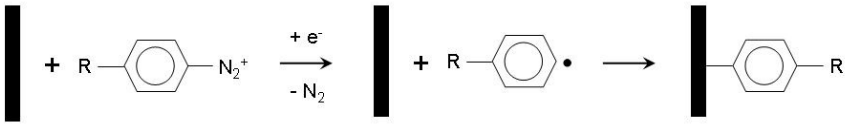

Figure 1.4. Reduction of aryldiazonium ionsleading to surface grafting.

A range of aryldiazonium ions can be synthesized from the corresponding aniline derivative by reaction with sodium nitrite. A wide variety of aryl derivatives with different R-groups have been grafted to carbon surfaces and are listed in Table 1. The electrochemically assisted grafting procedure involves either dipping the material into an aqueous acidic or nonaqueous electrolyte-solution of a aryldiazonium salt, or in a solution of aniline derivative (precursor) and sodium nitrite to generate aryldiazonium ion-modifiers in-situ[86].

Table 1. R-groups of diazonium ion-modifiers grafted on carbon surfaces.

R-group	References
Terphenyl	87
Stilbenzyl	2, 87
4-Nitrophenyl	14, 43, 52, 77, 78, 88-94
4-Carboxyphenyl	52, 88, 89
4-Bromophenyl	52, 88, 89, 95
4-Nitronaphthyl	52, 89
2-Methyl-3-chlorophenyl	52, 89
2', 3-Dimethylazobenzen-4'-yl	52, 89
3, 3' -Dimethoxy-biphenylene-4, 4' bisdiazonium	90
4-Methylphenyl	96-98
4-Ethylphenyl	97
4-Decylphenyl	98
4-Phenylacetate	52, 89, 90, 96, 98
4-Cyanophenyl	52, 89
4-Benzoylphenyl	52, 89
4-Acetamidolphenyl	52, 89, 90
4-Diethylaminophenyl	37, 88
Phenyl	52, 89, 99
9, 10-Anthraquinon-1-yl	52, 89
Azobenzen-4'-yl	100
1, 4-Benzenebisdiazonium	90
4-Benzoylbiocytin	101
4-Trifluoromethylphenyl	92, 97
4-Biphenyl	87, 97, 102, 103
4-Methoxyphenyl	96
4-Nitroazobenzen-4'-yl	43, 74, 87, 97, 104-107
4-Nitrobiphenyl	80, 87, 102, 103
Fluoren-4'-yl	103
4-Fluorosulfonimidephenyl	108
4-Hydroxy-3-nitrophenyl	109

Figure 1.4 shows the coupling of aryl groups directly to the carbon surface however additional reactions are possible through the attachment of radicals onto the grafted layer to

create extended multilayered networks. Additional reactions of film polymerization involve a radical, derived from the reduction of aryldiazonium ion moiety, attacking the already grafted aromatic group to give a cyclohexadienyl radical (*R3*). Aromaticity can be restored if the cyclohexadienyl radical reduces another aryldiazonium ion and lose a proton (*R4*). Repetition of this reaction would lead to polyphenylene layers as outlined in Scheme 1, pathway a). Addition of the radical can be made at different positions of the surface-bound aromatic ring to form the multilayered structure. It was reported that the rates of addition at the different positions are not very different and the electron-donating or withdrawing effect of the *para* substituent on the aromatic ring does not play an important role.[14] For steric reasons, the *ortho* position is the most likely sites for film growth for surface-bound *para* substituted aryl derivatives (R-group).[14, 37]

Scheme 1.1. Mechanism of film formation from reduction of aryldiazonium ions. Reproduced with permission from reference [85].

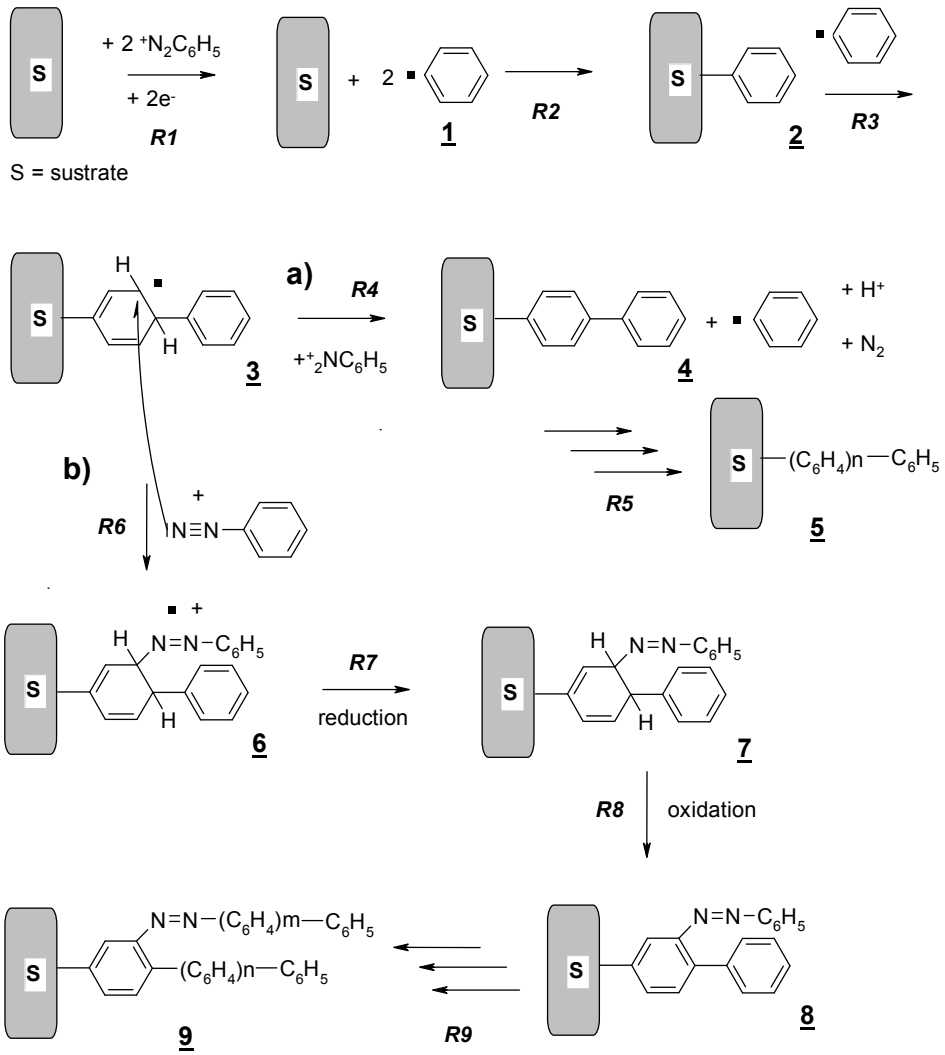

Formation of other linkages, such as azo (-N=N-) and hydrazine (-NH-NH-) are also possible.[77, 85, 88, 110] The presence of azo linkages within the polymeric structure of aryldiazonium-derived films is supported by spectroscopic and time-of-flight secondary ion mass spectroscopy (ToF-SIMS) evidence (also described to Chapter 4).[85] The azo linkage can form either when aryldiazonium ions react directly with the carbon surface containing activating phenol-like sites (Scheme 2)[77, 110], or when an aryldiazonium ion attacks on the cyclohexadienyl radical at the film resulting in the formation of azo-linked polymeric structures within the film (Scheme 1, pathway b).[85, 111]

Organic films electrografted to carbon surfaces by reduction of aryldiazonium ion modifiers have been characterized by a variety of techniques including voltammetry, X-ray photoelectron spectroscopy (XPS), Raman spectroscopy, IR spectroscopy, ToF-SIMS and scanning probe microscopy.[13, 14, 37, 43, 44, 52, 66, 74, 77, 78, 85, 87, 88, 100, 112-115] The films have been found to be stable in air and to ultrasonication in aggressive solvents.[13, 52, 81, 90] In addition, they exhibit good stability to thermal treatment up to ~ 1400 K in vacuum and are stable within a relatively wide potential window.[13, 52, 116] The stability of the grafted film is consistent with the formation of C-C bonds with the carbon surface. The formation of covalent C-C bond is also supported by spectroscopic and ToF-SIMS evidence.[114, 115] Spectroscopic analysis on metal surfaces grafted with aryldiazonium ions, revealed that the aryl films were grafted to the surface *via* a metal-carbon bond and that the films exhibit similar stability to films formed on carbon surfaces. The evidence of a surface bond between the metal surface and the film is inferred to aryl films grafted to carbon surfaces. ToF-SIMS analysis of GC grafted with aryldiazonium ions detected carbon-aryl fragments from the surface, which supported C-C bonding between the carbon surface and the aryl moiety.[114] The presence of polymeric C-aryl and oxygen-aryl fragments were also detected. The detection of these fragments is consistent with the formation of multilayered films and the reaction of aryl radicals with oxygen-containing functionalities on the surface of GC.[114]

Scheme 1.2. Mechanisms for azo group formation during surface grafting of aryldiazonium ions. Reproduced with permission from [85].

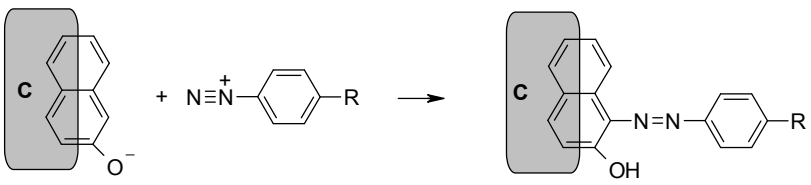

In studies of grafting reactions utilizing aryldiazonium salts, radicals were found to couple to both the edge and basal planes of graphitic carbon surfaces.[37, 117] A faster rate of derivatization has been observed at graphitic edge planes than basal planes with film growth appearing first at the edge plane sites at relatively short deposition times. A lower attachment coverage at the basal plane than the edge plane is found at longer electrolysis times. During modification, sporadic nucleations are observed at the graphitic edge steps followed by nucleations at defect sites of the basal plane. Clustered nucleations in the form of 'islands'- or 'mushroom'-like shapes were observed at relatively long electrolysis times.[37, 117] The observations suggest that the grafting of aryl radicals to the pristine basal plane is weak if occurring at all.[37, 117] These experimental findings are supported by more recent theoretical calculations comparing the binding of phenyl radicals to edge plane sites (zigzag and armchair sites) and basal plane sites. A covalent bond formed between an aryl radical and a basal plane carbon atom (Figure 1.5a) has calculated bond energy of -24 kJ mol^{-1}.[34, 117, 118] Grafting at edge plane armchair (Figure 1.5b) and zigzag sites (Figure 1.5c) have calculated bond energies of -107and -265 kJ mol^{-1}, respectively.[118] Consistent with the relatively more stable bond of zigzag sites, the zigzag edge of a graphene nanoribbon was found to be more reactive possessing a unique localized electronic state that shows a high affinity for the aryl group.[34, 118] The mechanism by which radicals react with the edge plane is unknown however it is reasonable to assume that the aryl radicals can react directly with the carbyne-like and carbene-like structures at graphitic carbon. In addition, it maybe possible for aryl radicals to react with phenolic functionalities and hydrogen-terminated sites at the carbon surface *via* hydrogen abstraction processes, resulting in surface grafting of the modifier. Reaction of aryl radicals at these sites yields layers that have compositions that are consistent with the film-fragments detected in ToF-SIMS for covalently grafted (C-aryl and C-O-aryl) films at GC (above).[85]

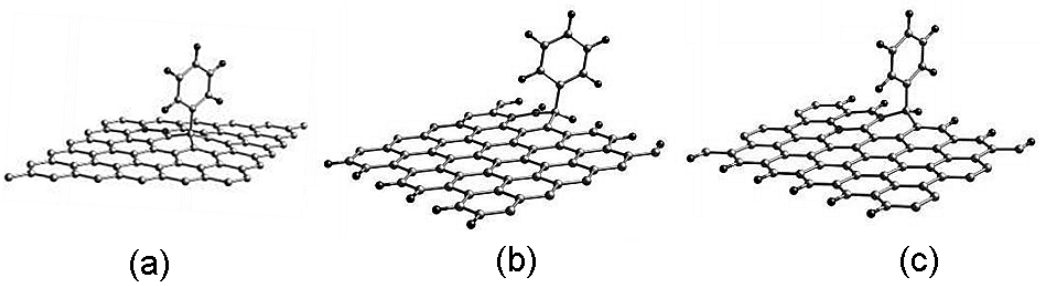

Figure 1.5. Optimized structures of phenyl groups grafted on a graphene sheet. Phenyl group grafted at a carbon atom of a (a) basal plane, (b) armchair site, and (c) zigzag site. Adapted with permission from reference [118].

The structure of films grafted by the reduction of aryldiazonium salts has been probed by electrochemical and AFM measurements. Electrochemistry is a useful surface characterization method when an electroactive modifier such as nitrophenyl, NP, is grafted to the surface. The electrochemical response of the modifier enables the grafting reaction to be monitored by voltammetry and the concentration of grafted groups to be estimated. Surface characterizations (voltammetry and spectroscopy) of electrografted films usually yield surface coverage ranging between 4–30 x 10^{-10} mol cm^{-2}.[43, 52, 76, 78, 88, 89, 94] Considering the theoretical surface coverage of an ideal close-packed monolayer of phenyl groups on a flat surface is approximately 12 x 10^{-10} mol cm^{-2},[78] it might seem reasonable to assume that the surface coverages indicate formation of a single monolayer or submonolayer (when surface roughness is taken into account). However, direct measurement with scanning probe microscopy reveals that both mono- and more often multilayered film structures are formed. Hence these surface coverages correspond to more than one molecular layer and are best represent, in practice, multilayered films.[43, 74, 87, 119] Films of several nanometers in thickness are frequently measured however films of up to 20 nm have also been found.[37, 43, 74, 87, 117] In a careful study, using an AFM depth profiling technique to measure film thickness, a linear relationship between the electrochemically determined surface coverage and film thickness was found for films electrografted from aryldiazonium salts.[43] It was demonstrated that the overall film density was approximately 21 % that of a close-packed layer with a surface coverage of approximately 2.5 x 10^{-10} mol cm^{-2} for each level of film with monolayer thickness (i.e. per monolayer-equivalent).[43] Hence the films are best described as loosely packed layers. With this film density, a surface coverage of phenyl groups of ~ 12 x 10^{-10} mol cm^{-2}, for example corresponds to a minimum of four phenyl layers. This highlights the importance of considering surface coverage and film thickness together. A similar surface concentration of modifiers (3-4 x 10^{-10} mol cm^{-2} per monolayer-equivalent) was found for aryldiazonium ion-modifiers grafted at gold surfaces. The similar surface concentration values suggests that a similar film formation process at gold surfaces.[120]

Preparation conditions such as aryldiazonium salt solution concentration, deposition (electrolysis) time and applied reduction potential can affect the properties of the resultant films.[13, 14] The final surface coverage of electrografted NP films has been shown to depend on the applied potential.[76, 99] In a report, the surface coverage of NP films grafted to GC increased from a value of approximately 6 x 10^{-10} mol cm^{-2} to 19 x 10^{-10} mol cm^{-2} after the applied overpotential was raised from -0.25 to -0.75 V (the overpotential is with respect to

the voltammetric peak for reduction of the aryldiazonium ion).[76] This type of dependence can offer a degree of control to the modification method to generate films with the desired properties. Films with monolayer thickness can be achieved under certain conditions such as when relatively low electrolysis overpotentials and/or short electrolysis times are applied for the method of electroreduction of aryldiazonium salts. For example, biphenyl and stilbene films with monolayer thickness were formed on PPF, when a single potential scan between 0.2 to -0.6 V *vs* SCE was performed in 1 mM diazonium ion acetonitrile-solution as confirmed by AFM measurement.[87] Spectroscopic studies have provided more detailed information about the film structures for these layers grafted to carbon. The studies indicate that phenyl containing mono- and multilayers are able to freely rotate about the surface, consistent with the formation of C-C bonds to the surface.[66] Free rotation of the surface-bound modifiers, such as nitrobiphenyl, nitroazobenzene and biphenyl, were found to have an average tilt angle with respect to the surface normal ranging approximately between 31 and 44 ^{o}.[66] Hence the modifiers are predominantly orientated upwards and are not chemisorbed flat on the carbon surface (PPF).

The versatility of this method is further demonstrated by recent reports of aryldiazonium ions spontaneously grafting to a variety of surfaces, which include carbon, silicon, iron, zinc and nickel.[53, 54, 115, 121] It is worth noting that the spontaneous reaction of aryldiazonium salts with carbon powder (carbon black) has been patented by Cabot Corp. and used industrially in the manufacturing of inks.[122] In general for carbon substrates, spontaneous electroless reactions are carried out by immersing the surface into the modifier-acetonitrile solution. The layers have been analyzed by cyclic voltammetry, infrared spectroscopy and XPS, which show that spontaneously grafted films form more slowly and contain more irregularities in film structures than the electrochemically prepared counterparts.[53, 54] AFM analysis of spontaneously grafted films on metal surfaces (Zn, Ni and Fe) revealed heterogeneously distributed multilayers of < 10 nm at the surface after immersion times of up to 3 h.[53, 54, 115] In general, lower surface coverages are found for spontaneously grafted films with surface coverages ranging between 2-6 x 10^{-10} mol cm^{-2} for films electrolessly grafted to GC.[53, 54] Spontaneous grafting is favoured on reducing metals (i.e. copper and iron) and with easily reduced aryldiazonium ions.[53, 54] Based on these observations, spontaneous grafting appears to be due to reduction of aryldiazonium ion by the metal with the metal surface acting as the reducing agent and the aryldiazonium ion as oxidant. The reducing ability of metal, such as copper and iron, is supported by their

relatively negative open circuit potentials, -0.15 and -0.5 V (*vs* SCE), respectively.[53] The spontaneous redox reaction of aryldiazonium ions with the surface will produce aryl radicals and it is assumed that grafting follows a similar surface grafting mechanism as that depicted in Scheme 1.1. However, the mechanism for spontaneous grafting of aryldiazonium ions at carbon remains unclear. GC has a relatively high open circuit potential (0.63 V *vs* SCE)[53] and hence it is unlikely that the mechanism of spontaneous grafting at carbon occur *via* redox reactions. Instead, it has been suggested that phenolic groups at GC surfaces (Figure 1.2) may undergo coupling reaction with aryldiazonium ions (Scheme 1.2), which may account in part for the spontaneous grafting reaction.[53, 54] However, the exact surface reaction is not understood.

1.3.2 Applications of surface modification by reduction of aryldiazonium salts

The stability of covalently attached layers on carbon surfaces offers a stable platform to carry out further chemistry and perform specific functions, which is suitable and have potential applications in molecular electronics and in the fabrication of sensors. Several examples of novel applications of aryldiazonium ion-grafted films on carbon surfaces are discussed below to demonstrate their recent uses.

Aryldiazonium ion-modifiers have been grafted to GC to construct interfaces that consist of molecular wires (MW) useful for applications in protein electrochemistry. In one example, a two-component modified GC surface was prepared by electrochemically reducing aryldiazonium ion derivatives of a carboxylic acid-derivatized-oligo(phenylethynylene) MW and a poly(ethylene glycol) (PEG) modifier.[7] The grafted molecular wire had a dual purpose at the interface. Firstly, it contained a carboxylic acid at the terminus, which was used for tethering of functional species. Secondly, it functioned as a wire in providing an electron-transfer pathway between the electrode and the tethered species. In contrast, the grafted PEG-based component had the purpose of resisting nonspecific adsorption of undesired proteins that might be present in the sample matrix (PEG-based diazonium ion-grafted films had previously been shown to resist the nonspecific adsorption of blood serum components, bovine serum albumin (BSA) and horseradish peroxidase (HRP)). To demonstrate the utility of the two-component interface, HRP was specifically immobilized to the interface *via* the reactive MW-tethers and used for the detection of H_2O_2.

The lowest detected H_2O_2 concentration for the system was 1 mM.[7] Although this may be a poor detection limit, the purpose of the studies was to demonstrate the mixed interface for immobilization applications and the use of MWs to probe immobilized species. In a second example, the enzyme, glucose oxidase (GOx), was coupled to a mixed film of carboxylic acid-derivatized-oligo(phenylethynylene) MW and carboxyphenyl (CP) modifiers on GC derived from the corresponding aryldiazonium ions.[8] The MWs in the mixed film was used to anchor and probe the electrochemistry of the active centre of the GOx enzyme (flavin adenine dinucleotide, FAD) that had been immobilized *via* attachment with the CP modifiers as anchorage (Figure 1.6). Additionally, the GOx-modified surface was able to directly convert glucose to gluconolactone, in the absence of oxygen, by the FAD-active centre of the immobilized GOx enzyme. This also shows that the activity of the enzyme was retained after immobilization.

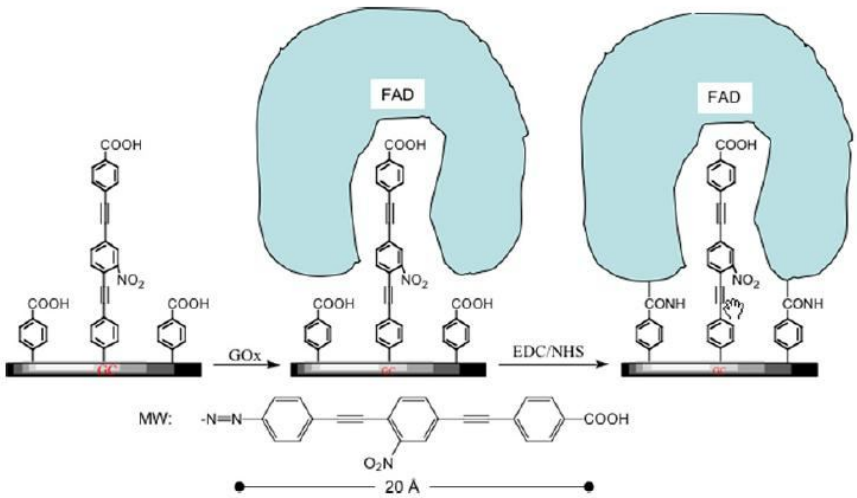

Figure 1.6. Idealized diagram of the steps involved in the fabrication of the modified electrode interface for achieving direct electron transfer to GOx. Also shown is the structure of the oligo(phenylethynyl) MW. Reproduced with permission from reference 8.

In a third example, CP films, derived from aryldiazonium ion-reduction methods, were grafted to GC surfaces and reacted with the amine group in a tripeptide, Gly-Gly-His, to immobilize it on the carbon surface.[123] Immobilized Gly-Gly-His is able to detect Cu^{2+} by forming a complex ion by coordinating to the metal ion. Hence, the Gly-Gly-His-modified surface was used as a chemical sensor for copper ions and the sensor demonstrated a detection limit of ~ 2 nM.[123] The sensor was fabricated on GC using aryldiazonium ion-reduction and it showed stability in the function of the sensor over long term exposure to air.[123] As demonstrated by the above examples, the method of surface grafting of aryldiazonium ions offers a useful approach to form stable film of functional modifiers that can be used as reactive tethers and as a connection for active centres of immobilized

biomolecules (i.e. DNA, proteins, enzymes), which has an important role in the fabrication of chemical and biosensors.[7, 8, 123-125]

The use of molecules in electronic circuits is an active area of research. Molecular junctions composed of molecular films sandwiched between two conductors (i.e. electrically connected at both sides) have been fabricated *via* modification methods utilizing the reduction of aryldiazonium ions.[1, 3, 107, 126-130] Molecular layers of biphenyl-like structures (i.e biphenyl, nitroazobenzene, stilbene) have been formed on PFF *via* reduction of the corresponding diazonium ions. Metal conductors such as mercury, copper and metal oxides such as, titanium oxides and aluminium oxides have been deposited on top of the grafted molecular films to complete the molecular junction.[1, 3, 107, 126-130] The stability of films grafted from aryldiazonium ions is an asset during the metal deposition step, which can cause heating of the grafted layers.

When a potential is applied between the two conductors, the resistance (or conductance) in the molecular junction changes. The resistance of PPF/molecule/Cu/Au junctions is strongly dependent on the structure and thickness of the molecular layer, ranging from 0.13 Ω cm^2 for a nitrobiphenyl monolayer, to 4.46 Ω cm^2 for a biphenyl monolayer, and 160 Ω cm^2 for a nitrophenyl multilayer (thickness = 4.3 nm).[107, 126, 128] Junctions incorporating nitroazobenzene films, i.e. PPF/nitroazobenzene/AlO_x/Au also exhibit interesting electronic behaviour such as conductance switching, where the conductance of the junction varies greatly (e.g. resistance difference ~10^5 times) upon an applied potential-pulse.[107, 126, 128] This substantial variation in conductance was caused by a change in the grafted molecular layer to a 'quinoid'-like structure that effectively conjugates with the carbon electrode and thus, increase the electronic coupling between the film and PPF (Figure 1.7).[3, 126, 128] This has the effect of providing a lower energy barrier or pathway for electron injection into the film and hence cause conductance changes. The switch in conductance can persist for several minutes before returning to the initial state. A similar conductance switching behaviour has also been found at aryldiazonium ion-grafted films on carbon surfaces in the absence of the metal conductor contact.[102]

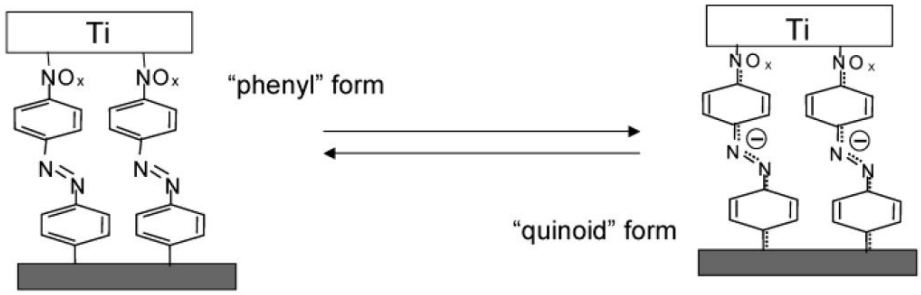

Figure 1.7. Diagram of PPF/nitroazobenzene/Ti junction showing conductance switching behaviour from an initial 'phenyl'-like form to a 'quinoid'-like form in the nitroazobenzene molecular layer. Reproduced from reference 128.

The attractive feature of using films grafted from the aryldiazonium ion for these systems is the stability and relatively low energy barrier for electrons to inject into the junction. The molecular junctions (i.e. PPF/molecule/metal) fabricated are stable for long periods of time (i.e. months), endure and function within a wide temperature window (-150 to 100 ^{o}C), and withstand millions of potential cycles.[3, 126, 128] It is worth noting that there is no solvent or supporting electrolyte in the junction. These systems could have useful functions in molecular memory devices.

1.4 Research work

The overall objective of the work in this thesis is to further expand and develop the understanding of thin films covalently grafted to carbon surfaces, and also to extend the scope of modification methods for carbon substrates. Specific aims of this thesis are outlined below.

Aims

- To gain further insight into the structure and reactivity of films grafted to GC and PPF *via* aryldiazonium salts

- To make a detailed investigation of the potential-dependent behaviour of films grafted *via* arylacetates, in particular to examine the previously reported unusual properties of the films

- To expand the available nonelectrochemical modification methods for GC and PPF

- To develop new methods for preparing mixed films and patterned films consisting of two different modifiers

1.5 References

1. McCreery, R. L., *Analytical Chemistry* **2006,** 78, 3490.
2. Ranganathan, S.; Steidel, I.; Anariba, F.; McCreery, R. L., *Nano Letters* **2001,** 1, 491.
3. McCreery, R. L., *Chemistry of Materials* **2004,** 16, 4477.
4. Corgier, B. P.; Marquette, C. A.; Blum, L. J., *Biosensors & Bioelectronics* **2007,** 22, 1522.
5. Corgier, B. P.; Marquette, C. A.; Blum, L. J., *Journal of the American Chemical Society* **2005,** 127, 18328.
6. Rudiger, O.; Abad, J. M.; Hatchikian, E. C.; Fernandez, V. M.; De Lacey, A. L., *Journal of the American Chemical Society* **2005,** 127, 16008.
7. Liu, G. Z.; Gooding, J. J., *Langmuir* **2006,** 22, 7421.
8. Liu, G. Z.; Paddon-Row, M. N.; Gooding, J. J., *Electrochemistry Communications* **2007,** 9, 2218.
9. Savage, G., *Cabon-Carbon Composites*. Chapman & Hall: 1993.
10. Harris, P. J. F., *Critical Reviews in Solid State and Materials Sciences* **2005,** 30, 235.
11. Chu, P.; Li, L., *Materials Chemistry and Physics* **2006,** 96, 253.
12. McCreery, R. L., In *Electroanalytical Chemistry*, Bard, A. J., Ed. Dekker: New York, 1991; Vol. 17.
13. Downard, A. J., *Electroanalysis* **2000,** 12, 1085.
14. Pinson, J.; Podvorica, F., *Chemical Society Reviews* **2005,** 34, 429.
15. Jenkins, G.; Kawamura, K., *Nature* **1971,** 231, 175.
16. Jenkins, G.; Kawamura, K.; Ban, L., *Proceedings of the Royal Society* **1972,** A327, 501.
17. Ergun, S.; Tiensuu, V., *Nature* **1959,** 183, 1668.
18. Heiduschka, P.; Munz, A.; Gopel, W., *Electrochimica Acta* **1994,** 39, 2207.
19. McCreery, R.; McDermott, M.; Kneten, K., *Journal of Physical Chemistry* **1992,** 96, 31240.
20. McCreery, R.; Packard, R.; Bowling, R., *Journal of American Chemical Society* **1989,** 111, 1217.
21. Chen, P.; McCreery, R. L., *Analytical Chemistry* **1996,** 68, 3958.
22. Cline, K.; McDermott, M.; McCreery, R., *Journal of American Chemical Society* **1994,** 98, 5314.
23. Scherson, D.; McIntyre, R.; Gerischer, H., *Journal of Physical Chemistry* **1987,** 91,

1930.

24. McIntyre, R.; Scherson, D.; Storch, W.; Gerischer, H., *Electrochimica Acta* **1987,** 32, 51.

25. Brown, N.; You, H., *Surface Science* **1990,** 237, 273.

26. Brown, N.; You, H., *Journal of Materials Chemistry* **1991,** 1, 469.

27. McCreery, R.; McDermott, M.; McDermott, C., *Analytical Chemistry* **1993,** 65, 937.

28. Harris, P., *Philosophical Magazine* **2004,** 84, 3159.

29. Tougas, T.; Collier, W., *Analytical Chemistry* **1987,** 59, 396.

30. Ranganathan, S.; McCreery, R. L., *Analytical Chemistry* **2001,** 73, 893.

31. Hoekstra, K. J.; Bein, T., *Chemistry of Materials* **1996,** 8, 1865.

32. Tougas, T.; Collier, W., *Analytical Chemistry* **1987,** 59, 2269.

33. Radovic, L. R.; Bockrath, B., *Journal of American Chemical Society* **2005,** 127, 5917.

34. Jiang, D.; Sumpter, B.; Dai, S., *Journal of Chemical Physics* **2007,** 126, 134701.

35. Shiu, K.; Shi, K., *Analytical Chemistry* **2002,** 74, 879.

36. Elings, V.; Wudl, F., *Journal of Vacuum Science & Technology A* **1988,** 6, 412.

37. Kariuki, J. K.; McDermott, M. T., *Langmuir* **2001,** 17, 5947.

38. Swain, G.; Chen, Q., *Langmuir* **1998,** 14, 7017.

39. Kim, J.; Song, X.; Kinoshita, K.; Madou, M.; White, B., *Journal of the Electrochemical Society* **1998,** 145, 2314.

40. Kostecki, R.; Schnyder, B.; Alliata, D.; Song, X.; Kinoshita, K.; Kotz, R., *Thin Solid Films* **2001,** 396, 36.

41. Ranganathan, S.; McCreery, R.; Majji, S.; Madou, M., *Journal of the Electrochemical Society* **2000,** 147, 277.

42. Brooksby, P. A.; Downard, A. J.; Yu, S. S. C., *Langmuir* **2005,** 21, 11304.

43. Brooksby, P. A.; Downard, A. J., *Langmuir* **2004,** 20, 5038.

44. Ray, K.; McCreery, R., *Analytical Chemistry* **1997,** 69, 4680.

45. Andrieux, C. P.; Gonzalez, F.; Saveant, J. M., *Journal of the American Chemical Society* **1997,** 119, 4292.

46. Barbier, B.; Pinson, J.; Desarmot, G.; Sanchez, M., *Journal of the Electrochemical Society* **1990,** 137, 1757.

47. Downard, A. J.; Tan, E. S. Q.; Yu, S. S. C., *New Journal of Chemistry* **2006,** 30, 1283.

48. Cruickshank, A. C.; Tan, E. S. Q.; Brooksby, P. A.; Downard, A. J., *Electrochemistry Communications* **2007,** 9, 1456.

49. Vase, K. H.; Holm, A. H.; Norrman, K.; Pedersen, S. U.; Daasbjerg, K., *Langmuir*

2007, 23, 3786.

50. Vase, K. H.; Holm, A. H.; Pedersen, S. U.; Daasbjerg, K., *Langmuir* **2005,** 21, 8085.

51. Vase, K.; Holm, A.; Norrman, K.; Daasbjerg, K.; Pedersen, S., *Langmuir* **2008,** 24, 182.

52. Allongue, P.; Delamar, M.; Desbat, B.; Fagebaume, O.; Hitmi, R.; Pinson, J.; Saveant, J.-M., *Journal of American Chemical Society* **1997,** 119, 201.

53. Adenier, A.; Cabet-Deliry, E.; Chausse, A.; Griveau, S.; Mercier, F.; Pinson, J.; Vautrin-Ul, C., *Chemistry of Materials* **2005,** 17, 491.

54. Adenier, A.; Barre, N.; Cabet-Deliry, E.; Chausse, A.; Griveau, S.; Mercier, F.; Pinson, J.; Vautrin-Ul, C., *Surface Science* **2006,** 600, 4801.

55. Devadoss, A.; Chidsey, C. E. D., *Journal of American Chemical Society* **2007,** 129, 5370.

56. Gallardo, I.; Pinson, J.; Vila, N., *Journal of Physical Chemistry B* **2006,** 110, 19521.

57. Ssenyange, S.; Anariba, F.; Bocian, D. F.; McCreery, R. L., *Langmuir* **2005,** 21, 11105.

58. Ababou-Girard, S.; Sabbah, H.; Fabre, B.; Zellama, K.; Solal, F.; Godet, C., *Journal of Physical Chemistry C* **2007,** 111, 3099.

59. Brooks, S. A.; Dontha, N.; Davis, C. B.; Stuart, J. K.; O'Neill, G.; Kuhr, W. G., *Analytical Chemistry* **2000,** 72, 3253.

60. Brooks, S. A.; Ambrose, W. P.; Kuhr, W. G., *Analytical Chemistry* **1999,** 71, 2558.

61. Nowall, W. B.; Dontha, N.; Kuhr, W. G., *Biosensors & Bioelectronics* **1998,** 13, 1237.

62. Dontha, N.; Nowall, W. B.; Kuhr, W. G., *Analytical Chemistry* **1997,** 69, 2619.

63. Sun, B.; Colavita, P.; Kim, H.; Lockett, M.; Marcus, M.; Smith, L.; Hamers, R., *Langmuir* **2006,** 22, 9598.

64. Colavita, P.; Sun, B.; Tse, K. Y.; Hamers, R., *Journal of American Chemical Society* **2007,** 129, 13554.

65. Flatt, A. K.; Chen, B.; Taylor, P. G.; Chen, M. X.; Tour, J. M., *Chemistry of Materials* **2006,** 18, 4513.

66. Anariba, F.; Viswanathan, U.; Bocian, D. F.; McCreery, R. L., *Analytical Chemistry* **2006,** 78, 3104.

67. Allongue, P.; de Villeneuve, C. H.; Cherouvrier, G.; Cortes, R.; Bernard, M. C., *Journal of Electroanalytical Chemistry* **2003,** 550-551, 161.

68. Allongue, P.; De Villeneuve, C. H.; Pinson, J.; Ozanam, F.; Chazalviel, J. N.; Wallart, X., *Electrochimica Acta* **1998,** 43, 2791.

69. Adenier, A.; Bernard, M.-C.; Chehimi, M. M.; Cabet-Deliry, E.; Desbat, B.; Fagebaume, O.; Pinson, J.; Podvorica, F., *Journal of American Chemical Society* **2001,** 123, 4541.

70. Adenier, A.; Cabet-Deliry, E.; Lalot, T.; Pinson, J.; Podvorica, F., *Chemistry of Materials* **2002,** 14, 4576.

71. Chausse, A.; Chehimi, M. M.; Karsi, N.; Pinson, J.; Podvorica, F.; Vautrin-Ul, C., *Chemistry of Materials* **2002,** 14, 392.

72. Boukerma, K.; Chehimi, M. M.; Pinson, J.; Blomfield, C., *Langmuir* **2003,** 19, 6333.

73. Fave, C.; Leroux, Y.; Trippe, G.; Randriamahazaka, H.; Noel, V.; Lacroix, J. C., *Journal of the American Chemical Society* **2007,** 129, 1890.

74. Brooksby, P. A.; Downard, A. J., *Journal of Physical Chemistry B* **2005,** 109, 8791.

75. Paulik, M. G.; Brooksby, P. A.; Abell, A. D.; Downard, A. J., *Journal of Physical Chemistry C* **2007,** 111, 7808.

76. Downard, A. J., *Langmuir* **2000,** 16, 9680.

77. Saby, C.; Ortiz, B.; Champagne, G. Y.; Belanger, D., *Langmuir* **1997,** 13, 6805.

78. Liu, Y.-C.; McCreery, R. L., *Journal of American Chemical Society* **1995,** 117, 11254.

79. Wang, J.; Firestone, M. A.; Auciello, O.; Carlisle, J. A., *Langmuir* **2004,** 20, 11450.

80. Lud, S. Q.; Steenackers, M.; Jordan, R.; Bruno, P.; Gruen, D. M.; Feulner, P.; Garrido, J. A.; Stutzmann, M., *Journal of the American Chemical Society* **2006,** 128, 16884.

81. Pinson, J.; Saveant, J. M.; Hitmi, R.,9213983, 1992.

82. Bahr, J. L.; Yang, J. P.; Kosynkin, D. V.; Bronikowski, M. J.; Smalley, R. E.; Tour, J. M., *Journal of the American Chemical Society* **2001,** 123, 6536.

83. Bahr, J. L.; Tour, J. M., *Chemistry of Materials* **2001,** 13, 3823.

84. Harnisch, J. A.; Gazda, D. B.; Anderegg, J. W.; Porter, M. D., *Analytical Chemistry* **2001,** 73, 3954.

85. Doppelt, P.; Hallais, G.; Pinson, J.; Podvorica, F.; Verneyre, S., *Chemistry of Materials* **2007,** 19, 4570.

86. Baranton, S.; Belanger, D., *Journal of Physical Chemistry B* **2005,** 109, 24401.

87. Anariba, F.; DuVall, S. H.; McCreery, R. L., *Analytical Chemistry* **2003,** 75, 3837.

88. D'Amours, M.; Belanger, D., *Journal of Physical Chemistry B* **2003,** 107, 4811.

89. Delamar, M.; Hitmi, R.; Pinson, J.; Saveant, J. M., *Journal of American Chemical Society* **1992,** 114, 5883.

90. Delamar, M.; Desarmot, G.; Fagebaume, O.; Hitmi, R.; Pinson, J.; Saveant, J. M., *Carbon* **1997,** 35, 801.

91. Xu, J.; Huang, W.; McCreery, R. L., *Journal of Electroanalytical Chemistry* **1996,** 410, 235.

92. Kuo, T.-C.; McCreery, R. L.; Swain, G. M., *Electrochemistry & Solid-State Letters* **1999,** 2, 288.

93. Liu, S. Q.; Shi, Z.; Dong, S. J., *Electroanalysis* **1998,** 10, 891.

94. Ortiz, B.; Saby, C.; Champagne, G. Y.; Belanger, D., *Journal of Electroanalytical Chemistry* **1998,** 455, 75.

95. Belanger, D.; Chamoulaud, G.; Ghodbane, O., *Electrochemistry Communications* **2004,** 6, 254.

96. Downard, A. J.; Roddick, A. D., *Electroanalysis* **1995,** 7, 376.

97. Yang, H.; McCreery, R., *Analytical Chemistry* **1999,** 71, 4081.

98. Downard, A. J.; Roddick, A. D., *Electroanalysis* **1997,** 9, 693.

99. Downard, A. J.; Prince, M. J., *Langmuir* **2001,** 17, 5581.

100. Liu, Y.-C.; McCreery, R. L., *Analytical Chemistry* **1997,** 69, 2091.

101. Dequaire, M.; Degrand, C.; Limoges, B., *Journal of the American Chemical Society* **1999,** 121, 6946.

102. Solak, A. O.; Eichorst, L. R.; Clark, W. J.; McCreery, R. L., *Analytical Chemistry* **2003,** 75, 296.

103. Anariba, F.; Steach, J. K.; McCreery, R. L., *Journal of Physical Chemistry B* **2005,** 109, 11163.

104. McDermott, M.; Rostami, A., *e-Journal of Surface Science and Nanotechnology* **2006,** 4, 419.

105. Kalakodimi, R. P.; Nowak, A. M.; McCreery, R. L., *Chemistry of Materials* **2005,** 17, 4939.

106. Nowak, A. M.; McCreery, R. L., *Journal of the American Chemical Society* **2004,** 126, 16621.

107. Anariba, F.; McCreery, R. L., *Journal of Physical Chemistry B* **2002,** 106, 10355.

108. Creager, S.; Liu, B.; Mei, H.; DesMarteau, D., *Langmuir* **2006,** 22, 10747.

109. Radi, A.-E.; Montornes, J. M.; O'Sullivan, C. K., *Journal of Electroanalytical Chemistry* **2006,** 587, 140.

110. Toupin, M.; Belanger, D., *Journal of Physical Chemistry C* **2007,** 111, 5394.

111. Andrieux, C. P.; Pinson, J., *Journal of the American Chemical Society* **2003,** 125, 14801.

112. Liu, G.; Liu, J.; Böcking, T.; Eggers, P.; Gooding, J., *Chemical Physics* **2005,** 319,

136.

113. Itoh, T.; McCreery, R. L., *Journal of the American Chemical Society* **2002,** 124, 10894.

114. Combellas, C.; Kanoufi, F.; Pinson, J.; Podvorica, F. I., *Langmuir* **2005,** 21, 280.

115. Combellas, C.; Delamar, M.; Kanoufi, F.; Pinson, J.; Podvorica, F. I., *Chemistry of Materials* **2005,** 17, 3968.

116. M.G. Paulik; P.A. Brooksby; A.D. Abell; Downard, A. J., *unpublished results*.

117. Kariuki, J. K.; McDermott, M. T., *Langmuir* **1999,** 15, 6534.

118. Jiang, D. E.; Sumpter, B. G.; Dai, S., *Journal of Physical Chemistry B* **2006,** 110, 23628.

119. Yu, S. S. C.; Downard, A. J., *e-Journal of Surface Science and Nanotechnology* **2005,** 3, 294.

120. Paulik, M. G.; Brooksby, P. A.; Abell, A. D.; Downard, A. J., *Journal of Physical Chemistry C* **2007,** 111, 7808.

121. Downard, A.; Garrett, D.; Lehr, J.; Miskelly, G., *Journal of American Chemical Society* **2007,** 129, 15456.

122. Cooke; Galloway, C.; Bissell, M.; Adams, C.; Yu, M.; Belmont, J.; Amici, R., *U.S Pat. 6 110 9994 A*. Cabot Corp.: 2003.

123. Gooding, J.; Liu, G.; Ngyuyen, Q.; Chow, E.; Bocking, T.; Hibbert, D., *Electroanalysis* **2006,** 18, 1141.

124. Teh, H.; Gong, H.; Dong, X.; Zeng, X.; Tan, A.; Yang, X.; Tan, S., *Analytica Chimica Acta* **2005,** 551, 23.

125. Blankespoor, R.; Limoges, B.; Schollhorn, B.; Syssa-Magale, J. L.; Yazidi, D., *Langmuir* **2005,** 21, 3362.

126. McCreery, R. L.; Wu, J.; Kalakodimi, R. P., *Physical Chemistry Chemical Physics* **2006,** 8, 2572.

127. McGovern, W. R.; Anariba, F.; McCreery, R. L., *Journal of the Electrochemical Society* **2005,** 152, E176.

128. McCreery, R.; Dieringer, J.; Solak, A. O.; Snyder, B.; Nowak, A. M.; McGovern, W. R.; DuVall, S., *Journal of the American Chemical Society* **2003,** 125, 10748.

129. McCreery, R. L.; Viswanathan, U.; Kalakodimi, R. P.; Nowak, A. M., *Faraday Discussions* **2006,** 131, 33.

130. Ssenyange, S.; Yan, H. J.; McCreery, R. L., *Langmuir* **2006,** 22, 10689.

Chapter 2. Experimental Methods

2.1 Introduction

This chapter outlines the general methods and materials used in the work of this thesis. Specific chemicals, methods and materials are given in the appropriate chapters under the experimental section.

2.2 General chemicals and materials

Solutions

Milli-Q (MQ) water, > 18 MΩ cm, was used for all aqueous solutions. Phosphate buffered saline (PBS), pH 7.4, was prepared from 0.04 M phosphate buffer (PB) with added 0.1 M NaCl. PB was made from oven-dried KH_2PO_4 (1.179 g) and Na_2HPO_4 (4.302 g) dissolved in 1 L of MQ water. Acetonitrile (HPLC grade) was dried over CaH_2 for at least two days and refluxed under N_2 for at least two hours prior to distilling in an N_2 atmosphere before use for electrochemistry.

Prep of tetrabutylammonium tetraflouroborate

Tetrabutylammonium tetraflouroborate ($TBABF_4$) electrolyte was prepared by mixing tetraammonium hydroxide (TBAOH, 40 %, Acros Organics) and fluoroboric acid (40 %, BDH). 5 mL of HBF_4 was diluted to 25 mL with MQ water and added to 20 mL of TBAOH that was diluted to 100 mL with MQ water with stirring. The white precipitate was washed with MQ water and filtered under vacuum. The electrolyte was air-dried under suction overnight, followed by oven-drying for 5 days at 50 ^{o}C and drying under vacuum at 80 ^{o}C for at least one day. The dried electrolyte was stored under vacuum.

Synthesis of aryldiazonium salts

Aryldiazonium tetrafluoroborate salts were synthesized using literature methods.[1] The general procedure is described here. 5 mmol of aromatic amine was dissolved in 2 mL of 40% fluoroboric acid pre-diluted with 2 mL of MQ water. The mixture was cooled in an ice bath with constant stirring. 5 mmol of sodium nitrite dissolved in 1 mL of MQ water was slowly added to aromatic amine mixture with stirring. The precipitate formed was cooled in a salted acetone-ice bath for 10 min. The product was collected in an ice cooled plastic filter.

The product was washed with ice-cooled 5% fluoroboric acid, methanol, MQ water and ether. The product was recrystallized in acetonitrile and dried under vacuum suction overnight in the dark. The product was stored under vacuum in the dark. ***Caution: diazonium salts should be handled with care as they can be explosive.***

Synthesis of citrate-capped gold nanoparticles

Gold nanoparticle solution was prepared by following previously reported procedures using the citrate-reduction method.[2] All glassware was washed with aqua regia solution (3:1 $HCl:HNO_3$) and MQ water before use. All solutions were filtered through a 0.45 μm membrane filter before use. A stirred 500 mL solution of 1 mM chloroauric acid was brought to a 'rolling' boil in a 1 L round bottomed flask fitted with a condenser. 50 mL of 38.8 mM sodium citrate solution was quickly added to the round bottomed flask. The solution was refluxed for 1 h with stirring and cooled to room temperature without stirring. The gold nanoparticle solution was stored in the dark. The average particle diameter was 13 nm, characterized by transmission electron microscopy (JEOL 1200EX electron microscope operating at 80 eV) with the assistance of Mr. Manfred Ingerfeld (School of Biological Sciences, University of Canterbury). This is consistent with the size reported in the literature.[2]

2.3 Carbon electrodes

Glassy carbon

Prior to use, GC plates (15 mm x 15 mm x 3 mm) and GC rods (diameter 3 mm) (Tokai Carbon Co. Ltd) were polished with a slurry of 0.05 μm alumina on a Leco polishing cloth and ultrasonicated in successive baths of acetone, methanol and isopropyl alcohol (IPA) for 10 min in each solvent. After ultrasonication, the GC electrodes were dried with a stream of N_2. GC plates were also ultrasonicated in MQ water and acetonitrile and dried with N_2 before use for electrochemistry.

Fabrication of pyrolyzed photoresist film (PPF)

Pyrolyzed photoresist film (PPF) preparation followed similar methods to those described previously.[3-5] The standard procedure adopted for the work in this thesis is described here. Two coats of positive photoresist AZ4620 (Clariant) were spin-coated on pre-cut square pieces (1.5 cm x 1.5 cm) of Si(100) wafers (Silicon Quest and Micro Materials) at 3000 rpm

and soft-baked at 95 ^{o}C for 20 min between coats. Spin-coated samples were stored overnight at 45 ^{o}C before pyrolysis in a Radatherm furnace (Model 2216e tube furnace) in a forming-gas atmosphere (95 % $N_{2\,(g)}$ + 5 % $H_{2\,(g)}$). The temperature was held at 500 ^{o}C for 20 min followed by 750 ^{o}C for another 20 min and finally 1050 ^{o}C for 1 h. After pyrolysis at 1050 ^{o}C for 1 h, the furnace was turned off and allowed to cool to room temperature under a forming-gas atmosphere before removing PPF surfaces from the furnace. PPF surfaces were ultrasonicated for 10 s in successive baths of acetone, methanol and isopropyl alcohol (IPA) and dried with N_2 and stored under vacuum. PPF surfaces were also ultrasonicated in acetonitrile for 30 s before use for electrochemistry. Only PPF samples with sheet resistances < 25 ohms/square were used for modification. The sheet resistance of PPF surface was measured using a home-built probe device that contained two gold wires fixed in a square geometry and connected to a common voltmeter. (N.B. Sheet resistance represents the parallel resistance of an infinite number of infinitely thin parallel sheets. Sheet resistance is expressed as ohms per square area (ohms/square) and is applicable to 2-D systems. The 3-D system-equivalent is resistivity (ρ), and sheet resistance is equal to the average resistivity of a layer multiplied by the thickness of the layer).

2.4 Electrochemistry

Instruments

Electrochemical measurements were performed using computer-controlled EG & G PAR potentiostat model 173 coupled to Powerlab 4SP (ADInstruments) or computer-controlled EG & G PAR potentiostat model 273A.

Electrochemical cell set-up and electrodes

Electrochemical cells were stored inside a HNO_3 acid bath. Cells were thoroughly washed with MQ water and acetone and dried at 45 ^{o}C before use. GC plates and PPF surfaces were mounted horizontally on an insulated metal stage under a glass cell secured with 4 springs. GC rods were fitted vertically through the cell top. A hole in the bottom of the cell was positioned on top of a Viton O-ring that sealed the solution above the sample (Figure 2.1). Electrical contact was maintained with a copper strip externally connected to the sample. The O-ring defined the geometric area of the working carbon electrode. A 008 Viton O-ring defined a geometric working area of ~ 0.26 cm^2 and a 007 Viton O-ring defined

a working area of ~ 0.12 cm^2. In general, a 008 O-ring was used for electrode modification and 007 O-ring was used for subsequent scans at the modified surface, unless otherwise stated. In all experiments, electrochemistry was carried out in a three-electrode cell with the carbon surface as the working electrode and a Pt wire as the auxiliary electrode. For aqueous electrochemistry, the reference electrode was a saturated calomel electrode (SCE). In nonaqueous conditions, a Ag wire pseudo-reference electrode was used. The hydroxymethylferrocene/ferrocenium ($FcOH/FcOH^+$) couple appeared at $E_{1/2}$ = 0.5 V (*vs* Ag wire) in acetonitrile solution + 0.1 M $TBABF_4$ (abbreviated as acetonitrile-electrolyte). Solutions for electrochemistry were degassed with N_2 for at least 15 min and kept in an N_2 atmosphere during measurement.

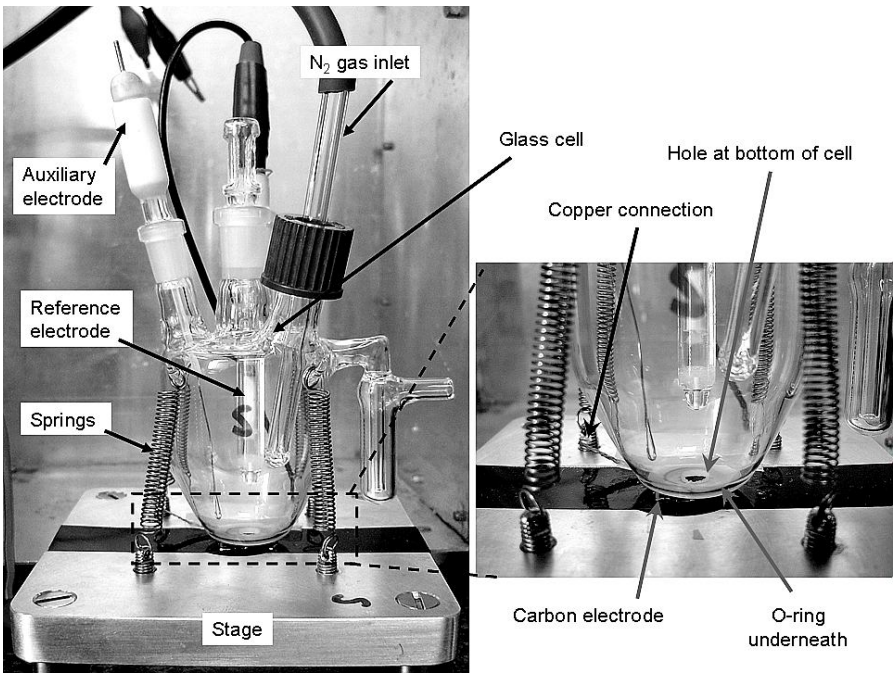

Figure 2.1. Photographs of the electrochemical cell set-up.

2.5 Photochemistry

Photolysis was carried out at room temperature in air either in an in-house built photoreactor (Nanofabrication workshop, Department of Electronic and Electrical Engineering, University of Canterbury) fitted with 365 nm UV lamps (UV intensity ~ 1 mW cm^{-2}) or in a Rayonet Srinivason-Griffin model photochemical reactor. The Rayonet

photoreactor can be equipped with different wavelength-lamp tubes (RPR 2537 Å or 3650 Å). More details about the photochemical procedure are given in Chapter 7.

Photomasks

Photomasks used in photo-patterning experiments (Chapter 7) were made from glass and chrome. The photomasks had features containing either inter-digitated arrays of lines with widths ranging from 200 μm to 30 μm (Figure 2.2, mask 1) or arrays of lines with widths ranging from 105 μm to 10 μm (Figure 2.3, mask 2). Table 1 shows the dimensions of the line-features in mask 2.

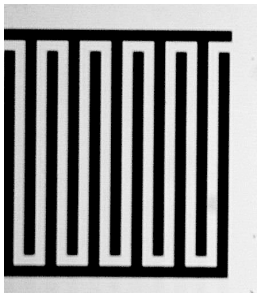

Figure 2.2. Diagram of the pattern of inter-digitated array of lines in mask 1.

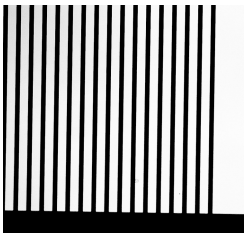

Figure 2.3. Diagram of one pattern of an array of lines in mask 2.

Table 1. Dimensions of the line-features in mask 2.

Feature	Line	Line width μm	Distance of gap between lines μm
1	array	105	200
2	single	105	none
3	array	50	100
4	array	25	100
5	single	50	none
6	array	50	150
7	single	10	none
8	array	10	45
9	single	25	none

2.6 Atomic Force Microscopy (AFM)

The atomic force microscope (AFM) consisted of a Nanoscope® DimensionTM 3100 controller (Digital Instruments) integrated with a Nanoscope® IIIa scanning probe microscope controller (Digital Instruments). All measurements were performed in noncontact tapping mode. Silicon cantilevers from Ultrasharp were used. Noncontact model NSC 37 (also known as NSC 12) cantilevers were used in AFM depth profiling experiments and model NSC 15 cantilevers were used for topographical imaging. Chart 2.1 shows the specifications of the silicon cantilevers and tips from the manufacturer. The images were collected with a resolution of either 256 or 512 samples per line and a scan rate of < 1 Hz. The data were collected in ambient air conditions and each scan was duplicated to ensure that any features observed were reproducible.

Chart 1. Manufacturer specifications of silicon AFM cantilevers and tips used

NSC 37

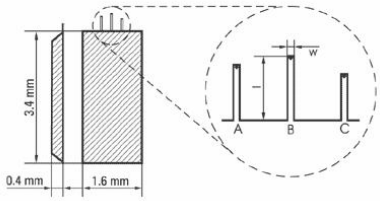

Specification

Cantilever Type	Cantilever Length, l ± 5, µm	Cantilever Width, w ± 3, µm	Cantilever Thickness, µm			Resonant Frequency, kHz			Force Constant, N/m		
			min	typical	max	min	typical	max	min	typical	max
A	300	35	1.7	2.0	2.3	23	28	34	0.20	0.35	0.70
B	350	35	1.7	2.0	2.3	17	21	24	0.10	0.30	0.40
C	250	35	1.7	2.0	2.3	33	41	49	0.35	0.65	1.2

NSC 15

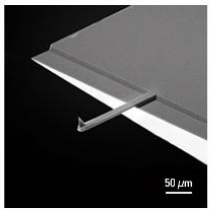

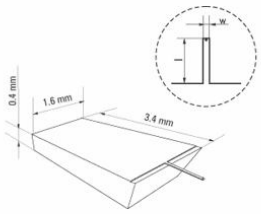

Specification

Cantilever Type	Cantilever Length, l ± 5, µm	Cantilever Width, w ± 3, µm	Cantilever Thickness, µm			Resonant Frequency, kHz			Force Constant, N/m		
			min	typical	max	min	typical	max	min	typical	max
A	125	35	3.5	4.0	4.5	265	325	400	20	40	75

Depth profiling experiments were performed at PPF surfaces following previously reported procedures.[5] The general method involved using an AFM tip to mechanically remove a section of film from the modified PPF surface and measuring the depth of the trench created by scanning across the scratch with an AFM tip. The technique of 'scratching' away a section of film utilized a chip configuration that has three silicon cantilever tips (NSC 37), of different lengths. Two out of the three tips (tips b and c, Chart 2.1), the longest and the shortest, were utilized. The laser on the AFM was focused on the shortest top while the camera visual system was aligned to the longest tip. As the shorter approaches the surface to begin a tapping mode scan, the longer tip (not in resonance) imbeds into the surface film and effectively scratches the film from the PPF surface (Figure 2.4). The size of the scratch is typically ~ 10 µm x 1.3 µm. After scratching, the tips were withdrawn from the PPF surface and the AFM alignment was refocused onto the longer tip which was used in tapping mode to scan the scratch. Alternatively, the scratch was scanned with a separate new tip (NSC 15). Loose debris from the scratch was removed by gentle air convection near the AFM tip. The average cross-sectional plot of the AFM image was used to determine the depth of the film. In some cases, scratching of the bare PPF surface was also carried out to determine the depth of PPF removed by AFM scratching. The maximum depth of PPF removed was 0.3 nm.

Depth profiling experiments were regularly carried out on bare PPF to determine whether film thickness data required an adjustment of 0.3 nm. This depended on the batch of PPF used for modification.

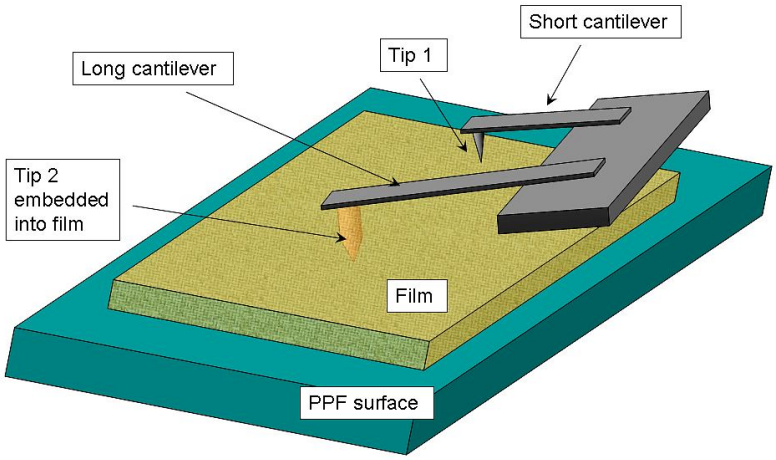

Figure 2.4. Diagram of AFM depth profiling experiment, which shows tip 1 engaged in noncontact tapping mode whilst tip 2 is physically imbedded into the film creating a trench.

For each surface, at least two scratches were made and two AFM scans were taken for each scratch for analysis. From the AFM cross-sectional plot collected for a scratch, at least 8 paired data points were collected where each pair contained one point from within the scratch and one outside. The height differences of the film were recorded and two new random locations were selected. AFM data have estimated uncertainty and standard deviations of ± 0.2 nm unless otherwise stated. Reported surface roughness values (R_a) are an arithmetic average of measured mean roughness values obtained from twenty randomly selected areas (each approximately 1 μm x 1 μm) of the surface film. Each mean surface roughness value was calculated using the NanoScope software.

2.7 Optical microscopy and scanning electron microscopy (SEM)

An Olympus BX60 (inverted light) microscope coupled with a digital Olympus DP10 camera was used for optical microscopy. It provided 5 to 100 X magnification. The microscope was fitted with a polarizer offering differential interference contrasting settings for viewing the carbon surface.

Scanning electron microscopy (SEM) images were obtained using a Raith 150 e-beam lithography system operating with a 10 keV acceleration voltage and aperture at 30. The

aperture and stigmation of the system was carefully adjusted before capture of SEM images. Magnification of less than 100,000 X typically gave the best images.

2.8 Contact angle measurement

Contact angle measurements were made by delivering a 2 μL drop of MQ water from a microsyringe onto the surface of the sample mounted on an illuminated horizontal stage. The image of the static water droplet was captured by an Edmund Scientific video camera and software. Five measurements were taken on each side of the droplet for each sample, and the average water contact angle was calculated for the stated *n* number of individual samples. Contact angles have an estimated uncertainty of ± 2 ^{o} unless otherwise stated.

2.9 UV-Visible Spectroscopy

Spectra were collected with a GBC Scientific UV/VIS 920 Spectrometer, using a 500 to 190 nm scan range, 1 nm slit width, 0.067 nm scan interval and 150 nm/min scan speed. A quartz cuvette with 1 cm pathlength contained the sample, and all samples were referenced to air from the dual beam.

2.10 X-ray photoelectron spectroscopy (XPS)

X-ray photoelectron spectroscopy (XPS) analysis and peak-fitting of XPS data were carried out by Dr. Byrony James, Department of Chemical and Materials Engineering at University of Auckland. XPS data were obtained on GC plates using a Kratos Axis Ultra DLD spectrometer equipped with a monochromatic Al Kα energy source (1486.6 eV), operated at 150 W. Wide scans were recorded with a step size of 1 eV and pass energy of 160 eV from 1100 to 0 eV. For narrow scans, the step size was 0.1 eV and a pass energy of 20 eV was used, unless otherwise stated. Peak positions were referenced to aromatic carbon at 284.7 eV.

2.11 Software

Spartan

Spartan software was used to calculate the molecular length of modifiers. Modifiers were drawn as attached to a sp^3 carbon atom (assuming a carbon-modifier single bond is

formed). Structures were drawn in the extended conformation and the maximum modifier length was calculated and used for film thickness analysis.

Linkfit

Surface concentrations of electroactive groups were determined by measuring the charge associated with voltammetric peaks. The Linkfit software[6] was used to perform curve-fitting to electrochemical data to determine peak areas in cyclic voltammograms. A range of polynomial baselines were fitted to the voltammogram prior to the curve-fit to determine an appropriate baseline to use for the set voltammograms. Baselines from 1st to 3rd polynomial order were fitted to determine how the baseline influences surface concentration values. The largest difference between the surface concentration determined from 1st order polynomial baselines and 3rd order polynomial baselines is approximately 20 %. This is assumed as the typical uncertainty for calculated absolute surface concentration values unless data deviations between samples are larger than 20 %. 3rd order polynomial baselines are predominantly applied as they appeared to best represent and fit peaks in voltammograms. For the same series of experiments, the same baseline was used to maintain consistency. Lorentzian, Gaussian, or a mixture of Lorentzian-Gaussian peaks was subsequently fitted to the recorded voltammetric peak *via* the Levenberg-Marquardt algorithm to best simulate the voltammetric peak. The peak area was determined by integration. The charge (Q) associated with the voltammetric peak is calculated from the peak area (A.V), determined by curve-fitting (above), divided by scan rate (v, V. s^{-1}) used to collect the voltammogram. Surface concentrations (Γ, mol cm^{-2}) was calculated according to Equation 2.1, where n is the number of electrons involved in the redox process, F is Faraday's constant (96485 C mol^{-1}) and A is the geometric area of the electrode (cm^2). More information about surface concentration analysis is also given in Chapters 3 and 4.

$$\Gamma = Q / nFA \qquad (2.1)$$

2.12 References

1. Downard, A. J.; Prince, M. J. *Langmuir* **2001**, *17*, 5581-5586
2. Grabar, K. C.; Freeman, R. G.; Hommer, M. B.; Natan, M. J. *Analytical Chemistry* **1995**, *67*, 735-743
3. Kim, J.; Song, X.; Kinoshita, K.; Madou, M.; White, R. *Joural of the Electrochemical Society* **1998**, 145, 2314-2319
4. Ranganathan, S.; McCreery, R. L. *Analytical Chemistry* **2001**, *73*, 893-900
5. Brooksby, P. A.; Downard, A. J. *Langmuir* **2004**, *20*, 5038-5045
6. Loring, J. S. *Linkfit* **2004**

Chapter 3. Carbon surface modification by electrochemical reduction of aryldiazonium ions

3.1 Introduction

The modification of GC and PPF surfaces by reduction of aryldiazonium salts has been reviewed in Chapter 1. Scheme 3.1 shows the surface grafting reaction, which for carbon substrates leads to the formation of C-C bonds between the surface and the modifier layer.

Scheme 3.1. Reduction of aryldiazonium ion resulting in surface attachment.

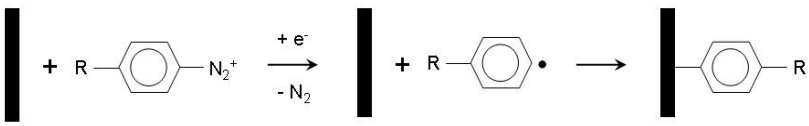

As described in Chapter 1, additional reactions are possible, which involves the aryldiazonium ion or the generated radicals attacking the grafted modifiers leading to polymerization (Scheme 1.1). These polymerization reactions result in film growth generating complex polymeric film structures. Also, other linkages may be present in the film such as azo (-N=N-) and hydrazine (-NH-NH-) groups as a result of the polymerization reactions.[1,2] In general, loosely packed multilayered films with typical film thickness of approximately 2-4 nm are formed as a result of film growth from polymerization reactions by this method.[3-6] Films of different thicknesses can be prepared by controlling the applied conditions. Experimental parameters such as the concentration of modifier, electrolysis time and applied potential can control the film growth.[3,7]

In this chapter, the grafting of 4-nitrobezenediazonium ion to GC and PPF is introduced and the experimental conditions used for film formation with 4-nitrobenzenediazonium salt are described. Standard procedures are established for surface modification of carbon surfaces using electroreduction of aryldiazonium ion-modifiers. Films grafted from aryldiazonium ion to GC and PPF are characterized using techniques which include a combination of atomic force microscopy (AFM), electrochemistry and water contact angle measurements. The work aims to gain further insight into the properties and

structure of films grafted from aryldiazonium salts. The experiments described in this chapter lay the groundwork for the later chapters; more detailed studies on the reduction of nitrophenyl (NP) films derived from 4-nitrobenzenediazonium ions form the subject of Chapter 4.

3.2 Experimental

3.2.1 Electrochemistry

Standard procedure for preparation of NP films on carbon surfaces

Two consecutive voltammetric scans typically between 0.3 to -0.45 V in 4-nitrobenzenediazonium salt in acetonitrile-electrolyte solution were carried out using a carbon electrode (GC or PPF), and the potential was then held at $E_{app} = E_{p,c} - 150$ mV (i.e. $E_{app} = -0.45$ V), where $E_{p,c}$ is the cathodic peak potential of the modifier (Figure 3.1), for a specified electrolysis time, t, typically between 30 to 600 s. The NP films were ultrasonicated in acetonitrile for 5 min to remove any weakly adsorbed material before electrochemical or AFM analysis.

3.3 Results and Discussion

3.3.1 Electrochemical grafting of NP films to GC surfaces

Electrochemistry was used to investigate the formation and properties of films on GC surfaces. Figure 3.1 show the first two cyclic voltammetric scans obtained for the reduction of 4-nitrobenzenediazonium salt at a GC electrode. The acetonitrile solution contained 0.6 mM of 4-nitrobenzenediazonium tetrafluoroborate with 0.1 M $TBABF_4$ as supporting electrolyte. In the first cycle, there is a large reduction peak appearing at $E_{p,c} \sim -0.30$ V. After stirring the solution by bubbling with N_2, a second scan was recorded. In the second scan, the reduction peak disappears and the residual current becomes smaller with repeat scanning. The loss of the cathodic peak is consistent with the behaviour of an electrode being passivated by the grafting of a surface film. The grafted film impedes electron-transfer across the electrode interface. Hence the continued electrochemical reduction of 4-nitrobenzenediazonium ion at the surface is increasingly inhibited by the formation of the grafted layer. The self-passivating response of the modified surface is typical of those reported in literature by other workers.[3,5,6,8-10] Formation of the grafted film is attributed to

the surface-grafting reaction described in Scheme 3.1.[9] Scheme 3.1 expresses the simplest form of the grafting reaction; other reactions are possible as discussed in Chapter 1.

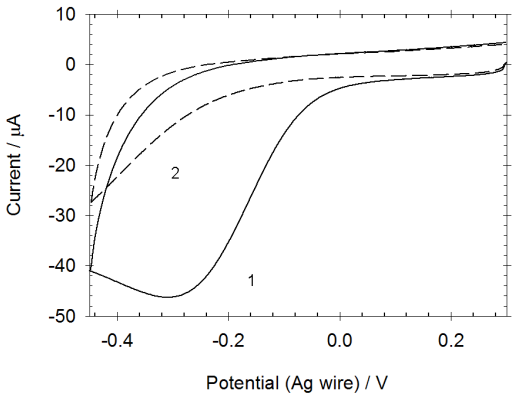

Figure 3.1. First two cyclic votammetric scans, with stirring between scans, obtained at a GC surface (geometric area = 0.26 cm^2) for the reduction of 0.6 mM 4-nitrobenzenediazonium salt in acetonitrile + 0.1 M $TBABF_4$ (v = 200 mV s^{-1}).

The process involves the electrochemical reduction of 4-nitrobenzenediazonium cation, which generates reactive aryl radicals near the electrode interface. The attack of radicals at the surface results in covalent grafting of the modifier to the carbon substrate. The process is entropically favoured with the chemically irreversible loss of N_2 from the diazonium ion moiety. Unless otherwise stated, all NP films were prepared at GC electrodes in acetonitrile with 0.1 M $TBABF_4$ (supporting electrolyte) using a standard procedure involving two consecutive voltammetric scans between 0.3 and -0.45 V in 0.6 mM 4-nitrobenzenediazonium salt solution, followed by holding the potential at E_{app} = -0.45 V (i.e. $E_{app} = E_{p,c} - 150$ mV). The purpose of the voltammetric scans is to ensure that grafting was indeed occurring at the particular carbon surface. This procedure was adopted as the standard method for the preparation of diazonium-derived films at carbon surfaces in this work (Section 3.2). The films were ultrasonicated in acetonitrile for 5 min to remove any weakly adsorbed material on the surface before transferring to 0.25 M H_2SO_4 for electrochemical analysis.

3.3.2 Electrochemistry and surface concentration measurement of NP films electrochemically grafted to GC surfaces

Films derived from the 4-nitrobenzenediazonium ion exhibit redox chemistry based on the electrografted surface-bound nitrophenyl (NP) moiety. This redox chemistry provides a

convenient means to monitor the films. The electroactivity of NP moiety can be observed in with cyclic voltammetry in both aqueous and nonaqueous conditions. Under nonaqueous conditions, the NP group is reversibly reduced in a one-electron process[11], and in protic conditions, the NP moiety is irreversibly reduced by four to six electrons as described below.[9] For the work described in this thesis, reduction in aqueous solutions was used to monitor NP films. The voltammetric reduction peak is larger and the experimental measurement is easier to carry out in aqueous compared with nonaqueous solution. The latter requires a rigorously dry solvent environment to prevent irreversible conversion of the NP group to reduced nitrogen products with unknown stiochiometry. Figure 3.2 shows the first and second cyclic voltammograms recorded in 0.25 M H_2SO_4 for a GC surface electrografted with a NP film using an electrolysis time, *t*, of 600 s. The voltammetric response is consistent with those reported by other workers.[5,8,12] The cyclic voltammograms show a large irreversible reduction peak at $E_{p,c} \sim$ -0.7 V in the first scan, which disappears in the second scan. Broad oxidation peak(s) between 0.2 V and 0.6 V and their associated reduction peaks are observed only after electroreduction, and remain in subsequent scans. The disappearance of the large cathodic peak (peak i) in the second and subsequent cycles indicates a chemically irreversible process has occurred during the reduction. The major peak is assigned to the electroreduction of NP groups to aminophenyl groups (AP) (Equation 3.1a) and hydroxylaminophenyl groups (APOH) (Equation 3.1b).[5,8,9,13] The reversible redox couple between 0.2 V and 0.6 V (peaks ii and iii) is assigned to the APOH/ nitroso (-Ph-NHOH)/(-Ph-NO) redox couple described in Equation 3.1c.[5,8,9,13] APOH is formed from the incomplete electroreduction of the NP film (Equation 3.1b). The formation of AP groups is based on known redox chemistry of NP groups and the obvious discrepancy between the changes involved in the reduction of NP groups and oxidation of APOH (taking the stiochiometries of the reactions into account). A more detailed study of NP reduction is presented in Chapter 4.

$$\text{Carbon-Ph-}NO_2 + 6H^+ + 6e^- \rightarrow \text{Carbon-Ph-}NH_2 + H_2O \qquad (3.1a)$$

$$\text{Carbon-Ph-}NO_2 + 4H^+ + 4e^- \rightarrow \text{Carbon-Ph-NHOH} + H_2O \qquad (3.1b)$$

$$\text{Carbon-Ph-NHOH} \leftrightarrow \text{Carbon-Ph-NO} + 2H^+ + 2e^- \qquad (3.1c)$$

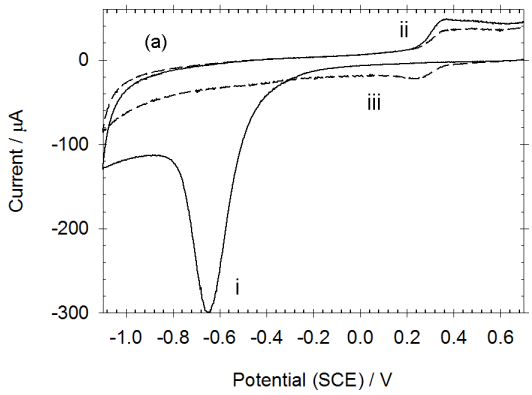

Figure 3.2. First two cycles of cyclic voltammograms recorded in 0.25 M H_2SO_4 for a NP film (t = 600 s) grafted to GC (geometric area of electrode 0.26 cm^2, v = 200 mV s^{-1}).

The voltammograms also reveal that nearly all the electroactive NP groups in the surface-grafted film are reduced in the first scan. Hence quantitative evaluation of the peak areas of the cyclic voltammograms recorded for the reduction of NP films can give information about the surface concentration of electroactive NP groups grafted at the surface. The effect of the electrolysis time (t) used for the electrografting on the surface concentration of NP groups was investigated by recording the NP voltammetric responses for a series of films prepared using t ranging from 30 to 600 s. Each individual film was analyzed in aqueous H_2SO_4 after preparation. The voltammetric peaks for the electroreduction of GC-Ph-NO_2 (Figure 3.2, i) and the oxidation peak for GC-Ph-NHOH (Figure 3.2, ii) were curve-fitted and the absolute charges related to each redox process were determined from the curve-fitted peak areas. Taking account of the relationship between the –Ph-NO_2 reduction peak (four- and six-electron processes), -Ph-NHOH oxidation peak (two-electron process) and the number of electrons involved in each redox process, the charge can be converted to the total surface coverage of electroactive NP groups. Equation 2.1 (Chapter 2) expresses the relationship between surface coverage (Γ) and the charge (Q) of the redox process, where n is the number of electrons involved in the redox process, F is Faraday's constant (96487 C mol^{-1}) and A is the geometric surface area of the electrode. Detailed calculation procedures for the estimation of grafted NP groups determined from voltammetry are given in the appendix.

The relationship between the calculated concentration of electrografted NP groups and modification time for each film is shown in Figure 3.3. (N.B. the grafting time excludes two consecutive voltammetric scans used in the standard modification procedure). The initial rate of increase in the amount of modifier grafted to the surface is rapid. The surface concentration is approximately 80 % of its maximum after 30 s electrolysis and reaches a

maximum after ~ 120 s. The rapid achievement of a high surface concentration is expected for a short electrolysis time since two (modification) voltammetric scans also preceded the applied electrolysis in the standard method film preparation. Surface coverages reach a maximum limiting surface concentration value of approximately 2.3±0.4 x 10^{-9} mol cm^{-2}. This is consistent with estimates reported by other groups for films prepared under similar modification conditions in acetonitrile (Chapter 1).[3,5,8,9]

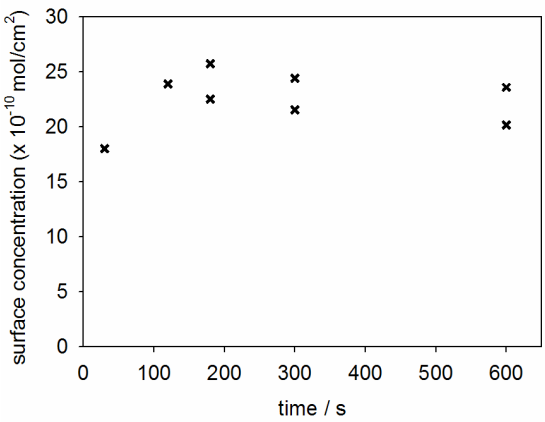

Figure 3.3. Plot of surface concentration of electroactive NP groups grafted to GC *vs* electrolysis time (applied after two consecutive voltammetric scans) for NP films prepared using 0.6 mM 4-nitrobenzenediazonium modifying solution.

As described in Chapter 1, theoretical calculations of an ideal close packed monolayer of phenyl groups attached to a flat surface has a surface concentration of approximately 1.2 x 10^{-9} mol cm^{-2}.[14] Considering this interpretation, the NP films generated here would be equivalent to approximately two close packed NP layers. However, the measured values are given with respect to the geometric electrode area and the actual surface area will be larger than the geometric area if surface topography is taken into account. Hence the grafted films appear consistent with a close-packed monolayer.[12,15] It should be noted that the surface coverage is a lower limit for the number of groups grafted to the surface because some NP groups maybe electroinactive in the film environment. A second interpretation provided by Downard *et al* indicated that a monolayer-equivalent of a phenyl film has a surface concentration of approximately 2.5 x 10^{-10} mol cm^{-2} (Chapter 1).[5] Using this interpretation, the surface coverage of ~ 2.3 x 10^{-9} mol cm^{-2} obtained for the NP films prepared in this work reflect molecular layers with a thickness of approximately five monolayer-equivalents (assuming a surface roughness factor of ~ 2 for GC)[12,16]. This suggests that the films prepared with the standard procedure in this work are multilayered films. Further evidence is presented in the sections below.

3.3.3 $Fe(CN)_6^{3-}$ redox probe voltammetry at NP-modified GC surfaces

Evaluation of the cyclic voltammetric behaviour of solution redox probes at film-modified carbon electrodes can provide further insight into the films' chemical and physical properties and is a commonly used method for surface analysis.[7,17] Cyclic voltammetry experiments were carried out in aqueous solution with $Fe(CN)_6^{3-}$. $Fe(CN)_6^{3-}$ is a redox probe that is known to undergo outer-sphere electron-transfer and it is also a probe that is sensitive to the nature of the electrode surface.[18] Figure 4 shows the electrochemical response of the $Fe(CN)_6^{3-/4-}$ redox couple at a) a polished GC surface and b) a NP modified GC surface (t = 600 s). Comparison of the two voltammograms reveal that the redox response is significantly suppressed by the presence of the grafted NP film. The blocking effect of the NP film is consistent with those reported by other workers of whom also observed the disappearance of the voltammetric response of the redox probe.[5,8] (Note that the large ΔE_p value at polished GC is most likely due to both slow heterogeneous electron-transfer kinetics at this GC electrode and uncompensated iR drop arising from the relatively large current).

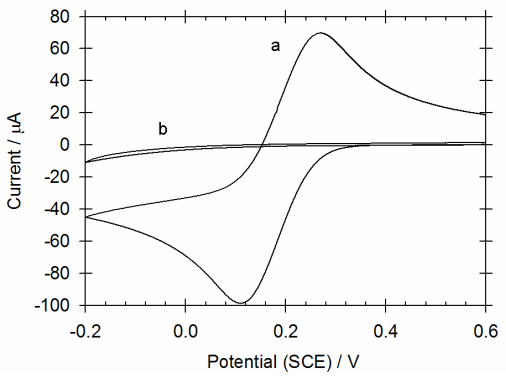

Figure 3.4. Cyclic voltammetric response of 4.5 mM $Fe(CN)_6^{3-}$ + 0.1 M KCl, using v = 200 mV s^{-1} at (a) polished GC surface and; (b) NP-modified GC surface (geometric area = 0.07 cm^2, t = 600 s).

The suppressed voltammetric probe response is attributed to the NP film acting as an insulating layer or physical barrier between $Fe(CN)_6^{3-}$ species in solution and the carbon electrode, increasing the distance for electron-transfer at the surface.[1,7] The barrier properties of NP films are examined in more detail using PPF substrates, which is presented in Section 3.3.7.

3.3.4 Water contact angle measurement of NP-modified GC surfaces

The wettability of NP films electrografted to GC surfaces was examined by static water contact angle measurements. NP films prepared with standard methods (t = 600 s) were placed on an illuminated stage. A drop of Milli-Q water was delivered to the surface of the film by a microsyringe and the image of the static water droplet was captured. Figure 5 shows an image of a water droplet on a GC surface electrografted with a NP film. The internal angle that the edge of the droplet makes with the surface is the measured contact angle. Analyzing the angles between the droplet and the surface on both sides, the average static water contact angle for NP films was found to be 58 ^{o}. In contrast, a polished GC surface has a measured average contact angle of 50 ^{o}. The increase in contact angle and hence decrease in wettability upon modification of GC with NP films is consistent with the deposition of a more hydrophobic layer on the surface. The water contact of *p*-nitrobenzenethiol self-assembled on gold surfaces is typically reported in the range 65 to 70 ^{o}.[19] The difference in contact angle for NP-modified GC surfaces compared to NP-terminated self-assembled monolayers on gold surfaces is unclear. However, it may be attributed to differences in film roughness and structure (More information on the film structure of NP films is described in later sections). Films can appear relatively more hydrophilic than expected if the surface texture of the film is rough. This is due to invasion of the wetting liquid (i.e. water) and weak pinning effect of the liquid droplet rested in the grooves and texture of the film.[20,21]

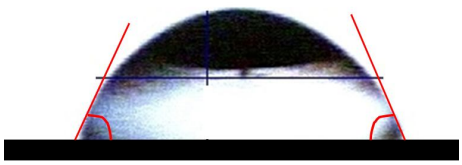

Figure 3.5. Static water contact angle image of a water droplet sitting on top of a GC surface grafted with a NP film.

3.3.5 Characterization of NP films electrochemically grafted to PPF surfaces

For comparison, similar procedures to those used for GC were also carried out for modification of PPF. Electrografted NP films were prepared at PPF surfaces and subsequently ultrasonicated in acetonitrile for 5 min and dried under a stream of nitrogen to clean and remove loose debris before characterization. Figure 6 shows the first two cyclic

voltammetric scans recorded at PPF for the electroreduction of 4-nitrobenzenediazonium salt in acetonitrile. Similar self-passivating behaviour to that observed at GC surfaces (Figure 3.1) is also observed at PPF. The first scan in the modifying solution at PPF shows an irreversible reduction peak at $E_{p,c}$ ~ -0.3 V, which disappears rapidly upon repeat scanning. This process is consistent to the formation of a NP film grafted to the surface. The grafted film attenuates electron-transfer across the surface preventing continuing reduction of aryldiazonium ions.

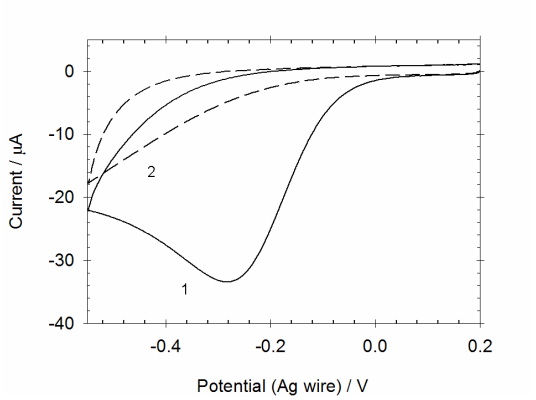

Figure 3.6. First two cyclic votammetric scans, with stirring between scans, obtained at a PPF surface for the reduction of 0.6 mM of 4-nitrobenzenediazonium salt in acetonitrile + 0.1 M $TBABF_4$ with v = 200 mV s^{-1}.

3.3.6 Electrochemistry and surface concentration measurement of NP-modified PPF surfaces

The redox chemistry of surface-bound NP groups was exploited to monitor a series of NP films that were prepared on PPF surfaces with two diazonium modifier concentrations, 0.6 and 5 mM, and electrolysis times ranging from 10 to 600 s. Figure 3.7 shows the cyclic voltammograms (first two cycles) obtained in H_2SO_4 for a PPF surface electrografted from 0.6 mM 4-nitrobenzenediazonium salt solution. The observed voltammetric response of NP moieties at PPF in protic solution is similar to that observed at GC surfaces (Figure 3.2). Figure 3.7 shows the irreversible reduction of NP groups at $E_{p,c}$ ~ -0.85 V in the first scan; the peak disappears in scan 2. Partially reversible redox features from the –Ph-NHOH/-Ph-NO redox couple are observed between 0.2 and 0.6 V after electroreduction.

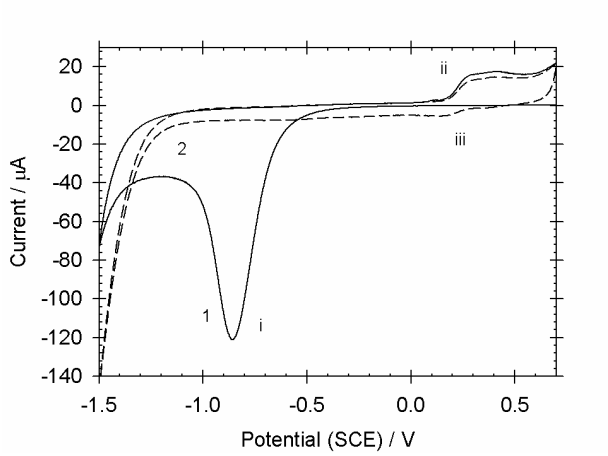

Figure 3.7. First two cycles of cyclic voltammograms recorded in 0.25 M H_2SO_4 for a NP film (t = 600 s) grafted to PPF (geometric area of electrode 0.12 cm^2, v = 200 mV s^{-1}).

Quantitative analysis of the charge associated with the redox processes was carried out using curve-fitting to help establish the surface concentration of NP groups at PPF. The effect of electrolysis time on the amount of NP modifiers electrografted to PPF was determined for the two modifier concentrations (0.6 and 5 mM). The calculated surface coverage data obtained at PPF are presented in Figure 8. For both concentrations of modifier, the data show that near limiting surface coverage of NP films are formed at relatively short electrolysis times. More than 60 % of the maximum surface concentration is reached within 10 s of electrolysis for films prepared in a modifier concentration of 0.6 mM, whilst for films derived from 5 mM diazonium ion modifier solution, around 90 % of the maximum coverage was reached within the same electrolysis time. Clearly, the modifier concentration has an effect on the rate of formation of the surface film. It is reasonable to suggest that a higher concentration of modifiers generate a relatively high concentration of radicals that can graft to the surface and hence may establish the film at a faster rate. The films approach maximum limiting surface concentration values of approximately 2.3±0.4 x 10^{-9} mol cm^{-2} and 1.8±0.4 x 10^{-9} mol cm^{-2} after 300 s for films formed in modifier concentrations of 0.6 and 5 mM, respectively. For 5 mM-derived films (crosses) there is no apparent increase in NP surface coverage beyond 60 s of electrolysis. In contrast, for 0.6 mM-derived films (triangles), it is unclear whether a higher surface concentration would be obtained at longer electrolysis times (for t > 300 s). The variation in surface concentration and maximum values are consistent with estimates reported by other groups for films prepared under similar modification conditions in acetonitrile (Chapter 1).[3,5,8,9]

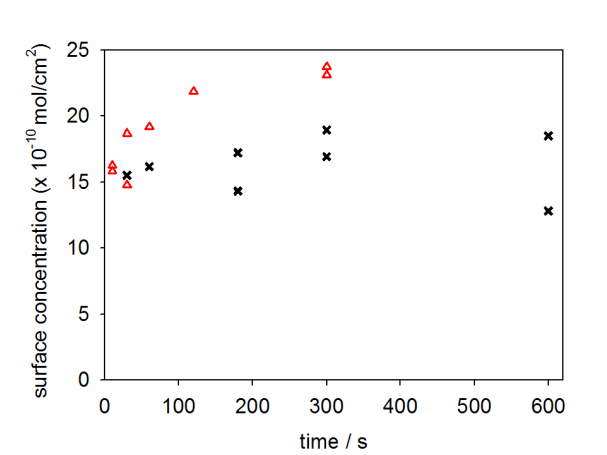

Figure 3.8. Plot of surface concentration of electroactive NP groups grafted at PPF *vs* electrolysis time (applied after two consecutive voltammetric scans) for NP films prepared using 4-nitrobenzenediazonium modifying solution with concentrations (triangles) 0.6 mM; and (crosses) 5 mM.

As explained earlier, a monolayer-equivalent of NP groups on PPF has been reported to correspond to a surface concentration of 2.5 x 10^{-10} mol cm^{-2}.[5] Hence the films electrografted to PPF are multilayered in structure and at their highest surface concentration have an estimated minimum of seven to nine layers. Further evidence for multilayered NP films is presented in Section 3.3.8. The data in Figure 8 also show that the NP films generated from 5 mM diazonium ion modifier solution have a surface coverage of electroactive NP groups approximately 20 % lower than films derived from a modifier concentration of 0.6 mM. This has not been reported by other workers that had used different concentrations of diazonium ion-solution for modification.[9] It is likely that the lower apparent film coverage is the result of more NP groups in the 5 mM-derived films being electroinactive within the multilayer network formed during electrografting. It is reasonable to propose that for relatively thick films, some NP groups may be inaccessible to solvents and ions or at too great a distance from the electrode for efficient electron-transfer. This might be particularly true for films derived from 5 mM of diazonium ion solution, which is assumed to produce relatively more radicals leading to a less uniform film structure (see later) and hence causing these NP films to be more electroinactive.

3.3.7 $Fe(CN)_6^{3-}$ redox probe voltammetry at NP-modified PPF surfaces

The surface film bonded to PPF was analyzed by comparing the cyclic voltammetry of the $Fe(CN)_6^{3-}$ redox probe before and after electrografting procedures. Figure 9 shows the

voltammetric response of $Fe(CN)_6^{3-}$ obtained at 1) bare PPF surface, and 2) after electrografting a NP film to PPF. The unmodified PPF surface shows a chemically reversible voltammetric response for $Fe(CN)_6^{3-}$ redox couple (Figure 9, scan 1). The ΔE_p value is assumed to be largely due uncompensated *i*R drop arising from the relatively large current as noted for GC in Section 3.3.3. At the PPF surface grafted with NP film, there is a very marked decrease in the apparent rate of electron-transfer of the $Fe(CN)_6^{3-}$ species. The modified PPF surface exhibits a large blocking effect to the $Fe(CN)_6^{3-}$ redox reaction, similar to that observed at NP-modified GC (Figure 4).

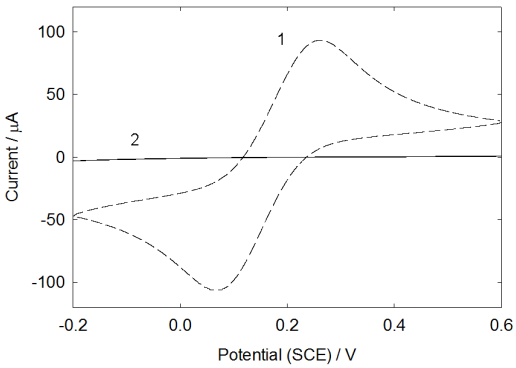

Figure 3.9. Cyclic voltammetric response of 3.1 mM $Fe(CN)_6^{3-}$ + 0.1 M KCl, using v = 200 mV s^{-1} at (1) bare PPF surface and; (2) NP-modified GC surface (geometric area = 0.12 cm^2, t = 600 s).

Considering a simple model, a molecular film is expected to influence the observed rate constant (k^o_{obs}) for electron-transfer of the redox probe according to equation 3.2, where an ideal close-packed layer model is assumed.[22] d is the average distance for electron-transfer, β is the tunneling parameter, which depends on the chemical nature of the layer, and k^o is the standard heterogeneous rate constant at the bare surface.

$$k^o_{obs} = k^o \exp(-\beta.d) \qquad (3.2)$$

Hence, the main factors that will affect the apparent rate of electron-transfer are the chemical nature of the film and the distance of electron-transfer (i.e. thickness of the film). A β value of 0.2 $Å^{-1}$ has been reported for substituted phenyl layers grafted to GC *via* reduction of aryldiazonium ions,[23] while for aliphatic self-assembled monolayers on gold surfaces β values are typically between 0.78-0.97 $Å^{-1}$.[24-27] Self-assembled monolayers of thiols that incorporate conjugated phenylene-ethylene units have intermediate β values in the range 0.36–0.57 $Å^{-1}$.[28,29] The effectiveness of the blocking properties of NP films in this work to

$Fe(CN)_6^{3-}$ redox chemistry indicates that the films are insulating with little or no defect sites or pinholes that permit $Fe(CN)_6^{3-}$ to undergo electron-transfer reaction at or near the surface and produce a voltammetric response. Other factors that may contribute to the blocking effect include hydrophobic and electrostatic interactions of the system, which can increase the effective distance of closest approach for electron-transfer beyond the physical thickness of the film (i.e. d > thickness of the film). $Fe(CN)_6^{3-}$ redox probe is hydrophilic that is likely to interact less favourably with NP film, which is relatively more hydrophobic. Hence this would lead to a larger distance of closest approach for electron-transfer beyond the physical thickness of the layer.

On the basis of the results in this work and using DigiSim software, estimates of k^o_{obs} and k^o for $Fe(CN)_6^{3-}$ redox couple at the bare and film covered electrodes were made. The rate constant ratio, k^o_{obs}/k^o, was approximately < 10^{-5}. Substitutions into Equation 3.2, and with $d \approx 3.5$ nm (see later), give an estimation for β of ≥ 0.33 Å^{-1}. This β value is larger than that reported by McCreery *et al* for phenyl layers (0.2 Å^{-1})[23] but is consistent with the values obtained for self-assembled monolayers that consists of conjugated phenylene-ethylene systems (0.36–0.57 Å^{-1}).[28,29] The reported β value of (0.2 Å^{-1})[23] for phenyl layers is most likely to be underestimated since the β value was calculated by assuming that monolayers of phenyl groups (i.e. d = monolayer thickness) were obtained by electroreduction of aryldiazonium ions. As described in the following section, multilayered films of 3-4 nm are typically formed by reduction of aryldiazonium ions under similar conditions. Hence the assumption made by the workers in the report that monolayers are formed under their applied conditions (i.e. 1 mM aryldiazonium salt, $E_{app} = E_{p,c} - 200$ mV, t = 10 min)[23] is most likely inaccurate, giving an underestimated β value.

3.3.8 AFM examination of NP-modified PPF surfaces

Atomic force microscopy (AFM) experiments were conducted to investigate changes in film thickness and topography at PPF surfaces upon electrochemical modification with NP films. PPF has a low surface roughness, which facilitates these measurements. NP films were prepared on PPF using standard procedures and were ultrasonicated in acetonitrile for 5 min to remove non-covalently bound material before microscopy analysis. AFM depth profiling experiments involve using an AFM tip to mechanically remove a section of the NP film from

the modified PPF surface. The trench that is created in the film is subsequently profiled by AFM to directly measure the thickness of the film. Figure 10 (bottom panel) shows a typical AFM image of a trench scratched out by an AFM tip at a PPF surface electrografted with a NP film. Figure 10 (top panel) shows an average cross-sectional profile of a trench created at a NP film on PPF. A small amount of surface debris can remain at the edge of the trench after AFM scratching hence depth profiling measurements of the trench are made away from those regions. Film thickness was determined from the statistical average of data points collected from the average cross-sectional profile from at least two trenches created at random locations on the film. The bare PPF area outside of the modified area containing the film was also regularly AFM 'scratched' and profiled for reference. At bare PPF, the technique scratched to an average maximum depth of 0.3 nm and hence AFM film thickness data were adjusted by this value.

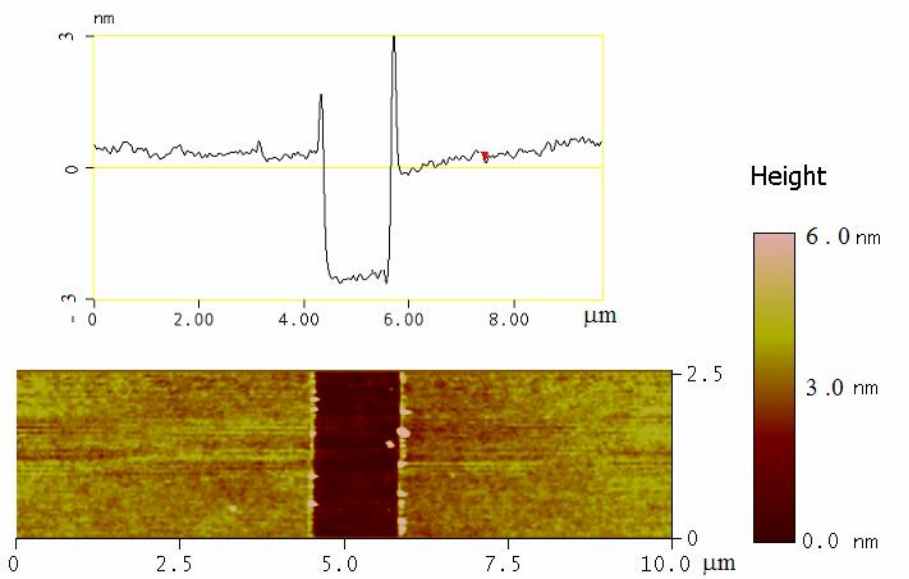

Figure 3.10. Top: Average profile of the trench generated in a NP film. **Bottom:** AFM image of a scratched NP film grafted to PPF (t = 180 s).

The effect of electrolysis time on film thickness was investigated by preparing films using electrolysis times ranging from 10 to 600 s. Figure 3.11 shows film thickness collected from films prepared using two aryldiazonium ion modifier concentrations, 0.6 mM (crosses) and 5 mM (circles). The data show an increase in film thickness with increasing electrolysis time for films prepared from both modifier concentrations. In both cases, 3 to 4 nm NP films are formed at the surface within approximately 180 s of electrolysis. An extended electrolysis time (600 s) was included for films prepared using 5 mM of aryldiazonium modifier, and

these films are seen to reach a film height of approximately 3.8 nm.

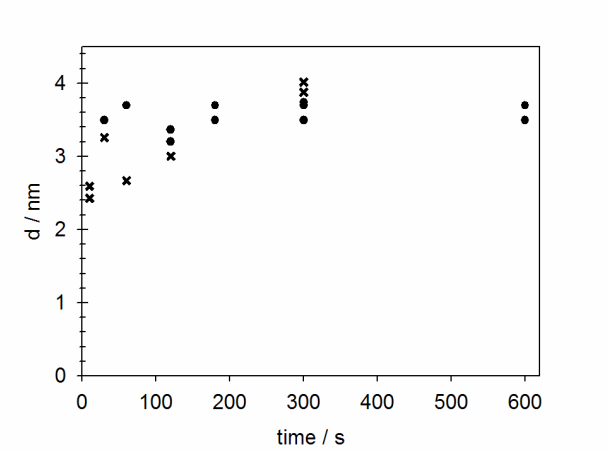

Figure 3.11. Plot of AFM thickness *vs* electrolysis time for NP films electrochemically modified in 4-nitrobenzenediazonium ion modifying solution with concentrations (crosses) 0.6 mM; and (circles) 5 mM.

Assuming, for simplicity, that the average molecular orientation of the film is perpendicular to the PPF surface and the length of the NP modifier is 0.7 nm, the maximum average film thickness of NP films formed here corresponds to films of approximately five layers. Clearly, the films generated in this study are multilayered in structure. The direct measurement of film thickness thus confirms the conclusion reached by measured surface concentration of NP groups in the film (Section 3.3.6). Multilayered structures can form when the aryl radicals produced during the electrochemical process attacks the grafted layer (Scheme 1.1). The data also show film growth at E_{app} = -0.45 V (i.e. overpotential of 150 mV) stops at approximately 4 nm indicating that electron-transfer becomes inefficient for continued film growth across that distance and the process becomes self-passivated. AFM results for NP films in this work are consistent with those reported by Downard *et al*, where the workers also generated NP films on PPF with a film height between 1.5–4 nm.[5] McCreery *et al* also observed multilayered film formation for their substituted biphenyl films electrografted to PPF.[4] Using a contact mode AFM depth profiling method, the workers showed that multilayers of up to ~ 6 nm were generated by reduction of aryldiazonium ion with similar applied conditions as used in this work. In the case of nitroazobenzenediazonium ion-modifiers (molecular length ~ 1.4 nm), films corresponding to approximately four layers were shown to form at PPF by the workers.[4] McDermott *et al* grafted films of 15-25 nm in thickness to GC by reduction of aryldiazonium ions with an overpotential of 250 mV and electrolysis time of 30 min.[10] As described previously, film growth is influenced by applied potential and modification time and hence relatively thinner films produced in this work is

due to a lower applied overpotential (i.e. 150 mV) and shorter deposition times.[10]

Inspection of the lower AFM image in Figure 3.10 reveals that the as-formed films are topographically uniform (surface roughness, R_a ~ 0.4 nm) with no visible defects or aggregates at the surface. This observation, directly obtained by AFM, is consistent with the result inferred by $Fe(CN)_6^{3-}$ redox probe voltammetry, where the complete blocking effect suggests a compact and uniform surface film with no pinholes or defects.

Comparison of electrochemical and AFM data reveals a linear correlation for films derived from 0.6 mM 4-nitrobenzenediazonium modifier. The data shown for the films in Figures 8 and 11 for 0.6 mM-derived NP films are shown as a plot of film height *vs* surface coverage in Figure 3.12 (circles). The straight line in the figure was forced through zero and is a line of best fit for the data set, with slope = 6.3 x 10^{-10} mol cm^{-2} nm^{-1} and R^2 = 0.64. Considering the length of grafted NP modifier (0.7 nm), this gives an estimated average surface coverage of approximately 4.4±0.9 x 10^{-10} mol cm^{-2} for a monolayer- equivalent thickness of NP groups grafted at PPF. This experimentally determined monolayer-equivalent surface coverage corresponds to approximately 34 % of the theoretical ideal monolayer of phenyl groups at a planar surface (12 x 10^{-10} mol cm^{-2}). Hence, the non-close packed film structure is expected to have significant free-volume occupied by solvents and ions.

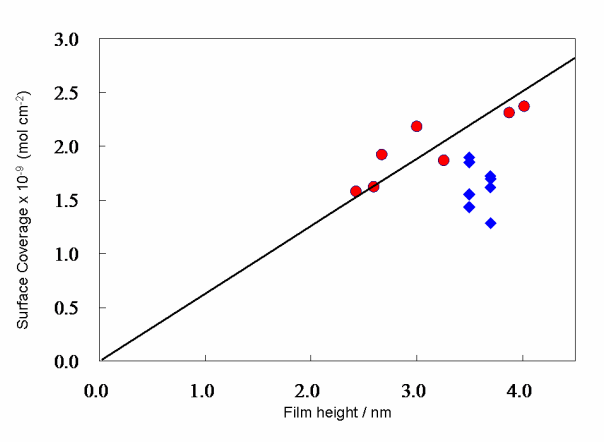

Figure 3.12. Plot of surface coverage of electroactive NP groups against initial film thickness for NP films electrochemically modified in 4-nitrobenzenediazonium modifying solution with concentrations; circles: 0.6 mM (with line of best-fit); and diamonds: 5 mM. The line of best fit for NP films derived from 0.6 mM modifier solution has slope = 0.63 x 10^{-9} mol cm^{-2} nm^{-1} and R^2 value = 0.64.

The surface concentrations of NP groups determined in this work is greater than the monolayer-equivalent surface coverage of 2.5 x 10^{-10} mol cm^{-2} reported by Downard and Brooksby for their NP films.[5] Possible reasons for the difference are likely to be related to the different conditions used for the preparation of the films. In the earlier report, NP films were prepared from aryldiazonium salts in both acetonitrile and aqueous acid solutions, and with a modifier concentration of 0.7 mM. Examination of the data reported in the earlier work show that films prepared in aqueous acid were generally more dense than those prepared in acetonitrile. If the data for the films prepared in aqueous conditions are excluded, the film density would be close to 3.2 x 10^{-10} mol cm^{-2} per monolayer-equivalent.[5] Additional disparities may be in part due to different curve-fitting of voltammetric peak areas, in particular with respect to the choice of baseline applied. Electroinactive NP groups in the films can also lead to underestimation of the amount of grafted NP groups and hence result in a lower than expected film density. Taking these factors into consideration, the NP films prepared in this work using 0.6 mM modifying solution may be more electroactive than those reported by the earlier workers however, the reason for such a difference is not understood.

In contrast to the data discussed above, NP films derived from 5 mM modifying solution (Figure 3.12, diamonds) did not yield a useful relationship between surface coverage and film thickness. Fewer NP groups were electrochemically detected in 5 mM-derived films than in films of similar thickness derived from 0.6 mM modifier solution. This is most likely the result of NP groups being electroinactive in the film environment, as previously observed for nitroazobenzene multilayers.[6] It is reasonable to assume that with higher aryldiazonium ion concentration, a higher concentration of radicals is produced at the surface, possibly resulting in a more dense film structure. The increased film density may significantly limit solvent and ion penetration into the film and may cause NP groups to be electroinactive.

3.4 Conclusion

The electrochemical reduction of diazonium cations leads to the grafting of the modifier to the carbon surface. The electrografting of 4-nitrobenzenediazonium was demonstrated at both GC and PPF surfaces. The electrochemically attached NP films were monitored and evaluated by electrochemistry and AFM, which together, give a powerful approach to investigating properties of surface films. Electrochemical investigations revealed that electrografting yield very similar films at GC and PPF. Electrochemical analysis showed that the NP films, at both type of carbon surfaces, have a strong blocking effect to electron-transfer to the $Fe(CN)_6^{3-}$ redox probe, voltammetric response of electroactive surface-bound NP groups and self-passivating electrografting behaviour upon repeat scanning or electrolysis. It is reasonable to conclude that very similar NP films with the same chemical and physical properties are formed at GC and PPF. Hence, it is assumed that results obtained for films electrografted from aryldiazonium ions are equally applicable for both GC and PPF; these surfaces will be used interchangeably in the following chapters. For experimental practicality, voltammetric experiments such as the investigation of $Fe(CN)_6^{3-}$ redox probe response at modified surfaces are carried out at GC. All film thickness measurements are made at films grafted to PPF surfaces, where the low surface roughness of PPF can facilitate more accurate measurements. AFM results are consistent with the results inferred by electrochemistry. AFM analysis showed that topographically uniform NP films with a thickness of approximately 4 nm is produced using these simple grafting procedures. The films are confirmed to be multilayered in structure and some films have an estimated compactness of approximately 34 % of an ideal close packed layer.

3.5 References

(1) Saby, C.; Ortiz, B.; Champagne, G. Y.; Belanger, D. *Langmuir* **1997**, *13*, 6805.

(2) Doppelt, P.; Hallais, G.; Pinson, J.; Podvorica, F.; Verneyre, S. *Chemistry of Materials* **2007**, *19*, 4570.

(3) Pinson, J.; Podvorica, F. *Chemical Society Reviews* **2005**, *34*, 429.

(4) Anariba, F.; DuVall, S. H.; McCreery, R. L. *Analytical Chemistry* **2003**, *75*, 3837.

(5) Brooksby, P. A.; Downard, A. J. *Langmuir* **2004**, *20*, 5038.

(6) Brooksby, P. A.; Downard, A. J. *Journal of Physical Chemistry B* **2005**, *109*, 8791.

(7) Downard, A. J. *Electroanalysis* **2000**, *12*, 1085.

(8) Ortiz, B.; Saby, C.; Champagne, G. Y.; Belanger, D. *Journal of Electroanalytical Chemistry* **1998**, *455*, 75.

(9) Allongue, P.; Delamar, M.; Desbat, B.; Fagebaume, O.; Hitmi, R.; Pinson, J.; Saveant, J.-M. *Journal of American Chemical Society* **1997**, *119*, 201.

(10) Kariuki, J. K.; McDermott, M. T. *Langmuir* **2001**, *17*, 5947.

(11) Bard, A.; Lund, H. *Encyclopedia of Electrochemistry of the Elements (Organic Section)*; Dekker, 1973; Vol. XIII.

(12) Tan, E. S. Q.,Assembly of Organic Layers onto Carbon Surfaces, University of Canterbury, 2006.

(13) Rubinstein, I. *Journal of Electroanalytical Chemistry* **1985**, *183*, 379.

(14) Liu, Y.-C.; McCreery, R. L. *Journal of American Chemical Society* **1995**, *117*, 11254.

(15) Liu, G. Z.; Liu, J. Q.; Bocking, T.; Eggers, P. K.; Gooding, J. J. *Chemical Physics* **2005**, *319*, 136.

(16) Liu, G.; Liu, J.; Böcking, T.; Eggers, P.; Gooding, J. *Chemical Physics* **2005**, *319*, 136.

(17) Davies, T. J.; Moore, R. R.; Banks, C. E.; Compton, R. G. *Journal of Electroanalytical Chemistry* **2004**, *574*, 123.

(18) Ranganathan, S.; McCreery, R. L. *Analytical Chemistry* **2001**, *73*, 893.

(19) Jakubowicz, A.; Jia, H.; Wallace, R. M.; Gnade, B. E. *Langmuir* **2005**, *21*, 950.

(20) Bico, J.; Tordeux, C.; Quere, D. *Europhysics Letters* **2001**, *55*, 214.

(21) Tuteja, A.; Choi, W.; Ma, M. L.; Mabry, J. M.; Mazzella, S. A.; Rutledge, G. C.; McKinley, G. H.; Cohen, R. E. *Science* **2007**, *318*, 1618.

(22) Miller, C.; Cuendet, P.; Graetzel, M. *Journal of Physical Chemistry* **1991**, *95*, 877.

(23) Yang, H.; McCreery, R. *Analytical Chemistry* **1999**, *71*, 4081.

(24) Smalley, J.; Feldberg, S.; Chidsey, C.; Linford, M.; Liu, Y. *Journal of Physical*

Chemistry **1995**, *99*, 13141.

(25) Becka, A.; Miller, C. *Journal of Physical Chemistry* **1992**, *96*, 2657.

(26) Finklea, H.; Hanshew, D. *Journal of American Chemical Society* **1992**, *114*, 3173.

(27) Weber, K.; Hockett, L.; Creager, S. *Journal of Physical Chemistry B* **1997**, *101*, 8286.

(28) Sachs, S.; Dudek, S.; Hsung, R.; Sita, L.; Smalley, J.; Newton, M.; Feldberg, S.; Chidsey, C. *Journal of American Chemical Society* **1997**, *119*.

(29) Creager, S.; Yu, C.; Bamdad, C.; O'Connor, S.; MacLean, T.; Lam, E.; Chong, Y.; Olsen, G.; Luo, J.; Gozin, M.; Kayyem, J. *Journal of American Chemical Society* **1999**, *121*, 1059.

Chapter 4. Reduction of nitrophenyl films electrografted to carbon surfaces

4.1 Introduction

Modification of surfaces by a range of methods often employs the nitrophenyl (NP) derivative as a model compound. Utilizing a modifier that contains the NP moiety has the advantage of producing surface films that can be detected spectroscopically and electrochemically, thus confirming the success of the grafting reaction. For the latter approach, by measuring the charge associated with the electrochemical reduction of electroactive NP moieties, either in nonaqueous or aqueous conditions, it is possible to estimate the surface concentration of the film.[1] The NP moiety is also a versatile precursor to diverse functionalities. The conversion of the NP functionality to a variety of nitrogen derivatives in synthetic organic chemistry is well-known and is used routinely in organic synthesis. Common methods for reduction of the NP functionality often use chemical reducing agents in rigorous conditions such as Zn + NaOH, Fe + HCl and Sn + HCl.[1,2] However, such harsh conditions are undesirable for modified surface applications as the procedure may cause damage to the surface or grafted film. Relatively milder chemical reductions with In powder + NH_4Cl and Na_2S are also effective methods used in synthetic chemistry and may be suitable in surface chemistry.[2-4] Hence the latter method is investigated for reduction of NP films in the work described in this chapter.

In addition to chemical methods, electrochemical reduction in protic conditions (most commonly aqueous acid or 1:9 EtOH:H_2O + 0.1 M KCl) can transform NP moieties in surface films to reactive reduced nitrogen derivatives.[5-16] The reduced nitrogen derivatives can react with carboxylic acids and their activated derivatives through the formation of amide linkages. It is generally assumed that reduction affords the aminophenyl (AP) and hydroxylaminophenyl (APOH) groups through the reactions described in Equations 3.1 (Chapter 3).[8] A four-electron reduction of NP yields the APOH group which may be further reduced to AP in a second two-electron step (Equations 3.1).

Simultaneous grafting of NP film and reduction of the NP moiety during modification of carbon surfaces in aqueous acidic conditions has also been demonstrated.[5,12] The chemical reduction of NP-modified carbon powder using Sn + HCl has been reported to lead to a useful material for subsequent coupling reactions.[17] Other novel approaches to selectively reduce NP groups of a grafted film and assembly of metal nanoparticles have also been reported.[18,19] The electroreduction of NP groups and subsequent reaction with appropriate functional groups have been reported for films grafted to a variety of carbon surfaces, which include diamond, GC, carbon fibers and screen-printed graphite electrodes.[9-12,20-25] In an interesting application, NP films grafted to screen-printed graphite electrodes were reduced in aqueous acidic solution and used as reactive tethers to immobilize an enzyme, acetylcholinesteras (Drosophila melanogaster), used for the detection of organophosphate pesticides. The reduction of NP film-modified surfaces can be utilized for biomolecular immobilization applications useful in the development of biosensors.[10]

Despite the widespread uses of NP-derivatized carbon materials, there are some aspects of the films and reactions that are not well understood. Interestingly, although electrochemical reduction of NP films is assumed to lead to the formation of AP groups, this product has not been confirmed by direct electrochemical detection. The efficiency of NP reduction in different media has not been explored and the relative reactivities of the reduced films towards amide bond formation reactions are unknown. Additionally, conflicting interpretations of XPS spectra of NP films appear in the literature. Spectra of freshly grafted films show a N 1s peak for the nitro group (405-406 eV) and in addition, a peak at approximately 400 eV corresponding to a reduced aromatic N moiety. There are a number of possible explanations for the origin of the 400 eV peak; the most frequently proposed are either amine groups arising from reduction of NP during XPS analysis[26,27], or azo functionalities derived from diazonium ion groups incorporated in the film during grafting.[28-30]

The work in this chapter aims to examine the physical and chemical properties of NP films derived from diazonium ion-modifiers, before and after reduction of the NP groups. Investigations are carried out on the electrochemical and chemical reduction, and subsequent coupling reactions, of NP films grafted to GC and PPF using a combination of electrochemical, XPS and AFM measurements. The efficiency and products of electrochemical reduction in 0.25

M H_2SO_4, 1:9 EtOH:H_2O + 0.1 M KCl and 20 mM benzoic acid in acetonitrile-electrolyte solution are compared with chemical reduction using Na_2S. The yields of electroactive products formed by coupling reactions of the reduced films with carboxylic acid and acid chloride derivatives are quantified with the aim of identifying the reduction method which gives the film with the greatest activity for amide bond formation reactions. In this work, analysis with both electrochemical and XPS techniques aims to provide further insight into the N 1s XPS spectra of freshly grafted and also reduced NP films.

4.2 Experimental Section

4.2.1 Electrochemistry

A Viton O-ring defined the geometric area of the working electrode (0.26 cm^2, unless stated otherwise). All voltammetric scans were performed using v = 200 mV s^{-1} unless otherwise stated. Electrochemical modification of carbon surfaces was carried out in acetonitrile solutions containing 0.6 mM of 4-nitrobenzenediazonium salt and 0.1 M $TBABF_4$. The standard modification procedure involved two initial scans from 0.3 V to -0.40 V, followed by electrolysis at -0.40 V for 600 s (i.e. E_{app} = $E_{p,c}$ – 150 mV). Modified surfaces were ultrasonicated in acetonitrile for 5 min prior to further analysis.

Electrochemical reduction of NP films was carried out in either 0.25 M H_2SO_4, or EtOH:H_2O solutions (1:9 by volume) containing 0.1 M KCl, or acetonitrile solutions containing 20 mM benzoic acid and 0.1 M $TBABF_4$. The standard reduction procedure in aqueous solvents involved four cyclic scans from 0.7 to -1.1 V (H_2SO_4) or -1.5 V (EtOH/H_2O). Ten scans between 0.7 and -1.8 V (*vs* Ag wire) were used for reduction in benzoic acid-acetonitrile solution. All treated samples were sonicated in the solvent in which they were reduced for 5 min and dried with N_2. Unless stated otherwise, all reductions were carried out using the standard procedures.

All redox probe voltammetry was obtained in 4.5 mM $Fe(CN)_6^{3-}$ in 0.1 M KCl aqueous solution) using a GC rod electrode (diameter = 3.0 mm).

4.2.2 Chemical Reduction of NP films

NP films were immersed in a stirred EtOH:H_2O solution (1:1 by volume) containing 0.8 M disodium sulfide for 3 h at 40-60 ºC. The treated samples were ultrasonicated in EtOH, Milli-Q water and acetonitrile for 5 min and dried with N_2.

4.2.3 Coupling reaction of 4-nitrobenzoyl chloride, 4-fluorobenzoyl chloride and 4-nitrobenzoic acid with reduced NP films

Reduced NP films were incubated for 18 h, with stirring, in a 200 mM 4-nitrobenzoyl chloride (NBCl) dichloromethane (DCM) solution, neat 4-fluorobenzoyl chloride (FBCl) or PBS solution containing 4 mM 4-nitrobenzoic acid (NBA), 20 mM EDC, and 20 mM NHS. After reaction, samples were sonicated for 5 min in DCM or MQ water and dried with N_2. To measure the surface concentration of coupled groups, the samples were mounted in the electrochemical cell using an O-ring that defined a smaller area (0.12 cm^2) than that used for preparation and reduction of the electrografted film.

4.2.4 Assembly of gold nanoparticles at reduced films

Reduced NP films grafted to PPF were immersed in Au nanoparticle solution for 1 h, followed by thorough washing with MQ water and drying with N_2.

4.3 Results and Discussion

4.3.1 Electrochemical and contact angle characterization of reduced films

The reduction of NP films electrografted to planar carbon surfaces was performed under various conditions. The effectiveness of the reduction process, the reduced products and the chemical reactivity of the resultant surface films were established by using water contact angle measurements, electrochemistry and X-ray photoelectron spectroscopy (XPS). XPS analysis is described later in the chapter. NP films were prepared on GC electrodes using standard procedures (Section 4.1.2). As described in the previous chapter, the NP films produced are loosely packed multilayered films with an approximate film thickness of 4 nm. The as-prepared NP films were ultrasonicated in acetonitrile before the modified surfaces were transferred to the

following solutions to carry out electrochemical reduction of the NP groups: aqueous 0.25 M H_2SO_4; EtOH:water (1:9) + 0.1 M KCl; and 20 mM benzoic acid in acetonitrile + 0.1 M $TBABF_4$. For simplicity, these reduction media will be referred to as H_2SO_4, $EtOH/H_2O$ and BA/ACN, respectively. Figures 1a-c) show the first two voltammetric scans recorded at the NP-modified GC electrodes in each medium.

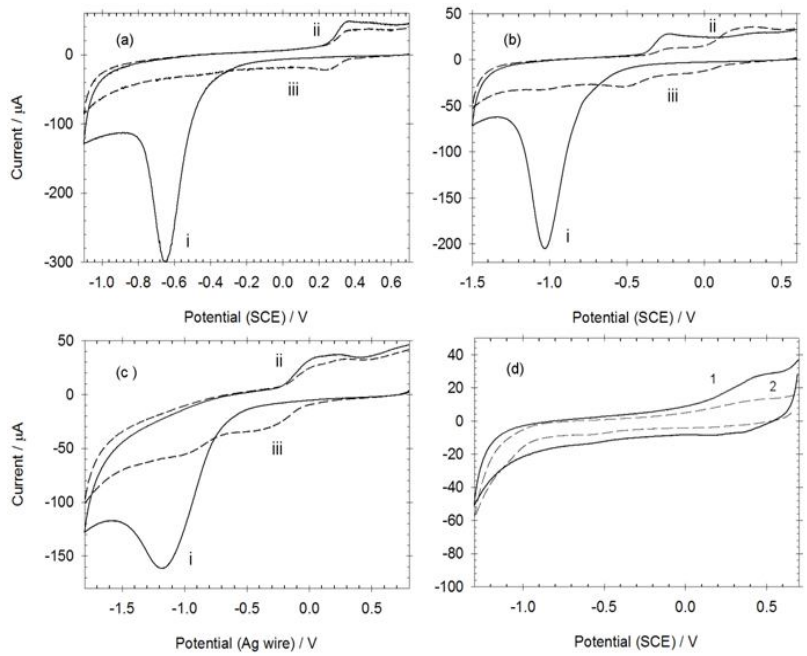

Figure 4.1. First two consecutive scans of NP-modified GC in: (a) H_2SO_4; (b) $EtOH/H_2O$ and (c) BA/ACN. (d) Voltammogram 1, first scan in 0.25 M H_2SO_4 of NP-modified GC after reduction with Na_2S; voltammogram 2, scan in 0.25 M H_2SO_4 of an unmodified GC surface. Scan rate = 200 mV s^{-1} for all voltammograms.

In the first scan, there is a single chemically irreversible reduction process (i) and a relatively small and broad oxidation process which appears to be two closely-spaced peaks (ii). The second scans at the grafted electrodes show the disappearance of the large reduction process and the appearance of small reduction processes (iii) associated with the oxidations (Chapter 3). The voltammograms in Figures 4.1a) and b) closely match others in the literature for reduction of NP films in similar media.[5,14,31] The similarity of the voltammograms in Figures 1a-c) show that reduction in BA/ACN also follows the same pathway, although the reduction is less complete after the first scan. The potentials of all voltammetric peaks in Figure 4.1 depend on the medium, shifting to more positive potentials as the H^+ activity increases; this influence of pH

is consistent with the widely accepted assignments for the redox processes, represented by equations 3.1. Peak (i) is due to the $6e^-$ reduction of NP to AP groups (equation 3.1a) and also includes NP reduction to APOH groups (equation 3.1b). Peaks (ii) and (iii) arise from the APOH/nitrosophenyl couple (equation 3.1c) after electroreduction.

The reversible APOH/nitroso couple (equation 3.1c) gives a single oxidation and reduction peak in homogeneous solution[32], whereas in Figure 4.1, the grafted films show two closely-merged oxidation and reduction peaks of similar size. The voltammograms for reduction of NP films in this region are variable. One pair of peaks is sometimes observed while in other voltammograms, two peaks of variable relative magnitudes are found in the region. Similar variations are seen in voltammograms reported by other workers.[5,14,31] This may show that in some experiments, electroreduction of the NP film results in formation of small amounts of two compounds which can be oxidized at similar potentials, or alternatively, that the film environment can cause splitting of the two charge transfer steps of the APOH/nitroso couple. For convenience, the process(es) appearing between 0.3 and 0.6 V will be referred to as the APOH/nitrosophenyl couple. NP films were also chemically reduced by gentle heating of the modified electrode in ethanolic Na_2S solution for 3 h. The resulting reduced NP films were then examined in H_2SO_4 to detect any residual NP groups (Figure 4.1d), scan 1). Comparing Figures 4.1a) and d) scan 1 reveals that after chemical reduction the cathodic peak related to NP reduction is absent and that there are small peaks attributed to the APOH/nitrosophenyl couple. In comparison, scan 2 of Figure 4.1d) shows the voltammetric response of an unmodified, polished GC surface in 0.25 M H_2SO_4; no peaks are present between 0.3 and 0.6 V. This shows that chemical reduction has reduced the NP groups in the film rather than detached the film from the surface. The electrochemical response of reduced films was also examined in the more positive potential region. Standard reduction conditions (Section 4.2) were used, i.e. the films electroreduced in H_2SO_4 and $EtOH/H_2O$ were cycled four times over the potential ranges shown in Figures 4.1a) and b), respectively, whereas ten scans were performed in the BA/ACN medium because the reduction appears to require more cycles in this medium (Figure 4.1c). All reduced films were ultrasonicated in the media that they were reduced in before electrochemical analysis in H_2SO_4 in the positive potential region. Figures 4.2a-c) show voltammograms obtained in 0.25 M H_2SO_4 of electroreduced films, and Figure 4.2d) shows a film chemically reduced in ethanolic Na_2S. The cyclic voltammograms of the reduced films reveal redox couples centered

between 0.3 and 0.6 V (above) followed by a broad irreversible oxidation at $E_p \approx 0.9$ V. The latter peak is assigned to the oxidation of AP groups, as reported for AP films grafted directly to gold surfaces by the reduction of the corresponding diazonium salt.[33] For comparison, cyclic voltammograms were obtained in H_2SO_4 for a bare GC electrode (scan 1, Figure 4.2e), and also for an as-prepared NP film which has not been reduced (scan 2). The absence of any redox response from these electrodes confirms that the redox processes in Figures 4.2a-d) are a consequence of reduction of the NP film. The observation of the AP oxidation process in Figures 4.2a-c) provides, for the first time, direct electrochemical evidence that NP groups are converted predominantly to AP groups during reduction in protic media. Furthermore, inspecting Figures 4.2a-d) suggests that reduction in different media gives qualitatively similar results, and this is supported by static water contact angle measurements of the reduced films. Polished GC gives an angle of ~ 50º and the angle increases to ~ 58º after grafting an NP film. As expected, the water contact angle decreases after reduction of NP films, giving an average value, for all films, of approximately 41º. There is no significant difference between films reduced by electrochemical or chemical reduction in different media.

Evaluation of the surface concentrations of functional groups in the reduced film helps to assess the effectiveness of the reduction methods. Surface concentrations of electroactive groups can be determined from the charge associated with each redox process. Table 4.1 lists the charge associated with each redox process, obtained from curve-fitting voltammograms obtained during reduction of NP films, and subsequent oxidation of the reduced films in H_2SO_4. The NP reduction charge, I, was estimated from the large reduction peak obtained in the first scan to negative potentials of the NP films in each medium. The charges, II and III, associated with AP and APOH oxidation, respectively, were obtained from the first scan to positive potentials in 0.25 M H_2SO_4, after the standard reduction procedures. The charge for formation of AP groups, IV, (i.e. the charge associated with the reaction in equation 3.1a) was calculated by assuming that charge I is the sum of charges for reactions 3.1a and 3.1b and that the contribution of reaction 3.1b can be accounted for as twice the charge for reaction 3.1c (i.e. double the charge of III). (Although the processes giving rise to the redox couple(s) in the region 0.3 - 0.6 V are uncertain (two separate species each undergoing two-electron charge transfers, or a single species undergoing successive one-electron charge transfers), for simplicity a two-electron process, represented by equation 3.1c, is assumed for the whole oxidation manifold.) The

surface concentrations of APOH and AP groups in the reduced films can be calculated from charges III and IV, respectively, assuming the stoichiometries shown in equations 3.1c and 3.1a. The sum of these values gives an estimation of the surface concentration of NP groups in the as-prepared NP-modified surface.

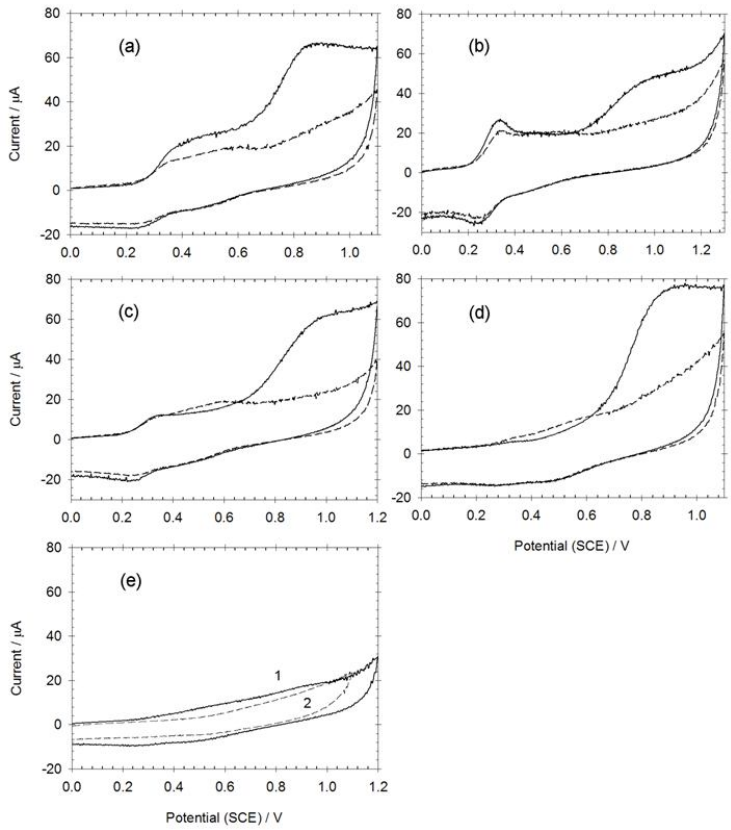

Figure 4.2. Cyclic voltammograms (200 mV s^{-1}) recorded in 0.25 M H_2SO_4 of (a-d): NP-modified GC after reduction in (a) H_2SO_4, (b) EtOH/H_2O, (c) BA/ACN and (d) Na_2S; (e) Voltammogram 1, unmodified GC surface; voltammogram 2, NP-modified GC prior to reduction.

Table 4.1. Charge and surface concentration data obtained from cyclic voltammograms of NP films reduced using different conditions.

reduction method	measured charge (C cm^{-2})			calculated charge (IV)[d] for formation of AP (C cm^{-2})	surface concentration (mol cm^{-2})		
	NP reduction (I)[a]	AP oxidation (II)[b]	APOH oxidation (III)[b]		AP	APOH	NP[e]
H_2SO_4	1.0×10^{-3}	3.4×10^{-4}	1.3×10^{-4}	7.4×10^{-4}	1.3×10^{-9}	6.7×10^{-10}	2.0×10^{-9}
$EtOH/H_2O$	1.2×10^{-3}	2.4×10^{-4}	1.4×10^{-4}	9.2×10^{-4}	1.6×10^{-9}	7.3×10^{-10}	2.3×10^{-9}
BA/ACN	9.6×10^{-4}	3.6×10^{-4}	1.1×10^{-4}	7.4×10^{-4}	1.3×10^{-9}	5.8×10^{-10}	1.8×10^{-9}
Na_2S	-	3.2×10^{-4}	3.8×10^{-5}	-	-	2.0×10^{-10}	-

[a] determined from the first reduction scan of the NP film; [b] after reduction of the NP film as described in the Experimental Section; [c] calculated from surface concentrations, assuming that the APOH groups undergo a two-electron oxidation; [d] calculated as charge I - (2 x III); [e] calculated as the sum of surface concentrations of AP and APOH

A limitation of the above analysis is that charge I is measured from the first reduction scan, whereas charge III for oxidation of APOH groups is measured after multiple reduction cycles during which reduction continues, albeit at a much lower rate. The consequence is underestimation of charge IV and hence underestimation of the concentration of AP (and NP) groups in the reduced films. Consideration of the voltammograms in Figures 4.1a) - c) indicates the underestimation will be greatest for the film reduced in BA/ACN because reduction of the film is least complete after one reduction scan in this medium. This effect must account for, in part, the discrepancy arising between the charges directly measured for oxidation of AP groups (charge II) which is highest for the film reduced in BA/ACN, and the calculated surface concentration of AP groups which is lowest for the film reduced in BA/ACN.

Despite the limitations described above, trends in the data are reliable for comparisons. The data in Table 4.1 establish that for all reduction methods, the major electroactive product is the AP group. The yield of APOH groups is lowest for chemically reduced films and similar for all electroreduced films. The calculated surface concentration of electroactive NP groups prior to electroreduction ranges from 1.8 to 2.3×10^{-9} mol cm^{-2}, however as discussed above, the calculation method underestimates the concentration to a variable extent. Considering that all films are expected to have the same concentration of NP groups, since they were prepared using the same standard procedure, the largest calculated value (2.3×10^{-9} mol cm^{-2}) must reflect the

best estimate. This surface concentration is larger than that measured for a NP film grafted under essentially the same conditions and subsequently electrochemically examined in anhydrous acetonitrile-electrolyte solution. In that medium, the one-electron reversible reduction of NP groups gave an estimated surface concentration of 1.2 x 10^{-9} mol cm^{-2}.[34] The difference can be attributed to two factors: 1) For film-modified electrodes, there is a large uncertainty associated with establishing an appropriate baseline from which to calculate voltammetric peak areas. Background currents for the grafted electrodes change after reduction of the film because the film permeability changes (compare Figures 1d) scan 1 and 2e) voltammogram 2), hence it is difficult to establish a 'correct' baseline for calculating peak areas. This difficulty is greater when fitting irreversible rather than reversible voltammetric peaks, and charge data I and II in Table 4.1 have an estimated associated uncertainty of 20 %. 2) The electroactivity of NP groups may depend on the medium used for reduction of the film and it is possible that not all NP groups are detected and contribute to the overall charge measured in acetonitrile solution, resulting in an underestimation of surface concentration. Notably, voltammetric determination of surface concentrations of these multilayer films must be applied with caution. However, the consistency in the procedure used for curve-fitting analysis in this work means that calculated surface concentrations can be meaningfully compared, and that trends in the data are reliable. Alternatively, determining the surface concentration of AP groups from the charge associated with their electrooxidation (charge II) is not helpful because the number of electrons involved in the oxidation process is unknown. In homogeneous aqueous solution, the electrooxidation of aromatic amines is followed by coupling reactions.[35] Such reactions must be of limited importance for AP groups in the film environment, however the important film-based reaction pathways are not known.

4.3.2 Reaction of reduced NP films with carboxylic acid and acid chloride derivatives.

Generating an amine-terminated surface is synthetically useful for coupling of molecular species (Section 4.1). Investigations with 4-nitrobenzoic acid (NBA) and 4-nitrobenzoyl chloride (NBCl) were carried out to compare the amount of coupling reaction between these species and the surface-amine groups at each type of reduced film. These amine-reactive species were chosen because the amount of coupled product can be readily determined by electroreduction of the electroactive nitroaryl moiety. A series of NP films were prepared at GC

surfaces and subsequently reduced by the methods described earlier, and reacted with either NBA in PBS solution with EDC and NHS as activating agents, or with NBCl in DCM. Figures 3a and b show voltammetric responses obtained in 0.25 M H_2SO_4 of H_2SO_4-reduced NP films after coupling NBA and NBCl, respectively. The voltammograms were obtained by scanning from 0 to 1.3 V to inspect for unreacted surface-amine groups that did not participate in the coupling reactions with the amine-reactive species. In the reverse scan to -1 V, the reductions of the amide-coupled surface-bound nitroaryl products can be detected. In Figure 4.3a, redox peaks from unreacted AP and APOH groups can be seen after reaction of the film with NBA. The presence of the residual AP and APOH groups indicate that the coupling reaction is incomplete even after 18 h of reaction. In contrast, barely discernible redox features are observed in the positive potential region after coupling with NBCl (Figure 4.3b), indicating a higher yield of coupling with the AP and APOH groups. As expected, the voltammograms also show a larger peak for nitroaryl reduction at the NBCl- than NBA-coupled film. The reduction peaks from the amide-coupled nitroaryl products in the voltammograms were analyzed and the concentration of electroactive NP groups coupled to each type of reduced film was estimated.

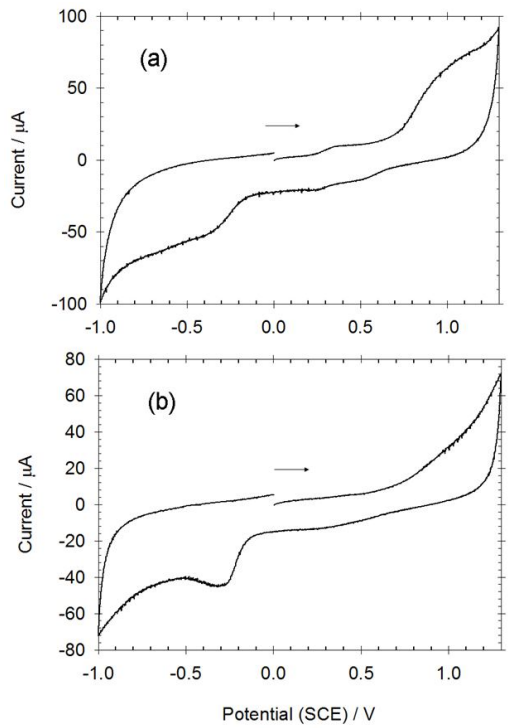

Figure 4.3. Cyclic voltammograms (200 mV s^{-1}) recorded in 0.25 M H_2SO_4 of NP-modified GC reduced in H_2SO_4 and reacted with (a) NBA and (b) NBCl.

Figure 4.4 shows data for films reduced in H_2SO_4, $EtOH/H_2O$, BA/ACN and Na_2S and reacted with NBA and NBCl, the open triangles, shows the concentration of coupled NP groups for films reacted with NBA in aqueous conditions. The estimated amount of coupled nitroaryl species is approximately 4.6±0.9 x 10^{-10} mol cm^{-2} for all the reduced films and does not appear to depend on the method used to reduce the initial NP film. In contrast, when the coupling reaction was carried out with the corresponding acid chloride derivative in nonaqueous conditions, the yield of coupled nitroaryl product depended on the method of preparation of the initial reduced film. As expected, yields are generally higher for NBCl coupling which is consistent with acid chlorides being intrinsically more reactive than carboxylic acids. Figure 4.4, crosses, shows that the yield is highest for NP films that were electroreduced in H_2SO_4 ($\Gamma \sim 10$ x 10^{-10} mol cm^{-2}) and lowest for films electroreduced in BA/ACN ($\Gamma \sim 5.1$ x 10^{-10} mol cm^{-2}), differing in coupling yields by a factor of two. Although cyclic voltammogram in Figure 4.3b shows an almost complete disappearance of electroactive AP and APOH groups after reaction with NBCl, the yields of electroactive coupled groups are less than quantitative (approximately 50% for the H_2SO_4-reduced film). This is most likely the result of some AP and APOH groups reacting to yield nonelectroactive coupled products, presumably because they are electrochemically inaccessible in the film environment. Hence the calculated yields (and also for those coupling reactions in aqueous conditions) must represent lower limits.

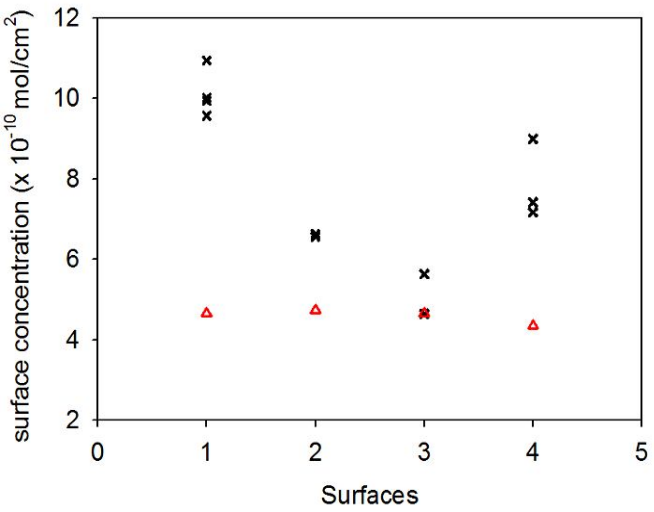

Figure 4.4. Plots of surface concentration of electroactive NP groups coupled to reduced NP films by reaction with Δ: NBA and x: NBCl. Initial NP films where reduced in: (1) H_2SO_4; (2) $EtOH/H_2O$; (3) BA/ACN and (4) Na_2S.

Despite the limitations of determining surface concentration from NP moiety using curve-fitting (described above), comparisons between films and coupling methods can be made. The different behaviours of the films to the two coupling procedures can be attributed to the different reaction environments. For aqueous reactions with NBA, the relatively low yields suggest that coupling occurs in the outer layer(s) of the films only, whereas the higher coupling yields obtained for reactions with NBCl in DCM may indicate coupling within the multilayer films. Steric constraints associated with the activated carboxylic acid-NHS complex, and/or film shrinkage and compaction in the aqueous medium may account for the restriction of the reaction to the outer film surface. As noted earlier, all reduced films exhibited the same water contact angles. This indicates that all films have a similar composition at their outer surface and hence it is unsurprising that their reactivity towards amide bond formation reactions at the outer layers is similar. The same steric constraints did not appear to restrict reaction with NBCl in DCM indicating that the functional groups within the films may be more accessible in this medium. Unlike well-organized self-assembled monolayers of alkane thiols assembled on gold surfaces, the branching growth of these diazonium ion-derived multilayered films result in loose packing of modifier groups and a free-volume of up to approximately 53 % (see later in Section 4.3.6).[6,31] The loosely-packed structure appears to give dynamic mechanical properties to the films and enables the films to respond to their environment. In several studies of films grafted to carbon and gold surfaces by reduction of aryldiazonium salts and oxidation of amines, it show that exposing organic thin films to different solvents and applied potentials leads to easily measurable changes in film properties such as thickness, water contact angle and blocking properties towards solution redox probes.[36,37] The present findings in this chapter, which indicate that different film structures result from different reduction treatments, is another example of surface films responding to their environment.

4.3.3 Assembly of gold nanoparticles at reduced NP films

Dense layers of citrate-capped gold nanoparticles have been reported to assemble to protonated amine-terminating layers on surfaces, such as gold and silicon, from self-assembled layers of aminothiophenol groups and AP-terminated silane, respectively.[18,38,39] Hence it was of interest to assemble anionic gold nanoparticles to AP layers derived from the reduction of NP

film. A significant amount of AP groups (pK_a of aniline is 4.6) are expected to be protonated when the reduced surfaces are incubated in gold nanoparticle solution, which has a pH 4.2 and citrate-capped gold nanoparticles are expected to assemble on the modified surface.[40] PPF was employed as the substrate since it is a smooth surface (surface roughness ~ 0.6 nm or less) that can prevent accumulation of nanoparticles in pits and scratches. NP films were prepared at PPF and subsequently reduced using standard chemical and electrochemical reduction methods (Section 4.1.2) and incubated with gold nanoparticle solution for 1 h. Particle-count analysis of SEM images of gold nanoparticle assemblies on each reduced surface was carried out to determine the density of the assemblies. Table 4.2 lists the average nanoparticle densities (np μm^{-2}) on NP films reduced by standard methods. The table also includes data for gold nanoparticle assembles on NP films electrochemically reduced in 20 mM benzoic acid in aqueous 0.1 M KCl and 20 mM naphthalene acetic acid in acetonitrile-electrolyte. The NP films reduced in nonaqueous conditions with benzoic acid and naphthalene acetic acid show the expected interaction with nanoparticles to form dense gold assemblies (Figure 4.5) whereas surprisingly, there is only adventitious, nonspecific adsorption at the surfaces reduced in aqueous conditions. As-formed NP films prepared in acetonitrile did not specifically assembly gold nanoparticles in the absence of favourable electrostatic interactions.

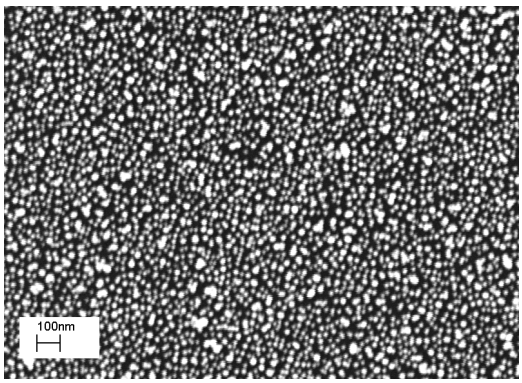

Figure 4.5. SEM image of a BA/ACN reduced NP film grafted to PPF after incubation in a solution of citrate-capped gold nanoparticles.

Table 4.2. Density of gold nanoparticle assembly on reduced NP films grafted to PPF.

	NP film reduction method						
	none	H_2SO_4	EtOH/H_2O	BA/ACN	Na_2S	BA/aq[a]	NA/ACN[b]
nanoparticle density (np/μm^2)	47	10	44	1175 ± 150 (n = 2)	33	50 ± 3 (n = 2)	590

[a] electroreduction in 20 mM benzoic acid in aqueous 0.1 M KCl; [b] electroreduction in 20 mM naphthalene acetic acid in acetonitrile-electrolyte.

In an attempt to understand the factors that effect gold nanoparticle assembly, experiments were repeated on all the reduced films after adding HCl to the nanoparticle solution to lower the pH to 2, however no increases in nanoparticle assembly were observed. In another set of experiments, NP films that had been reduced in BA/ACN were subsequently transferred to 0.25 M H_2SO_4 and scanned four times within the potential limits used to reduce films in that medium. The treated films were incubated in as-prepared gold nanoparticle solution however the surfaces did not assemble nanoparticles indicating that treatment in aqueous acid changed the film to markedly decrease the number of favourable electrostatic interactions. Conversely, a NP film that had been reduced in 0.25 M H_2SO_4 and subsequently treated to the electrochemical reduction conditions in BA/ACN did not assemble nanoparticles. The results for the variable assembly of gold nanoparticles on reduced films are not understood. A permanent change may take effect in the structure of NP films after treatment in aqueous conditions, which may result in the non-assembly of gold nanoparticles. What this change might be is not clear at present. These intriguing results highlight another example of complex film behaviour arising from the multilayer structure.

4.3.4 XPS characterization of NP films before and after reduction: survey spectra.

XPS was employed to monitor the NP films electrografted to GC surfaces and reduced by the different procedures. XPS spectra were obtained by Dr. Byrony James at University of Auckland. Peak fits to narrow scans were also performed by Dr. James. Survey spectra (not shown) were obtained for at least two samples of each type, giving the data shown in Table 4.3. Table 4.3 shows good reproducibility for each type of sample, confirming reproducible preparation and handling of samples.

As expected, the % N at the NP-grafted surfaces (samples 1-4) is significantly greater than at bare GC (sample 16) and there is an increase in % O consistent with the grafting of a NP film. The N:C ratio is less than predicted for a NP film which is attributed to a large contribution from the underlying GC surface to the C peak. The N:O ratio (~ 1:1.5) is also less than the expected ratio of (1:2) for a NP film suggesting that some N atoms in the film are associated with only one O atom, or none. This is consistent with the presence of reduced N species in the film (see below). The atomic % of each element is similar for all reduced samples after treatment using different reduction methods (samples 5 - 15). There is an increase in the atomic % C and a decrease in N and O, however the O:N ratio of the reduced films is significantly greater than expected, even when the contribution of surface O is considered. A decrease in the atomic % N after reduction has been reported previously for NP films and was proposed to be from the cleavage of some grafted film from the surface.[8] However, the origin of the decrease in atomic % N and the high O:N ratio observed in the present work is not entirely clear. AP groups formed on gold surfaces by the reduction of a 4-nitrothiophenol monolayer[41] and by electroreduction of the aminobenzene diazonium ion[33] have been suggested to interact with atmospheric carbon dioxide and water giving carbonate anions (CO_3^{2-} and/or HCO_3^-). The involvement of carbonate anions is also consistent with recent observations of an increase in O signal after modification of GC with ethylenediamine.[36] These counter-anion species would increase the measured atomic % C and O and decrease that of N, as observed for the reduced films here. Other factors such as shrinkage of films during reduction may contribute to the relatively high C signal in the reduced films as more of the carbon substrate will be sampled. The decrease in film height of NP films after electroreduction in H_2SO_4 determined by AFM[31] (Section 4.3.6), is consistent with the decrease in N and increase in C signal arising from a greater contribution of C from the GC surface at the thinner film. Hence, the unexpected XPS signal intensities for samples 5-15 is tentatively attributed to the incorporation of species derived from atmospheric carbon dioxide and water, with a contribution from film shrinkage.

Table 4.3. Normalized atomic % of N, O and C obtained from XPS core level spectra for NP films grafted to GC.

		atomic %		
NP film reduction method	sample	N	O	C
none	1	8.28	13.19	78.53
none	2	9.03	12.27	78.70
none	3	8.75	14.79	76.46
none [a]	4	6.74	14.39	78.87
H_2SO_4	5	6.33	10.62	83.04
H_2SO_4 [b]	6	6.54	11.24	82.23
EtOH/H_2O	7	4.83	10.05	85.13
EtOH/H_2O [c]	8	5.23	10.39	84.38
BA/ACN	9	6.67	10.47	82.85
BA/ACN	10	6.75	11.86	81.39
Na_2S	11	4.61	10.30	85.09
Na_2S	12	5.63	10.01	84.36
H_2SO_4 and reacted with FBCl	13	5.56	10.80	83.64
Na_2S and reacted with FBCl	14	5.10	11.43	83.47
Na_2S and reacted with FBCl	15	6.50	10.01	83.49
Polished GC blank [d]	16	1.85	9.26	88.89

[a] grafted using $E_{app} = E_{p,c} + 150$ mV for 900 s
[b] one standard scan followed by electrolysis at -1.4 V for 1 h
[c] two cycles between -0.6 and -1.4 V
[d] GC cycled six times between 0 and - 1.2 V at 100 mV s^{-1}, in blank acetonitrile-electrolyte solution

4.3.5 XPS characterization of NP films before and after reduction: N 1s spectra.

Closer examination with high resolution XPS was made for N spectra. Peaks could be fitted to the observed XPS signals to elucidate the components contributing to the overall N signal. Figure 4.6 shows typical N 1s core level spectra and the peak-fittings for an as-prepared NP film (a) and for films reduced by each standard method (b - e). In addition, XPS spectra for films reacted with 4-fluorobenzoyl chloride (FBCl) after reduction in H_2SO_4 (f) and with Na_2S (g) are also shown in Figure 4.6. The data obtained for all samples, after peak fitting, are presented in the bar graph shown in Figure 4.7.

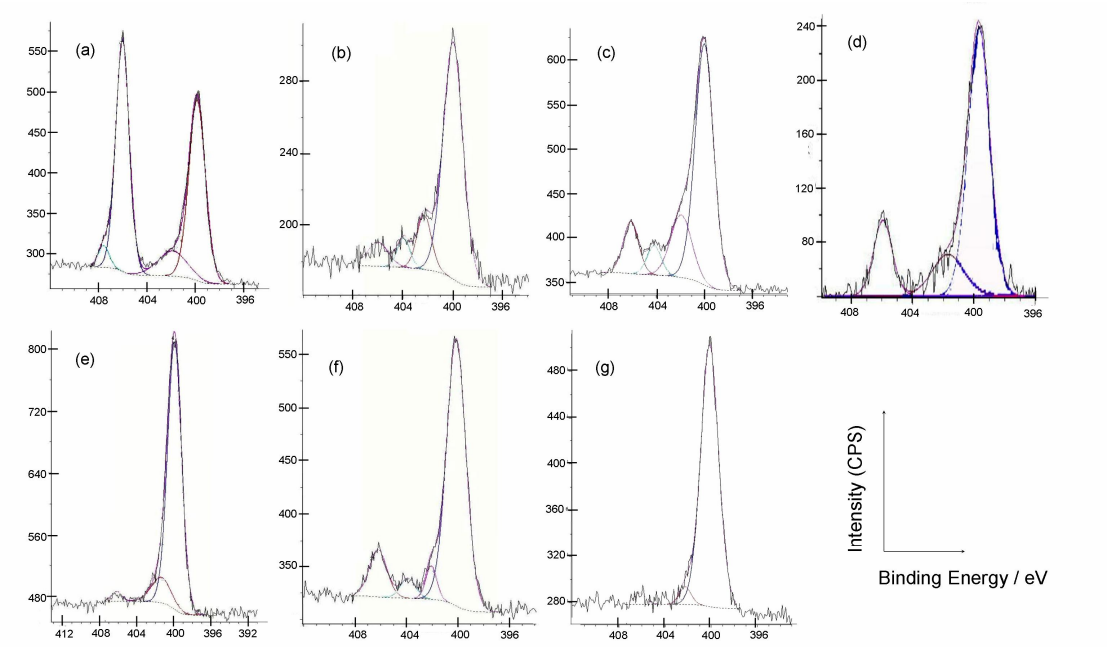

Figure 4.6. XPS N 1s core level spectra of NP-modified GC: (a) as-prepared (b-g) reduced in (b) H_2SO_4, (c) EtOH/H_2O, (d) BA/ACN, (e) Na_2S, (f) H_2SO_4 followed by reaction with FBCl and (g) Na_2S followed by reaction with FBCl.

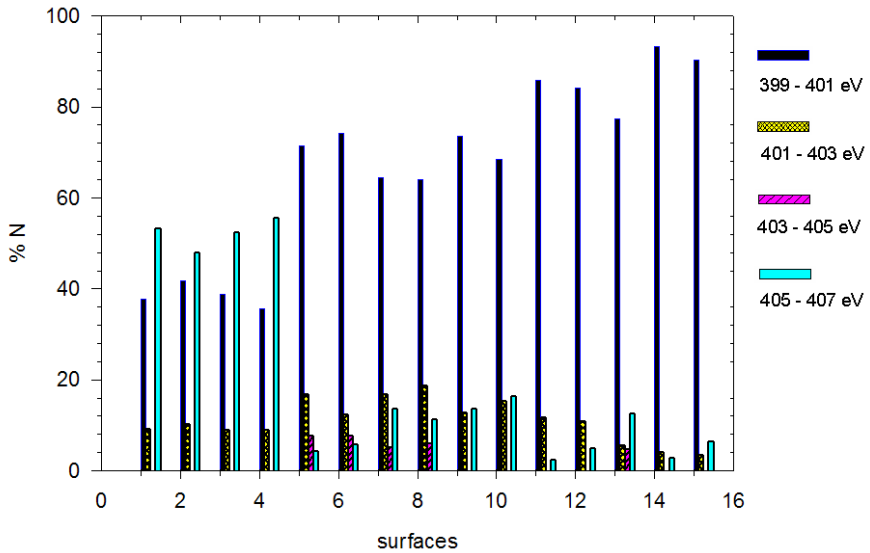

Figure 4.7. Atomic % of N calculated from XPS N 1s core level spectra for NP-modified GC. 1-3: as-prepared; 4: as-prepared, grafted using $E_{app} = E_{p,c} + 150$ mV for 900 s; 5: reduced in H_2SO_4; 6: reduced in H_2SO_4 at $E_{app} =$ -1.4 V for 1 h; 7: reduced in EtOH/H_2O; 8: reduced in EtOH/H_2O by two cycles between -0.6 and -1.4 V; 9-10: reduced in BA/ACN; 11-12: reduced with Na_2S; 13: reduced in H_2SO_4 and reacted with FBCl; and 14-15: reduction with Na_2S and reacted with FBCl.

Figure 4.6a shows that the N 1s region of as-prepared NP films can be well-fitted with two main peaks at 406.0 and 399.9 eV, and two small peaks at 401.9 and 407.6 eV. The major peaks have been reported many times in the literature and are assigned to the nitro group and a reduced N species, respectively. A peak at 407 eV has been observed in the XPS spectra of NP groups assembled on an aminosilane layer on silicon and, along with a 400 eV peak, was attributed to the nitro group.[42] However, the origin of two peaks for the nitro moiety is not clear. The peak at 401.9 eV is discussed below. Several explanations have been proposed accounting for the reduced N peak observed at 399.9 eV. Reports in literature describe the reduction of NP groups to AP groups during XPS analysis. However the reported conversion rate is variable, possibly depending on the substrate. Thus Adenier and coworkers found significant conversion of the 406 eV peak to the 400 eV peak over 120 scans for a NP film grafted to Zn[26], whereas for a 4'-nitro-1,1-biphenyl film on ultrananocrystalline diamond, Lud and coworkers observed that the peak at 400 eV increased from 20 to 85% of total N over 753 min.[43] For 3-(4-nitrophenoxy)-propyltrimethoxysilane (NPPTMS) on silicon, conversion of nitro to amine was almost complete after 447 min of continuous exposure to X-ray irradiation.[44] Hence, to examine whether nitro-reduction occurs during XPS analysis in the present work, the 406 eV peak of a NP film was monitored over two timescales during XPS measurements. Figure 4.8a shows the data obtained in snapshot mode for data collected over a 1 s scan. However, it should be noted that the sample is exposed to irradiation for 10 s per scan, giving a total exposure time of 20 min after 120 scans. The data in Figure 4.8b were obtained with 60 s acquisition time with the NP film exposed to the X-rays for approximately 3.5 min per scan, giving a total exposure time of nearly 6 h. The data in Figure 4.8 were fitted with a line of best fit. The line in Figure 4.8a, has a slope of 0.0054 atomic % per scan, strongly supporting that there is no change in signal intensity over the first 20 min of X-ray exposure. For the longer timescale measurement in Figure 4.8b, the slope is -0.046 atomic % per scan corresponding to a very small decrease in the 406 eV peak over 6 h. Considering that the XPS data of Figures 5 and 6 were obtained with a total X-ray exposure time of approximately 2 h, it is clear that the peak observed ca. 400 eV in samples 1- 4 (Figure 4.7) cannot arise from reduction of NP groups during XPS analysis.

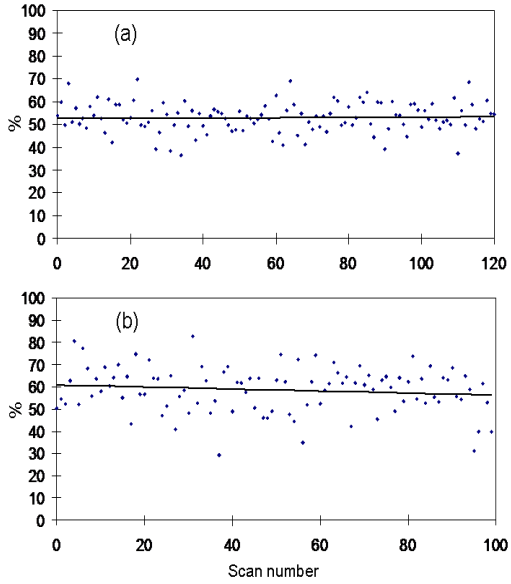

Figure 4.8. Plot of atomic % of N associated with peak at ca. 406 eV calculated from XPS N 1s core signal of NP-modified GC *vs* number of scans. (a) 10 s exposure to X-rays per scan, trendline: y = 0.0054x + 53, and (b) 3.5 min exposure to X-rays per scan, trendline: y = -0.046x + 61.

If reduced N species are present in the as-prepared NP film, another possibility is that NP groups are reduced to AP groups during film grafting. To explore this possibility, a NP film was prepared using an applied potential 300 mV less negative than the standard grafting potential (i.e. 150 mV more positive than the NP reduction peak potential). Surface 4 in Figure 4.7 shows the XPS results for that sample. Comparing surface 4 (grafted at the less negative potential) with surfaces 1-3 (grafted using the standard procedure), shows that for surface 4, the reduced N (ca. 400 eV) accounts for a slightly smaller % of the total N signal than for the other NP films. However this difference is insignificant compared with the total atomic % of reduced N, confirming that reduction of NP during grafting is not a major factor. Importantly, this is consistent with the electrochemical results which show that there are no electrooxidizable AP groups in the as-formed NP films (Figure 4.2e). (Note however, the low background current of the voltammogram of the NP film between 0 and 1.1 V in 0.25 M H_2SO_4 (Figure 4.2e), scan 2) compared with those of the reduced films in Figures 4.2a-d), which reveal that ion and solvent penetration into the as-prepared NP film is limited. Hence the possibility of a low concentration of reduced N sites that are electroinactive within the bulk film structure cannot be discounted.)

Considering that the reduced N species are unlikely to be amines introduced during grafting or XPS analysis, the major contributor to the reduced N peak obtained from as-formed NP films is most likely azo groups arising from the diazonium moiety. In homogeneous solution, azobenzene moieties are electroactive however, it has been demonstrated that the azo groups in nitroazobenzene multilayered films are electroinactive.[6] As described previously in Chapters 1 and 3, several workers have proposed possible pathways for formation of azo linkages in multilayered films derived from diazonium ions. Shortly after completion of the present work, Pinson and coworkers proposed the reactions shown in Scheme 1.1. This scheme shows that azo linkages are formed when diazonium ion-modifiers attack at a radical site on the grafted film during film growth.[28,29,45] The 400 : 406 eV peak ratio for as-prepared NP films (Figure 4.7, surfaces 1-3) suggests that there is approximately one azo linkage per NP-modifier grafted at the surface.

Examining the XPS data for reduced NP films reveals significant decrease of the nitro peak at 406 eV is observed after reduction of NP films. Comparing the spectra obtained after reduction by the various methods (Figure 4.6b-e) and the data of Figure 4.7, it is clear that chemical reduction with Na_2S gives the lowest residual nitro content (2.4 and 4.9 % of total N for Surfaces 11 and 12) and the cleanest conversion to reduced N species at ca. 400 eV. The peak at ca. 400 eV is also consistent with the assignment to azo groups initially present in the film and to AP groups formed by electrochemical or chemical reduction. Assuming the azo content of all films is the same, the % N present as AP groups depends on the reduction method, and it decreases in the order $Na_2S > H_2SO_4 \approx$ BA/ACN > EtOH/H_2O. For reduced films, the peak near 402 eV is assigned to both APOH and/or nitrosophenyl groups and to protonated AP groups.[29,46-48] As discussed above, results from survey spectra suggest the presence of anions derived from the atmosphere (CO_3^{2-} and/or HCO_3^-) in the reduced films and hence protonated AP groups are also expected to be present. However, the magnitude of the signal at ca. 402 eV does not follow the same trend as that of the AP signal at ca. 400 eV indicating there is a second species contributing to this signal. Formation of APOH /nitrosophenyl moieties is indicated in the voltammograms of the reduced films and is consistent with the observed binding energy. The APOH /nitrosophenyl species may also be present in the initial as-formed films contributing to the signal at ca. 402 eV. At very mild negative potentials (for example, -50 mV *vs* SCE in 50 mM H_2SO_4), reduction of 4-nitrothiophenol films was shown to give the corresponding NHOH

derivative[41,49] and hence it is reasonable to propose the formation of a small amount of the same species during electrografting of NP films from ACN solution, with a low concentration of residual water. These groups can be electroinactive inside the as-prepared NP films. Inspection of Figure 4.6c, d and data sets 7-10 in Figure 4.7 reveals that films electroreduced in H_2SO_4 and $EtOH/H_2O$ also have a distinct peak at ca. 404 eV. This peak is not present in the films reduced electrochemically in BA/ACN and chemically by Na_2S, nor in as-prepared NP films. Examination of the film electrochemical data and the observed reactivity of the films towards amide bond formation did not reveal any insight into the nature or the origin of the species giving rise to this signal. Notably, the signal appears in the same binding energy region as a shakeup peak arising from aminobenzene moieties observed at electrografted NP films on Si surfaces.[50] The 402 eV peak observed in the spectra in this work may be attributed to this aminobenzene species. However, the reason for the presence of the 402 eV peak in NP films reduced electrochemically in aqueous conditions is not understood. Reaction of 4-fluorobenzoyl chloride (FBCl) with films reduced in H_2SO_4 and with Na_2S, gives the spectra shown in Figures 4.5f-g and data sets 13 -15 in Figure 4.7. The relative size of the peak at ca. 400 eV increases and that at ca. 402 eV decreases after reaction. The 400 eV peak is assigned to amide N and also to unreacted amine and azo functionalities. FBCl is expected to react with both amino and APOH functionalities forming an amide bond and hence the changes in the spectra are consistent with the assignment of the 402 eV peak to APOH /nitrosophenyl and protonated AP moieties. Monitoring the F signal of FBCl-coupled reduced surfaces was not useful. The F signals were weak and varied apparently randomly. It has previously been noted that F-containing phenyl films gave very weak F signals.[51] This is not understood but may be a result of F atoms becoming labile upon exposure to XPS beam.

Comparing the electrochemical and XPS results the following general points can be made:

- the relative amounts of AP species determined by electrochemical and XPS are different to each other. For example, XPS analysis showed that $EtOH/H_2O$-reduction gave the least amount of AP groups whilst electrochemical analysis revealed that reduction in $EtOH/H_2O$ gave the highest amount of AP groups.

- XPS is able to detect nonelectroactive species in the as-prepared and reduced NP films that electrochemistry cannot otherwise identify their presence. For example, XPS analysis identifies the presence of azo- species in as-prepared NP films and residual NP species in the reduced films however electrochemistry did not detect their presence.

4.3.6 $Fe(CN)_6^{3-}$ redox probe voltammetry at, and AFM depth profiling of, NP films before and after electroreduction and potential excursions

Monitoring of NP films before and after electroreduction in H_2SO_4 was carried out with redox probe voltammetry. The effects of the electrochemical polarization step in aqueous and nonaqueous environments on film properties were also explored. As described previously in Chapter 3, as-formed NP films have a strong electron-transfer resistance in $Fe(CN)_6^{3-}$ redox probe voltammetry, evident in Figure 4.9a) scan (i) here. Figure 4.9a also shows the voltammetric response of $Fe(CN)_6^{3-}$ at a polished GC for comparison (scan ii). After standard electroreduction in H_2SO_4, the reduced surface was ultrasonicated in Milli-Q water for 3 min and re-examined in $Fe(CN)_6^{3-}$ probe solution. The voltammetric response of the reduced surface (Figure 4.9b) shows that the apparent rate of electron-transfer of $Fe(CN)_6^{3-}$ is markedly increased after reduction of the NP moiety. Scans to negative potentials and/or reduction of the NP film must generate an interface that allow $Fe(CN)_6^{3-}$ to undergo more rapid electron-transfer at the modified electrode. Several explanations may account for the voltammetric changes. One obvious possibility is desorption or the creation of pinholes in the film. This possibility was investigated in further experiments (below).

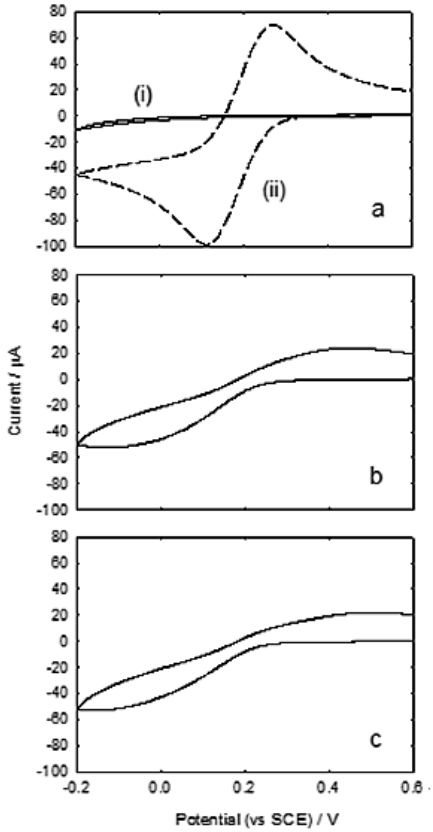

Figure 4.9. Cyclic voltammograms obtained in 4.5 mM $K_3Fe(CN)_6$ + 0.1 M KCl for a GC electrode (a) (scan i) grafted with a NP film using standard procedure; (scan ii) at polished GC; (b) NP film-modified GC after standard electroreduction in H_2SO_4; (c) after holding the potential at $E_{app} = E_{p,c} - 150$ mV for 600 s in acetonitrile-electrolye solution.

The reversibility of the system was investigated by returning the reduced surface into acetonitrile-electrolyte solution, in the absence of aryldiazonium ions, and treatment to the film formation conditions, i.e. applied potential of $E_{app} = E_{p,c} - 150$ mV for 600 s. The modified electrode was then returned to $Fe(CN)_6^{3-}$ solution for probing. Figure 4.9c shows the $Fe(CN)_6^{3-}$ voltammetry of the surface after voltammetry in acetonitrile. Comparing Figures 4.9a)i) and 4.9b), reveal that there is only slight changes in the cyclic voltammograms, which suggests that the barrier properties of film remain largely unchanged after scans to negative potentials in acetonitrile-electrolyte solution. Clearly, the increase in the apparent rate of electron-transfer across the modified electrode after reduction cannot be attributed solely to solvent effects.

AFM depth profiling experiments were carried out on NP films grafted to PPF before and

after standard electrochemical reduction in H_2SO_4. Table 4.4 shows the film thickness measured at each individual film before and after electroreduction. Comparing the film heights before and after electrochemical reduction in H_2SO_4, the data shows a decrease in the average film thickness for all reduced NP films. The thickness decrease ranges from 11 to 53 % and does not appear to depend on whether the initial film is relatively thick or thin.

Table 4.4. Film thickness data for NP films electrografted to PPF, derived from 0.6 mM and 5 mM diazonium salt modifying solutions using the listed electrolysis times, before and after two standard electroreduction cycles in 0.25 M H_2SO_4.

electrolysis time	as-formed film thickness	film thickness after reduction in H_2SO_4	thickness difference
s	nm	nm	%
10[a]	2.6	1.7	35
10[a]	2.4	1.1	53
30[a]	3.3	1.7	47
60[a]	2.7	2.3	15
120[a]	3.0	2.1	30
300[a]	3.9	2.4	38
300[a]	4.0	1.9	53
30[b]	3.5	2.5	29
60[b]	3.7	3.3	11
120[b]	3.4	2.0	39
120[b]	3.2	1.7	46
180[b]	3.5	2.5	29
180[b]	3.7	3.3	11
300[b]	3.7	3.0	20
300[b]	3.5	2.5	29
300[b]	3.7	3.3	11
600[b]	3.5	2.5	29
600[b]	3.7	3.3	11

[a] Prepared in 0.6 mM 4-NB diazonium salt modifying solution. [b] Prepared in 5 mM 4-NB diazonium salt modifying solution.

The observed decrease in average film height may be attributed to two possible factors: 1) the loss of material from the film; and/or 2) film shrinkage. The former would give an irreversible change in film thickness whilst the latter might be expected to be a reversible effect. Hence to investigate the reversibility of the film changes, a 4.1 nm NP film was electroreduced in H_2SO_4 to give a film thickness of 2.9 nm. The film was returned to acetonitrile-electrolyte solution (in the absence of modifier) and the potential used for film preparation, i.e. $E_{app} = E_{p,c} - 150$ mV, was re-applied for 600 s. Re-examination with AFM revealed that the film thickness of the film was now 3.8 nm returned close to its initial as-formed thickness (Table 4.5). The reversible

shrinking and swelling of the films from 4.1 nm to 2.9 nm and back to 3.8 nm demonstrates that there is no large-scale loss of film during reduction. No large pinholes or bare electrode areas were detected by AFM. Correlating the AFM results here with the results of probe voltammetry (Figure 4.9b, c), highlights that the changes in $Fe(CN)_6^{3-}$ voltammetry appear to be unrelated to the physical changes in film thickness. Reversible changes in film thickness of ~ 25 % indicate that there are corresponding amounts of free volume in the as-prepared films, consistent with a loosely packed film structure. The reversible swelling and shrinking processes are similar to those recently reported for nitroazobenzene films.[6] For the nitroazobenzene films, the changes in film thickness (> 50 %) were suggested to be due to potential-induced penetration of ions and solvent. This is also likely for NP films where entrapped ions and solvents can move in and out of the loosely packed multilayered film in different solvent environments, a process which is likely to be influenced by potential cycling.

Table 4.5. AFM film thickness data for a NP film electrografted to PPF after various treatments. Treatments were applied as shown in descending order in the table.

NP film treatment	conditions	applied potential, Time V , s	thickness nm
as-prepared film	-	-	4.1
acid reduction	0.25 M H_2SO_4	0.7 V to -1.3 V, 2 scans	2.9
film formation conditions	acetonitrile[a]	-0.3 V , 600 s	3.8
positive polarization	acetonitrile[a]	1.5 V , 600s	3.6

[a] Treated in the presence of 0.1 M $TBABF_4$ supporting electrolyte.

The solubility and swelling of polymers in solvents can be predicted by comparing solubility parameters. Solubility parameters (δ) describe the degree of interaction between materials and can provide a good indication of solubility. Materials with a similar solubility parameter value will be able to interact with each other resulting in solvation, miscibility or swelling. Hence it is reasonable to predict film behaviour using these values. Assuming a simple model that polyphenylene diazonium ion-derived films have a 'polystyrene-like' structure (δ ~ 9 $cal^{1/2}$ $cm^{3/2}$), the film is predicted to swell and interact favourably with acetonitrile (δ ~ 12 $cal^{1/2}$ $cm^{3/2}$) and less favourably with water (δ ~ 24 $cal^{1/2}$ $cm^{3/2}$).[52] These predictions are also consistent with AFM film thickness results (above).

The examination of reduced films with a combination of AFM and redox probe voltammetry as described above reveals electroreduction induces changes in the film that promote electron-transfer to solution-based redox probe. These changes cannot be reversed in blocking properties. The combination of results has shown that the major factor contributing to the changes in blocking properties of the film is unrelated to large scale loss of film material or film swelling and compacting effects. The results may be due to changes in electrostatic or hydrophilic interactions between the redox probe and the film. Furthermore, similar changes in the volatmmetric response of redox probes at aryldiazonium ion-derived film-modified GC after polarization to negative potentials have been observed by other workers, which they have attributed to potential-induced changes in the electronic properties of the film-modified surface *via* a conductance switching mechanism (Chapter 1).[53,54] These effects cannot be discounted for the film prepared in this work however further experiments, for example using a neutral or cationic redox probe, are needed to gain a better understanding of the observed film behaviour.

4.3 Conclusions

Electrochemical analysis of reduced NP films demonstrates that electro- and chemical reduction give AP as the main product. The AP product generated from the reduction processes was directly detected by voltammetry. However, this chapter also highlights the limitations of electrochemical estimation of surface concentrations, and interpretations should be applied with caution. Voltammetric and XPS investigations both show that reduction with ethanolic Na_2S is a simple and effective reduction procedure that gives the cleanest conversion to AP groups. XPS establishes that electroinactive azo and APOH/nitrosophenyl species are present in NP films and also, unreacted NP groups are present in the film after reduction treatments. Chemical reduction leaves the smallest percentage of unreacted NP groups, while reduction in BA/ACN, the largest. Despite these differences in reduction yields, when the reduced films are reacted with NBA in aqueous conditions, the yield of coupled product appears to be the same for all films. Results are consistent with coupling reactions taking place only in the outer part of the film, probably due to steric constraints. Higher yields are found when reduced films are reacted with NBCl in DCM and are consistent with coupling within the films. Under those conditions, films reduced in BA/ACN give the lowest yield of electroactive product and those reduced in H_2SO_4 the highest.

The opposite effect is observed for electrostatic assembly of citrate-capped gold nanoparticles, with the highest particle-count at BA/ACN reduced films, and no assembly at H_2SO_4- and EtOH/H_2O-reduced surfaces. The observations suggest that the structures of the reduced films can be subtly affected by the medium in which they are prepared and that structure influences film properties. Voltammetric monitoring of the reaction of NBCl with the reduced films reveals that the decrease in concentration of AP and APOH groups is not matched by the appearance of an equal concentration of coupled product, emphasizing that electroactivity of groups within the film is affected by the film environment. Electrochemical analysis shows that as-prepared NP films do not incorporate detectable amounts of electrooxidizable groups however XPS analysis shows that a low concentration of APOH/nitrosophenyl groups is generated during grafting. Furthermore, the reduced N XPS signal ca. 400 eV is assigned to azo groups, which are known to be electroinactive in the film environment.

AFM and electrochemical analysis show that NP films remain largely, if not completely, intact after electroreduction in H_2SO_4 despite some changes to film properties. Further work is needed to elucidate the origins of the induced changes to blocking properties of the film. AFM analysis established reversible film thickness changes during polarization, which is attributed to swelling and shrinking of the film.

In summary, NP films are loosely packed and exhibit complex film behaviour. However, they are robust and useful precursor to AP groups for coupling reactions. Conditions used to reduce NP groups can have a significant influence on the resultant reactivity of the film.

4.5 References

(1) Bard, A.; Lund, H. *Encyclopedia of Electrochemistry of the Elements (Organic Section)*; Dekker, 1973; Vol. XIII.

(2) Ono, N. *The Nitro Group in Organic Synthesis*; John Wiley & Sons, Inc., 2001.

(3) Huber, D.; Andermann, G.; Leclerc, G. *Tetrahedron Letters* **1988**, *29*, 635.

(4) Hartman, W.; Silloway, H. *Organic Syntheses* **1955**, *3*, 82.

(5) Brooksby, P. A.; Downard, A. J. *Langmuir* **2004**, *20*, 5038.

(6) Brooksby, P. A.; Downard, A. J. *Journal of Physical Chemistry B* **2005**, *109*, 8791.

(7) Saby, C.; Ortiz, B.; Champagne, G. Y.; Belanger, D. *Langmuir* **1997**, *13*, 6805.

(8) Ortiz, B.; Saby, C.; Champagne, G. Y.; Belanger, D. *Journal of Electroanalytical Chemistry* **1998**, *455*, 75.

(9) Ruffien, A.; Dequaire, M.; Brossier, P. *Chemical Communications* **2003**, 912.

(10) Vakurov, A.; Simpson, C. E.; Daly, C. L.; Gibson, T. D.; Millner, P. A. *Biosensors & Bioelectronics* **2004**, *20*, 1118.

(11) Delamar, M.; Hitmi, R.; Pinson, J.; Saveant, J. M. *Journal of American Chemical Society* **1992**, *114*, 5883.

(12) Allongue, P.; Delamar, M.; Desbat, B.; Fagebaume, O.; Hitmi, R.; Pinson, J.; Saveant, J.-M. *Journal of American Chemical Society* **1997**, *119*, 201.

(13) Liu, Y.-C.; McCreery, R. L. *Journal of American Chemical Society* **1995**, *117*, 11254.

(14) Wang, J.; Firestone, M. A.; Auciello, O.; Carlisle, J. A. *Langmuir* **2004**, *20*, 11450.

(15) Nassef, H. M.; Radi, A. E.; O'Sullivan, C. K. *Electrochemistry Communications* **2006**, *8*, 1719.

(16) Nassef, H. M.; Radi, A. E.; O'Sullivan, C. K. *Journal of Electroanalytical Chemistry* **2006**, *592*, 139.

(17) Wildgoose, G. G.; Leventis, H. C.; Davies, I. J.; Crossley, A.; Lawrence, N. S.; Jiang, L.; Jones, T. G. J.; Compton, R. G. *Journal of Materials Chemistry* **2005**, *15*, 2375.

(18) Kim, K.; Lee, I. *Langmuir* **2004**, *20*, 7351.

(19) Kim, K.; Lee, I.; Lee, S. *Chemical Physics Letter* **2003**, *377*, 201.

(20) Bath, B. D.; Martin, H. B.; Wightman, R. M.; Anderson, M. R. *Langmuir* **2001**, *17*, 7032.

(21) Delamar, M.; Desarmot, G.; Fagebaume, O.; Hitmi, R.; Pinson, J.; Saveant, J. M. *Carbon* **1997**, *35*, 801.

(22) Ge, F. Y.; Tenent, R. C.; Wipf, D. O. *Analytical Sciences* **2001**, *17*, 27.

(23) Yang, W.; Baker, S. E.; Butler, J. E.; Lee, C. s.; Russell, J. N.; Shang, L.; Sun, B.; Hamers, R. J. *Chemistry of Materials* **2005**, *17*, 938.

(24) Wang, J.; Carlisle, J. A. *Diamond and Related Materials* **2006**, *15*, 279.

(25) Shin, D. C.; Tokuda, N.; Rezek, B.; Nebel, C. E. *Electrochemistry Communications* **2006**, *8*, 844.

(26) Adenier, A.; Cabet-Deliry, E.; Chausse, A.; Griveau, S.; Mercier, F.; Pinson, J.; Vautrin-Ul, C. *Chemistry of Materials* **2005**, *17*, 491.

(27) Combellas, C.; Delamar, M.; Kanoufi, F.; Pinson, J.; Podvorica, F. I. *Chemistry of Materials* **2005**, *17*, 3968.

(28) Doppelt, P.; Hallais, G.; Pinson, J.; Podvorica, F.; Verneyre, S. *Chemistry of Materials* **2007**, *19*, 4570.

(29) D'Amours, M.; Belanger, D. *Journal of Physical Chemistry B* **2003**, *107*, 4811.

(30) Hurley, B. L.; McCreery, R. L. *Journal of the Electrochemical Society* **2004**, *151*, B252.

(31) Yu, S. S. C.; Downard, A. J. *e-Journal of Surface Science and Nanotechnology* **2005**, *3*, 294.

(32) Rubinstein, I. *Journal of Electroanalytical Chemistry* **1985**, *183*, 379.

(33) Lyskawa, J.; Belanger, D. *Chemistry of Materials* **2006**, *18*, 4755.

(34) Downard, A. J. *Langmuir* **2000**, *16*, 9680.

(35) *Organic electrochemistry : an introduction and guide* 3rd ed.; Lund, H.; Baizer, M. M., Eds.; Marcel Dekker: New York 1991.

(36) Cruickshank, A. C.; Tan, E. S. Q.; Brooksby, P. A.; Downard, A. J. *Electrochemistry Communications* **2007**, *9*, 1456.

(37) Paulik, M. G.; Brooksby, P. A.; Abell, A. D.; Downard, A. J. *Journal of Physical Chemistry C* **2007**, *111*, 7808.

(38) Zhu, T.; Fu, X.; Mu, T.; Wang, J.; Liu, Z. *Langmuir* **1999**, *15*, 5197.

(39) Mendes, P. M.; Jacke, S.; Critchley, K.; Plaza, J.; Chen, Y.; Nikitin, K.; Palmer, R. E.; Preece, J. A.; Evans, S. D.; Fitzmaurice, D. *Langmuir* **2004**, *20*, 3766.

(40) Downard, A. J.; Tan, E. S. Q.; Yu, S. S. C. *New Journal of Chemistry* **2006**, *30*, 1283.

(41) Tsutsumi, H.; Furumoto, S.; Morita, M.; Matsuda, Y. *Journal of Colloid and Interface Science* **1995**, *171*, 505.

(42) Moon, J. H.; Kim, J. H.; Kim, K.; Kang, T. H.; Kim, B.; Kim, C. H.; Hahn, J. H.; Park, J. W. *Langmuir* **1997**, *13*, 4305.

(43) Lud, S. Q.; Steenackers, M.; Jordan, R.; Bruno, P.; Gruen, D. M.; Feulner, P.; Garrido, J. A.; Stutzmann, M. *Journal of the American Chemical Society* **2006**, *128*, 16884.

(44) Mendes, P.; Belloni, M.; Ashworth, M.; Hardy, C.; Nikitin, K.; Fitzmaurice, D.; Critchley, K.; Evans, S.; Preece, J. *Chemphyschem* **2003**, *4*, 884.

(45) Hurley, B. L.; McCreery, R. L. *Journal of the Electrochemical Society* **2003**, *150*, B367.

(46) Saito, N.; Maeda, N.; Sugimura, H.; Takai, O. *Langmuir* **2004**, *20*, 5182.

(47) Rosario-Castro, B. I.; Fachini, E. R.; Hernandez, J.; Perez-Davis, M. E.; Cabrera, C. R. *Langmuir* **2006**, *22*, 6102.

(48) Liu, S. Q.; Tang, Z. Y.; Shi, Z.; Niu, L.; Wang, E. K.; Dong, S. J. *Langmuir* **1999**, *15*, 7268.

(49) Nielsen, J. U.; Esplandiu, M. J.; Kolb, D. M. *Langmuir* **2001**, *17*, 3454.

(50) Roodenko, K.; Gensch, M.; Rappich, J.; Hinrichs, K.; Esser, N.; Hunger, R. *Journal of Physical Chemistry B* **2007**, *111*, 7541.

(51) Garrett, D. *Personal Communication*.

(52) Barton, A. *CRC Handbook of solubility parameters and other cohesion parameters*; 2nd Edition ed.; CRC Press LLC, 1991.

(53) Solak, A. O.; Eichorst, L. R.; Clark, W. J.; McCreery, R. L. *Analytical Chemistry* **2003**, *75*, 296.

(54) McDermott, M.; Rostami, A. *e-Journal of Surface Science and Nanotechnology* **2006**, *4*, 419.

Chapter 5. Carbon surface modification by electrochemical oxidation of arylacetates

5.1 Introduction

The anodic oxidation of acetates is an important reaction in electrochemical synthesis, forming a range of hydrocarbon compounds.[1-4] The reaction involves the electrooxidation of an acetate functional group with subsequent decarboxylation of the structure, yielding either carbon-based radicals or carbocations depending on the acetate reactant.[5, 6] The radical can sometimes be oxidized to the corresponding carbocation at the potential at which it is formed; when the product is formed from the carbon-based radical, it is referred to as the Kolbe reaction, and when the product is formed from the carbocation, it is termed a non-Kolbe reaction. The electrochemical oxidation of arylacetates at carbon electrodes was first reported to result in the formation of surface films around ten years ago but the reaction has received comparatively little attention since then.[5] There are a few reports in which the reaction is used to generate modified carbon felts with potential applications in combinatorial synthesis and electrocatalysis.[7-9] A few studies of the mechanism of the electrochemical oxidative decarboxylation reaction, and characterization of surface films by spectroscopy, scanning tunneling microscopy (STM) and electrochemistry have been reported[5, 7, 9], but the physical and chemical stability and structure of the resultant layers is largely unknown. This was the motivation behind the work described in this chapter.

The mechanism of the surface reaction for the covalent grafting of arylacetates to carbon surfaces was proposed to be similar to a non-Kolbe reaction, as shown in equations (5.1) – (5.4). It was reported that the cleavage of the carboxylate is fast and the radical ($E_{oxidation}$ ~ 0.7 V *vs* SCE) is formed very close to the electrode surface and is easily oxidized to the corresponding carbocation leading to C-C bond formation with surface carbon and surface-coupling.[5, 6] Although Savéant and coworkers proposed that the carbocation is the species, which couples to the carbon surface, the more recent elucidation of radical-based grafting mechanisms with aryldiazonium ions suggests that the radical is the more likely species (reaction 5.5), in particular during multilayered film formation (Chapter 1). However, both types of reactive species, carbocation and

arylmethyl radicals, may participate in surface grafting to form C-C covalent linkages with the carbon surface. Electrochemical oxidation of arylacetates -modifiers has been demonstrated on both glassy carbon (GC) and highly ordered pyrolytic graphite (HOPG), and hence suggests that reactive species react and graft to both graphitic edge and basal plane sites. It remains unclear whether electrografting occurs at the pristine basal plane of HOPG or at defect sites on the basal plane. Estimated surface coverage at GC is approximately three times that at basal plane HOPG, which indicates that grafting at graphitic edge sites is faster than at graphitic basal sites.[5] This is likely to be attributed to the higher reactivity of edge than basal plane carbon similarly observed for radical-based surface derivatization for the reduction of aryldiazonium ions as discussed in Chapter 1.[10, 11]

$$RCO_2^- - e^- \Leftrightarrow RCO_2^{\bullet} \quad (5.1)$$

$$RCO_2^{\bullet} \rightarrow R^{\bullet} + CO_2 \quad (5.2)$$

$$R^{\bullet} - e^- \Leftrightarrow R^+ \quad (5.3)$$

$$\text{Carbon Surface} + e^- + R^+ \rightarrow \text{Carbon Surface—R} \quad (5.4)$$

$$\text{Carbon Surface} + R^{\bullet} \rightarrow \text{Carbon Surface—R} \quad (5.5)$$

In the initial report of carbon surface derivatization by electrochemical oxidation of arylacetates, intriguing aspects of film behaviour were described.[5] For film preparation, a two-step grafting process was shown to give films with higher surface coverage than those prepared with a single grafting. Surfaces were first grafted using potential scans just encompassing the acetate oxidation peak. After disappearance of the oxidation peak, a new peak is observed at a potential between the initial peak and the peak for oxidation of the surface film. Oxidation at the potential of the new peak in acetate modifier solution leads to further grafting. Voltammetry of surface-attached groups on GC confirmed an increase in modifier surface coverage and STM images showed a denser film on HOPG after the second grafting compared to single grafting. A second intriguing finding from the same study is that the films could be electrochemically erased from the surface by treatment in blank acetonitrile-electrolyte solution. Erasing was achieved by holding the potential of the grafted glassy carbon (GC) electrode slightly positive of the peak for irreversible oxidation of the surface-bound groups. After this treatment, electrodes were found to exhibit the same behaviour as a bare GC electrode, towards solution-based redox species. Hence, it was

concluded that the surface film had been removed.

The work described in this chapter was prompted by the reports of second grafting and erasing processes for films formed by oxidation of arylacetates at carbon surfaces. This chapter is aimed at examining the film properties and effect of applied potential on these films using a combination of atomic force microscopy (AFM) and electrochemistry. In particular, the surface coverage of electroactive groups, changes in film thickness and ability of the film to inhibit electron-transfer to a solution redox probe are monitored before and after subjecting the films to applied potential excursions (beyond ± 1.5 V) in acetonitrile-electrolyte solution.

5.2 Experimental

5.2.1 Reagents and Materials

1-napthalene acetic acid (Sigma), *p*-nitrophenyl acetic acid (Aldrich), *p*-methoxyacetic acid (Koch-Light laboratories) and tetrabutylammonium hydroxide (TBAOH) in 1 M methanol (Aldrich) were used as received.

5.2.2 Electrochemistry

Arylacetic acids were converted to the corresponding acetate in the electrochemical cell by dissolving the aryl acetic acid in acetonitrile and slowly adding 0.9 molar equivalents of TBAOH in methanol. Films were prepared on GC and PPF surfaces using acetonitrile solutions containing 5.2 mM of the arylacetate and 0.1 M $TBABF_4$. For the standard modification procedure, two voltammetric cycles at 200 mV s^{-1} were recorded between 0 and 1.4 V and then the working electrode potential was maintained for the selected time 100 mV more positive than the modification peak, i.e. $E_{app} = E_{p,a} + 100$ mV. For PPF samples, the modified surface was thoroughly washed with pure acetonitrile and dried with nitrogen gas. Modified GC was ultrasonicated in pure acetonitrile for 30 s and dried with nitrogen gas.

An O-ring defined the geometric area of the PPF working electrode (0.26 cm^2 for electrode modification and 0.12 cm^2 for subsequent scans at the modified surface). A conventional glass cell was used with the glassy carbon (GC) disk electrode (diameter = 3.0 mm). All voltammetry of $Fe(CN)_6^{3-}$ (3 mM in 0.2 M KCl aqueous solution) was obtained

with scan rate = 200 mV s^{-1}.

For practical reasons, experiments involving voltammetric determination of film surface coverage and examination of the $Fe(CN)_6^{3-}$ response at the modified surface were carried out at GC. All AFM film thickness measurements were made on PPF, using similar procedures to those described in Chapters 3 and 4 for diazonoium ion-derived films. Scans in acetonitrile-electrolyte solution to negative potentials were obtained at 20 V s^{-1} and to positive potentials at 200 mV s^{-1}. Each voltammogram was obtained with a freshly prepared film.

5.2.3 UV Visible Spectroscopy

Spectra were collected with a GBC Scientific UV/VIS 920 Spectrometer, using a 500 to 190 nm scan range, 1 nm slit width, 0.067 nm scan interval and 150 nm/min scan speed. A quartz cuvette with 1 cm pathlength contained the sample, and all samples were referenced to air from the dual beam. Solutions for UV analysis were prepared by adding aliquots (0 - 100 μL) of 0.1 M TBAOH in methanol to a 10 mL solution of 5.9 mM 1-naphthylmethylacetic acid (NM-COOH) in acetonitrile giving twelve different solution compositions. From each solution, 40 μL was further diluted to 4 mL with methanol-acetonitrile solvent and the UV spectrum recorded.

5.3 Results & discussion

5.3.1 Grafting and Electrochemistry

Initial experiments were aimed at identifying arylacetates with suitable film-forming properties at GC and PPF surfaces. Chart 5.1 shows the three arylacetates chosen for this investigation. Their selection was based on previous reports of electrochemical grafting of arylacetates to GC and HOPG electrodes.[5] Thus 4-nitrobenzylcarboxylate ($NB\text{-}COO^-$), 1-naphthylmethylcarboxylate ($NM\text{-}COO^-$) and 4-methoxybenzylcarboxylate ($MeOB\text{-}COO^-$) were reported to readily form passivating films on GC electrodes on repeat cycling through the acetate oxidation peak. Furthermore, films prepared from $NB\text{-}COO^-$ and $NM\text{-}COO^-$ exhibit additional redox chemistry based on the electroactive nitrophenylmethyl (NB) and naphthylmethyl (NM) groups, respectively. This provides a convenient means to examine the

films electrochemically. The calculated lengths of the modifiers from the carbon surface atom to the outermost atomic radii are listed in Table 5.1.

Chart 5.1. Acetate-modifiers used for electrochemical grafting.

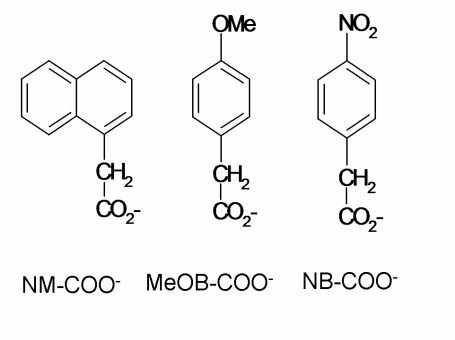

Table 5.1. Molecular lengths calculated for acetate-modifiers.

modifier	molecular lengths nm
NM	0.72
MeOB	0.82
NB	0.84

For electrochemical modification, carbon electrodes were placed in acetonitrile-electrolyte solution containing arylacetates. Figure 5.1 shows two consecutive voltammetric scans of NM-COO^- (panels a and b), MeOB-COO^- (panels c and d) and NB-COO^- (panel e) in acetonitrile solution at GC and PPF surfaces. The acetates were generated in situ (Section 5.2.2); this method is described in more detail in the following section. The voltammograms show oxidation peaks between 1.1 and 1.4 V, which are attributed to the reactions described by equations (5.1), (5.2) and (5.5), above. On repeat scans (with stirring in between scans) the peak current decreases. This electrode behaviour is consistent with a passivating film forming on the electrode surface inhibiting the continuation of the electrooxidation process. To gain further evidence for the formation of surface films, grafting was carried out by holding the potential at $E_{app} = E_{p,a} + 100$ mV for a specified time. The modified electrodes were ultrasonicated and/or rinsed in acetonitrile and transferred to an aqueous $Fe(CN)_6^{3-}$ solution for voltammetric investigations. Figure 5.2 shows the response of $Fe(CN)_6^{3-}$ before and after the grafting step at the GC and PPF surfaces. The changes in the response of the redox probe at all the acetate-grafted surfaces

provides evidence for a surface film that decreases the apparent facilitation of electron transfer to $Fe(CN)_6^{3-}$ in solution.[12, 13] Similar suppression of redox probe responses were observed for aryldiazonium ion-derived films (as shown in Chapters 3 and 4)[14-16], which suggests that films of similar structure are generated by this method. A relatively weaker blocking property of NB film-modified GC is shown in Figure 5.2d. This is due to an incompletely formed film, which was prepared with a shorter electrolysis time. In contrast, significantly less blocking arylacetate-derived films were reported by Savéant *et al* for films prepared for 600 s using similar conditions to those described in this work.[5] As discussed later in this work (Section 5.3.6), the weaker blocking properties are due to the films being treated to negative potential excursions prior to analysis in redox probe solution. Detailed investigations on the effect of negative applied potential are presented in Section 5.3.6.

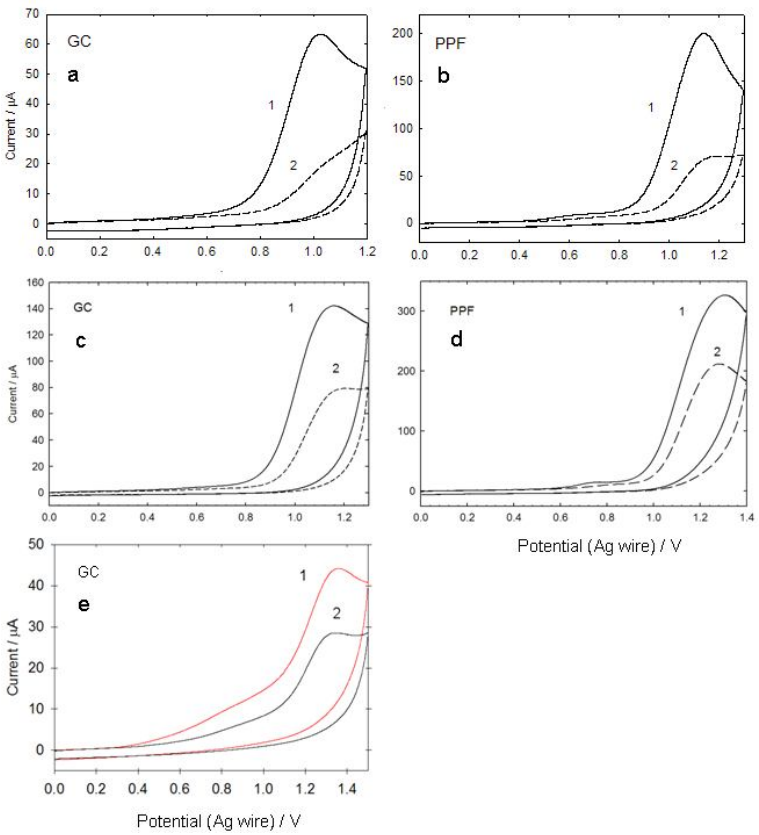

Figure 5.1. Cyclic voltammograoms of the first two scans, with stirring between scans (ν = 200 mV s^{-1}), recorded at GC (a, c, e) and PPF (b, d) surfaces in 5.2 mM arylacetates in acetonitrile-electrolyte (a and b) NM-COO^-,(c and d) MeOB-COO^-, and (e) NB-COO^-.

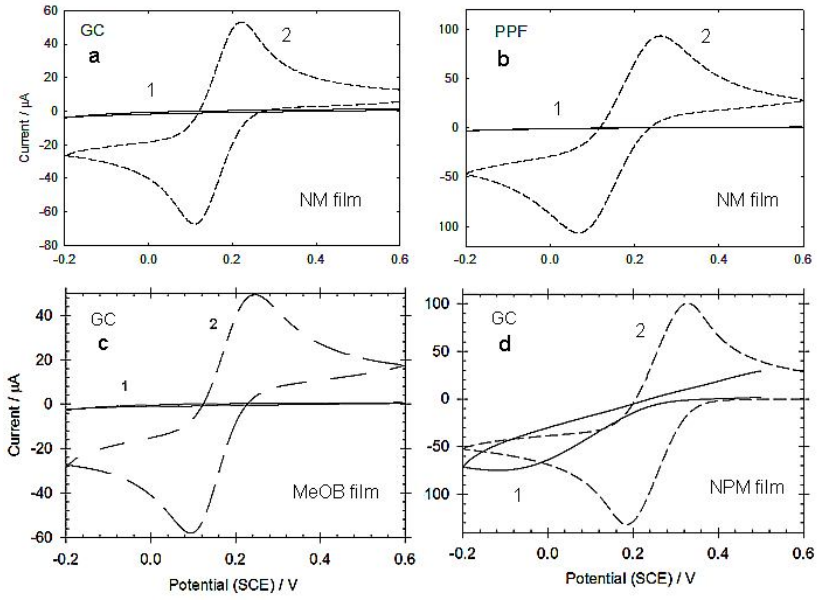

Figure 5.2. Cyclic voltammetry of 3.1 mM $Fe(CN)_6^{3-}$ in aqueous 0.2 M KCl at GC (a, c, d) and PPF (b) surfaces. Scans 1 are recorded at film-modified surfaces and scans 2 at unmodified surfaces. Voltammograms are collected at (a and b) NM film (t = 300 s); (c) MeOB film (t = 300 s); (d) NB film (t = 120 s).

For the NM-COO^- and MeOB-COO^- modifiers, the similarity of the ratio of peak currents for scans 1 and 2 of the grafting process at GC and PPF [Figures 5.1a) c) and b) d)], and the blocking effects of the grafted films of NM at each surface [Figures 5.2a) and b)] suggest similar rates of film formation and film properties at both GC and PPF surfaces. In contrast to the results described above, NB-COO^- showed different electrochemical behaviour at GC and PPF. Although NB-COO^- was electrooxidized with similar results to the other arylacetates at GC, inconsistent results were obtained at PPF. NB-COO^- did not reproducibly show an irreversible oxidative peak for electrooxidative grafting at PPF even though reproducible results were obtained at GC. This appears to be the first example where GC and PPF have dissimilar electrochemical behaviour for a surface coupling reaction. The reasons underlying this difference are not certain but may be related to the low roughness and adsorption properties of PPF (Chapter 1) that may inhibit the surface-grafting using the NM-COO^- modifier.[17] Adsorption of NB-COO^- modifier at sites on the carbon surface may be required prior to surface grafting of which it is less favourable at PPF. Another example of different behaviour of GC and PPF has subsequently been reported for the spontaneous grafting of 4-NB diazonium ion in acetonitrile where the aryldiazonium ion-modifier grafts to GC surfaces but does not graft to PPF however no explanation was given to this finding.[18] The electrooxidation of acetates has been reported to be dependent on the nature of the

electrode material, and it has been reported that the electrooxidation of acetates at gold and platinum electrodes gives poorly defined and irreproducible responses.[19] Hence the difference in electrografting behaviour at the two different carbon surfaces is consistent with this observation. However, the reason behind this difference is not understood.

5.3.2 Neutralization of acetic acids to generate acetates

Acetates were generated in-situ in the electrochemical cell by addition of methanolic TBAOH to an acetonitrile solution containing the corresponding arylacetic acid. This procedure was examined in more detail to determine the amount of TBAOH to add. Addition of up to 0.4 molar equivalent amount of base to the acetic acid increased the current for oxidation of the acetate. Thereafter, the current did not significantly increase. It is assumed that at high concentration of acetate, the film formed during the oxidative scan significantly passivates the electrode during the scan and hence affects the observed peak current. Figure 5.3 shows voltammograms obtained at a GC electrode in acetonitrile solution containing electrolyte only (1), the parent 4-nitrobenzylcarboxylic acid (5.9 mM) in the presence of electrolyte, methanol and water (2), and TBAOH in the presence of electrolyte (3). Scans 1 and 2 show no significant redox activity at the grafting potential confirming that the parent acetic acid is not oxidized in the selected potential window. Scan 3 shows there is a large oxidation peak at $E_{p,a}$ ~ 1 V when TBAOH is added to the acetonitrile-electrolyte solution. This is attributed to oxidation of hydroxide ion. To avoid the presence of unreacted hydroxide ion (and the associated oxidation peak), a slightly less than 1 equivalent stoichiometric amount of base was added to create the acetate-modifier.

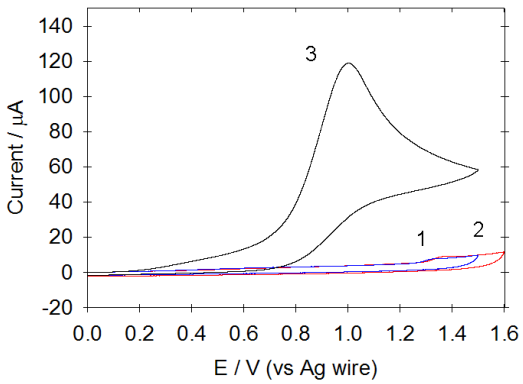

Figure 5.3. Cyclic voltammograms of a GC electrode obtained in acetonitrile-electrolyte solutions (ν = 200 mV s^{-1}). (1) Blank electrolyte, (2) 5.9 mM NB-COOH (in the presence of 50 μL MeOH and 50 μL H_2O), and (3) 5.2 mM TBAOH.

UV spectroscopy was used to monitor the neutralization reaction, and to establish the concentration of the acetate in grafting solutions. Aliquots of 0.1 M TBAOH in methanol were added to 5.9 mM NM-COOH in acetonitrile to generate twelve solutions containing NM-COOH and NM-COO$^-$, including a solution containing only the acid. Figure 5.4 (top panel) shows the UV spectra of (a) NM-COOH solution (5.9 mM), (b) NM-COO$^-$ solution (5.9 mM NM-COOH + 10 mM TBAOH), and (c) solution used for electrografting to carbon (5.9 mM NM-COOH + 5 mM TBAOH). The UV bands of NM-COOH and NM-COO$^-$ in the mixed acetonitrile/methanol solvent system are measurably different and hence the ratio of NM-COOH to NM-COO$^-$ in solution could be determined.

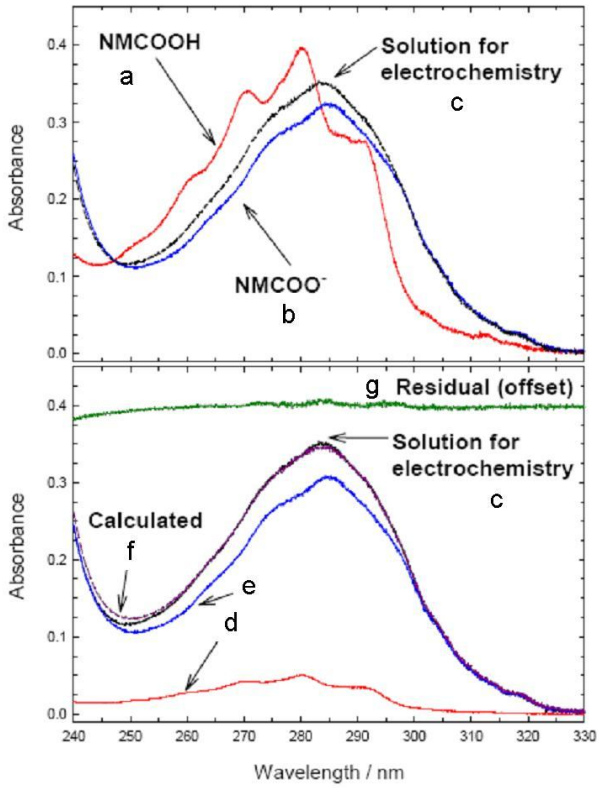

Figure 5.4. Top Panel. UV spectra of : (a) 5.6 mM NM-COOH in 10 ml acetonitrile + 50 µL methanol; (b) 5.5 mM NM-COO$^-$ in 10 ml acetonitrile + 50 µL methanol + 10 mM base (TBAOH in methanol); (c) the solution used for electrochemical grafting (5.9 mM NM-COOH + 5 mM base). **Bottom Panel:** The absorbance of (d) NM-COOH and (e) NM-COO$^-$ represent the relative amounts of each species calculated to be present in the electrochemical solution, based on a linear curve-fit of the measured spectrum. Hence, the calculated spectrum of this linear fit (i.e. the co-addition of the (d) and (e) traces) is shown as trace (f). The residual between the measured and calculated is trace (g), and has been offset for clarity. The linear regression of the UV data was carried out by Dr. Paula Brooksby for the measured electrochemical solution was $y = Ax + Bz$, where y is the calculated spectrum, x the NM-COOH spectrum and z is the NMCOO$^-$ spectrum. The coefficients are $A = 1.27 \times 10^{-1}$ and $B = 9.49 \times 10^{-1}$. From this, the concentration of [NMCOOH] is calculated to be 0.71 mM and [NMCOO$^-$] is 5.20 mM.

Principal component regression analysis (singular value decomposition, SVD, and linear regression methods) of the measured spectra was performed by Dr. Paula Brooksby (University of Canterbury). One significant advantage of SVD analysis is that the outcome gives the number of species that are present and is also a standard method to determine whether there are side products created in the neutralization reaction. The SVD results for the region from 247 to 330 nm for all 12 samples gave two statistically significant spectra that form the basis for all of the measured data. Reducing the data set to those with excess added base gave only one significant spectrum (i.e. the spectrum of NM-COO^-). This confirms that the reaction between NM-COOH and TBAOH gives NM-COO^- as the only product exclusively. Using the spectra of NM-COOH and NM-COO^- in the linear regression analysis of the spectrum of the (diluted) grafting solution showed that the solution contained 0.7 mM NM-COOH and 5.2 mM NM-COO^- as confirmed in Figure 5.4 (lower panel). Grafting solutions of MeOB-COOH and NB-COOH were prepared in the same manner, using nominally 5.9 mM of arylacetic acid and 5 mM TBAOH, and hence it is assumed that all grafting solutions contain 5.2 mM of the corresponding arylacetate.

5.3.3 Characterization of as-prepared NM films and MeOB films

GC surfaces were modified with NM-COO^-, NB-COO^-, and MeOB-COO^- and the electroactivity of their grafted films was examined. All films were prepared under standard conditions at GC surfaces with t = 300 s unless stated otherwise. Following the grafting step, the modified electrodes were cleaned and transferred into blank acetonitrile-electrolyte solutions. On scanning in the positive potential direction, NM film undergoes an irreversible oxidation at 1.8 V (Figure 5.5a)) that is close to the potential for irreversible oxidation of solution phase 1-methylnaphthalene.[5] For MeOB film, an irreversible oxidation is seen in the voltammograms at 1.7 V, (Figure 5.5b)). This peak is also present for solution-phase MeOB-COOH and provides evidence for surface modification.[5] On scanning in the negative potential direction, NM film and NB film exhibited redox processes centered near -2.6 V and -1.0 V, respectively (Figure 5.6). These processes can be assigned to a one-electron transfer to surface-attached naphthyl- and nitrophenyl-containing groups to form radical anions, which are oxidized back during the reverse scan.[5, 20] This process is not chemically reversible for NM film at scan rates lower than 20 Vs^{-1}.[5, 20] The voltammetric responses of these films are consistent with those observed in the initial report by Savéant *et al*.[5]

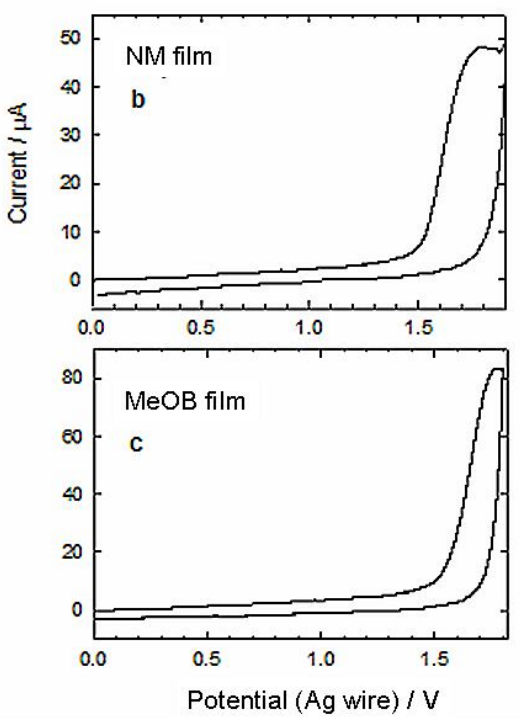

Figure 5.5. Cyclic voltammetry of a) NM modified GC and b) MeOB modified GC in acetonitrile-electrolyte (ν = 200 mV s^{-1}).

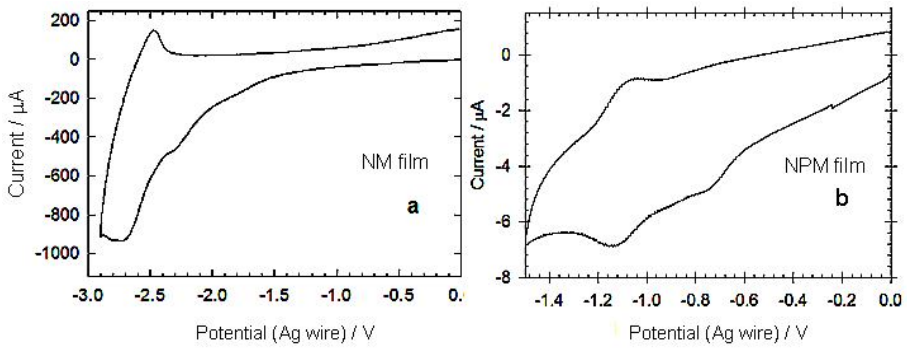

Figure 5.6. Cyclic voltammetry of a) NM modified GC (20 V s^{-1}) and b) NB film-modified GC in acetonitrile-electrolyte (ν = 200 mV s^{-1}).

Also apparent in Figure 5.6 are small pre-waves associated with the NB/NB^- and NM/NM^- redox couples. Pre-waves have been observed many times in the voltammetry of electroactive films, grafted using both the oxidation of arylacetates and reduction of aryldiazonium ions, however the origin of these pre-waves is unknown. The reasons may be related to the presence of modifier groups in different film environments however this was not investigated in this work. The NB film-modified GC electrodes were also scanned in 0.25 M H_2SO_4 (Figure 5.7) after scanning in blank acetonitrile-electrolyte solution and ultrasonicating in acetonitrile before electrochemical examination. The cyclic voltammogram

is consistent with those obtained at NP films prepared from the electroreduction of aryldiazonium salts (Chapters 3 and 4).[14, 16, 21, 22] The surface-bound nitroaryl groups are irreversibly converted to various reduced nitrogen-products as described in Chapters 3 and 4. Hence, the surface concentration of NB groups was determined by scanning in the two different environments: acetonitrile-electrolyte solution and 0.25 M H_2SO_4.

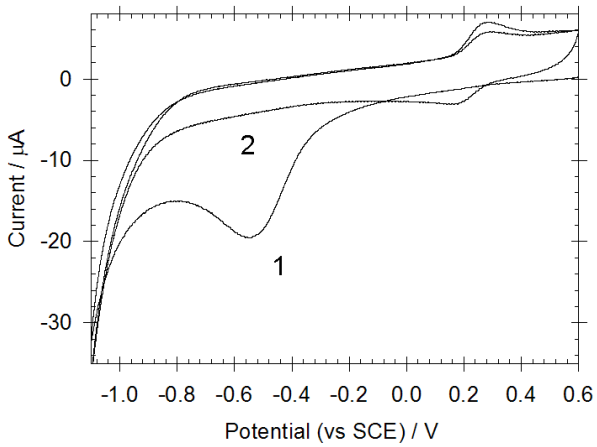

Figure 5.7. First two consecutive voltammetric scans of NB modified GC recorded in 0.25 M H_2SO_4 (ν = 200 mV s^{-1}).

The surface coverages of NB and NM groups were estimated for a series of films prepared from NM-COO^- and NB-COO^- on GC using electrolysis times between 30 and 1200 s. Figure 5.8a) shows that on the first voltammetric scan for NM film, overlapping of the pre-peaks with the main NM film reduction peak gives a significantly larger area for the cathodic peaks than the corresponding anodic peak. However, the second and subsequent scans have approximately equal areas for the cathodic and anodic peaks and hence the area of the second scan cathodic peak was used to determine the absolute charge associated with the NM/NM^- redox reaction. For NB film, the cathodic peak from the first voltammetric scan (Figure 5.6b) was used to determine the surface concentration. On repeat scanning the NB redox response decreases in magnitude due to irreversible reduction of NB groups in the presence of adventitious water (Chapter 3). Assuming a one-electron transfer, the surface concentration, Γ, of electroactive NB and NM groups was obtained by curve-fitting and is shown in Figures 9 and 10. Figure 5.9 shows a plot of surface concentration of NM groups *vs* electrolysis time (applied after two voltammetric scans). The amount of NM grafted to the GC surface does not appear to increase after approximately 60 s of electrolysis. The average surface concentration of NM groups for films was approximately 1.7±0.3 x 10^{-10} mol cm^{-2}. The surface concentration value determined for NM film is in good agreement with that

reported by Savéant and co-workers who reported a surface concentration of 1.5 x 10^{-10} mol cm^{-2}.[5] Figure 5.10 shows the surface concentration of NB groups *vs* electrolysis time calculated by obtaining voltammograms in acetonitrile solution (Δ) and aqueous H_2SO_4 (X).

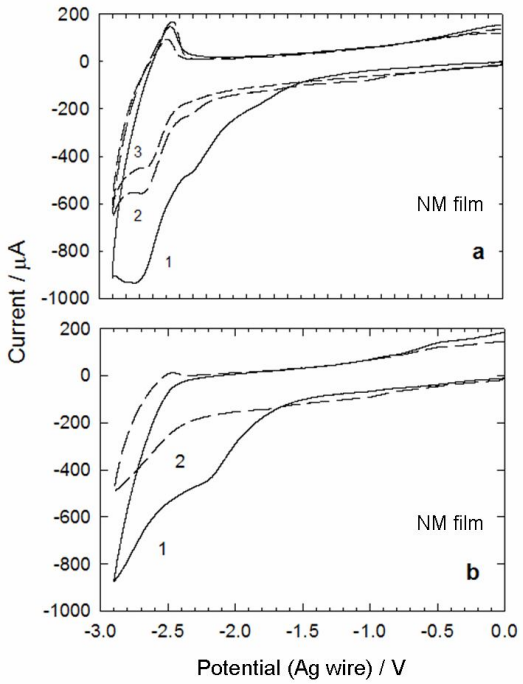

Figure 5.8. Consecutive scans (v = 20 V s^{-1}), of NM modified GC in acetonitrile-electrolyte solution. a) Film grafted for 300s at $E_{app} = E_{p,a}$ + 100 mV; b) Film grafted for 300 s at $E_{app} = E_{pa}$ + 100 mV followed by 120 s at $E_{app} = E_{p,a}$ + 500 mV.

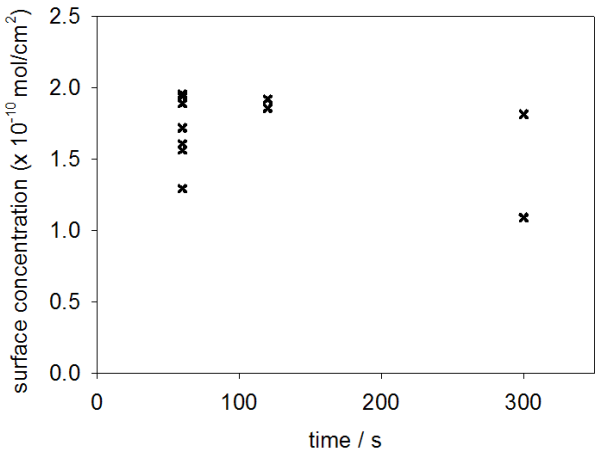

Figure 5.9. Graph showing the estimated surface concentration of electroactive NM groups in NM film *vs* electrolysis time (applied after two voltammetric scans).

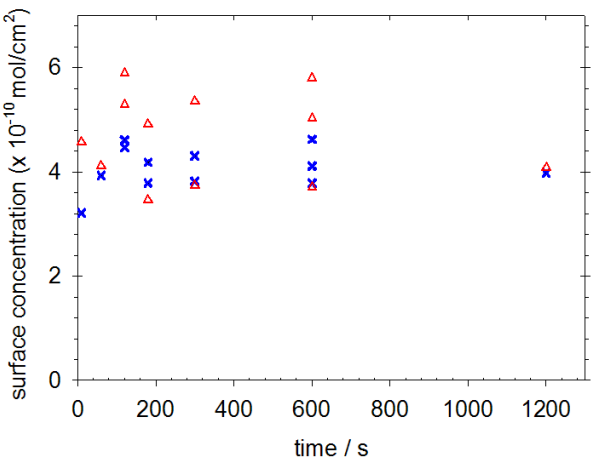

Figure 5.10. Graph showing the estimated surface concentration of electroactive NB groups in NB film *vs* electrolysis times (applied after two voltammetric scans). Surface concentrations were determined by scanning in (Δ) acetonitrile + 0.1 M $TBABF_4$; and (x) 0.25 M H_2SO_4.

In both media, the concentration of grafted NB groups increases rapidly and reaches significant surface coverage after just 10 s of electrolysis. The data show that the concentration of electroactive groups does not vary significantly for electrolysis times between 60 and 1200 s. This suggests that film growth is rapid and nearly complete within 60 s. The average surface concentration of NB films was approximately 4.2±0.8 x 10^{-10} mol cm^{-2} determined from voltammetry in acetonitrile-electrolyte solution. The surface concentration of NB film determined from voltammetry in aqueous H_2SO_4 is approximately 4.0±0.8 x 10^{-10} mol cm^{-2}. Considering that scans were performed in aqueous H_2SO_4 after acetonitrile-electrolyte solution and that the process is not fully reversible in acetonitrile (due to adventitious water), these values agree well with each other. Savéant and co-workers reported a value of 2.5 x 10^{-10} mol cm^{-2} for a film prepared with the NB-COO^- modifier at GC.[5] The difference in the surface concentration of NB is most likely due to the different preparation conditions used to generate the films. Lower concentration of NB-COO^-, applied overpotential and a shorter electrolysis time were used by Savéant and co-workers for the preparation of their NB films and hence a lower surface concentration was reported. Films produced by electrooxidation of arylacetates in this work are relatively low density with surface concentrations lower than films derived from reduction of aryldiazonium ions (Γ ~ 2.3 x 10^{-9} mol cm^{-2}, Chapters 3 and 4). This may be attributed to electroinactive NB groups present within the film and/or the grafting reactions of arylacetates may be intrinsically less efficient than aryldiazonium ions. The latter maybe related to the difference in reactivity of carbocations and/or arylmethyl radicals with the carbon surface as well as the grafted film.

5.3.4 AFM examination of as-prepared films

Thickness measurements of NM and MeOB films were undertaken using AFM depth profiling. Figure 5.11 shows an AFM image of NM film and a profile scan of a trench created in the film. The as-prepared film has a regular topography with a low film surface roughness (R_a = 0.29 nm). Tables 5.2 and 5.3 show the film thickness (d) for sixteen NM films prepared using standard conditions and electrolysis times between 30 and 300 s, and four MeOB films prepared using an electrolysis time of 300 s. The as-prepared films have thickness ranging between 2.0 and 3.1 nm for NM films, and 3.3 and 4.7 nm for MeOB films. These films are clearly greater than one molecular layer thick.

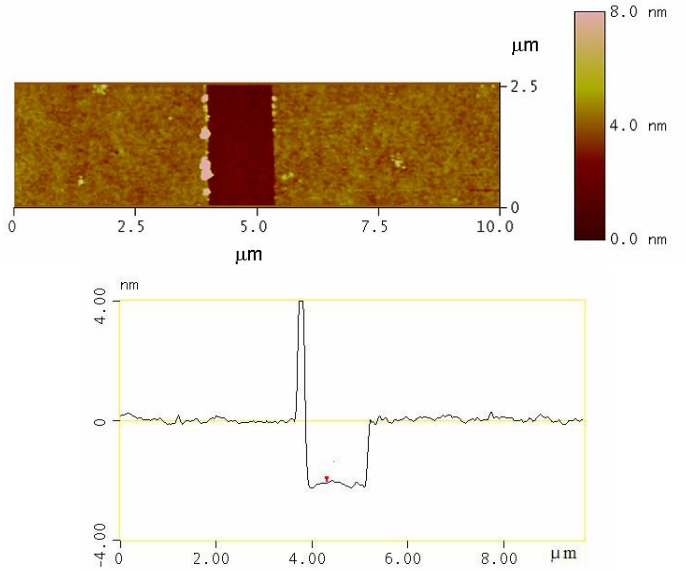

Figure 5.11. (Top) AFM image of a trench created in NM film grafted at PPF **(Bottom)** average profile of the trench created in NM film.

Table 5.2. NM film thickness and surface roughness, before and after sequential potential excursions in acetonitrile-electrolyte, for films prepared using standard conditions, and times listed.

preparation	as-prepared		after -2.9 V[a]		after E_{app}[b]		after 1.9 V[c]	
t	d	R_a	d	R_a	d	R_a	d	R_a
s	nm	nm	nm	nm	nm	nm	nm	nm
300	2.1	0.22	1.6	0.61	2.4	0.35		
300	3.1	0.69	2.1	0.99	2.9	0.77		
300	2.9	0.33	2.2	0.49				
300	2.0	0.26	1.1	0.53	3.0[d]	0.48		
300	2.0	0.30					2.4	0.36
300	2.0	0.35						
300	2.1	0.29						
120	2.9	0.50						
30			1.6	0.53			2.6	0.66
30			1.6	0.70				
60			1.2	0.40				
60			1.3	0.40				
120			1.1	0.52				
120			1.3	0.48				
300			1.3	0.64				
300			1.4	0.58			2.7	0.77

[a] two scans with $v = 20$ V s^{-1}. [b] $E_{app} = E_{p,a} + 100$ mV, $t = 300$ s; potential was applied after two standard scans to -2.9 V. [c] $t = 120$ s. [d] Potential applied in the presence of 5.2 mM NM-COO$^-$.

Table 5.3. MeOB film thickness and surface roughness, before and after potential excursions in acetonitrile-electrolyte, for films prepared using standard conditions and an electrolysis time of 300 s.

as-prepared		after -1.8 V, 300 s		after 2 V, 120 s	
d	R_a	d	R_a	d	R_a
nm	nm	nm	nm	nm	nm
3.3	0.51	3	0.83		
4.7	0.57	3.3	1.1[a]		
3.7	0.52			6.1	0.73
4.1	0.44			6.2	0.52

[a] Value obtained from arithmetic average of 10 areas.

As shown in Table 5.1, the lengths of the NM and MeOB modifiers from the carbon surface atom to the outermost atomic radii are 0.72 and 0.82 nm respectively. Assuming that the average molecular orientation of the film is perpendicular to the surface, AFM measurements provide direct evidence that these films are multilayered and the measured thicknesses correspond to 3–4 molecular layers for NM films and 4–6 molecular layers for MeOB films. Formation of multilayers by oxidation of arylacetates has not previously been reported. Films of similar thickness (typically 3-4 nm) are formed by the electroreduction of aryldiazonium ions (Chapter 3), which suggests that a similar mechanism to multilayer-film growth may be operative. The mechanism by which multilayers form was not specifically investigated but presumably proceeds *via* attack of arylmethyl radicals at the surface-attached film, analogous to the mechanism proposed for the formation of multilayer films during grafting from aryldiazonium salts (Chapter 3).[10, 11, 21, 23]

5.3.5 Two-step grafting of NM films and effect of grafting potential on NM films and MeOB films

The surface concentration and film thickness data for NM films (Figure 5.9 and Table 5.2) show that the growth of NM films is self-limiting at a fixed potential and that the NM films have substantial electron-transfer resistance to redox probe. Beginning with a NM film that had reached its maximum thickness during the initial grafting step ($E_{app} = E_{p,a} + 100$ mV), and scanning in a positive potential direction in a NM-COO^- modifier solution reveals a new modification peak (more details below). Incrementing E_{app} to a more positive potential was found to lead to further film growth. Figure 5.8b shows consecutive cyclic voltammograms of NM film in acetonitrile-electrolyte solution for a film grafted for 300 s at $E_{app} = E_{p,a} + 100$ mV followed by 120 s at $E_{app} = E_{p,a} + 500$ mV. After the second grafting step, the first scan shows the peak associated with reduction of NM film merged with the solvent limit. The second scan shows reduction and oxidation of the NM groups, although less well-defined than for single-grafted films. While it is not possible to reliably obtain an estimate of the surface coverage from the voltammograms of the two-step grafted films, visual inspection of Figures 8a) and 8b) indicate the peak shapes are similar and hence the peak areas are not greatly different. In contrast, film thickness measurements (Table 5.4) gave values ranging from 11.6 to 13.4 nm for the films formed by the two-step grafting procedure, compared with 2.0 to 3.1 nm for films formed at $E_{app} = E_{p,a} + 100$ mV (Table 5.2). The thicker films correspond to multilayered structures ranging between 16 and 19 molecular

layers. The apparent similarity of voltammetric peak areas for reduction of NM groups for films with thickness ranging from 2 to 13 nm provides clear evidence that not all surface groups are electroactive or survive the grafting process. Hence, voltammetrically determined surface concentration does not necessary accurately represent the amount of material incorporated in the surface film. A similar conclusion has been reached for aryldiazonium ion-derived films as previously described in Chapters 3 and 4.[23, 24]

Table 5.4. Films prepared by two-step grafting and by single grafting at $E_{app} > E_{p,a} + 100$ mV.

film	$E_{app} = E_{p,a} + x$		
	x	time	d
	mV	s	nm
NM	100	300	
	500	30	12.5
NM	100	300	
	500	30	11.6
NM	100	300	
	500	300	13.4
NM	100	300	
	500	300	13.3
NM	300	300	5
NM	500	300	21.6
NM	500	300	17.4
MeOB	500	300	14.3
MeOB	800	300	16.7
MeOB	800	300	18.4

Voltammetric scans were recorded over a wide potential range from 0 to 2.5 V in the NM-COO^- modifier solution to investigate the significance of the new modification peak (second grafting step). In the first cycle, Figure 5.12a), there are four peaks observed which are labeled (i) – (iv). Peak (i) is oxidation of the acetate and peak (iii) is assigned to oxidation of surface-bound NM groups (by comparison in Figure 5.5a). Peak (iv) appears at the potential where the naphthylmethyl-based oxidation of NM-COOH is observed (in the same medium, NM-COOH exhibits a single, broad irreversible oxidation peak at 2 V) and hence (iv) is tentatively assigned to oxidation of NM moiety of NM-COO^- and NM-COOH in solution.

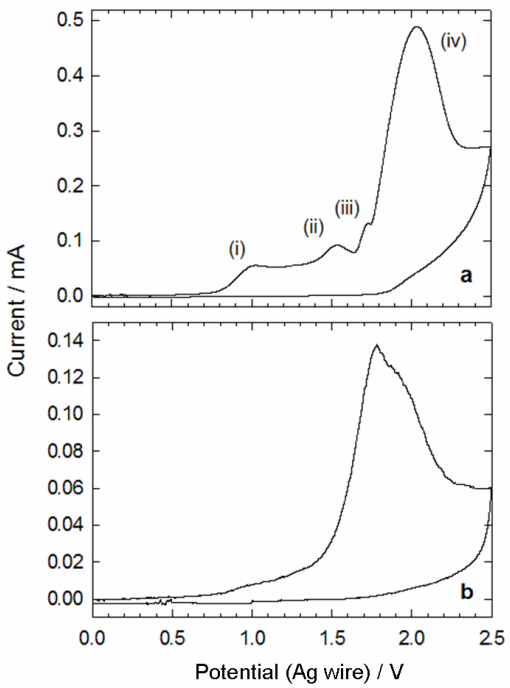

Figure 5.12. Cyclic voltammograms (200 mV s^{-1}) at GC of 5.2 mM NM-COO^- in acetonitrile-electrolyte solution. a) First scan and b) second scan, with solution stirring between scans.

The peak current for this process is consistent with that assignment. As is the observation that the oxidation process giving rise to peak (iv) does not appear to be involved in the grafting process, nor does it appear in the voltammetry of NM film. On the other hand, the shape of the peak is not consistent with a simple diffusion-controlled process. Peak (ii) corresponds to that assigned by earlier workers to oxidation of adsorbed acetate, and it is this process that was proposed to be responsible for the second (distinct) grafting step.[5] However, the voltammograms of Figure 5.12 show significant anodic current at potentials positive of ~ 0.8 V and it is not possible to associate the current at 1.3 V, for example, exclusively with peak (i) or peak (ii). In the second scan, Figure 5.12b), only a broad oxidation peak is observed that is assumed to arise from merging of the processes giving peaks (i) - (iv) in the first scan.

Single graftings (300 s) were also undertaken at higher potentials more positive than the standard electrolysis potential, i.e. 300 mV and 500 mV more positive than $E_{p,a}$. As shown by the data in Table 5.3, these procedures generated films of relatively similar thickness and properties to those prepared by two individual grafting steps (Table 5.4). For films prepared with MeOB-COO^-, qualitatively similar results (Table 5.4) were obtained. Single step

grafting at $E_{app} = E_{p,a}$ + 500 mV and + 800 mV generated films with thickness 14.3 and 17.4 nm, respectively, considerably thicker than the films prepared under standard conditions (single step, $E_{app} = E_{p,a}$ + 100 mV, $d \sim 4$ nm). The thick films correspond to multilayers ranging between 17 and 21 molecular layers. From the observations, it is clear that the final film thickness increases with the potential used for grafting. Similar behaviour has been reported for aryldiazonium ion-derived films, and can be explained by the self-inhibiting nature of the films (Chapter 3).[11, 25-27] Downard revealed the potential dependence of surface concentration for films derived from aryldiazonium ions, where increased applied overpotentials gave increased surface concentrations of grafted material at GC.[26] She showed that films with surface coverages of 6 x 10^{-10} mol cm^{-2}, 12 x 10^{-10} mol cm^{-2} and 19 x 10^{-10} mol cm^{-2} were obtained when overpotentials 250 mV, 500 mV and 750 mV were applied, respectively.[26] Similarly, films with thicknesses between 15 and 25 nm have been generated by electroreduction of aryldiazonium ions with an applied overpotential of 450 mV.[11] Hence, an increase in overpotential is required to drive electron-transfer across the insulating film for continuation of film growth to a greater thickness. From these investigations, it appears the previously reported second grafting step of electrooxidation of arylacetates has no significance beyond being just a grafting step at higher applied overpotential than usually utilized.

5.3.6 Film changes induced by scans to negative potentials

Changes in film thickness and $Fe(CN)_6^{3-}$ redox response at NM film and MeOB film grafted surfaces were monitored to establish the effects of negative potential excursions on the properties of the films. Modifiers were grafted to GC and PPF surfaces using standard conditions. After measuring the film thickness and surface roughness, and recording the voltammetric response of $Fe(CN)_6^{3-}$, the as-prepared films were transferred to acetonitrile-electrolyte solution and treated to negative potential excursions. After treatment, the film thickness and surface roughness were re-measured, and scans in $Fe(CN)_6^{3-}$ and NM-COO^- were obtained at the treated surfaces.

Figure 5.13 shows voltammograms of $Fe(CN)_6^{3-}$ obtained at a) NM film- and b) MeOB film-modified surfaces. Scan (ii) is at the as-prepared films and scan (iii) at the grafted surfaces after two repeat scans between 0 and -2.9 V at 20 Vs^{-1} in acetonitrile-electrolyte solution. Scan (i), obtained at bare GC, is shown for comparison. For both films, the apparent

rate of electron transfer to $Fe(CN)_6^{3-}$ is greatly increased at the grafted surface after scans to -2.9 V. When a grafted surface, which has been treated to negative potential scans is returned to an acetonitrile solution containing the acetate-modifier, oxidation of the acetate is observed, with a peak current approximately 30 % of that obtained at a freshly polished electrode (not shown).

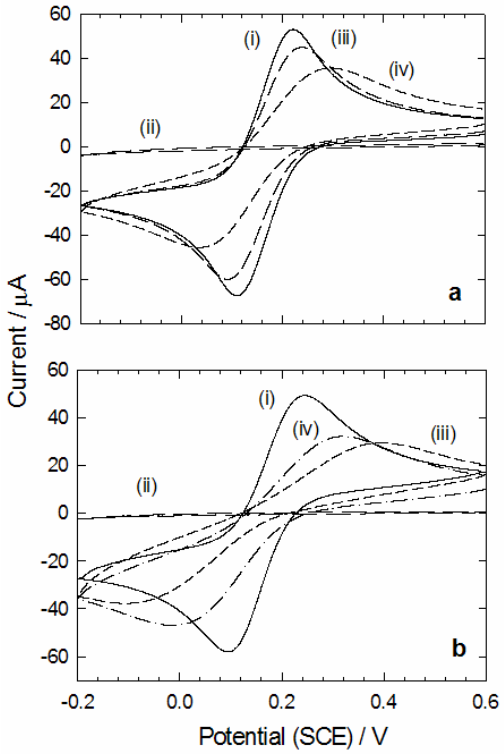

Figure 5.13. Cyclic voltammetry in 0.2 M KCl of a) 3.7 mM $Fe(CN)_6^{3-}$ at (i) polished GC, (ii) NM-modified GC, (iii) NM-modified GC after 2 scans to -2.9 V at 20 V s^{-1} , (iv) NM film after 30 scans to -1.8 V at 200 mV s^{-1} followed by holding at -1.8 V for 120 s; b) 3.1 mM $Fe(CN)_6^{3-}$ at (i) a polished GC, (ii) MeOB -modified GC (300 s), (iii) MeOB -modified GC after 2 scans to -2.9 V at 20 V s^{-1}, (iv) MeOB-modified GC after holding at -1.8 V at for 300 s.

For NM film, AFM measurements (Table 5.2) revealed a ~ 30 % reduction in average film thickness and a large increase in film surface roughness after scanning to -2.9 V. However, no large pinholes extending through the films could be detected in AFM examinations. The effects of applying less negative potentials were also examined. Figure 5.13a, scan (iv) is the voltammogram of $Fe(CN)_6^{3-}$ obtained at a NM film-grafted electrode after 30 scans between 0 and -1.8 V in acetonitrile-electrolyte solution at 200 mV s^{-1}, followed by 120 s at E_{app}=-1.8 V. Figure 5.13b, scan (iv) is the voltammogram of $Fe(CN)_6^{3-}$ obtained at MeOB film after applying a potential of -1.8 V to the electrode in acetonitrile-electrolyte solution for 300 s.

Comparing voltammograms (iii) and (iv) in Figure 5.13 reveals that polarization to the less negative potential of -1.8 V causes similar changes the blocking properties of NM and MeOB films as do potential excursions to -2.9 V. Potential excursions to -1.8 V also decrease the blocking properties of $Fe(CN)_6^{3-}$ at NM and MeOB film-modified GC electrodes, compared to that of freshly prepared films. AFM monitoring of MeOB films showed that film thickness is decreased and roughness increased by treatment at -1.8 V (Table 5.3). Evidently, similar changes are induced in the films when the less negative potential is applied, but for a longer time.

To probe the reversibility of film changes, NM film-grafted surfaces that had been cycled twice to -2.9 V and examined using electrochemistry and AFM were returned to acetonitrile-electrolyte solution and the potential used for film preparation, i.e. $E_{app} = E_{p,a} +$ 100 mV, was re-applied for 300 s (in the absence of modifier). After this treatment, the film thickness returned to the same value (within experimental uncertainty) as the initial films however the surface roughness remained higher than for as-prepared films (Table 5.2). Film blocking properties were not reversed by this treatment and the voltammetry of $Fe(CN)_6^{3-}$ was not altered and was the same as that shown in Figure 5.13a, scan (iii).

The results described above demonstrated that there is no significant cleavage of layers from the film during potential excursions to negative potentials but there is a decrease in blocking properties of the film. The changes in film thickness are consistent with potential-induced swelling and shrinking processes, similar to those reported for nitroazobenzene films.[23] For those films, thickness decreased during reduction in aqueous acid, and then increased when more positive potentials were applied in acetonitrile-electrolyte solution. The present results cannot be attributed to the effects of different solvents, and hence must arise from potential-induced changes in film solvation or the concentration of electrolyte ions entrained within the films. Structural changes to the film, such as orientation and packing of groups, may also be a contributing factor in the observed film changes.

The observation that two potential scans to -2.9 V significantly increases the facilitation of electron transfer to $Fe(CN)_6^{3-}$ at all film-grafted surfaces, indicates there are additional changes to the films that are unrelated to film shrinkage. Studies of films grafted *via* reduction of aryldiazonium ions (Chapter 4) have revealed similar changes in film thickness

and the apparent barrier properties of the films after negative potential excursions but different interpretations were proposed for the origin of the changes. Bélanger *et al* covalently grafted multilayer organic films to GC electrodes by electroreduction of aryldiazonium ions, and examined the stability of the films at various potentials in aqueous media.[15] Significantly increased apparent facilitation of electron transfer to solution redox probes were observed at film-modified surfaces after the films had been subjected to high positive and negative polarizations. The workers proposed that desorption of non-covalently grafted modifiers accompanied hydrogen, oxygen or chlorine evolution at very negative and positive potentials, leaving behind a thin layer (sub-monolayer) of covalently-attached modifier on the surface. A different explanation was offered by McCreery and co-workers to account for an increase in the apparent rate of electron transfer for probe species at aryldiazonium ion-generated films on GC, after negative potential polarization in acetonitrile solution.[28] The researchers reported that by treating the modified surfaces to negative potential excursions to ~ -2 V gave rate enhancement to solution-based redox probes. The workers proposed that electrons from the GC surface are injected into the films containing biphenyl and nitrobiphenyl groups leading to a quinoid structure containing a C=C double bond between the aromatic film and the graphitic substrate. This structure results in a smaller HOMO-LUMO energy gap and a more conducting state (Chapter 1).[28] The report described Raman spectral changes in the surface-bound NB moiety, consistent with the films exhibiting quinoid characteristics. The increase in electronic coupling between the π system of the graphitic substrate and the grafted film leads to a higher electronic conductance state.[28] This increased electronic conductance state was referred to as an "ON" state.[28] Similar rate enhancements towards solution redox probe species after negative potential polarization was also observed by McDermott *et al* for nitroazobenzene and 1-(-2-bisthienyl)-4-aminophenyl films electrografted to GC. These workers also proposed that a conductance switching mechanism was operative in those films.[29, 30]

The reversibility of changes in film thickness observed here for the arylacetate-derived films is not consistent with large scale loss of film during negative potential excursions as proposed by Bélanger *et al* (above). However, modifiers may be desorbed to leave nanometer-sized bare areas. The minimum lateral resolution of the AFM instrument is in the order of 10 nm, and hence areas on this length-scale or smaller, cannot be imaged properly. The increase in film surface roughness after potential scans to -2.9 V is consistent with such changes in the film. When electron-transfer occurs at a surface partially covered with an

insulating film, with bare areas that are small and closely spaced relative to the diffusion layer thickness, the standard heterogeneous rate constant for electron transfer appears to increase as surface coverage decreases.[31] The changes in voltammetric response of $Fe(CN)_6^{3-}$ at the modified electrodes, particularly at NM film treated with repetitive scans to -1.8 V, are qualitatively consistent with this model. After polarization at the grafting potential, the film swells back to its initial thickness but the nano-sized pinholes created in the film during negative potential treatment largely remains. This would account for the increases in surface roughness and irreversible changes in blocking properties of the treated films compared with as-prepared films.

A mechanism involving electrostatically-driven physisorption and desorption of modifiers can account for the generation of holes with nanometer sized dimensions in the films. During the formation of the film, the positive charge of the electrode surface would promote simple physisorption of the negatively charged acetate, in addition to the covalent coupling (grafting). Subsequent treatment of the grafted electrode at negative potentials will have the opposing effect with electrostatic repulsions removing physisorbed acetate material. The stability of the films during positive potential excursions is also consistent with this mechanism (see below). Considering conductance-switching as an alternative explanation to film desorption for the effects of scans to negative potentials, this phenomenon cannot be discounted but several observations suggest it is unlikely for these acetate-derived films. The methyl link in arylmethyl grafted films may prevent conjugation with the electrode and the formation of a quinoid-like structure and hence it may not be possible for the modified electrode to switch conductance states. Measurements of surface concentration and film thickness for NM film provide convincing evidence that, at least for thick films grafted by a two-step procedure, a large proportion of the film is nonelectroactive. This observation would be difficult to reconcile if the film itself was conducting (i.e. ON). Further, after scans to negative potentials, applying a potential more positive than the peak for irreversible oxidation of the film, does not change the $Fe(CN)_6^{3-}$ response, hence there is no evidence for switching the conductivity off, even after irreversible oxidation of surface-bound groups.

In another set of experiments, NM film-grafted surfaces which had been cycled twice to -2.9 V were returned to the acetate modifying solution and grafted at $E_{app} = E_{p,a} + 100$ mV for 300 s. The film thickness was monitored by AFM. The film was 2.0 nm after the initial grafting, 1.1 nm after negative potential excursions, and after re-grafting the measured

thickness was 3.0 nm (Table 5.2). Considering the magnitude of potential-induced film swelling and the experimental uncertainties, it is unclear whether there is further film growth on top of the existing film during the re-grafting step. On the other hand, there were dramatic changes in the $Fe(CN)_6^{3-}$ response after re-grafting. The voltammograms were indistinguishable to that shown in Figure 5.13a, scan (i), showing no redox features associated with $Fe(CN)_6^{3-}$. Similarly, the restoration of the barrier properties of the film after re-grafting at the initial grafting potential can be explained by the modifiers 'filling-in' the bare areas, generated during negative potential excursions.

5.3.7 Film changes induced by applying positive potentials

NM film and MeOB film can be irreversibly oxidized between 1.7 and 1.8 V (Figure 5.5). Savéant and co-workers reported previously that acetate-derived films can be erased by applying a potential slightly beyond the irreversible oxidation peak for the film.[5] Thus the effect of oxidation of NM and MeOB films on film properties was examined in a series of experiments similar to those described above. After applying a potential of 1.9 V (120 s) and 2.0 V (300 s) in acetonitrile-electrolyte to freshly prepared NM films and MeOB films, respectively, the voltammetric response of $Fe(CN)_6^{3-}$ was the same as that at the as-prepared films, i.e. the films remained very blocking to electron-transfer. Oxidation of NM-COO^- was not detected when the NM film-grafted electrode was replaced in modifier solution (5.2 mM NM-COO^- in acetonitrile + 0.1 M $TBABF_4$). When oxidized NM film was scanned to -2.9 V (v = 20 V s^{-1}) in acetonitrile solution the reversible NM/NM^- couple was found to be absent. Oxidation of naphthyl groups in the presence of low concentrations of adventitious water is expected to yield naphthaquinyl derivatives,[32] however voltammetry revealed no new redox features that could be attributed to such species. Oxidizing NM film at 1.8 V led to the same changes, whereas after 120 s at 1.7 V, the NM/NM^- couple showed diminished peak currents.

AFM measurements confirmed that the films remained largely intact after oxidative treatment. Table 5.2 shows that the thickness of a NM film was the same (within experimental uncertainty) after 120 s at 1.9 V in acetonitrile-electrolyte, whereas there was a significant increase in film thickness for MeOB film after 300 s at 2.0 V in acetonitrile-electrolyte (Table 5.3). AFM measurements provided direct evidence that grafted films cannot be erased by irreversible oxidation of electroactive groups in the films under the

conditions applied here. The observed swelling of MeOB film after oxidative treatment maybe related to the applied potential, as discussed above, rather than film redox chemistry. Although irreversible oxidation of aryl groups must change the molecular structure of the films to some extent, the grafted layers exhibit excellent stability to positive applied potentials in acetonitrile-electrolyte solutions.

5.4 Conclusion

This work demonstrates the first electrografting of organic films on PPF *via* electrooxidation of arylacetates. The technique is a versatile method for carbon modification when an acetic acid moiety can be neutralized to give an arylacetate group available on the modifier for electrografting. This offers an alternative approach when the desired diazonium salt derivative is unavailable. Multilayer organic films were formed on both GC and PPF from arylacetate derivatization under the experimental conditions applied here. As-prepared films dramatically reduced the apparent rate constant for electron-transfer to solution species. Although the grafted groups can be electrochemically oxidized, film thickness measurements and the voltammetric response of solution species demonstrated that the films maintain their integrity after positive potential polarization treatment at $\leq$ 2.0 V (*vs* Ag wire) in acetonitrile-electrolyte solution. On the other hand, polarization to potentials more negative than -1.8 V in the same medium led to significant changes in film properties. The film becomes effectively less blocking with the apparent rate constant for electron-transfer to solution species increasing to close to that for a bare, polished electrode. Moreover, this effect is not reversed when a positive potential is applied. In contrast, AFM analysis showed that there is a small decrease in film thickness, but this can be reversed by application of positive potentials attributed largely to film swelling/compaction behaviour. Hence films are not substantially removed by this negative polarization treatment (nor by positive polarization), and results are consistent with desorption of physisorbed, rather than covalently coupled modifier, leading to a film containing holes of nanometer dimensions.

5.5 References

1. Utley, J., *Chemical Society Reviews* **1997,** 26, 157.
2. Utley, J., *Chemistry & Industry* **1994,** 6, 215.
3. Moeller, K., *Tetrahedron* **2000,** 56, 9527.
4. Lund, H., *Journal of the Electrochemical Society* **2002,** 149, S21.
5. Andrieux, C. P.; Gonzalez, F.; Savéant, J.-M., *Journal of the American Chemical Society* **1997,** 119, 4292.
6. Andrieux, C. P.; Gonzalez, F.; Savéant, J. M., *Journal of Electroanalytical Chemistry* **2001,** 498, 171.
7. Coulon, E.; Pinson, J.; Bourzat, J. D.; Commercon, A.; Pulicani, J. P., *Langmuir* **2001,** 17, 7102.
8. Coulon, E.; Pinson, J.; Bourzat, J.-D.; Commercon, A.; Pulicani, J.-P., *Journal of Organic Chemistry* **2002,** 67, 8513.
9. Geneste, F.; Cadoret, M.; Moinet, C.; Jezequel, G., *New Journal of Chemistry* **2002,** 26, 1261.
10. Kariuki, J. K.; McDermott, M. T., *Langmuir* **1999,** 15, 6534.
11. Kariuki, J. K.; McDermott, M. T., *Langmuir* **2001,** 17, 5947.
12. Cui, X.; Jiang, D.; Diao, P.; Li, J.; Tong, R.; Wang, X., *Journal of Electroanalytical Chemistry* **1999,** 470, 9.
13. Diao, P.; Guo, M.; Jiang, D.; Jia, Z.; Cui, X.; Gu, D.; Tong, R.; Zhong, B., *Journal of Electroanalytical Chemistry* **2000,** 480, 59.
14. Ortiz, B.; Saby, C.; Champagne, G. Y.; Belanger, D., *Journal of Electroanalytical Chemistry* **1998,** 455, 75.
15. D'Amours, M.; Belanger, D., *Journal of Physical Chemistry B* **2003,** 107, 4811.
16. Saby, C.; Ortiz, B.; Champagne, G. Y.; Belanger, D., *Langmuir* **1997,** 13, 6805.
17. Ranganathan, S.; McCreery, R. L., *Analytical Chemistry* **2001,** 73, 893.
18. Downard, A.; Garrett, D.; Lehr, J.; Miskelly, G., *Journal of American Chemical Society* **2007,** 129, 15456.
19. Galicia, M.; Gonzalez, F. J., *Journal of the Electrochemical Society* **2002,** 149, D46.
20. Lund, H.; Baizer, M. M., *Organic electrochemistry : an introduction and guide* 3rd ed.; Marcel Dekker: New York 1991.
21. Brooksby, P. A.; Downard, A. J., *Langmuir* **2004,** 20, 5038.
22. Delamar, M.; Hitmi, R.; Pinson, J.; Savéant, J. M., *Journal of American Chemical Society* **1992,** 114, 5883.
23. Brooksby, P. A.; Downard, A. J., *Journal of Physical Chemistry B* **2005,** 109, 8791.
24. Combellas, C.; Delamar, M.; Kanoufi, F.; Pinson, J.; Podvorica, F. I., *Chemistry of Materials* **2005,** 17, 3968.
25. Anariba, F.; DuVall, S. H.; McCreery, R. L., *Analytical Chemistry* **2003,** 75, 3837.

26. Downard, A. J., *Langmuir* **2000,** 16, 9680.
27. Blankespoor, R.; Limoges, B.; Schollhorn, B.; Syssa-Magale, J. L.; Yazidi, D., *Langmuir* **2005,** 21, 3362.
28. Solak, A. O.; Eichorst, L. R.; Clark, W. J.; McCreery, R. L., *Analytical Chemistry* **2003,** 75, 296.
29. McDermott, M.; Rostami, A., *e-Journal of Surface Science and Nanotechnology* **2006,** 4, 419.
30. Fave, C.; Leroux, Y.; Trippe, G.; Randriamahazaka, H.; Noel, V.; Lacroix, J., *Journal of American Chemical Society* **2007,** 129, 1890.
31. Davies, T. J.; Moore, R. R.; Banks, C. E.; Compton, R. G., *Journal of Electroanalytical Chemistry* **2004,** 574, 123.
32. Lagrost, C.; Carrie, D.; Vaultier, M.; Hapiot, P., *Journal of Physical Chemistry A* **2003,** 107, 745.

Chapter 6. Carbon surface modification *via* photochemical reaction of alkene- and alkyne-modifiers, and photoactivation of organic films with oxalyl chloride

6.1 Introduction

Modifiers can be grafted to planar carbon surfaces through nonelectrochemical methods however these methods are relatively less common. The methods may employ thermal or light activation to induce coupling reactions with the carbon surface. Grafting of aromatic and aliphatic layers to graphitic carbon surfaces through thermal reaction of alkynes and alkenes have been reported.[1, 2] Thermal modification procedures generally involve heating the graphitic carbon surface immersed in deoxygenated neat liquids of the modifiers (alkene or alkyne) at temperatures above 160 ºC inside sealed vessels in the absence of air. Spectroscopic and voltammetric studies on these thermally attached films established that grafting occurred with formation of C-C bonds to the surface.[2] The mechanism of thermally assisted grafting of alkene and alkyne to graphitic carbon surfaces is unknown however it may occur *via* coupling reactions through surface radical-based reactions or Diels-Alder-type reactions. Surface carbon radicals have been reported to form by heat treatment of the surface under vacuum.[3] These radicals and/or carbene-like structures present within graphtic carbon may react with the alkene (or alkyne) modifiers *via* abstraction and/or insertion reactions in which covalent bonds can form between the modifier and the surface, respectively. Alternatively, coupling can occur between alkenes (and alkynes) with alkene-like functionality of graphitic carbon surface through Diels-Alder [4+2] and [2+2] cycloaddition reactions as depicted in Scheme 6.1.[4, 5] It is reasonable to expect that the carbyne-like structures that maybe present in graphitic carbon can also participate in Diels-Alder-type reactions. Films formed by thermal grafting of alkenes and alkynes are stable to ultrasonication in various solvents and to at least 100 voltammetric scans in acetonitrile-electrolyte solution[2] and hence are consistent with the formation of covalent bonds. Electrochemical and spectroscopic studies have established that these thermally grafted films have estimated surface concentrations indicative of monolayers and atomic force microscopy (AFM) data revealed that the films are approximately one molecular layer thick.[1, 2] Although the films appear to be close-packed monolayers, scrutiny of the reported AFM data support that these films are loosely packed monolayers.[2]

Scheme 6.1. Depiction of possible Diels-Alder-like reactions of alkene and alkyne with graphitic carbon surface. Reproduced with permission from reference 2.

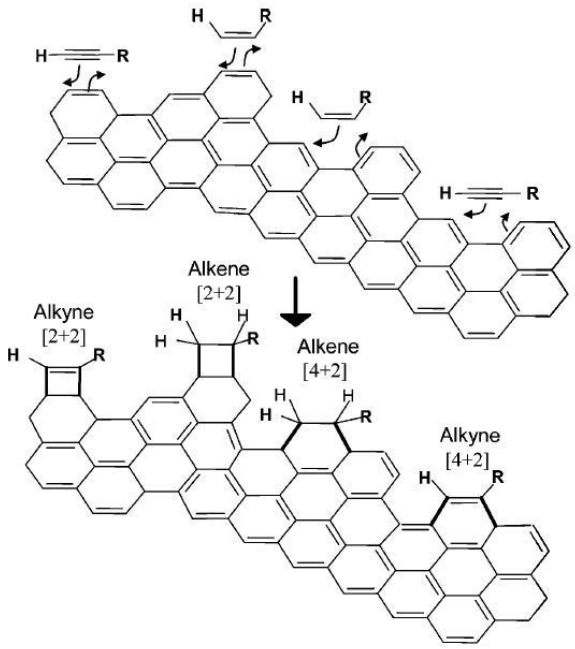

Photochemical reactions can also lead to grafting of modifiers to carbon surfaces and studies have shown that alkenes can be induced to react with hydrogen-terminated diamond[6-8], carbon nanofibers[9] and glassy carbon (GC).[10, 11] More recently, the photografting of alkenes on amorphous carbon films has also been reported.[12, 13] DC-magnetron sputtering was used to prepare carbon films, which were subsequently treated with radio frequency hydrogen plasma. The carbon substrate has a sp^2 carbon content of more than 85 %.[12] Spectroscopic analysis of the amorphous carbon film revealed an absence of any significant absorbance from C-H bonds and hence was assumed to contain relatively low hydrogen content. The modification procedure involved drop-coating the carbon surface with neat liquids of alkenes, most often with trifluoroacetic acid protected 10-aminodec-1-ene (TFAAD), which possesses a latent amine group at the terminus useful for further reaction.[12, 13] UV irradiation at 254 nm in a nitrogen-atmosphere for 12 h led to surface modification. Spectroscopic studies estimated a surface concentration of TFAAD of approximately 10 x 10^{-10} mol cm^{-2} grafted to amorphous carbon surface, which was claimed to indicate a close packed monolayer.[12] However, film thickness and morphology of the layers were not reported and hence the film structure of the layers are unknown. Hydrogen-terminated GC photografted with TFAAD was reacted with biotin to give a functional platform used to demonstrate frequency-dependent electrochemical impedance spectroscopy detection of

biotin-avidin binding. TFAAD was also photografted to amorphous carbon and used to immobilize DNA molecules. These DNA-modified surfaces were integrated into a quartz crystal microbalance (QCM) and used for real-time biosensing in the detection of complementary DNA sequence.[12] These photografted alkene surfaces are demonstrated to be a useful starting point for formation of amine-terminated surfaces for biomolecular immobilization applications.[10, 12]

While these reactions may appear similar to those well-established for the photografting of alkenes at hydrogen-terminated silicon[14-17] and diamond,[7, 18-21] many aspects of the mechanism of grafting to graphitic carbon remains unclear. Previous studies on diamond surfaces have reported that the functionalization reaction is initiated by the emission of photoelectrons (internal photoemission) from the surface into the liquid alkene layer.[7, 21] The overall grafting process can be divided into two stages: 1) the creation of a surface radical (or dangling bond) and 2) the subsequent reaction of the surface radical with alkene. In the case of diamond, the generation of a surface radical is associated with direct photoemission of an electron that forms an alkene-based radical anion in solution, and is unrelated to cleavage of C-H bonds at the surface.[7, 13, 21] The process is depicted in Scheme 5.2. A surface radical is generated when the alkene-based radical anion abstracts hydrogen from C-H bond at the surface.[7, 13, 21] Once such a surface-bound radical species is formed, propagation reactions can proceed by reaction of the radical species with additional alkenes (neutral or radical) similar to those for photochemical functionalization of silicon.[7, 13, 14, 21-23] Theoretical calculations and photocurrent experiments there show that graphitic carbon can also eject photoelectrons and hence the mechanism for photografting of alkenes to amorphous carbon is suggested to be the same as for diamond surfaces.[12, 13, 21] Note however, diamond is a sp^3 material whereas the amorphous carbon material was shown to be 85 % sp^2 carbon. In addition, the hydrogen content of the amorphous carbon material has been reported to be low (above) and hence grafting involving hydrogen abstraction-related reaction as the major pathway appears unlikely. Hence it seems surprising that the photografting mechanism could be the same for diamond and amorphous carbon.

Scheme 6.2. Proposed mechanism of surface grafting of alkene: (a) electron ejection and solution radical formation; (b) hydrogen abstraction from the diamond surface; (c) interaction of surface radical with another alkene in solution; (d) resulting surface-bound radical species. Reproduced with permission from reference 21.

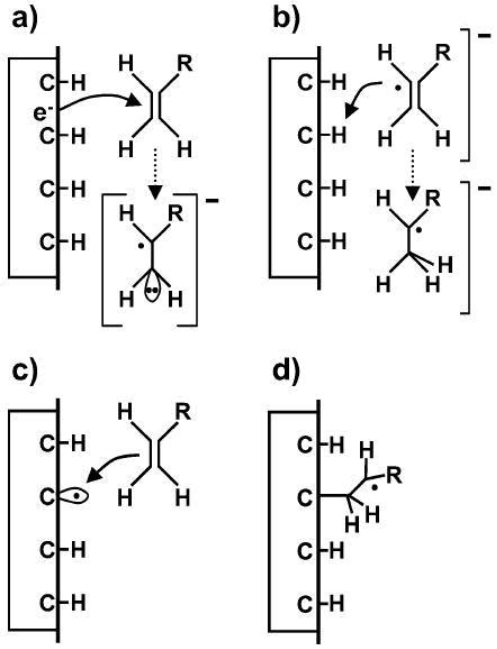

The preparation of carboxylic acid-terminated or other types of amine-reactive surfaces is of interest as an alternative starting platform to amine-terminated surfaces, which can be utilized for immobilization of molecular species. Hydrocarbons can be converted to amine-reactive species using oxalyl chloride. Oxalyl chloride has been utilized in organic synthesis to functionalize molecules such as cubanes with acid chlorides.[24, 25] Oxalyl chloride cleaves into chlorocarbonyl (and other) radicals under UV irradiation and the radicals readily insert into C-H bonds to give functionalities which include reactive acid chlorides. Equations 6.1 – 6.3 show the reported steps for the generation of radicals which subsequently lead to the formation of acid chloride derivatives and other products.[25] The photochemical procedure has been used to introduce acid chloride functionalities into alkyl terminated silicon surfaces by exposing the surface film to UV light and gaseous oxalyl chloride.[26] The photochemical reaction of oxalyl chloride to activate photografted surfaces to give a reactive interface for coupling amines is examined in this chapter.

$$Cl^{\bullet} + {}^{\bullet}COCOCl \Leftrightarrow (COCl)_2 + h\nu \Leftrightarrow 2({}^{\bullet}COCl) \quad (6.1)$$

$$RH + {}^{\bullet}COCl \rightarrow R^{\bullet} + CO + HCl \quad (6.2)$$

$$R^{\bullet} + (COCl)_2 \rightarrow RCOCl + {}^{\bullet}COCl \quad (6.3)$$

Mixed molecular layers are important in preparing platforms that contain multiple modifiers giving surfaces with specific functions, such as binding of protein and resistance to non-specific adsorption.[27] Important issues in platform design include the control over the spacing, orientation and density of the immobilized species on the surface. The self-assembly of thiols on gold surfaces is a widely used method for preparing mixed components on surfaces.[28-30] Thiol-based modifiers can be adsorbed to gold surfaces by immersing the surface in a mixture of thiols or by sequentially exposing the surface to a series of thiol solutions. However, these mixed layers suffer from disadvantages concerning the poor long-term stability of the system. Disadvantages include a tendency to desorb during electrochemical and temperature treatments.[31-33] Additionally, it is also difficult to control the amount of each component deposited when working with thiol mixtures with different adsorption rates. Alternatively, the electroreduction of mixtures of aryldiazonium ions has recently been used to prepare mixed layers in one-pot.[27, 34] The process forms covalent substrate-C linkages and hence stable electrografted films. The workers coupled electroactive molecular species, such as ferrocenemethylamine derivatives, to the mixed film and observed electron-transfer through the layer, demonstrating that the films are useful for electrochemical studies of immobilized redox centres.[34] However, it is difficult to control the amount of each component being deposited when working with a diazonium ion-mixture since the reduction of each species will occur at a different effective overpotential leading to different rates of surface grafting. A low coupling yield for amines (~ 10 %) to the mixed layer was found, which is undesirable for immobilization applications. The grafting of an aliphatic carboxylic acid derivatives and acid chlorides may lead to higher amounts of immobilized amine on carbon surfaces and are of interest.

The aim of this chapter is to explore the photografting of alkene- and alkyne-modifiers to GC and PPF surfaces, without prior treatment with hydrogen plasma. The simple approach of using polished GC and as-prepared PPF samples, spin-coating with modifier and photolyzing in air is used. Film properties will be investigated and have been characterized by contact angle measurements, atomic force microscopy (AFM) and electrochemistry. This work also aims to investigate the photochemical preparation of different types of films that react with amines, in high yield, for potential use as amine-reactive interfaces. The investigated methods include activation of films with oxalyl chloride. The preparation of mixed layers *via* electroreduction of aryldiazonium ions in combination with photochemical methods is also explored.

6.2 Experimental Section

6.2.1 Materials and reagents

1-decene, *1H, 1H, 2H*-perfluoro-1-decene, 1-ethyl-3-(-3-dimethylaminopropyl) carbodiimide hydrochloride (EDC) (all Alfa Aesar), N-hydroxysuccinimide (NHS), ethyl decylenate, 1-undecylenic acid, 4-decylaniline (all Sigma-Aldrich), ethynylferrocene (Acros Organics), ethylene diamine (en), oxalyl chloride (both Merck), 4-nitro-4-aminoazobenzene (NAAB) (AnalaR, BDH) were used as received. The tetrafluoroborate salts of 4-carboxybenzenediazonium and 4-decylbenzenediazonium were synthesized using standard procedures (Chapter 2).

6.2.2 Electrochemistry

An O-ring was used to define the geometric area of the working electrode (0.26 cm^2 for electrode modification and 0.12 cm^2 for subsequent scans at the modified surface). Cyclic voltammograms of $Fe(CN)_6^{3-}$ (5 mM in 0.1 M KCl aqueous solution) were obtained with scan rate (v) = 200 mV s^{-1}.

6.2.3 Modification of carbon surfaces

For the standard photografting procedure, cleaned carbon surfaces were spin-coated with two coats of the neat alkene, or alkene or alkyne dissolved in acetonitrile solution (1000 rpm for 30 s). Based on the density of neat alkene and the mass deposited (approximately 3.2 mg over a surface area of 225 mm^2), the volume spin-coated was approximately 2 μL. Unless stated otherwise, samples were irradiated at 254 nm inside a Rayonet Srinivason-Griffin photochemical reactor (equipped with six RPR 2537 Å reaction lamp tubes) for 1 h at room temperature in air. The treated samples were ultrasonicated in acetonitrile for 30 s and dried with N_2 before characterization.

Electrochemical modification of carbon surfaces was carried out in acetonitrile + 0.1 M $TBABF_4$ solutions containing 2 mM 4-carboxybenzenediazonium tetraflouroborate or 3 mM decylbenzenediazonium tetraflouroborate. The standard modification procedure involved two initial scans from 0 V to E_f at 200 mV s^{-1}, followed by electrolysis at (E_f – 150) mV. Electrolysis time was 300 s and E_f was -0.45 V for 4-carboxybenzenediazonium salt, and 600 s and -0.40 V for 4-decylbenzenediazonium salt.

6.2.4 Photoactivation with oxalyl chloride

Modified carbon surfaces were photochemically activated by drop-coating with 4 drops of neat oxalyl chloride solution and irradiating at 254 nm inside a Rayonet photoreactor for 30 min. The treated samples were then sonicated in acetonitrile solution for 30 s and dried with N_2.

6.2.5 Preparation of mixed layers

Mixed layers were prepared on PPF in a stepwise fashion first by photografting 1-undecylenic acid, which was spin-coated with 200 mM of 1-undecylenic acid and the surface was photolyzed in air for 1 h in a Rayonet reactor. The photografted surface was then electrochemically modified by electroreduction of 0.6 mM 4-NB diazonium tetraflouroborate dissolved in acetonitrile + 0.1 M $TBABF_4$. One voltammetric scan at 200 mV s^{-1} from 0.2 to -0.5 V was performed for the electroreduction.

6.2.6 Coupling of amines to modified surfaces

Amines were coupled to the acid chloride derivatized (photoactivated by oxalyl chloride) surfaces by incubating the modified surfaces in stirred acetonitrile solutions of en (20 mM) for 1 h, or NAAB (4 mM) for 18 h. Carboxylic acid derivatized surfaces were incubated in a stirred acetonitrile or PBS solution of either en (20 mM) or NAAB (4 mM), containing EDC (20 mM) and NHS (4 mM) for 18 hr. All samples were then sonicated for 30 s in acetonitrile or PBS solution and dried with N_2.

6.2.7 Assembly of gold nanoparticles

Gold nanoparticles were assembled on amine-terminated modified PPF surfaces by incubation in an as-prepared nanoparticle solution for 30 min followed by thorough rinsing with Milli-Q water and drying with N_2.

6.3 Results & Discussions

6.3.1 Preparation, water contact angle measurements and electrochemistry of photografted surfaces

Figure 6.1 shows the alkenes and alkyne utilized for photochemical modification and diazonium modifiers used in the study. **1** (1-decene), **3** (ethyl-10-undecylenate) and **4** (*1H, 1H, 2H*-perfluoro-1-decene) were spin-coated as the neat liquids and **2 (**1-undecylenic acid) and **5** (ethynylferrocene), solids at room temperature, were dissolved in acetonitrile giving 200 mM and 50 mM solutions, respectively. Two coats of the neat alkene or dissolved alkene/alkyne were spin-coated at 1000 rpm for 30 s to cover the carbon surface.

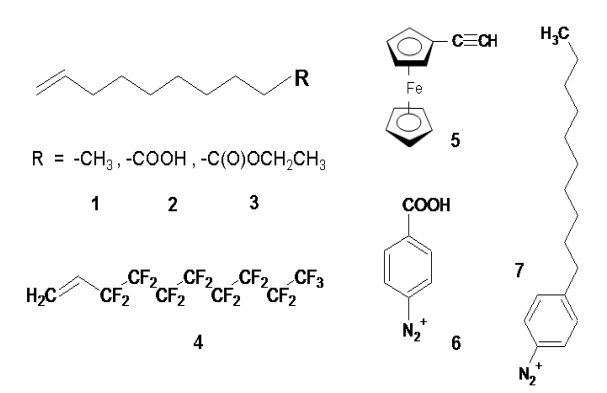

Figure 6.1. The alkenes and alkyne photografted to carbon surfaces, and diazonium cations used for electrochemical grafting. (**1**) 1-decene, (**2**) 1-undecylenic acid (**3**) ethyl-10-undecylenate (**4**) *1H, 1H, 2H*-perfluoro-1-decene (**5**) ethynylferrocene, (**6**) 4-carboxydiazonium ion and (**7**) decylbenzenediazonium ion.

In preliminary experiments, the basic conditions for achieving grafting of alkene to a carbon surface were established. Four pieces of polished GC plate were immersed in **1** (Figure 6.1), as the neat liquid, giving a solution thickness of approximately 1 mm above the surface. A second set of four samples was prepared by spin-coating **1** onto GC plates. Both sets of samples were irradiated at 254 nm, in air, inside a Rayonet reactor for photolysis times ranging from 1 to 9 h. Water contact angles were measured at 1, 3, 6 and 9 h intervals, giving the data shown in Figure 6.2. Note that each data point corresponds to one GC sample. Figure 6.2a shows the measured contact angles *vs* photolysis time for samples photolyzed in liquid. The samples exhibit a steady increase in contact angle from 50 º on the polished GC surface to 64 º after 9 h irradiation, indicating a more hydrophobic surface, which is

consistent with the grafting of **1** to the surface. The gradual change in contact angle is suggests that grafting is a slow process in liquid. Spin-coated samples gave a maximum contact angle of 68 º after 1 h irradiation and then a gradual decline in contact angle to 58 º after 9 h (Figure 6.2b). There appears to be a more rapid initial rate of surface attachment for the spin-coated samples. Assuming that the radicals are generated at the surface (see later), for samples photolyzed in the thicker layer of liquid, the radicals can diffuse further away from the surface whereas the radicals are more confined to the surface for spin-coated samples. The gradual decrease in contact angle observed for spin-coated samples (Figure 6.2b) may be a result of a film degradation process possibly by reaction with ozone occurring after prolonged irradiation of the surface film.[35, 36] Control samples of GC irradiated for 1 and 9 h in the absence of alkene did not show a change in contact angle indicating no significant oxidation of the surface. Samples that were spin-coated with alkene and protected from UV irradiation also showed (after ultrasonication) no change in contact angle, indicating UV light is necessary for grafting. A photolysis time of 1 h with spin-coated samples was adopted as the standard procedure for grafting alkenes.

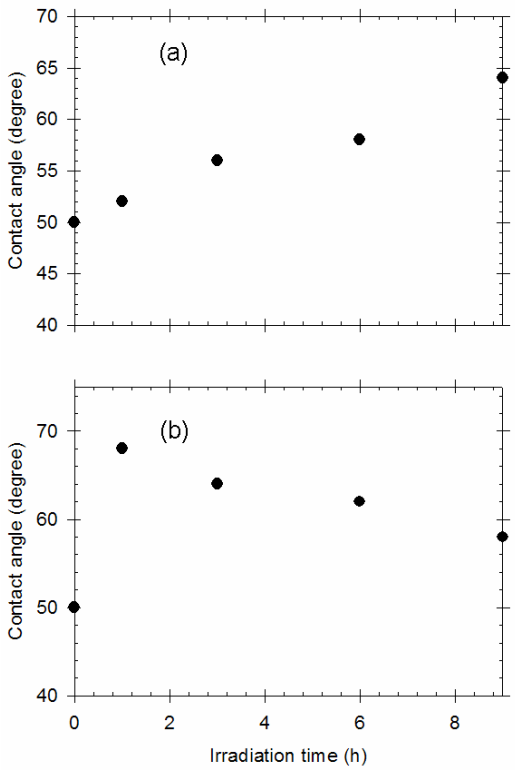

Figure 6.2. Plot of static water contact angle *vs* photolysis time for GC samples a) immersed in **1** and b) spin-coated with **1**.

The changes in the water static contact angles measured on bare and photografted GC and PPF surfaces for all modifiers are listed in Table 6.1. Films were prepared by standard procedures (Section 6.2), which involve spin-coating the selection of modifiers on the surface and irradiating with UV light for 1 h. The contact angle changes indicate that grafting has occurred for all modifiers and the changes are consistent with the expected chemical nature of the end groups of the modifiers. However, the measured angles are lower than the reported water contact angles of long chain alkanes with the same end groups assembled on gold or silicon surfaces. This may be the result of degradation of the alkene-derived layer after prolonged photolysis (above) and/or related to the texture of the layer (the effect of surface roughness on wettability was described in Section 3.3.4), which can influence the resultant contact angles of the film. Hence the lower contact angles measured on alkene layers may indicate that the photografted films are not close-packed.

Table 6.1. Static water contact angles on blank and photografted GC and PPF surfaces. Samples were prepared using standard procedures.

	modifier					
	none	**1**	**2**	**3**	**4**	**5**
contact angle (°) on GC	50 ± 2 (n = 5)	68 ± 2 (n = 5)	50 ± 2 (n = 5)	-	75 ± 2 (n = 2)	53 ± 2 (n = 5)
contact angle (°) on PPF	68 ± 2 (n = 5)	78 ± 2 (n = 2)	55 ± 2 (n = 2)	57 ± 2 (n = 2)	73 ± 2 (n = 2)	78 ± 2 (n = 2)
literature values		108 ± 2[a]	65[b], 79[c]	82 ± 4[d]	91 ± 1[e]	71 ± 2[f]

[a] 1-decene on silicon[17]; [b] undecylenic acid on silicon[37]; [c] undecylenic acid on silicon[17]; [d] ethyl undecylenate on silicon[38]; [e] 11-fluoro-1-decene on silicon[17]; [f] 2-aminoethylferrocenylmethylether coupled to decylenic acid on silicon.[39]

Photografting of ethynylferrocene, **5** (Figure 6.1), to GC and PPF surfaces was also examined using spin-coated samples. Spin-coated GC samples were photolyzed for 0.5, 1 and 2.5 h and the grafted surfaces examined using cyclic voltammetry. Figure 6.3a shows cyclic voltammograms (first scan and 27th scan), recorded in acetonitrile-electrolyte at v = 2 V s^{-1} of a GC surface photolyzed for 2.5 h. The expected chemically reversible Fc/Fc^{+} couple is clearly observed in the cyclic voltammogram with $E_{1/2}$ = 0.65 V *vs* Ag wire. A control sample, which was spin-coated with **5**, was stored in the absence of UV for 2.5 h and ultrasonicated in acetonitrile prior to electrochemical interrogation, showed no redox features in the same region. At the photolyzed surfaces, the voltammetric peak areas decrease over

the first five scans and then remain approximately constant during subsequent scans, consistent with attachment of the alkyne to the surface. Modified surfaces that had been scanned at least 5 times between 0 and 0.9 V, were scanned in acetonitrile-electrolyte solution at different scan rates. Figure 6.3b shows a linear relationship between the measured area of the cyclic voltammetric peaks and scan rate, as expected for surface-bound species.[40] Although the response clearly arises from immobilized species, the voltammograms do not show the theoretical peak widths or ΔE_p values for an electrochemically reversible surface-confined species. Several factors may contribute to this response: an inherently slow rate of electron transfer at this GC surface;[34] uncompensated *iR* drop; and nonequivalent environments for the grafted Fc groups, leading to a range of formal potentials.[41, 42]

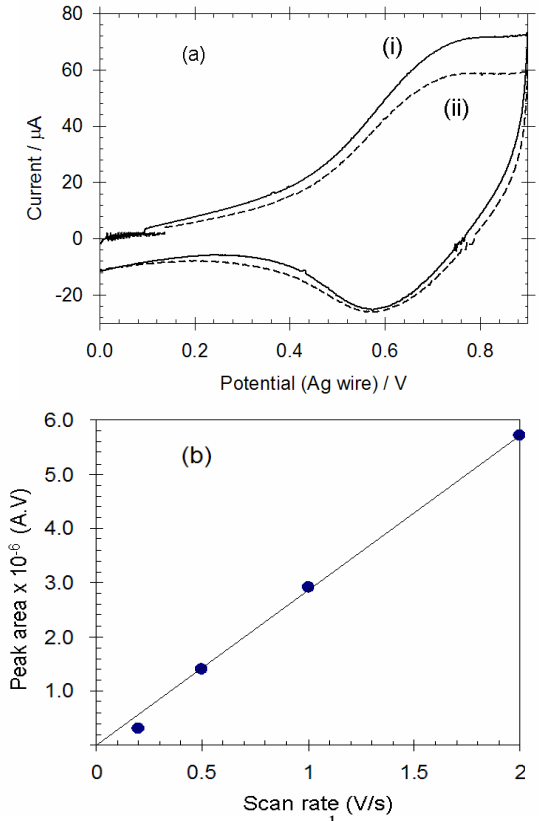

Figure 6.3. a) Cyclic voltammograms (v = 2 V s^{-1}) obtained in blank acetonitrile-electrolyte solution after 2.5 h photolysis of a GC surface spin-coated with **5**. i) 1st scan and ii) 27th scan. b) Plot of peak area *vs* scan rate, obtained in blank acetonitrile-electrolyte, for a GC surface spin-coated with **5** and photolyzed for 2.5 h.

The effect of photolysis time on surface concentration of Fc groups grafted to GC was monitored by calculating the surface concentration of Fc groups from the first cyclic voltammetric scan recorded at each photolyzed surface. The surface concentration data are shown and Table 6.2. The data show that the surface concentration on GC increases at a

decreasing rate as photolysis time increases and reaches a surface concentration value of approximately 3.6±0.7 x 10^{-10} mol cm^{-2} after 2.5 h of photolysis. Similarly, the same highest surface concentration value (within experimental uncertainty) is obtained after 2.5 h photolysis of spin-coated PPF samples and hence 2.5 h was chosen as the standard photolysis time for the alkyne modifier. This surface concentration value is similar to those obtained for thiol-based Fc modifiers self-assembled on gold surfaces (4-5 x 10^{-10} mol cm^{-2}).[43, 44] Those films are confirmed to be monolayers but a similar structure cannot be assumed for the photografted films in this work. Further experiments were carried out using PPF to investigate the structures of the photografted films and the results are presented in Section 6.3.4.

Table 6.2. Surface concentration of photografted ethynylferrocene at GC and PPF surfaces determined from first cyclic voltammetric scans.[a]

substrate	photolysis time min	surface concentration mol cm^{-2}	v V/s	solvent-electrolyte
GC	30	1.9 x 10^{-10} (n = 2)	0.2	aqueous 0.1 M $NaClO_4$
GC	60	3.0 x 10^{-10} (n = 3)	0.2	aqueous 0.1 M $NaClO_4$
GC	150	3.3 x 10^{-10} (n = 3)	0.2	aqueous 0.1 M $NaClO_4$
GC	150	3.9 x 10^{-10} (n = 2)	1	ACN-0.1 M $TBABF_4$
PPF	150	3.6 x 10^{-10} (n = 2)	1	ACN-0.1 M $TBABF_4$

[a] Each surface was a separate sample

The stability of these surfaces photografted with alkene and alkyne modifiers to ultrasonication and electrochemical analysis in various solvents suggests that the photografted layers are strongly bonded to the surface and hence is consistent with the formation of a C-C bond between the carbon surface and the film.

6.3.2 $Fe(CN)_6^{3-}$ redox probe examination at photografted surface

The blocking properties of surfaces photolyzed with **1** were examined using $Fe(CN)_6^{3-}$ as the redox probe. Cyclic voltammetric scans of $K_3Fe(CN)_6$ (5 mM in 0.1 M KCl) were collected at GC surfaces photolyzed for 1 and 9 h, after spin-coating with **1**. Figure 6.4

shows that at the surface photolyzed for 1 h, ΔE_p is larger (270 mV) and peak currents are smaller than at polished GC (ΔE_p = 200 mV) (The large ΔE_p value at polished GC is due to slow heterogeneous electron transfer kinetics at this GC surface, and also in part to uncompensated *iR* drop arising from the relatively large current). The small changes in the voltammogram at the grafted surface indicate that the photografted film is relatively thin and/or non-compact containing pinholes, which allow the redox probe to diffuse into the film and approach close to the GC surface. Additonal experiments showed that there were no further changes in the voltammograms when the photolysis time was extended from 1 to 9 h indicating that an increase in exposure time did not result in more grafting. This finding is consistent with the contact angle results. When the experiment was repeated with photolysis in liquid **1** (t = 9 h)**,** voltammograms recorded at the photolyzed surfaces were indistinguishable from those recorded at the polished surface, suggesting that the resultant surface film is thinner or less compact than the spin-coated samples. Hence the changes observed in the voltammograms of $K_3Fe(CN)_6$ (Figure 6.4) are consistent with formation of a partially blocked surface[45] and indicate that the amount of grafting is greater at spin-coated surfaces than at those immersed in liquid. This also suggests that the alkene layers photografted on carbon surfaces prepared by both approaches are loosely packed.

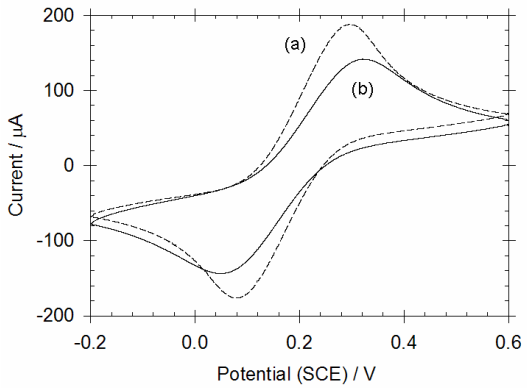

Figure 6.4. Cyclic voltammograms of 5 mM $K_3Fe(CN)_6$ + 0.1 M KCl obtained at GC: scan a) polished and scan b) after 1 h photolysis of surface spin-coated with **1**.

6.3.3 XPS examination of photografted surface

XPS survey spectra were obtained for two GC samples photografted with alkene **4**, giving the data shown in Table 6.3. There is good reproducibility between the samples, confirming reproducible grafting of **4**. The presence of a strong F peak at ca. 689 eV in the survey spectra confirms the attachment of **4**.[12, 13, 21] In contrast, no F signal was observed at

polished GC. The F:C ratio is between 0.03-0.04, which is less than predicted for films of **4.** The F:C ratio is also slightly less than that reported for TFAAD films grafted on hydrogen-terminated diamond and amorphous carbon surfaces (< 0.05).[12, 13, 21] This is mostly likely because there is a significant contribution to the C peak from the underlying GC surface. Table 6.3 shows that there is no significant increase in % O for photografted surfaces compared with polished GC, hence the GC surface does not appear to undergo detectable oxidation during photolysis in air. This is consistent with water contact angle measurements, which showed no change significant change in wettability after photolysis of a polished GC surface in the absence of modifier.

Table 6.3. Normalized atomic % of F, C and O obtained from XPS core level spectra for GC surfaces photografted with **4**.

		atomic %		
samples	sample	F	O	C
GC photografted with **4**	1	3.3	9.7	87
GC photografted with **4**	2	2.6	10.2	87.2
Polished GC [a]	3	--	9.3	88.9

[a] sample 16 presented in Chapter 4. GC cycled six times between 0 and 1.2 V at 100 mV s^{-1}, in acetonitrile-electrolyte solution.

6.3.4 AFM examination of photografted surfaces

The structure of surface films prepared by photografting of alkenes on PPF surfaces was investigated with AFM. Thicknesses of the grafted layers were measured by AFM depth profiling. Table 6.4 shows the data obtained for each modifier and lists the calculated molecular length of each modifier. As shown in Table 6.4, 1 h photografting of alkenes **1 - 3** gives surface films with average thickness ranging between 0.5 and 0.7 nm. Based on the relevant molecular dimensions, vertically aligned monolayer films of the alkenes are expected to be 1.2 to 1.5 nm thick, and even with significant tilt angles, the thicknesses of well-ordered monolayers of **1 - 3** would be greater than those observed. Considering that the average surface roughness values are close to the average thicknesses of these films, it is evident that the films are best described as loosely packed monolayers. This is confirmed by comparison of the topography and line profiles across modified surfaces and bare PPF (Figure 6.5). Modification with alkenes **1 – 3** greatly increases the surface roughness; there is a large increase in the peak-to-peak height variation as would be expected for loosely packed

monolayer films. A film of **2** was also prepared by photolyzing a spin-coated sample for 9 h. The measured water contact angle, average film thickness and surface roughness for this film was found to be the same, within experimental uncertainty, as for films prepared with 1 h photolysis using the standard procedures. This confirms that the film coverage cannot be increased by longer photolysis time and is consistent with the contact angle and electrochemistry results described earlier. As a comparison, Hamers and coworkers using XPS reported the formation of close packed monolayers from the photolysis of TFAAD modifiers to hydrogen-terminated amorphous carbon surfaces in the absence of air. However, thickness measurements of the film were not reported and hence the packing density and film structure is unknown and may likely be loosely packed. Allongue and coworkers studied the electrochemical grafting of aryldiazonium ions with alkyl *para* substitutents of $-(CH_2)_nR$ (n = 0-12) at hydrogen-terminated silicon surfaces.[46] The workers found that the surface concentration of grafted groups decreased as n increased, and proposed that long alkyl chains of attached modifiers screen vacant surface binding sites. The same effect may lead to low packing densities for the films prepared from aliphatic alkenes in this work.

In contrast to the results for films of **1** - **3**, AFM depth profiling of films of **4** and **5** gave thicknesses greater than expected for monolayer films. Figure 6.5, bottom panel shows the line-profiles recorded for films of **4**. As shown in Table 6.4, the average film thickness for **4** is 2.1 nm, which corresponds to between one and two molecular layers (assuming vertical alignment of the modifier). Photografting of **5** forms films that have an average thickness of 3.0 nm corresponding to a minimum arrangement of five molecular layers (AFM depth profiling was undertaken prior to electrochemical analysis). Considering the average roughness values and AFM line-profiles, these films appear to be loosely packed and multilayered in structure. A film of **5** was also re-examined with AFM after voltammetric scans in acetonitrile-electrolyte solution to determine the amount of Fc groups. The film was found to have the same thickness and roughness as the films prior to voltammetric measurements (Table 6.4). This result confirms that the film is stable to voltammetric scans in blank electrolyte with no large-scale loss of film material from the surface. The small decrease in the peak current for a film of **5** upon voltammetric scanning (Figure 6.4) is indicative of a partial loss of Fc electroactivity during scans to 0.9 V. This may be attributed to irreversible electrooxidation of some surface-bound Fc groups or reorientation of the Fc groups leading to electroinactivity of the groups within the film environment.[44]

Table 6.4. Average film thickness and surface roughness, calculated from two independent samples, of photografted PPF surfaces, and the calculated molecular lengths of the modifiers. Samples were prepared using standard procedures.

	modifier							
	none	**1**	**2**	**2**[a]	**3**	**4**	**5**[b]	**5**[c]
Av. film thickness (nm)	-	0.7	0.5	0.4	0.5[d]	2.1	3.0	3.1
Av. surface roughness (nm)	0.27	0.44	0.50	0.54	0.43	0.8	1.1	1.0
molecular length (nm)	-	1.2	1.3	1.3	1.5	1.3	0.6	0.6

[a] photolysis time was 9 h, water contact angle was 52 °; [b] spin-coated sample photolyzed for 2.5 h; data obtained prior to cyclic voltammetric measurements; [c] data obtained after cyclic voltammetric measurements; [d] ± 0.3 nm

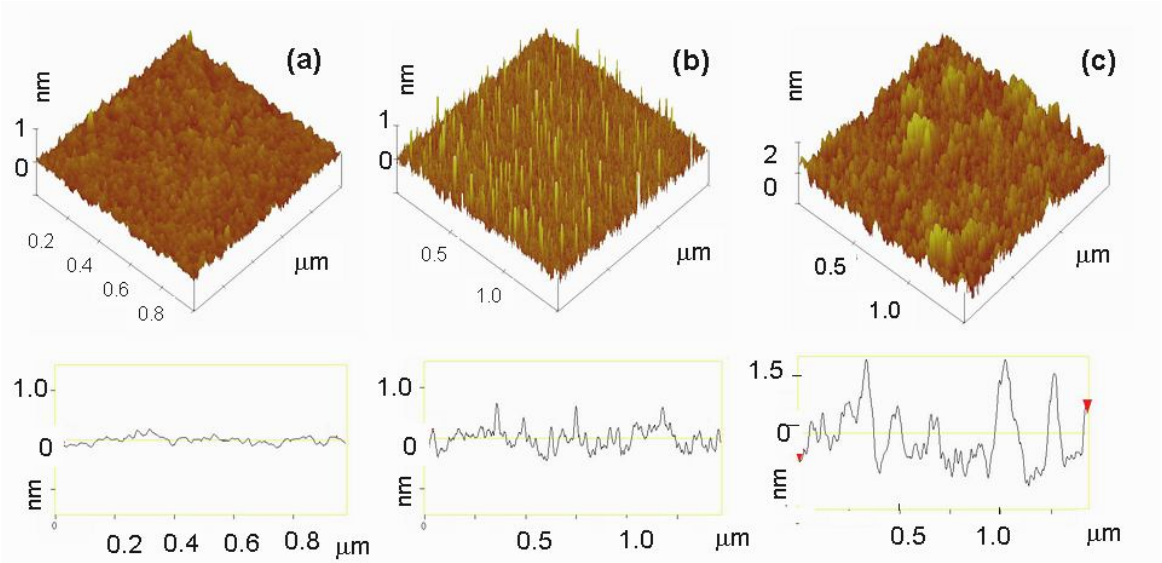

Figure 6.5. AFM topographical images and line profiles of a) bare PPF, b) PPF after photografting of **1** and c) PPF photografting of **4**.

As described earlier, the surface concentration of Fc groups in films of **5** prepared with 2.5 h photolysis was determined electrochemically to be approximately 3.6±0.7 x 10^{-10} mol cm^{-2} (Table 6.2). Hence each 'monolayer equivalent' in the 3 nm thick film of **5** has a maximum average surface concentration of Fc groups of approximately 0.7±0.1 x 10^{-10} mol cm^{-2}. The calculated surface concentration of an ideal close-packed monolayer of ferrocenylalkanethiol groups on a planar surface is 4.5 x 10^{-10} mol cm^{-2}, which is consistent with the surface concentration for monolayers of thiol-based Fc modifiers self-assembled on gold (4-5 x 10^{-10} mol cm^{-2}).[43, 44] Hence each monolayer-equivalent in the film of **5,** has a maximum ~ 16 % of a close-packed coverage of Fc groups, which confirms that the film is loosely packed. These photografted multilayered films have a lower film density than films

prepared by the reduction of aryldiazonium ions, which have film densities ranging between 21 and 34 %, as previously described in Chapter 3.[47] This may suggest photografting reactions at the surface are less efficient than electroreduction of aryldiazonium ions.

6.3.5 Photoactivation of modified surfaces with oxalyl chloride.

The preparation of amine-reactive surfaces with the use of oxalyl chloride as an activating agent was investigated by exposing alkyl terminating films to oxalyl chloride and UV light. Oxalyl chloride cleaves into chlorocarbonyl (and other) radicals under UV irradiation and the radicals readily insert into C-H bonds to give functionalities, which include reactive acid chlorides as described in Equations 6.1-6.3 (Section 6.1).[25] This photoactivation method was investigated with films of **1**, which were photografted to GC and PPF surfaces using the standard procedure to give alkyl-terminated films. Photografted samples were drop coated with oxalyl chloride and photolyzed further for 30 min. The derivatization of films of **1** with acid chloride groups was demonstrated by reacting the treated surfaces with the amines (Equation 6.4), ethylenediamine (en) and 4-nitro-4-aminoazobenzene (NAAB), giving surfaces abbreviated as carbon-**1**-en and carbon-**1**-NAAB, respectively.

$$\text{Surface-modifier-COCl} + \text{R-NH}_2 \rightarrow \text{Surface-modifier-CONHR} + \text{HCl} \qquad (6.4)$$

A GC sample photografted with **1** and treated with oxalyl chloride and irradiated with UV light was analyzed by contact angle measurements before and after incubation in en. A decrease in contact angle from 68 º for a film of **1** grafted to GC, to 55 º for GC-**1**-en is consistent with coupling of en (Films of en electrochemically grafted to GC have reported water contact angles of 48 º).[48] The presence of en in PPF-**1**-en films was also decisively demonstrated by the assembly of citrate-capped gold nanoparticles and SEM imaging. The micrographs in Figure 6.6 and the data in Table 6.5 reveal a large increase in nanoparticle density, from ~ 40 particles/μm^2 on the film of **1** prior to reaction, to ~ 370 particles/μm^2 after photoactivation with oxalyl chloride and reaction with en. This is consistent with the electrostatic interaction of the anionic citrate-capped gold nanoparticles with the film amine groups, which would be largely protonated at the pH of the nanoparticle solution (pH 4.2).[49] In the absence of favourable electrostatic interactions, very few nanoparticles assemble on

the film of **1**. Control samples prepared by incubating PPF-**1** in an acetonitrile solution of en, and PPF-**1** that was treated with oxalyl chloride in the absence of UV irradiation, were treated with gold nanoparticle solution, leading to particle-densities of no more than 50 particles/μm^2 (Table 6.5). This result confirms that en couples to the grafted film only after oxalyl chloride photo-treatment. For comparison, PPF was also photografted with **2** giving a surface terminated with carboxylic acid groups, was also reacted with en and EDC and NHS as coupling agents. The surface was cleaned and then incubated in citrate-capped gold nanoparticle solution. SEM microscopy revealed a particle-density of approximately 470 particles/μm^2. The particle-count on PPF-**2**-en is slightly higher than PPF-**1**-en surfaces (~ 370 particles/μm^2). This may suggest that the density of acid chloride groups available for reaction with en is lower than that of carboxylic acid groups possibly due to the hydrolysis of the acid chloride moieties by adventitious water. Another possibility is that reaction of both amines of en with acid chloride moieties may reduce the amines available for gold nanoparticle assembly.

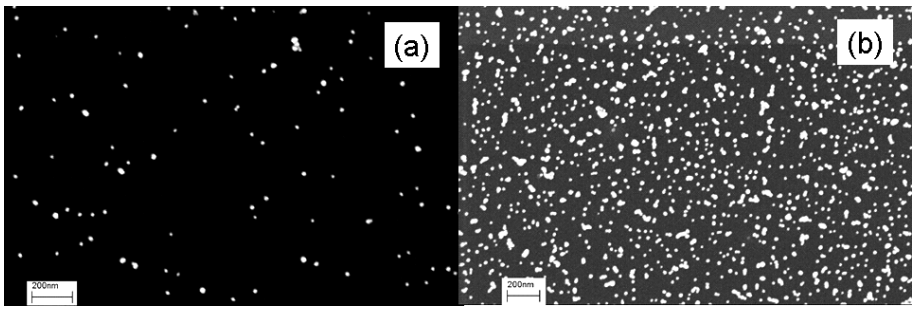

Figure 6.6. SEM images, after incubation in a solution of citrate-capped gold nanoparticles, of a) film of **1** photografted to PPF and b) PPF-**1**-en.

Reaction of oxalyl chloride and NAAB with films of **1** did not lead to contact angle changes however the success of the reactions was established by examining the voltammetry of the modified electrodes. Figure 6.7 (scan a) shows that when the GC-**1**-NAAB surface is scanned in PBS, there is a well-defined irreversible reduction peak at $E_{p,c}$ ~ -1.1 V, which can be assigned to reduction of the nitroaryl group (Chapters 3 and 4). The electroreduction proceeds with the transfer of 6 electrons to give the amine product (Equation 3.1a), or by 4 electrons to give the hydroxylamine product (Equation 3.1b).[50, 51] The hydroxylamine product can be oxidized on the return scan (Equation 3.1c), giving the broad oxidation peak at $E_{1/2}$ ~ 0.1 V.

Table 6.5. Density of gold nanoparticle assembly on film-modified PPF surfaces.

samples	particle density[a] np/μm^2
PPF	40
PPF[b]	20
PPF[c]	40
PPF-1	40
PPF-1[b]	44
PPF-1[c]	44
PPF-1-en	370
PPF-2	50
PPF-2-en	470
PPF-DP[b]	40
PPF-DP-en	600
PPF-NP	40
PPF-(2, NP)-en[d]	410

[a] an estimated uncertainty of approximately 15 % is associated with each particle-density value
[b] surface treated with oxalyl chloride only (without UV irradiation)
[c] surface treated with oxalyl chloride and incubated with en for 1 h (without UV irradiation)
[d] mixed layer photografted with **2** and subsequently electrografted with 4-NB diazonium ion

Voltammetric analysis of the nitroaryl signal of NAAB coupled to photoactivated films of **1** gave an average surface concentration of approximately 16.7±3 x 10^{-10} mol cm^{-2}. In contrast, as shown in Figure 6.7 (scan b), no redox processes are observed in a similar potential range for films of **1**, which have not been reacted with oxalyl chloride and NAAB. Similarly, the control surface prepared by treatment of polished GC with oxalyl chloride (in the absence of UV irradiation) and NAAB did not exhibit any redox chemistry.

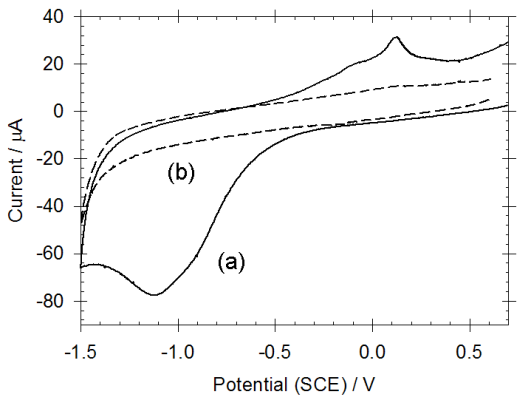

Figure 6.7. Cyclic voltammograms (v = 200 mV s^{-1}) recorded in PBS of (a) film of **1** photografted to GC and (b) GC-**1**-NAAB.

The reactivity of films of **2** on GC was compared with that of oxalyl chloride activated films of **1**, by reacting films of **2** with NAAB in the presence of EDC and NHS coupling agents under both aqueous and nonaqueous conditions. Assuming quantitative amide formation with all surface carboxylic acid groups, these results enable an estimate of the surface concentration of **2**. The average amount of coupled NAAB product was determined to be approximately $4.8 \pm 1 \times 10^{-10}$ mol cm^{-2} for the aqueous reaction while, for the nonaqueous reaction, an approximate average value of $9.4 \pm 2 \times 10^{-10}$ mol cm^{-2} was obtained. As expected, nonaqueous conditions favoured the desired coupling reaction due to the absence of competing reactions from the solvent (i.e. water). The surface concentration of **2** ($\sim 9.4 \times 10^{-10}$ mol cm^{-2}) is similar to that estimated for TFAAD alkene-derived films photografted on amorphous carbon (10×10^{-10} mol cm^{-2}).[52] This suggests that films of similar structures are formed on the two different types of graphitic carbon surfaces. A higher amount of NAAB was found to couple to photoactivated decene-derived films (GC-**1**-NAAB) than to carboxylic acid terminated films (GC-**2**-NAAB). This is attributed to the inherently more reactive acid chloride groups and also the possibility of more than one acid chloride group being formed per modifier within the film. Hence photoactivated films contain more anchoring points available for coupling with NAAB compared to surfaces photografted with **2**.

6.3.6 Comparison of amine-reactive photografted and activated films with films electrografted by reduction of aryldiazonium ions

Aryldiazonium ion-derived films, in particular carboxyphenyl (CP) films have been commonly used with EDC and NHS coupling agents for subsequent coupling reactions with amines,[27, 34] and hence form an interesting comparison with photografted and photoactivated films. Using the same conditions as for reaction with photografted films, NAAB was also reacted with CP films, prepared by electroreduction of 2 mM 4-carboxybenzenediazonium salt (**6**) in acetonitrile at GC surfaces. CP films were generated with standard methods using an applied potential of $E_{app} = E_{p,c} - 150$ mV for 300 s (Section 3.2). The CP film has a measured contact angle of approximately 30 ^{o}, consistent with the formation of a carboxylic acid terminated film grafted at the surface.[53] As expected, upon coupling with NAAB, the contact angle increases to approximately 41 ^{o}, consistent with the addition of a relatively more hydrophobic molecular species, to the film surface. The voltammetric response of

coupled NAAB in aqueous and nonaqueous reaction conditions was evaluated, giving an average surface concentration of approximately 5 ± 1 x 10^{-10} mol cm^{-2}, for all CP films. Henec reaction in the different media gives very similar results for the coupling conditions of NAAB to CP films (Table 6.6).

Table 6.6. Grafting methods at GC, conditions used for coupling NAAB to the film, and surface concentration of NAAB.

surface	film	grafting	oxalyl chloride	coupling medium	surface concentration (mol cm-2)	*n*
1	**2**	UV	no	aqueous	5 x 10^{-10}	4
2	**2**	UV	no	acetonitrile	9 x 10^{-10}	4
3	**1**	UV	yes	acetonitrile	17 x 10^{-10}	5
4	DP	electroreduction	yes	acetonitrile	7 x 10^{-10}	4
5	CP	electroreduction	no	aqueous	5 x 10^{-10}	2
6	CP	electroreduction	no	acetonitrile	5 x 10^{-10}	2

Photoactivation with oxalyl chloride was also examined at aryldiazonium ion-derived films. Decylphenyl (DP) films, which are alkyl terminated, were prepared using standard procedures by electroreduction of 3 mM decylbenzenediazonium cation (**7**) in acetonitrile at PPF and GC surfaces. There was an increase in the water contact angle at DP-modified GC surfaces, with a measured angle of ~ 78 ^{o}, compared to an average angle of ~ 50 ^{o} for polished GC surfaces (Table 6.1). DP films were reacted with amines by incubating with an acetonitrile solution containing 4 mM NAAB after photoactivation with oxalyl chloride using the standard procedure. The success of the reaction was evaluated by monitoring the attached amines with voltammetry and SEM after assembly of gold nanoparticles. Firstly, NAAB was coupled to photoactivated DP films in nonaqueous conditions, and a decrease in contact angle to 70 ^{o} was observed, consistent with the outer surface becoming less hydrophobic after coupling of NAAB. The voltammetric response of NAAB in PBS solution was also observed at the modified surface demonstrating successful coupling. The average surface concentration determined from electroreduction of coupled NAAB was approximately 7 ± 1 x 10^{-10} mol cm^{-2} (Table 6.6). Similarly, Sevy *et al* reported the coupling of polyethylenimine on silane layers photoactivated with gaseous oxalyl chloride however the amount of immobilized imine was not described.[26] Secondly, the coupling of en to

photoactivated DP films on PPF was demonstrated by the successful assembly of anionic gold nanoparticles. Particle-counts of SEM micrographs obtained for gold nanoparticle assembly at PPF-DP-en shows an increase in particle density from 44 particles/μm^2 measured for DP films (before activation) to 600 particles/μm^2, after coupling of en to the activated film (Table 6.5). Control samples of bare PPF incubated with en after treatment with oxalyl chloride (absence of UV light) yielded a density of approximately 20 particles/μm^2, which indicate that there is no direct attachment of en to PPF.

Table 6.6 shows the electrochemically determined surface concentrations of immobilized NAAB at each type of surface. Surface 3, prepared by photografting of **1** followed by photoactivation with oxalyl chloride gives the highest concentration of NAAB. The average value, ~ $17\pm3 \times 10^{-10}$ mol cm^{-2}, is greater than that calculated for monolayer coverage of an ideally flat surface (12×10^{-10} mol cm^{-2}).[54] However, GC and/or film-modified GC are not ideally flat and this value most likely reflects submonolayer coverage. Photoactivation of DP films with oxalyl chloride leads to a significantly lower concentration of coupled NAAB (surface 4) than found for surface 3. This could be due to a number of factors such as the surface concentration and/or morphology of the DP film, the influence of the aromatic group on the reaction with oxalyl chloride or the influence of the aromatic group on the reaction between acid chloride and NAAB. As explained earlier, surfaces 3 had a higher surface concentration of coupled NAAB than surface 2 possibly attributed to the greater reaction efficiency inherent for acid chloride moieties. After coupling NAAB in nonaqueous conditions, surface 2 (photografted aliphatic carboxylic acid-terminated film) has a higher concentration of NAAB than the aromatic counterpart of a CP film (surface 6). The conditions used to graft the underlying CP film are expected to result in a multilayered structure (Chapter 3) and hence it is likely that the surface concentration of CP groups is significantly greater than that of aliphatic carboxylic acids on surface 2. These considerations suggest that the lower concentration of NAAB on surface 6 is due to a lower coupling yield for the CP film. This could be attributed to steric crowding in the CP film and/or the electronic influence of the aromatic group on the reaction with NAAB. These results indicate that surfaces prepared with aliphatic modifiers give better films for further coupling of amine-bearing molecular species.

6.3.7 Preparation and characterization of mixed layers by photo- and electrochemical grafting

A popular system for modifying surfaces with organic films incorporating multiple components is with the self-assembly of thiols on gold surfaces (Section 6.1). However, as mentioned earlier, mixed self-assembled monolayers suffer from the same disadvantages of gold-thiol chemistry, most importantly poor long-term stability of the system.[31-33] An alternative approach is demonstrated here utilizing electroreduction of aryldiazonium salts and photografting of alkenes on carbon surfaces. The covalent C-C linkages mean that the resultant functionalized films are expected to be more robust and stable than self-assembled monolayers. Mixed component films were prepared in a stepwise fashion by photografting of alkenes followed by electroreduction of diazonium salts at the carbon surface. PPF surfaces were spin-coated at 1000 rpm with 200 mM of **2** dissolved in acetonitrile and photolyzed for 1 h. The PPF samples photografted with **2** were ultrasonicated and placed in an electrochemical cell to carry out electrografting of diazonium ions. One voltammetric scan at 200 mV s^{-1} from 0.2 to -0.5 V was performed in 0.6 mM 4-NB diazonium salt. The grafting procedure is expected to give submonolayer coverage of NP groups.[55] The resulting film consists of two components, aliphatic modifiers and aromatic modifiers. The successful addition of each component within the film was demonstrated by reaction of the individual components of the film with appropriate species, and subsequent examination by microscopy and electrochemistry. Figure 6.8 shows the voltammetric scan of the mixed film in 0.25 M H_2SO_4. A well-defined redox system is clearly observed in the cyclic voltammogram and is assigned to the electroreduction of the nitroaryl moiety that was introduced to the mixed film *via* the electrografting of the 4-NB diazonium salt at the **2**-modified PPF surface. A value of approximately $10 \pm 2 \times 10^{-10}$ mol cm^{-2} was found for the surface concentration of NP groups present within the mixed surface. This coverage value is less than the average value of ~ 16 x 10^{-10} mol cm^{-2}, for NP films prepared using the standard protocol and short preparation times at unmodified PPF surfaces (Chapter 3). The loosely packed nature of the photografted film as the first component allows substantial grafting of the NP aromatic modifier as the second component. This also demonstrates that the screening effect of vacant surface binding sites by the aliphatic film does not greatly decrease the electrochemically induced grafting at the modified electrode for the second modifier. Hence it is reasonable to assume that grafting of NP groups occurs at the bare sites within the loosely packed film of **2**. The diazonium ion-modifier may form multilayered aggregates by reaction with the aliphatic modifiers.

However, examination with SEM microscopy did not reveal any film-aggregate features in the mixed layer.

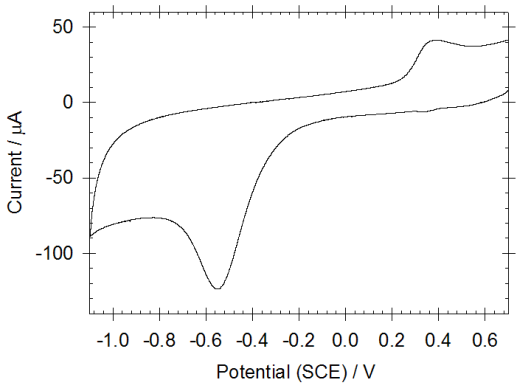

Figure 6.8. Cyclic voltammogram (v = 200 mV s^{-1}) recorded in 0.25 M H_2SO_4 of a mixed film attached to PPF consisting of photografted **1** and electrografted NP modifiers.

In order to demonstrate that the carboxylic acid groups of **2** remain exposed at the interface of the mixed layer rather than smothered with NP groups, the mixed film was reacted with en. A separate sample of a mixed film consisting of **2** and NP groups was prepared using the standard protocol (above) and was incubated with 20 mM of en in the presence of EDC/NHS reagents for amide coupling. The presence of coupled en in the mixed film was confirmed by the assembly of citrate-capped gold nanoparticles and SEM microscopy. Figure 6.9 shows the SEM images of the Au assemblies from electrostatic interaction of anionic nanoparticles with the film-bound amines (en). The SEM micrographs show dense nanoparticle assemblies formed on the mixed film. A particle-count reveals a particle density of 410 particles/µm^2 at the mixed surface. Control samples of surfaces containing only one component, either NP groups or a film of **2**, showed gold nanoparticle densities of no more than 50 particles/µm^2 (Table 6.5), confirming the coupling of en to the carboxylic acid moiety in the mixed surface. The particle density value obtained for the mixed surface is not significantly different to a single-component surface of PPF-**2**-en with a nanoparticle count of 470 particles/µm^2 (Table 6.5). This reveals that the photografted aliphatic carboxylic acid modifiers are available for coupling at the surface with no significant impact from the addition of the aromatic modifier. The aliphatic modifiers have a molecular length of 1.3 nm, thus when fully extended, the carboxylic acid termini will be accessible for coupling above the NP modifiers, which have a shorter molecular length of 0.7 nm. The aliphatic modifiers can maximize hydrophobic-hydrophobic intermolecular interactions with the neighbouring aromatic environment by adopting an extended structure,

which brings the carboxylic acid moiety to the film-solution interface. It is clear that the first modifier is not buried inhibiting it from further reaction.

Considering the requirements for a bi-functional surface, this procedure may be limited by the need for selecting an appropriate first modifier to produce relatively loosely packed films on the surface, allowing surface attachment of the second modifier. Nevertheless, this preparation method is experimentally simple and yields stable mixed films consist of both aliphatic and aromatic modifiers on the same surface. The formation of these mixed films *via* electro- and photochemical procedures provides a useful interface for further reaction.

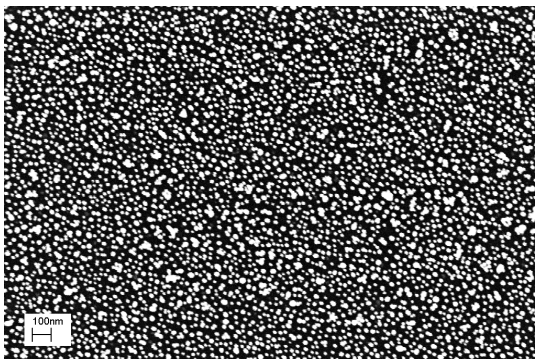

Figure 6.9. SEM micrograph, after incubation in a solution of citrate-capped gold nanoparticles, of a mixed film attached to PPF consisting of photografted **1** and electrografted NP modifiers after reaction with en.

6.3.8 Mechanism of film formation

The results described above show that UV photolysis of GC and PPF in the presence of alkenes leads to grafted organic layers, consistent with the formation of a C-C bond between the modifier and the surface. The same conclusion can be drawn concerning alkyne **5** (ethynylferrocene). As described earlier in Section 6.1, photografting of alkenes at hydrogen-terminated diamond has previously been demonstrated and the mechanism of the grafting reaction was proposed.[6, 7, 13, 21] In detailed studies, Hamers and coworkers have demonstrated that the photografting process is surface-mediated and suggest that grafting is initiated by photoemission of electrons from the surface, generating radical species derived from the alkene. Following formation of the radical species, Hamers and coworkers propose a sequence of reactions involving hydrogen abstraction from the surface (i.e. C-H bonds) leaving a radical, which reacts with additional alkene molecules (as described in Section 6.1).[21] Based on theoretical calculations and photocurrent experiments, which revealed that

graphitic carbon can both eject electrons upon photolysis with 254 nm light, the same mechanism is suggested for photografting of alkenes to hydrogen-terminated amorphous carbon.[12, 13, 21] For GC and PPF, which has not been subjected to hydrogen plasma treatment, it is reasonable to assume that photoemission of electrons from the surface leads to formation of radical species, however hydrogen abstraction from the surface may not be a major pathway to surface coupling (as described in Section 6.1). Radicals can directly attack both the edge and defective basal carbon sites of polished GC and PPF to form covalent bonds to the surface (as described for electrochemically assisted grafting reactions such as reduction of aryldiazonium (Chapter 1)) however the pathway leading from radical species to surface grafting is unclear. With the exception of **4** (*1H, 1H, 2H*-perfluoro-1-decene) and alkyne **5**, AFM measurements reveal that grafting yields loosely packed monolayers. The origin of the different grafting behaviours of **4** and **5** is not understood but surface concentration and film thickness measurements lead to the conclusion that the multilayer film of **5** is also loosely packed. A possible reason may be attributed to the stabilization of the e radical centre by the electron-rich fluorine groups and cyclopentanyl substituents of **4** and **5** during grafting, enabling the radicals to attack at the attached film as well as the electrode surface to generate multilayered structures. However, the grafting mechanism at films remains unknown.

6.4 Conclusion

A simple procedure involving photolysis of alkenes and alkyne for photografting has been demonstrated at both GC and PPF surfaces. The procedure should be applicable to a wide range of commercially available reagents and is experimentally simple, requiring neither hydrogen plasma treatment of the substrate nor reaction in an inert atmosphere. In contrast to electrochemical grafting methods, electrolyte is not required and only a small volume of solvent, or no solvent, is used. Unlike a recently reported method involving heat treatment of alkynes and an alkene, thermal stability of the R-group of the modifier is not important. Contact angle measurements, XPS, voltammetric and AFM analysis established that covalently grafted loosely packed monolayers with film thickness less than 1 nm are formed by the photochemical method, except for modifiers **4** and **5**, which generated loosely packed multilayered films of around 2-3 nm thick. For the electroactive modifier **5**, AFM and electrochemistry determined that the loosely packed multilayer had a maximum compactness of approximately 16 % of a close-packed layer. Photoactivation with oxalyl

chloride to functionalize alkyl-terminated films with acid chloride groups was demonstrated for photografted and electrografted films. Amine-reactive surfaces were prepared by this method and comparisons were made to other electro- and photochemical preparations. Aliphatic alkyl-alkene modifiers photografted to the surface that were photoactivated with oxalyl chloride had the highest yield of coupling with amines, while in general, aromatic modifiers (without activation) had the lowest amine-coupling yield. The photochemical procedures are also useful methods for the immobilization of gold nanoparticles to carbon surfaces. Preparation of carbon surfaces modified with two components was demonstrated by combining the different chemistry of electro- and photochemical reactions on carbon surfaces. This procedure yielded stable loosely packed mixed layers, which can provide a reliable starting point as a useful interface to couple molecular species utilizing different reactive tether components within the mixed layer. The grafting of each component can be managed by exploiting the different parameters that effect individual grafting, such as photolysis or electrolysis times. Selection of appropriate underlying (first) modifier-films on the surface so that the second modifier can also graft to the surface is an important consideration when applying this procedure. Despite this, the technique allows access to both aliphatic and aromatic functional groups on the same surface, opening up new opportunities for surface modification.

6.5 References

1. Ababou-Girard, S.; Sabbah, H.; Fabre, B.; Zellama, K.; Solal, F.; Godet, C., *Journal of Physical Chemistry C* **2007,** 111, 3099.
2. Ssenyange, S.; Anariba, F.; Bocian, D. F.; McCreery, R. L., *Langmuir* **2005,** 21, 11105.
3. Mazur, S.; Matusinovic, T.; Cammann, K., *Journal of American Chemical Society* **1977,** 99, 3888.
4. Wang, G. T.; Bent, S. F., *Journal of American Chemical Society* **2000,** 122, 744.
5. Roucoules, V.; Fail, C.; Schofield, W.; Teare, D.; Badyal, J., *Langmuir* **2005,** 21, 1412.
6. Strother, T.; Knickerbocker, T.; Russell, J. N.; Butler, J. E.; Smith, L. M.; Hamers, R. J., *Langmuir* **2002,** 18, 968.
7. Nichols, B. M.; Butler, J. E.; Russell, J. N.; Hamers, R. J., *Journal of Physical Chemistry B* **2005,** 109, 20938.
8. Yang, W.; Baker, S. E.; Butler, J. E.; Lee, C. s.; Russell, J. N.; Shang, L.; Sun, B.; Hamers, R. J., *Chemistry of Materials* **2005,** 17, 938.
9. Baker, S.; Tse, K. Y.; Hindin, E.; Nichols, B.; Clare, T.; Hamers, R., *Chemistry of Materials* **2005,** 17, 4971.
10. Lasseter, T. L.; Cai, W.; Hamers, R. J., *Analyst* **2004,** 129, 3.
11. Yang, W.; Auciello, O.; Butler, J.; Cai, W.; Carlisle, J.; Gerbi, J.; Gruen, D.; Knickerbocker, T.; Lasseter, T.; Russell, J.; Smith, L.; Hamers, R., *Nature Materials* **2003,** 1, 253.
12. Sun, B.; Colavita, P.; Kim, H.; Lockett, M.; Marcus, M.; Smith, L.; Hamers, R., *Langmuir* **2006,** 22, 9598.
13. Colavita, P.; Sun, B.; Tse, K. Y.; Hamers, R., *Journal of American Chemical Society* **2007,** 129, 13554.
14. Strother, T.; Cai, W.; Zhao, X.; Hamers, R.; Smith, L., *Journal of American Chemical Society* **2000,** 122, 1205.
15. Cicero, R. L.; Linford, M. R.; Chidsey, C. E. D., *Langmuir* **2000,** 16, 5688.
16. Sun, Q. Y.; de Smet, L.; van Lagen, B.; Wright, A.; Zuilhof, H.; Sudholter, E. J. R., *Angewandte Chemie-International Edition* **2004,** 43, 1352.
17. Sun, Q.; de Smet, L.; van Lagen, B.; Giesbers, M.; Thune, P.; van Engelenburg, J.; de Wolf, F.; Zuilhof, H.; Sudholter, E., *Journal of American Chemical Society* **2005,** 127, 2514.
18. Strother, T.; Knickerbocker, T.; Russell, J.; Butler, J.; Smith, L.; Hamers, R., *Langmuir* **2002,** 18, 968.

19. Tian, R.; Rao, T.; Einaga, Y.; Zhi, J., *Chemistry of Materials* **2006,** 18, 939.

20. Nebel, C.; Shin, D.; Takeuchi, D.; Yamamoto, T.; Watanabe, H.; Nakamura, T., *Diamond and Related Materials* **2006,** 15, 1107.

21. Nichols, B. M.; Metz, K. M.; Tse, K. Y.; Butler, J. E.; Russell, J. N.; Hamers, R. J., *Journal of Physical Chemistry B* **2006,** 110, 16535.

22. Sun, Q.; deSmet, L.; van Lagen, B.; Wright, A.; Zuilhof, H.; Sudholter, E., *Angewandte Chemie International Edition* **2004,** 43, 1352.

23. Sun, Q.-Y.; deSmet, L. C. P. M.; vanLagen, B.; Giesbers, M.; Thune, P. C.; vanEngelenburg, J.; deWolf, F. A.; Zuilhof, H.; Sudholter, E. J. R., *Journal of American Chemical Society* **2005,** 127, 2514.

24. Bashir-Hashemi, A.; Li, J., *Journal of Organic Chemistry* **1995,** 60, 698.

25. Hardee, J.; Bashir-Hashemi, A.; Gelber, N.; Qi, L.; Axenrod, T., *Journal of Organic Chemistry* **1994,** 59, 2132.

26. Husseini, G. A.; Niederhauser, T. L.; Peacock, J. G.; Vernon, M. R.; Lua, Y.-Y.; Asplund, M. C.; Sevy, E. T.; Linford, M. R., *Langmuir* **2003,** 19, 4856.

27. Gooding, J.; Liu, G., *Langmuir* **2006,** 22, 7421.

28. Chapman, R.; Ostuni, E.; Yan, L.; Whitesides, G., *Langmuir* **2000,** 16, 6927.

29. Frederix, F.; Bonroy, K.; Laureyn, W.; Reekmans, G.; Campitelli, A.; Dehaen, W.; Maes, G., *Langmuir* **2003,** 19, 4351.

30. Gong, P.; Lee, C.; Gamble, L.; Castner, D.; Grainger, D., *Analytical Chemistry* **2006,** 78, 3326.

31. Delamarche, E.; Michel, B.; Kang, H.; Gerger, C., *Langmuir* **1994,** 10, 4103.

32. Peng, D.; Lahann, J., *Langmuir* **2007,** 23, 10184.

33. Poirier, G., *Chemical Review* **1997,** 97, 1117.

34. Liu, G.; Liu, J.; Böcking, T.; Eggers, P.; Gooding, J., *Chemical Physics* **2005,** 319, 136.

35. Owens, T.; Ludwig, B.; Schneider, K.; Fosnacht, D.; Orr, B.; Holl, M., *Langmuir* **2004,** 20, 9636.

36. Bhurke, A.; Askeland, P.; Drzal, L., *Journal of Adhesion* **2007,** 83, 43.

37. Perring, M.; Dutta, S.; Arafat, S.; Mitchell, M.; Kenis, P. J. A.; Bowden, N. B., *Langmuir* **2005,** 21, 10537.

38. Liu, Y.-J.; Navasero, N. M.; Yu, H.-Z., *Langmuir* **2004,** 20, 4039.

39. Fabre, B.; Hauquier, F., *Journal of Physical Chemistry B* **2006,** 110, 6848.

40. Bard, A. J.; Faulkner, L. R., *Electrochemical Methods: Fundamentals and Applications*.3rd ed.; John Wiley: New York, 2001.

41. Honeychurch, M. J., *Langmuir* **1998,** 14, 6291.

42. Rowe, G. K.; Carter, M. T.; Richardson, J. N.; Murray, R. W., *Langmuir* **1995,** 11, 1797.

43. Chidsey, C. E. D.; Bertozzi, C. R.; Putvinski, T. M.; Mujsce, A. M., *Journal of the American Chemical Society* **1990,** 112, 4301.

44. Kondo, T.; Kanai, T.; Uosaki, K., *Langmuir* **2001,** 17, 6317.

45. Amatore, C.; Saveant, J. M.; Tessier, D., *Journal of Electroanalytical Chemistry* **1983,** 147, 39.

46. Allongue, P.; de Villeneuve, C. H.; Pinson, J., *Electrochimica Acta* **2000,** 45, 3241.

47. Brooksby, P. A.; Downard, A. J., *Langmuir* **2004,** 20, 5038.

48. Downard, A. J.; Cruickshank, A. C., *Unpublished work.*

49. Downard, A. J.; Tan, E. S. Q.; Yu, S. S. C., *New Journal of Chemistry* **2006,** 30, 1283.

50. Ortiz, B.; Saby, C.; Champagne, G. Y.; Belanger, D., *J. Electroanal. Chem.* **1998,** 455, 75.

51. Delamar, M.; Desarmot, G.; Fagebaume, O.; Hitmi, R.; Pinson, J.; Saveant, J. M., *Carbon* **1997,** 35, 801.

52. Sun, B.; Colavita, P. E.; Kim, H.; Lockett, M.; Marcus, M. S.; Smith, L. M.; Hamers, R. J., *Langmuir* **2006,** 22, 9598.

53. Brooksby, P. A.; Downard, A. J.; Packwood, D. M.; Garrett, D. G., *unpublished work*.

54. Liu, Y.-C.; McCreery, R. L., *Journal of American Chemical Society* **1995,** 117, 11254.

55. Anariba, F.; DuVall, S. H.; McCreery, R. L., *Analytical Chemistry* **2003,** 75, 3837.

Chapter 7. Carbon surface modification by photochemical grafting of azides

7.1 Introduction

Photochemical methods offer an alternative approach to electrochemical methods for forming stable surface films on carbon materials that is simple to carry out. As described in the previous chapter, UV photolysis of alkenes and alkynes at carbon surfaces can lead to surface modification. Azide and diazirine derivatives are photosensitive molecules that can generate reactive species that readily react with their neighbouring environments. Azide derivatives are commonly utilized as photoactive reagents in photoresists[1-4], surface 'click' chemistry[5-8], photoaffinity labeling and modification of polymers.[9-12] They have also been utilized for the photochemical modification of glassy carbon (GC).[13-16] Modification procedures generally involve drop-coating the carbon surface with a solution of dissolved azide and irradiating the sample with UV light. Photolysis of azide derivatives generate reactive nitrenes that can readily insert into a variety of chemical bonds such as C-H, O-H and N-H that may be present on the substrate leading to grafting of the modifier to the surface, presumably through covalent bonds as depicted in Scheme 7.1 (i.e. C-N or O-N bonds for graphitic carbon substrates).[12, 16-19] It is reasonable to suggest that nitrenes can also react *via* insertion reactions with the carbene- and carbyne-like structures that maybe present in graphitic carbon to form C-N covalent bonds. However, the mechanism and nature of the bond to the surface is unclear.

Scheme 7.1. Diagram of possible photografting reactions of azide with graphitic carbon surface upon photolysis.

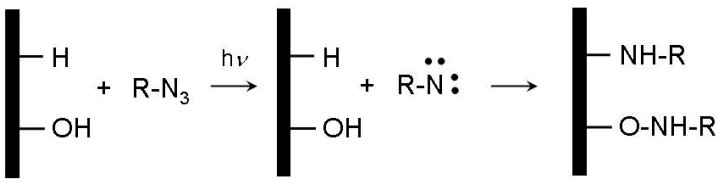

Generation of nitrenes can also lead to complex side-reactions, such as fragmentation and rearrangement processes, resulting in the formation of side-products.[12, 17, 18, 20] Scheme 7.2

shows some of the possible rearrangement reactions that can occur when nitrene species are formed after photolysis of aryl azide. Two forms of aryl nitrenes can form upon photolysis: singlet state (^{1}N, species 366) or triplet state nitrene (^{3}N, species 370). Singlet nitrenes is the principal species upon photolysis that can irreversibly form triplet nitrenes *via* intersystem crossing (Scheme 7.2, species 366 → species 370). Singlet nitrenes can insert preferentially into O-H or N-H bonds and insertion reactions with C-H bonds is favoured for triplet nitrenes.[15, 19] These nitrene species can also react with another nitrene to form azo products (species 369) or rearrange and form other reactive species (species 367 and 368).[12, 18] These other reactive species derived from nitrenes may also react with the carbon substrate and lead to surface grafting.

Scheme 7.2. Diagram of some of the possible rearrangement and chemical reactions of aryl azide upon UV photolysis. Reproduced with permission from reference 12.

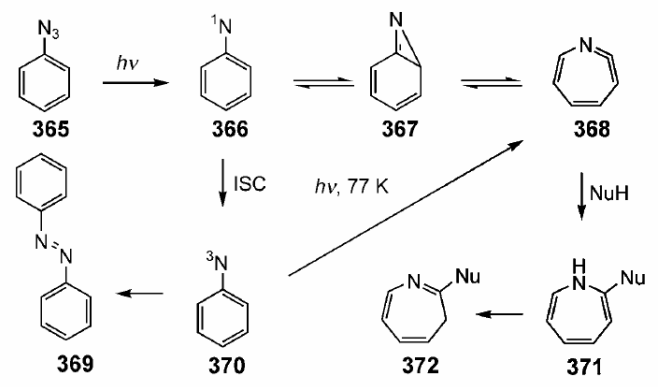

ISC = Intersystem crossing
NuH = nucleophile

Azides have been used to graft biotin to carbon surfaces. Photobiotin, the general name for azide derivatives of biotin, have been photografted to GC by drop-coating photobiotin that has been dissolved in EtOH-water onto a GC surface and exposing the sample to UV light. A UV laser was utilized to irradiate the surface and generate patterns. Patterning was demonstrated using two approaches: by using the laser was used to generate an interference pattern on the GC electrode,[13, 16] or by focusing the laser light through a microscope lens setup for direct writing of photobiotin patterns on the surface.[15, 16] The success of photografting and chemical patterning were established by fluorescence imaging of the grafted photobiotin patterns after reaction with a fluorescent avidin derivative. Patterned lines of biotin of approximately 5–20 μm width, were generated on the surface by the two

methods.[13, 15, 16] However, the fluorescence images revealed that some areas of the lines were not continuously labeled with avidin tags, showing signs of film heterogeneity. The inhomogeneous biotin lines may be due to cluttered biotin-avidin binding at the modified surface and/or degradation of fluorescent avidin from photo-bleaching. Film heterogeneity may also be due to a relatively low amount of nitrene-reactive sites available for grafting at GC.[16]

Diazirine is another photoactive species, which upon UV photolysis, can generate reactive species. Diazirines yield carbenes that can readily insert into a variety of bonds including O-H, C-H and C=C.[13, 21-24] Kuhr and coworkers made a comparison, using fluorescence microscopy, between films prepared on GC from carbene-generating biotin and photobiotin (nitrene-generating analogue).[16] After reaction with the fluorescent avidin tag, films grafted from carbene-generating biotin appeared more homogeneous in fluorescence imaging than films derived from the nitrene-analogue. This may be attributed to a relatively higher reactivity of the carbene species than nitrenes with the carbon surface, presumably due to carbene's ability to insert into C=C as well as C-H and O-H bonds at graphitic surfaces.[16] However, direct analysis and detailed investigations of chemical and physical properties of films grafted from azide and diazirine derivatives were not reported, and film structures are unknown.

The chemical patterning of two or more modifiers at surfaces can give spatially defined domains of functionality on the surface for desired applications. For example, a surface may have regions for carrying out coupling reactions and other regions designed to reduce nonspecific adsorption. The ultimate goal of patterned surface modification is to have control over the spacing, orientation and density of the immobilized species on the surface. There are several approaches to creating molecular patterns with multiple modifiers on surfaces. Scheme 7.3 shows the general strategies involved in achieving each patterning approach. These have been termed the 'fill-in', 'selective conversion' and 'build-up' methods.[25]

For the fill-in strategy of Scheme 7.3a, the first step involves generating a pattern of the first modifier on the surface with bare regions available to graft the second modifier in the second step. The first step can be achieved in a number of setup, for example by masking the surface with a nonpermanent material such as photoresist or poly(dimethylsiloxane) (PDMS).[25-30] The first modifier is grafted to the nonblocked regions and after removal of the

mask the second modifier is grafted to the regions that were previously masked. Another general strategy is to use microcontact printing and dip-pen lithography to form patterns of the first modifier on the surface.[30-32]

Scheme 7.3. Strategies for patterning surfaces consisting of two different functionalities. (a and b) fill-in approach, (c) selective conversion approach, and (d) build-up approach.

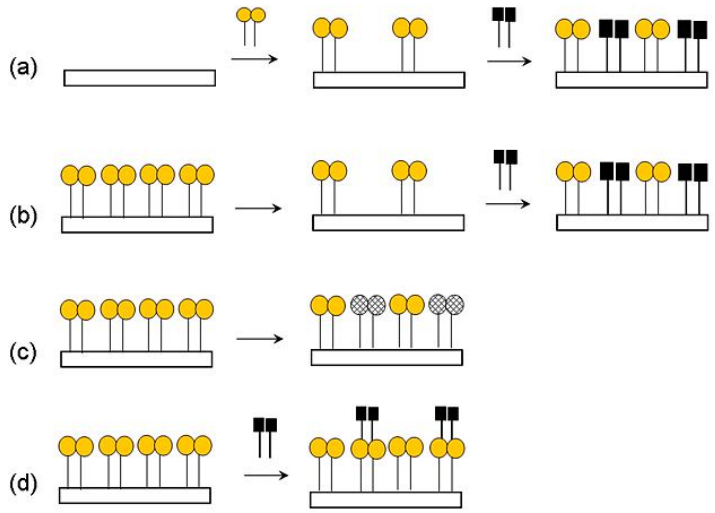

In Scheme 7.3b, a continuous film of the first modifier can be prepared with regions of the film mechanically removed and subsequently the second modifier is grafted in those regions. Modifiers can be selectively removed from the surface by techniques such as 'nanoshaving' and ablation, which utilizes the tip of an atomic force microscope (AFM) or energy beams (e.g. laser, ion-beam), respectively, to create bare regions for the second modifier to fill.[27, 29, 33] For the selective conversion method (Scheme 7.3c), regions of a grafted continuous layer are selectively modified so that the functional group of the film has a significantly different chemical or physical property to the remainder of the layer. This type of patterning is exemplified by in the selective deprotection of functional groups of surface films such as in the photo-deprotection of *tert*-butyl esters terminated films to reveal latent carboxylic acid groups on selected regions, by photolithographical techniques.[27, 29] The reduction of selected regions of a nitro-terminated surface film *via* photo-reduction of nitro groups in the presence of silver nanoparticles, or electroreduction carried out in PDMS microchannels on top of nitro-films are other examples of this strategy to generate patterned surface consisting of two different functionalities.[25, 29, 34-36] For the 'build-up' patterning strategy, a continuous film of the first modifier is formed on the surface and subsequently, a second modifier is coupled to regions of the first modifier film (Scheme 7.3d). This can be

achieved by selective introduction of the second modifier onto the continuous film by direct grafting methods such as stamping.[25-27, 29, 30] Alternatively, the second modifier can be coupled to specific regions on the first film by restricting coupling reactions in within PDMS microchannels.[30]

Recently, patterning of carbon surfaces incorporating two different modifiers on the surface was achieved by electrochemical methods involving aryldiazonium ions and amines.[25, 33] One report applied the fill-in approach (Scheme 7.3b), where a continuous film of the first modifier was grafted to pyrolyzed photoresist film (PPF) by reduction of aryldiazonium ions followed by removal of selected regions of the film by mechanical scribing with an AFM tip.[33] The exposed area was then electografted with a second type of aryldiazonium ion, giving a nanoscale pattern with dimensions of approximately 140 nm x 250 nm.[33] Similarly, in a different report, the fill-in strategy (Scheme 7.3b) was also demonstrated on PPF by soft lithography utilizing a PDMS mold to physically block selected regions of the surface during the electrografting of the first film from aryldiazonium ion.[25, 37] After removal of the PDMS mold, the bare areas are grafted with the second modifier *via* electrooxidation of amine to produce an aliphatic amine modified surface with approximately 20 μm lines of phenyl groups.[25] The addition of the second modifier using electrochemical methods has the possible undesired effect of film growth of the second modifier on top of the first layer. Hence, to avoid this possibility, electrochemically assisted patterning requires a sufficiently thick and passivating initial layer to ensure that the second modifier only grafts to the bare surface.

In a second approach, PDMS molds containing small microchannels (lines of ~ 20 μm widths) were also used to restrict working solutions for carrying out chemical reactions on top of film-modified PPF surfaces.[25] Following a selective conversion strategy (Scheme 7.3c), selective reductions were carried out inside the microchannels of a PDMS mold that had been applied on top of a nitrophenyl (NP) film derived from electroreduction of aryldiazonium ion. Acetonitrile solution containing benzoic acid (BA/ACN) was introduced into the microchannels to carry out electroreduction of regions of the NP film, generating aminophenyl (AP) groups.

The third approach to two-component patterning on carbon surfaces, followed a build-up approach (Scheme 7.3d), in which solutions of the second component were

introduced into PDMS microchannels sealed onto the first modifier film.[25] Patterned coupling reactions between an amine in solution and a carboxyphenyl (CP) film electrografted to PPF, and between an acid chloride derivative in solution and an amine-terminated film derived from electrooxidation of a diamine, were demonstrated utilizing PDMS microchannels.[25, 37]

The above examples using soft lithography share limitations associated with the use of PDMS molds. The mold has to physically contact and seal with the bare carbon surface or film-modified surface. PDMS is well-known to leave residues when the mold is removed or may give a poor seal at the contact.[30, 38, 39] Furthermore, not all solvents are compatible with the use of PDMS molds. Different solvents can cause PDMS molds to swell or dissolve. These effects can contaminate the surface and affect the clarity of the pattern.

This chapter aims to prepare and examine surface films formed by the photolysis of azides on carbon surfaces. GC and PPF surfaces are photografted with different azides and properties of the photolyzed surfaces are characterized by a combination of contact angle measurements, AFM and electrochemistry. This work in this chapter also aims to explore the use of film-modified surfaces for coupling of amine, carboxylic acid and other species. The preparation of patterned two component films on carbon surfaces by combination electro- and photochemical reactions are examined by integration of photolithographical methods into the photochemical modification procedure. This general approach to patterning avoids the use of PDMS molds or other masking materials and hence avoids possible surface contamination from undesired residues.

7.2 Experimental Section

7.2.1 Reagents and Materials

1-ethyl-3-(-3-dimethylaminopropyl) carbodiimide hydrochloride (EDC) (Alfa Aesar), N-hydroxysuccinimide (NHS), dihydroxyphenylacetic acid (DOPAC), 4-nitrobenzoyl chloride (all Sigma-Aldrich), azidoaniline and azidophenylisothiocynate (both Acros Organics) and 4-nitro-4-aminoazobenzene (NAAB, AnalaR, BDH) were used as received. The tetrafluoroborate salts of 4-carboxybenzenediazonium, 4-nitrobenzenediazonium, 4-methoxybenzenediazonium and 4-decylbenzenediazonium were synthesized using standard procedures (Chapter 2). 4-nitrophenyl azide was synthesized from 4-nitrobenzenediazonium salt using standard procedures (with minor modification) inside a yellow room.[20, 40] 4-nitrobenzenediazonium tetrafluoroborate was dissolved in cold acetonitrile and the solution was cooled in an ice-acetone bath with stirring. One equivalent of NaN_3 was dissolved in the minimum amount of water and added slowly to the diazonium salt solution. After the addition was complete, stirring was maintained for 30 min. The yellow solid was filtered and washed with cold water and acetonitrile. The solid was recrystallized in acetonitrile before use. Azides were stored in the dark and at ~ -4^{o}C moistened with acetonitrile. ***Caution: diazonium salts and azides are potentially explosive and should be handled with care.***

7.2.2 Electrochemistry

An O-ring was used to define the geometric area of the working electrode (0.26 cm^2 for electrode modification and 0.12 cm^2 for subsequent scans at the modified surface). Cyclic voltammograms of nitroaryl derivatized surfaces were obtained in 0.25 M H_2SO_4 unless otherwise stated. DOPAC-coupled and NAAB-coupled modified surfaces were voltammetrically scanned in PBS solution. Unless otherwise stated, all voltammetric scans were carried out with ν = 200 mV s^{-1}.

7.2.3 Modification of carbon surfaces

4-nitrophenylazide and azidophenylisothiocynate were dissolved in DCM solution while azidoaniline was only able to be dissolved in DMF solution. For the standard photografting procedure, cleaned carbon surfaces were spin-coated with two coats of the azide solution at 1000 rpm for 30 s followed by photolysis for 30 min. For solution photolysis, samples were immersed in DCM solution containing the azide modifier giving approximately 1 mm solution thickness above the surface. Samples were irradiated at 365

nm in either a Rayonet Srinivason-Griffin photochemical reactor (equipped with four RPR 3650 Å reaction lamp tubes, UV intensity ~ 1 mW cm^{-2}) or an in-house built photoreactor (365 nm lamp tubes, UV intensity ~ 1 mW cm^{-2}) at room temperature in air. The photolyzed samples were ultrasonicated in DCM or DMF for 5 min and dried with N_2 before characterization.

Electrochemical modification of carbon surfaces was carried out in acetonitrile with 0.1 M $TBABF_4$ and containing tetrafluoroborate salts of 2 mM 4-carboxybenzenediazonium, 3 mM decylbenzenediazonium, 0.6 mM 4-nitrobenzenediazonium or 2 mM 4-methoxybenzenediazonium. The standard modification procedure involved two initial scans from 0.3 V to E_f at 200 mV s^{-1}, followed by electrolysis at (E_f – 150) mV (*vs* Ag wire). Electrolysis time was 300 s and E_f was -0.45 V for 4-carboxybenzenediazonium salt, 600 s and -0.40 V for 4-decylbenzenediazonium salt, 60 s and -0.55 V for 4-methoxybenzenediazonium and 600 s and -0.30 V for 4-nitrobenzenediazonium salt.

NP films on PPF surfaces were reduced by carrying out ten voltammetric scans at 200 mV s^{-1} between 0.7 and -1.8 V (*vs* Ag wire) in acetonitrile containing 0.1 M $TBABF_4$ and 20 mM benzoic acid. Reduced surfaces were ultrasonicated in acetonitrile for 5 min before use.

7.2.4 Preparation of two-component layers

Two-component films were prepared by spin-coating two coats of 200 mM NPA in DCM at 1000 rpm for 30 s on top of surfaces electrochemically prepared with aryldiazonium salt-derived films (above), followed by UV irradiation for 30 min. The photolyzed samples were ultrasonicated in DCM for 5 min and dried with a stream of N_2.

7.2.5 Preparation of patterned two-component films

Patterned two-component films were prepared by spin-coating two coats of 20 mM azide dissolved in DCM or acetonitrile at 1000 rpm for 30 s on top of surfaces electrochemically prepared with aryldiazonium salt-derived films (above). A photomask (Chapter 2) was positioned above the spin-coated sample and subsequently irradiated with UV (365 nm) for 30 min (Scheme 7.4). The setup was fastened by external clips. As described in Chapter 2, the photomasks are made from glass and chrome and contained feature sizes from hundreds of microns to lines of 10 μm width. The photolyzed samples were ultrasonicated in DCM or acetonitrile for 30 s and dried with a stream of N_2.

Scheme 7.4. Diagram of the preparation of patterned two-component films.

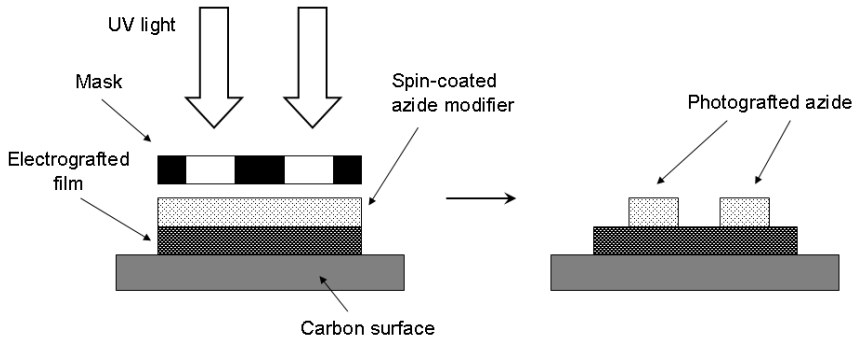

7.2.6 Coupling of carboxylic acid and acid chloride derivatives to modified surfaces

Modified surfaces were incubated in a stirred DMF solution containing DOPAC (50 mM), 20 mM EDC and 4 mM NHS or DCM solution containing 200 mM 4-NBCl for for 18 h. All coupled surfaces were ultrasonicated for 30 s in DMF or DCM and dried with N_2.

7.2.7 Coupling of amine derivatives to modified surfaces

Amines were coupled to modified surfaces by incubating the surface in a stirred acetonitrile solution of NAAB (4 mM) for 18 h. Coupled samples were ultrasonicated for 30 s in acetonitrile and dried with N_2.

7.2.8 Assembly of gold nanoparticles

Gold nanoparticles were assembled on modified PPF surfaces by incubation in an as-prepared nanoparticle solution. Single component films were incubated for 1 h and patterned two component films were incubated for 30 min followed by thorough rinsing with Milli-Q water and drying with N_2.

7.3 Results & Discussions

7.3.1 Preparation and electrochemical analysis of GC surfaces photografted with 4-nitrophenyl azide (NPA)

Figure 7.1 shows the azide modifiers used in the study: nitrophenyl azide (NPA), azidophenylisothiocynate (API) and azidoaniline (APA). The azidonitrophenyl (NPA) modifier was selected for initial investigations due to its electroactivity. GC electrodes were used as the carbon substrate The modifier was dissolved in DCM to give solutions ranging from 5 to 200 mM. A set of polished GC surfaces was modified with NPA by immersing the surfaces in DCM solutions of the modifier giving approximately 1 mm solution thickness above the surface. The samples were photolyzed at 365 nm (in solution) inside a photoreactor open to air. The concentration of dissolved NPA and the photolysis time were varied and the extent of photochemical modification was monitored by utilizing cyclic voltammetry to analyze the surface concentration of the NP group as a function of photolysis time. Another set of polished GC surfaces were modified by spin-coating two coats of the dissolved modifier onto the surface at 1000 rpm for 30 s before photolyzing as described above. The modified surfaces were ultrasonicated for 5 min in DCM to remove any non-covalently bound material.

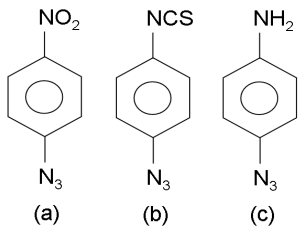

Figure 7.1. Azides used for photochemical grafting to carbon surfaces: (a) nitrophenyl azide (NPA), (b) azidophenylisothiocynate (API) and (c) azidoaniline (APA).

Figure 7.2 shows the cyclic voltammetry recorded in H_2SO_4 of GC surfaces photografted with NPA a) in solution and b) spin-coated. The voltammograms show the expected voltammetric response previously assigned (Chapters 3 and 4) to the electrochemical reduction of surface-bound NP groups in aqueous acidic conditions. In both sets of cyclic voltammograms, there is a large reduction peak ($E_{p,c}$ ~ 0.45 V) during the first scan which disappears on the second cycle, and also, a relatively broad reversible redox couple found at $E_{1/2}$ ~ 0.3 V. The amount of NPA photografted to the surface was determined from the

charge associated with the voltammetric response as described in Chapters 3 and 4. Figure 7.3 shows the relationship between the voltammetrically determined surface concentration of electroactive NP groups plotted as a function UV exposure time for two different NPA concentrations. For solution photolysis with 200 mM NPA (crosses), there is a rapid rise in the surface concentration of NP groups attached to the GC surface for irradiation up to 120 s, then a steady upward growth at a lesser rate towards an average surface concentration of approximately $3.7 \pm 0.7 \times 10^{-9}$ mol cm^{-2} at 1800 s. For solution photolysis with a lower NPA concentration (20 mM (circles)), the rate of increase of NP group photografted to GC and the limiting surface concentration are lower. An increase in the surface concentration is observed up to a photolysis time of 600 s giving an average surface concentration of approximately $2.5 \pm 0.5 \times 10^{-9}$ mol cm^{-2} for UV exposure beyond 600 s. The NP coverage of these films is comparable to that for films prepared by the electroreduction of 4-NB diazonium ion (~ 2.3×10^{-9} mol cm^{-2}, prepared using standard conditions in Chapter 4), which may suggest that films grafted by NPA reflect multilayers. Film structure of azide-derived films is examined in more detail using PPF substrates in the following sections.

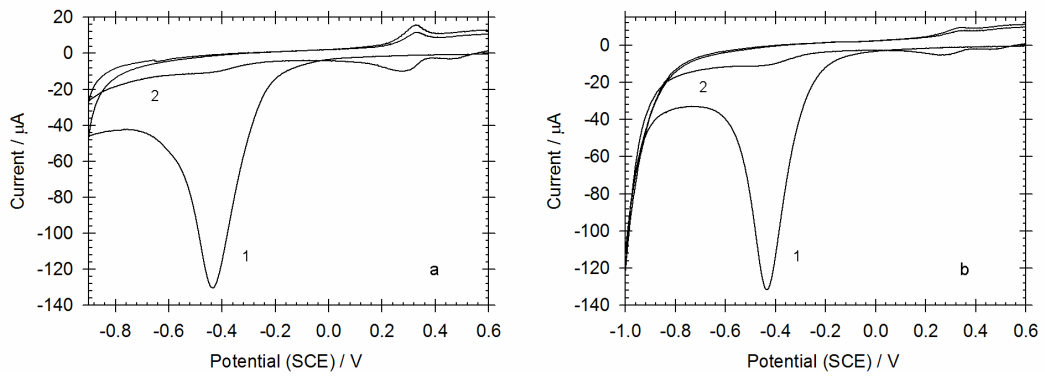

Figure 7.2. First two voltammetric scans recorded in 0.25 M H_2SO_4 for GC electrodes grafted with 200 mM NPA (t = 600 s) by a) solution-photolysis and b) spin-coated photolysis.

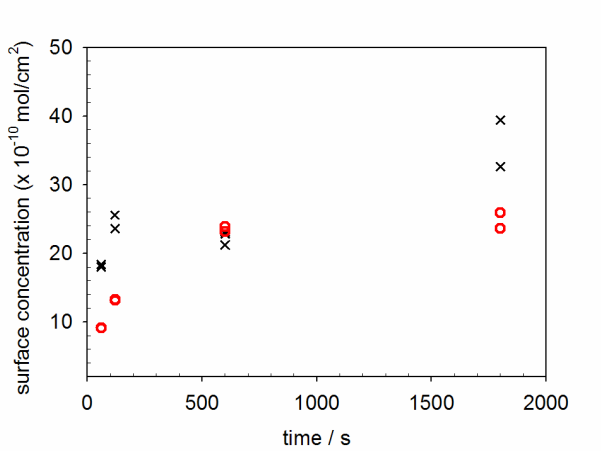

Figure 7.3. Graph showing the estimated surface concentration of electroactive NP groups grafted on GC *vs* solution photolysis time using NPA solutions with concentration (crosses) 200 mM and (circles) 20 mM.

Photografted films were also prepared by photolyzing spin-coated samples of NPA. Surface concentration data obtained at photolyzed spin-coated GC samples are shown in Figure 7.4. The maximum average surface concentrations reached are generally less than those measured for solution photolyzed samples. For GC samples prepared by spin-coating with relative high modifier concentrations (100 mM (Figure 7.4a, crosses) and 200 mM (Figure 7.4a, circles)), the surface concentration increases sharply with irradiation time, at irradiation times less than 600 s. Figure 7.4a shows these spin-coated samples reach a maximum surface concentration of ~ 2.2±0.4 x 10^{-9} mol cm^{-2}. In general, spin-coated samples give photografted films with lower surface concentrations than samples photolyzed in solution. This may be due to the amount of azide material present at the surface for photolysis and presumably, more azide is exposed to the surface for reaction in solution than spin-coated samples. The NP coverage for films prepared by this method is similar to those electrochemically prepared from 4-NB diazonium ion using standard methods (Γ ~ 2.3 x 10^{-9} mol cm^{-2}, Chapter 4), which may suggest that the films have similar structures. Further experiments were carried out on PPF substrate to investigate the structure of photografted films and are presented in the following section. For NPA derived films photolyzed for longer than 600 s with 200 mM azide solution, there is a difference between films formed by spin-coated (Figure 7.4a) and solution photolysis (Figure 7.3). This suggests that the yield of photografting is influenced by the amount of modifier directly in contact with the surface rather than the amount of material deposited on the surface. Films prepared by solution-photolysis continue to grow with an increase in surface concentration for UV irradiation times greater than 600 s. In contrast, for spin-coated samples there is no increase

in surface coverage after 600 s of irradiation. Figure 7.4b shows that the surface concentration of NP groups is less for films prepared by spin-coating lower NPA concentrations. For spin-coated samples with NPA concentration of 20 mM (crosses) and 5 mM (circles), the increase in surface concentration with photolysis time is initially rapid, however the final surface coverage, ~ 5±1 x 10^{-10} mol cm^{-2}, is lower than that of its higher modifier concentration counterpart. Presumably at these lower concentrations, the surface is not fully covered with spin-coated modifier. Hence thinner films may be formed at the surface as a result of less grafted material. Control GC samples that were spin-coated with the NPA modifier and stored in the dark (no UV irradiation) for 600 s did not show a voltammetric response.

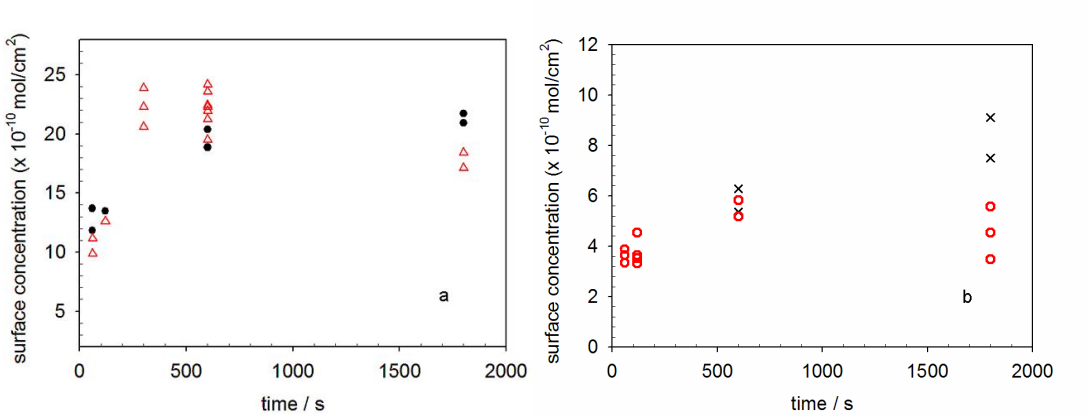

Figure 7.4. Graphs showing the estimated surface concentration of electroactive NP groups *vs* photolysis time for spin-coated GC samples prepared from NPA solutions with concentration (a) (dots) 100 mM and (triangles) 200 mM; (b) (crosses) 20 mM and (open circles) 5 mM.

The stability of the photografted layers to ultrasonication and electrochemical analysis in different solvents indicates that the photografted layers are strongly bonded to the surface and hence supports the formation of a covalent bond between the carbon surface and the films.

7.3.2 Electrochemical and AFM depth profiling analysis of PPF surfaces photografted with 4-nitrophenyl azide (NPA)

Similar approaches for photografting NPA to GC were also carried out for PPF modification. Figure 7.5 shows the amount of photografted NP groups on PPF surfaces

photolyzed with 200 mM of the modifier spin-coated (crosses) and immersed in solution (circles). For both types of samples, the surface coverage increases steadily up to 600 s giving a maximum value of ~ 6±1 x 10^{-10} mol cm^{-2}. Compared with GC samples prepared using the same conditions (Figures 7.3 and 7.4), the surface coverage of photografted material at PPF is lower. This is partly attributed to the differences in surface area arising from the larger surface roughness of GC (as described in Chapter 1). Another possibility may be that there is a higher concentration of nitrene-reactive sites on GC surfaces than PPF. Nitrenes are expected to graft to graphitic carbon surfaces *via* insertion into surface C-H and O-H bonds. The oxygen content of GC surfaces is typically greater than that of PPF, which may allow more insertion reactions by singlet nitrene to surface O-H bonds.[41, 42] Hence, it is reasonable to assume that this may attribute to a higher grafting yield for GC than PPF, since singlet nitrene is the principal species produced upon photolysis of azides (Section 7.1).

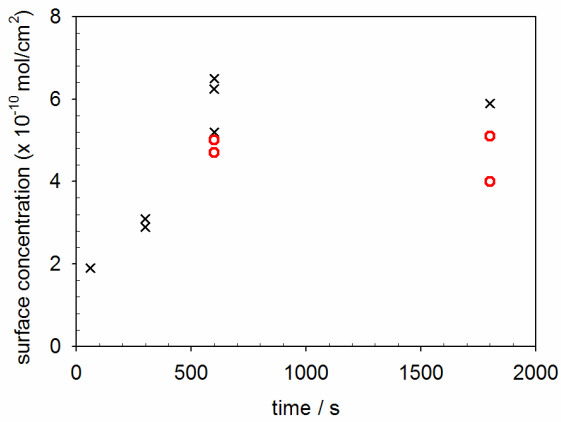

Figure 7.5. Graph showing the estimated surface concentration of electroactive NP groups *vs* photolysis time for photolyzed PPF prepared from 200 mM NPA solution by irradiation of spin-coated samples (crosses) and in solution (circles).

The physical properties of the azide-derived films prepared with varying exposure of UV irradiation were investigated by AFM. As-formed NPA-derived films were prepared with standard procedures by spin-coating 200 mM NPA solution at 1000 rpm on PPF surfaces followed by photolysis for times ranging from 60 to 1800 s. The photolyzed PPF samples were ultrasonicated in DCM for 5 min before AFM depth profiling examination. Figure 7.6 shows the average film thickness of NPA-derived films prepared at various irradiation times. The data reveal that after 60 s of UV irradiation, a film with an approximate height of 1 nm is formed, which indicates that films are established rapidly. There appears to be no growth in film height with increasing UV irradiation times. A photolyzed sample spin-coated with a faster spin rate at 4200 rpm (triangle) had a similar film height of approximately 0.8 nm, as those prepared with the standard spin rate. A smaller

amount of material is deposited of the higher spin rate and hence this result demonstrates that the photografted layers are the same as those prepared by the standard spin rate. Based on the theoretical molecular dimensions of the NPA modifier, vertical alignment of the molecule on the surface gives an expected film height of 0.8 nm (assuming that modifier is bonded *via* a C-N linkage with a carbon atom at the surface). As shown in Figure 7.6 (crosses), the measured film thickness ranged between 0.6 and 1 nm, which confirms that the films have an average film thickness that correlates to monolayer or sub-monolayer. This is further evident by AFM measurements of the NPA-derived film topography. The line profile shown in Figure 7.7 reveals that the photografted film greatly increases the peak-to-peak height variation and the average surface roughness (See Chapter 6 for AFM line profile of bare PPF). The average surface roughness values are also very close to the average film thickness of the films. The evidence confirms that the NPA photografted films are loosely packed monolayers.

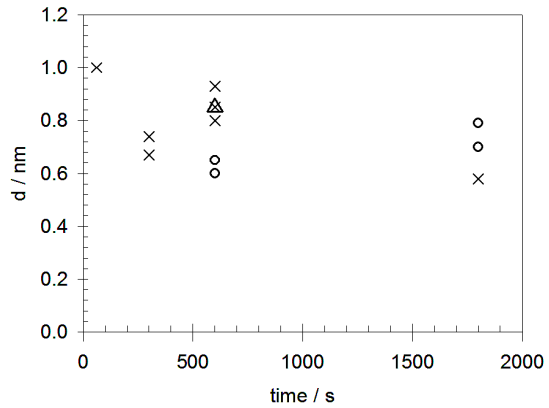

Figure 7.6. Plot of AFM thickness *vs* photolysis time for NP films prepared on PPF from 200 mM NPA solution by irradiation of spin-coated samples (crosses and triangles) and in solution (circles). Spin-coated samples were prepared from a spin-rate of 1000 rpm (crosses) and 4200 rpm (triangles).

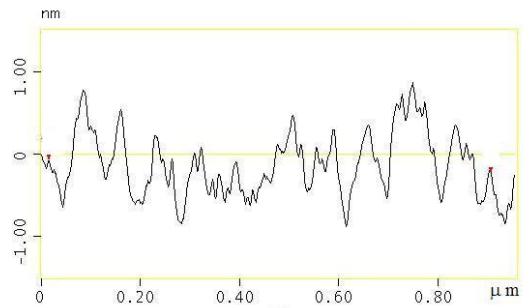

Figure 7.7. AFM line profile of PPF photografted with NPA *via* standard procedures (t = 600 s).

NPA-derived films prepared by solution photolysis were also investigated with AFM. As shown in Figure 7.6 (circles), the films have an average height of approximately 0.7 nm, which is similar to films produced from spin-coating procedures. Hence these films are also best described as loosely packed monolayers. In this respect, the loose packing arrangement of photografted NPA films is similar to photografted alkene-films described in Chapter 6. However, comparison of the relevant AFM line profiles (Figures 6.5a 6 and Figure 7.7 above) indicate that the NPA-derived films are more clump-like. The different morphology is mostly likely due to structural differences between aliphatic alkenes and aromatic NPA modifiers and different surface grafting reactions, which can influence the resultant film structures. It is also worth noting that Kuhr and coworkers reported, by utilizing fluorescent microscopy, photobiotin films photografted at GC were inhomogeneous.[13, 15, 16] This appears consistent with the loosely packed nature of the NPA-derived films determined by AFM analysis in this work (above).

Film thickness and surface concentration of NPA-derived films were correlated for films prepared by a photolysis time of 600 s. This yielded an estimated film density of approximately 6 x 10^{-10} mol cm^{-2} per monolayer-equivalent. This value is higher than the film density of loosely packed multilayered films prepared from electroreduction of 4-NB diazonium ions (4.4 x 10^{-10} mol cm^{-2} per monolayer-equivalent, Chapter 3)[43], which indicates that more modifiers are in the first layer of the film grafted to PPF by the photolysis of azide than electroreduction of aryldiazonium ion. This may reflect reaction of nitrenes with the carbon surface is more efficient than aryl radicals, possibly due to instrinically different reactivities of the reactive species.

7.3.3 Electrochemical analysis and reactions of GC surfaces photografted with azidophenylisothiocynate (API)

Photografting with the API modifier leads to a surface bearing isothiocyanate (-NCS) groups useful for further reaction. Isothiocyanate is a useful group to have at the surface because it is electrophilic and reacts selectively with primary amines to form a stable product. It is often utilized in reactions with proteins since they contain amine residues that are favoured for coupling.[44, 45] The derivatization of carbon surfaces with API was demonstrated and monitored by reaction of the surface-bound –NCS group with electroactive amine

(NAAB) to form an isothiourea bond (Equation 7.1).[44] Coupled surfaces will be abbreviated in the format: carbon-API-NAAB.

$$\text{-NCS} \quad + \quad \text{R-NH}_2 \quad \rightarrow \quad \text{-HN-C(=S)-NHR} \qquad (1)$$

Photografting of API to GC and PPF surfaces was examined using 20 mM solutions in DCM. GC samples were spin-coated with API and photolyzed for times ranging from 30 to 1800 s. The photolyzed samples were then ultrasonicated in DCM before incubation for 3 h at room temperature in stirred acetonitrile solution containing 4 mM NAAB. After reaction, samples were ultrasonicated in acetonitrile and analyzed in PBS buffer solution with cyclic voltammetry. A typical modified electrode voltammetric response is shown in Figure 7.8. The voltammogram shows a large reduction peak at $E_{p,c} \sim$ -1.1 V and a broad oxidative process centered $E_{1/2} \sim$ 0.2 V. This is the characteristic response from nitroaryl moieties as described in Chapters 3 and 4. The reaction with NAAB can also reveal information about the underlying –NCS film formed under different irradiation times. Figure 7.9 shows voltammetrically determined surface coverage of NAAB groups coupled to API-derived films prepared with a range of electrolysis times. The plot shows that the amount of immobilized NAAB increases with increasing electrolysis time used to prepare the underlying API film. The data can provide an estimate for the minimum surface concentration of photografted –NCS groups. Based on the surface concentration of coupled NAAB, the maximum surface coverage of the –NCS terminated film was approximately $2 \pm 0.4 \times 10^{-9}$ mol cm^{-2}. This value appears to be consistent with the surface concentrations obtained for NPA-derived films ($\Gamma \sim 0.4–2.5 \times 10^{-9}$ mol cm^{-2}, Section 7.3.1) and hence API-films of similar structure to NPA-films are formed.

The amine coupling yield of API-derived films is comparable to decene-derived films that have been photoactivated by oxalyl chloride (NAAB coupling capacity of $\sim 2 \times 10^{-9}$ mol cm^{-2}, Chapter 6) and greater than electrografted carboxyphenyl (CP) films prepared from aryldiazonium salt (NAAB coupling capacity of $\sim 5 \times 10^{-10}$ mol cm^{-2}, Chapter 6). This demonstrates that API-derived films terminated with –NCS groups are a useful amine-reactive interface for immobilization applications. The relatively high amine coupling capacity for API-derived films may reflect that more amine-reactive groups are grafted to the

surface by this photochemical procedure with azide than films prepared from other procedures described in the previous chapter. However, -NCS groups may instrinically be more reactive than –COOH and –COCl groups and hence lead to a higher amine coupling yield.

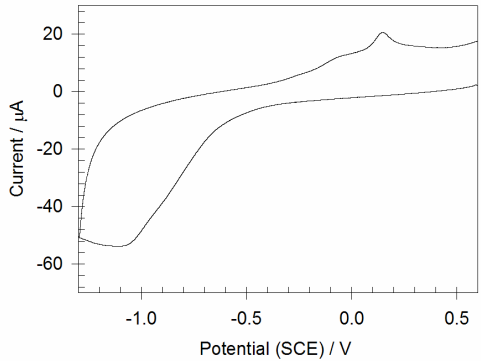

Figure 7.8. Cyclic voltammogram recorded in PBS of NAAB-coupled to a GC surface photografted with API (v = 200 mV s^{-1}).

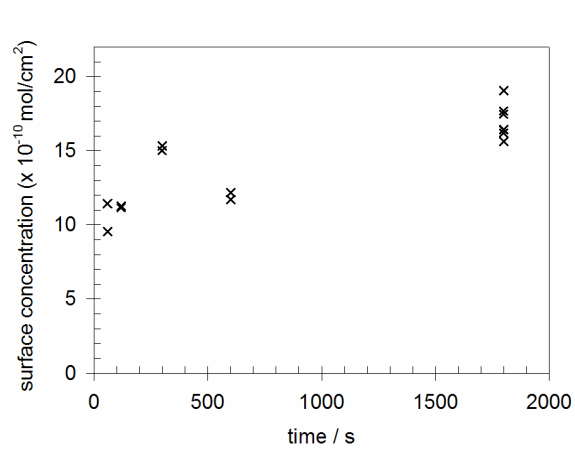

Figure 7.9. Graph showing the estimated surface concentration of NAAB coupled to GC surfaces grafted with API using a range of photolysis times.

7.3.4 AFM analysis of PPF surfaces photografted with azidophenylisothiocynate (API) and azidoaniline (APA)

AFM measurements were carried out for a series of films prepared by photografting API and APA to PPF using standard procedures with UV irradiation times ranging from 60 to 1800 s. Figure 7. 10 shows the data for film thickness growth with increasing UV irradiation time. The data show that the API photografted film is formed quickly and does not grow thicker with increasing UV exposure times beyond 200 s. The photografted film has a maximum average film height of up to ~ 1 nm. Comparing this measured film height

with the molecular height of the API modifier (1 nm), the photografted films are consistent with an average thickness of a monolayer. Qualitatively similar AFM results were obtained for PPF surfaces photografted with APA with an average film thickness of approximately 0.9 nm. Additionally, AFM line-profiles of the API-derived films reveal that there are large variations in the film height within the monolayer (Figure 7. 11). The average surface roughness values are also very close to the average film thickness of the films. The evidence confirms that API and APA photografted films are loosely packed monolayers. The AFM depth profiling results for the two types of photografted films are consistent with the results obtained with NPA. This indicates that the film structure of the three azides (NPA, API and APA) used in this work are similar (Section 7.3.2).

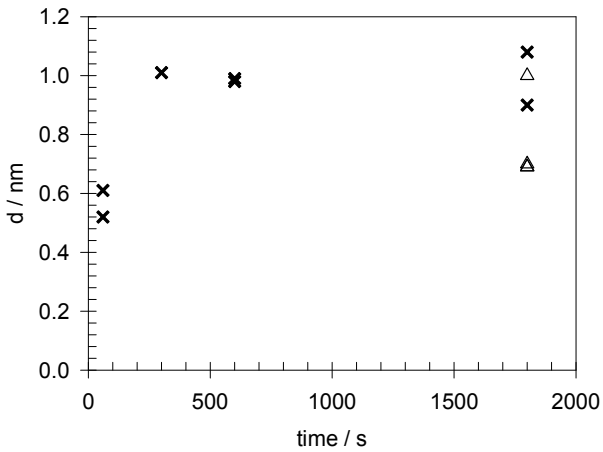

Figure 7.10. Plot of AFM thickness *vs* photolysis time for PPF photografted with API (crosses) and APA (triangles).

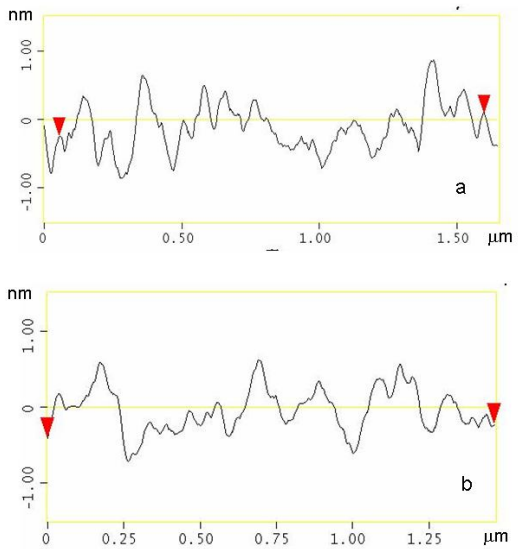

Figure 7.11. AFM line profiles of PPF photografted with (a) API and (b) APA.

7.3.5 Assembly of gold nanoparticles to carbon surfaces photografted with azide modifiers

Amine-terminated films generated by photografting of azides may assemble citrate-capped gold nanoparticles *via* electrostatic interactions, as described earlier for reduced NP films prepared from aryldiazonium salt (Chapter 4). Figure 7. 12 shows the SEM micrograph of a) a bare PPF surface and b) a PPF surface photografted with APA, after immersion in gold nanoparticle solution for 1 h. The presence of the amine-terminated photografted film is confirmed by the dense gold nanoparticle assembly, which has an approximate density of ~ 800 particles/μm^2 (n = 2). In contrast, a density less than ~ 40 particles/μm^2 is obtained at an unmodified PPF surface. The increase in particle density confirms the electrostatic interaction of anionic gold nanoparticles with the surface amine film (pK_a of aniline is 4.6), which would be substantially protonated in the nanoparticle solution (pH 4.2).

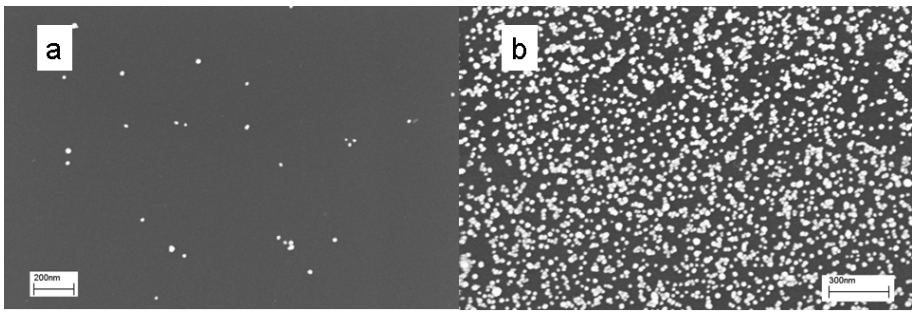

Figure 7.12. SEM micrographs of PPF surfaces after immersion in gold nanoparticle solution for 1 h. (a) bare PPF and (b) a PPF surface photografted with APA.

The appearance of dense nanoparticle assembly on APA grafted surface is typical of those observed for other amine-terminated films such as silane layers grafted on silicon and amine layers electrooxidized on carbon.[35, 46, 47] It also appears comparable with NP films electroreduced in BA/ACN that also show the expected electrostatic assembly with anionic gold nanoparticles (~ 1200 particles/μm^2, Chapter 4). PPF surfaces photografted with NPA and API using standard methods (Section 7.2) did not assemble gold nanoparticles, with SEM micrographs indistinguishable from those of unmodified PPF surfaces (Figure 7. 12a). This is the expected result consistent with an absence of electrostatic interaction between the film and particles. PPF surfaces photografted with NPA and electrochemically reduced in 0.25 M H_2SO_4 and 20 mM BA/ACN also did not assemble gold nanoparticles. It is unsurprising that H_2SO_4-reduced NP-terminated films did not assemble gold nanoparticles since similar behaviour was found in Chapter 4 for reduced NP films prepared from

aryldiazonium ions after reduction in aqueous acidic conditions. However, the absence of gold nanoparticle assembly at BA/ACN-reduced NPA-derived films is surprising and not understood. The reasons behind the disassembly of gold nanoparticles at these reduced NP-terminated films remain unclear however it may be influenced by film structure.

7.3.6 Coupling reactions of carboxylic acid and acid chloride species with carbon surfaces photografted with azidoaniline (APA)

Amine-terminated layers can be utilized for coupling reactions, as shown in Chapter 4 for reduced NP films. The success of coupling reaction of APA-derived surface films with 4-nitrobenzyl chloride (NBCl) was established by examining the voltammetry of the coupled surface. GC samples were photolyzed in the presence of APA, and after ultrasonication, were subsequently incubated in a DCM solution of NBCl (200 mM) for 18 h. The coupled surfaces were analyzed in 0.25 M H_2SO_4 after ultrasonication in DCM for 15 min. Figure 7.13 shows the expected voltammetric response of a surface-bound nitroaryl product, which involves the electroreduction of the nitroaryl moiety (Chapters 3 and 4). From measuring the charge associated with the redox processes involved in the reduction of the nitroaryl group, an average surface concentration of immobilized electroactive product was estimated to be approximately $7 \pm 1 \times 10^{-10}$ mol cm^{-2} (n = 3). Comparing with coupling reactions involving reduced NP films (Chapter 4), this amine-terminated surface had a higher coupling yield for NBCl species than NP films reduced in EtOH/H_2O and BA/ACN (NBCl coupling capacity ~ 5×10^{-10} mol cm^{-2}), but less than NP films chemically reduced in ethanolic Na_2S and electroreduced in H_2SO_4 (NBCl coupling capacity ~ 10×10^{-10} mol cm^{-2}). The differences in the coupling yield of NBCl may be due to differences in the amount of amine groups present in the films prepared by the different methods. The monolayer film structure of APA may allow NBCl to access the amine groups more easily for coupling reaction.

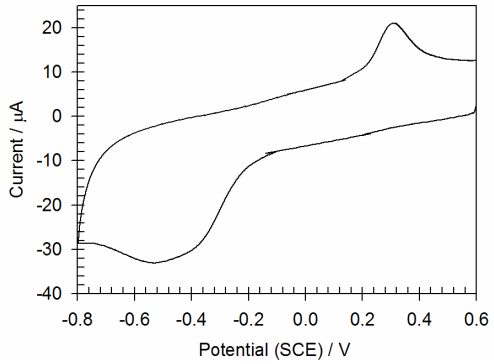

Figure 7.13. Cyclic voltammogram recorded in 0.25 M H_2SO_4 of NBCl-coupled to a GC surface photografted with APA (v = 200 mV s^{-1}).

The photografted GC surfaces bearing amine groups were also covalently reacted with the carboxylic acid group of dihydroxyphenylacetic acid (DOPAC) in the presence of EDC and NHS in DMF. The coupled surface is abbreviated as GC-APA-DOPAC. The coupled surfaces were ultrasonicated in DMF for 3 min before scanning in PBS solution. Figure 7.14a shows the voltammetric response of a coupled surface. The chemically reversible DOPAC redox system,[48-50] with $E_{1/2}$ ~ 0.16 V, is clearly observed. Analyzing the current of the oxidation peak in the cyclic voltammograms show the expected linear relationship between the oxidation peak current and scan rate for surface-bound species (Figure 7.14b).[51] The straight line is a line of best fit forced through zero and has a slope of 3 x 10^{-5} A V^{-1} s with R^2 = 0.99. Calculating the charge associated with the oxidation peak of surface-coupled DOPAC gives an estimated surface concentration of approximately 1.8±0.4 x 10^{-10} mol cm^{-2} (n = 2). The coupling yield of the carboxylic acid derivative, DOPAC, is lower than that of the acid chloride species, NBCl (above). This was also observed for reduced NP films used for coupling NBCl and 4-nitrobenzeneacetic acid (NBA) described in Chapter 4. The higher coupling yield obtained for NBCl is likely to be attributed to the intrinsically greater chemical reactivity of acid chloride for amine than carboxylic acid, and also the possible steric constraints when utilizing EDC and NHS to form bulky carboxylic acid-activated complex to aid amide coupling. It is worth noting that APA-modified surface immobilized less carboxylic acid species (i.e. DOPAC) than reduced NP films immobilized with NBA (coupling capacity ~ 4 x 10^{-10} mol cm^{-2}). However, this is most likely due to the different carboxylic acids, coupling media and reaction times applied in both cases.

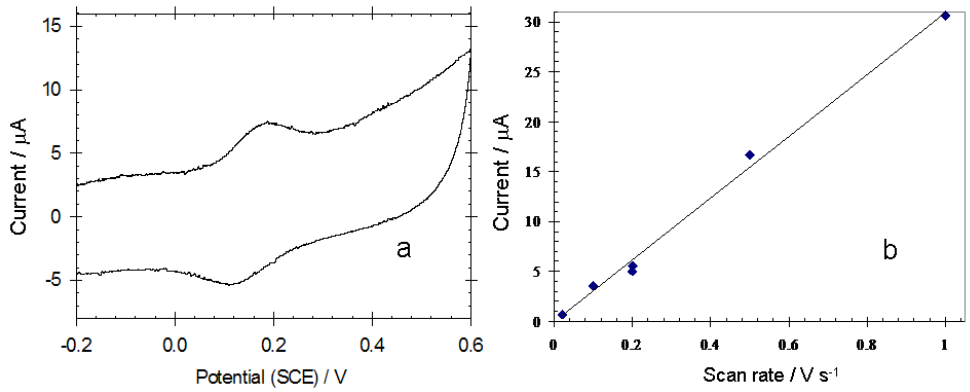

Figure 7.14. (a) Cyclic voltammogram (v = 200 mV s^{-1}) recorded in PBS solution of GC-APA-DOPAC. (b) Plot of oxidation peak current *vs* scan rate, obtained for GC-APA-DOPAC.

7.3.7 Formation and characterization of two-component films

The formation of two-component mixed films using electro- and photochemical reactions was demonstrated by utilizing azide and diazonium ion modifiers. Mixed component films were prepared on carbon in a stepwise fashion by electrografting with decylphenyl (DP) and methoxyphenyl (MeOB) moieties by reduction of the corresponding diazonium salts, followed by photografting of azide modifiers on top of the electrografted film. It is assumed that the nitrene generated from the azide can graft to the film-modified surface *via* insertion reactions. GC surfaces were initially electrografted with methoxybenzene- or decylbenzenediazonium ion-derived films using standard methods (Section 7.2). The films were characterized by water contact angle measurements, giving average angles of approximately 78 ^{o} (n = 4) and 45 ^{o} (n = 4) for DP and MeOB films, respectively. To graft the second modifier, two applications of 200 mM NPA dissolved in DCM solution were spin-coated on the electrografted DP and MeOB films followed by UV irradiation for 30 min. The photolyzed samples were ultrasonicated in DCM for 5 min and dried with a stream of N_2. The resultant coupled surfaces are abbreviated as carbon-DP-NPA and carbon-MeOB-NPA. For GC surface electrografted with DP film a decrease in contact angle from 78 ^{o} to 65 ^{o} was measured after photolysis with spin-coated NPA. Additionally, an increase in contact angle for MeOB film electrografted to GC, from 45^{o} to 65^{o}, was measured upon photochemical modification with NPA. Changes in water contact angles are consistent with the photochemically induced coupling of NPA to the surface of diazonium ion-derived films.

The successful photo-attachment of NPA was also demonstrated by the presence of the voltammetric response of the grafted NP layer in the two-component films. Figure 7.15 shows the first two voltammetric scans recorded in 0.25 M H_2SO_4 of a two-component film of GC-MeOB-NPA (solid line). The voltammogram shows the expected voltammetric response of photografted nitroaryl product, which have been assigned to the electroreduction of the nitroaryl moiety in aqueous acid (Chapter 4). A control sample was prepared by spin-coating NPA onto a MeOB film electrografted to GC, leaving in the dark (absence of UV light) for 30 min and then washing with DCM. Cyclic voltammetry (Figure 7.15, dashed line) reveals an absence of nitroaryl redox chemistry in the voltammogram indicating that the NP layer is only formed on the surface film upon UV irradiation. Analysis of the charge associated with the redox processes involved in the reduction of the electroactive nitroaryl groups (Chapters 3 and 4) gives an estimated average surface concentration of photografted NPA of approximately $11 \pm 2 \times 10^{-10}$ mol cm^{-2} (n = 3) for GC-MeOB-NPA. This value is similar to the surface concentration of NPA photografted to a polished GC surface under similar conditions (~ 17×10^{-10} mol cm^{-2}, [NPA] = 200 mM, t = 30 min, Figure 7.4), which suggests that similar amount of material is grafted on a film-modified surface and an unmodified surface. The mechanism of the grafting of azide to a molecular film is not known, presumably photogenerated nitrene inserts into C-H bonds that are present in the film.

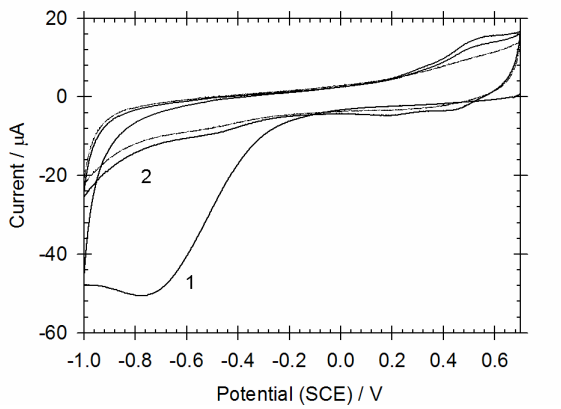

Figure 7. 15. Cyclic voltammograms recorded in 0.25 M H_2SO_4 for a two-component film of GC-MeOB-NPA (first two scans, solid line) and for GC-MeOB that had NPA modifier spin-coated on top and removed without UV irradiation (first scan, dashed line).

7.3.8 Pattern formation and visualization of two-component films utilizing nitrophenyl azide (NPA)

The chemical patterning of PPF surfaces with two-component films was demonstrated using a combination of photolithographical methods with the azide, NPA, and films grafted by the reduction of aryldiazonium salts. The patterning strategy involved a build-up approach (Scheme 7.3), which entailed the direct attachment of azide modifiers to specific regions by utilizing a mask to give patterned UV exposure, on top of PPF surfaces electrografted with a continuous aryldiazonium ion-derived film. This approach transfers the pattern of the mask to the surface, giving a patterned surface that contains two different functionalities, which can be exploited for further chemical reactions. The success of the patterning was confirmed directly by microscopy and also by reaction of the respective modifier-components with molecular species that can be characterized by voltammetry and microscopy.

For these experiments, continuous films of DP and carboxyphenyl (CP) were initially grafted to PPF surfaces by electrochemical reduction of the corresponding diazonium ion. To create the patterned surface, a few drops azide solution (DCM) were spin-coated on the electrochemically prepared films. The spin-coated samples were then exposed to 365 nm light through a glass and chrome mask, containing different patterns, for 30 min. The mask features are inter-digitated arrays of lines with widths of hundreds of micrometers to arrays of lines with 10 μm widths. After photolysis through the mask, the samples were ultrasonicated in DCM or ACN for 3 min and dried with N_2.

It is well established that SEM can be used to directly image SAMs patterned on gold and silicon surfaces and recently, the method was demonstrated for thin films grafted on carbon however the important factors are not clear.[25, 52, 53] Image contrast is due to the different scattering abilities of the modifiers or of impurities adsorbed on modifiers; even small differences in molecular structure of modifiers can give good contrast for visualization. Figure 7.16 shows SEM micrographs of DP-NPA and CP-NPA patterns, confirming the success of patterning of azide modifiers. Regions 1 in the SEM micrographs show the areas of the electrografted films (i.e. DP or CP film) and regions 2 show the areas of photografted NPA. The patterned two-component films here have a similar appearance, under SEM, to the patterned films generated by soft lithography with electrografting methods using amine and

aryldiazonium salt (Section 7.1).[25] 20 μm patterned lines were generated by utilizing PDMS microchannels to graft modifiers on top of molecular films.[25] In contrast, patterned lines with feature sizes of 100 μm to 10 μm are generated by utilizing photolithographical techniques, as shown in Figure 7.16. The patterned films could be formed reproducibly and shows the features transferred from the photo-mask. SEM was used as the standard visualization method to confirm successful patterning and accurate reproduction of the pattern. In further experiments, the CP-NPA patterned surface was placed in 0.25 M H_2SO_4 and standard electroreduction scans (Section 4.2) were carried out. The reduced patterned CP-NPA film was re-examined by SEM after ultrasonication in Milli-Q water giving the micrograph shown in Figure 7.17. The reduced CP-NPA pattern remains visible under SEM analysis demonstrating the stability of the photografted film in aqueous acidic conditions, supporting the proposed covalent attachment of azide to the surface films. The mechanism by which the photolyzed azide species can graft to the diazonium ion-derived film is unknown. However, as mentioned earlier, changes in water contact angle after photografting of azide on the underlying diazonium ion-derived film is consistent with nitrenes inserting possibly to the C-H bonds at the outer layer of polyphenylene structured films.

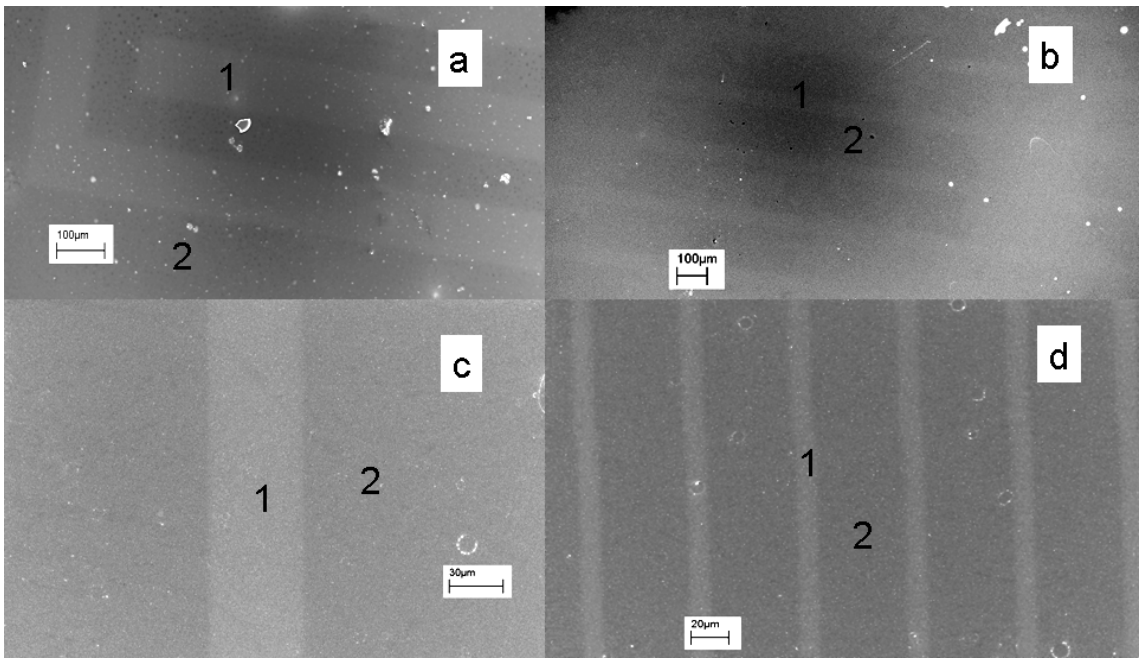

Figure 7.16. SEM micrographs of PPF surfaces patterned with two-component films of (a and b) DP-NPA and (c and d) CP-NPA. Region 1 is the location of electrografted film and region 2 is the location of photografted NPA.

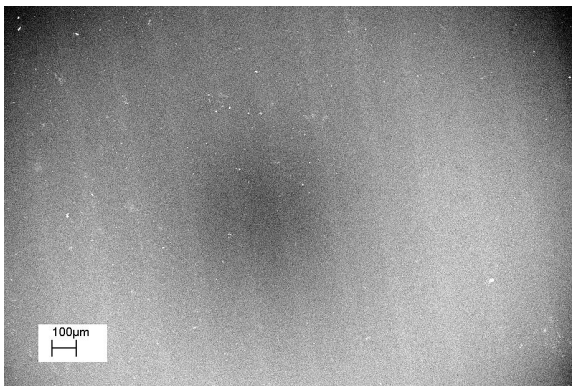

Figure 7.17. SEM micrographs of PPF surfaces patterned with CP-NPA after electroreduction in H_2SO_4.

Formation of condensation figures is another simple and nondestructive approach for visualizing patterned films at PPF surfaces. Water condensation figures are formed on a heterogeneous surface when water condenses, giving different size and distributions of droplets on areas of different wettabilities. This method has been applied to image films formed on gold, glass and carbon surfaces.[25, 54, 55] Figure 7.18 shows optical micrographs of condensation figures of DP-NPA and CP-NPA patterned PPF surfaces. The patterns (inter-digitated lines of 100 µm width) can be seen from the contrast in the images. Note that rapid water evaporation from the surface makes it difficult to obtain well defined condensation figures for the patterned surfaces especially for less hydrophilic films with patterns containing feature sizes smaller than 50 µm. However, this method offers a quick and simple approach to determining whether patterning is successful.

Control experiments were carried out to confirm the proposed reactions. No patterned features were detected by water condensation figures or SEM imaging at continuous DP or CP films that had been spin-coated with DCM and/or acetonitrile (without the azide modifier) and photolyzed through photo-masks. This confirms that the patterns obtained after photolysis with the azide modifier arise from the photografting of the azide to the underlying film.

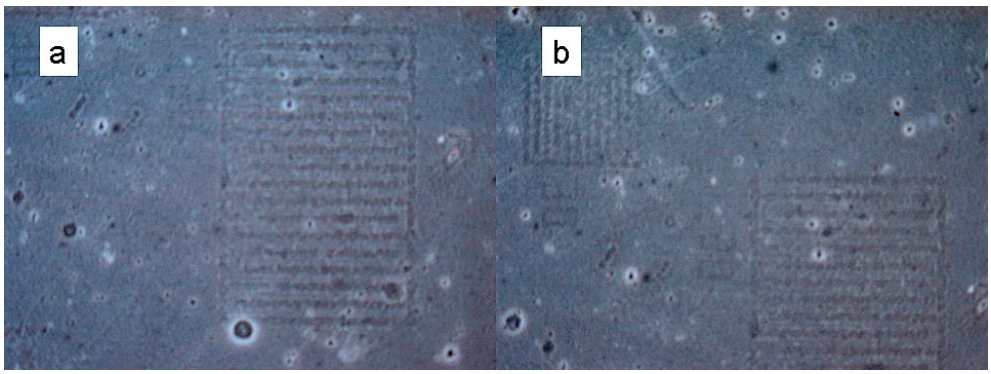

Figure 7.18. Optical micrographs obtained at 5 X magnification of condensation figures on PPF surfaces patterned with two-component films of (a) DP-NPA and (b) CP-NPA. Inter-digitated lines are the electrografted film and the other regions are areas of photografted NPA.

7.3.9 Pattern formation and visualization of patterned two-component films utilizing azidophenylisothiocynate (API)

Using similar procedures to those described above, API modifiers were successfully photo-patterned to PPF surfaces electrografted with an initial layer of DP or CP film. Figure 7.19 shows SEM micrographs of DP-API and CP-API patterns with feature size (i.e. line width) of approximately 50 μm, which has a similar appearance to the patterned two-component films utilizing NPA described in the previous section (Figure 7.16, Section 7.3.8). Regions 1 in the SEM micrographs show the areas of the electrografted films (i.e. DP or CP film) and regions 2 show the areas of photografted API. Patterned surfaces containing both electrophilic and nucleophilic modifiers on the surface were also prepared, by photo-patterning API modifiers on electrografted NP diazonium ion-derived films that had been electrochemically reduced in BA/ACN using standard conditions (Chapter 4). The patterned film is abbreviated as NP(BA/ACN)-API. Figure 7.20 shows an SEM micrograph of a NP(BA/ACN)-API patterned surface, with photografted API modifiers in the darker regions and the electroreduced NP film in the lighter regions. The patterned surfaces were incubated in gold nanoparticle solution for 30 min and rinsed before re-examination under SEM. Figure 7.21a shows gold nanoparticle assembly on the patterned film of NP(BA/ACN)-API. The image is of an area at the boundary of the pattern of the film-modified surface. In the regions containing AP groups from the BA/ACN-reduced NP film, gold nanoparticles assembled with an approximate density of 500 particles/μm^2 (Figure 7.21b). The patterned gold nanoparticle assemblies here have similar appearance to the assemblies formed at the patterned amine films created using soft lithography.[25] In contrast,

regions photografted with API had a lower gold nanoparticle density of approximately 90 particles/μm^2 (Figure 7.21c). This is consistent with API modifiers photografted to the underlying BA/ACN-reduced NP film and disrupting the assembly of gold nanoparticles to AP groups in the reduced NP film. In the underlying film, there may be unreacted amines and also secondary amines and these are expected to lead to some nanoparticle assembly.

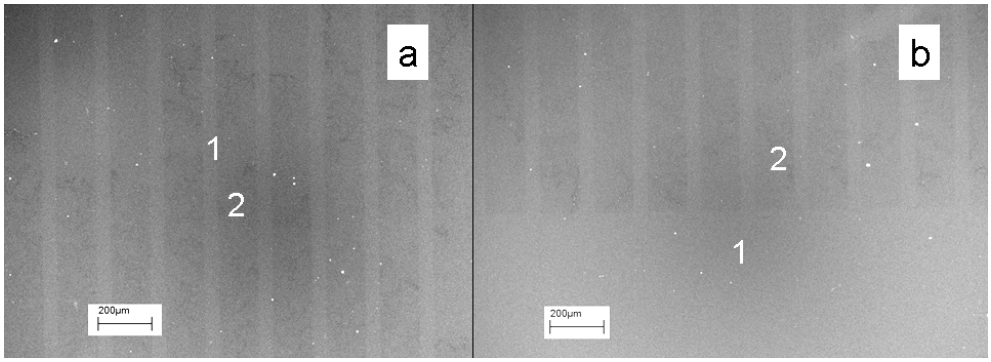

Figure 7.19. SEM micrographs of PPF surfaces patterned with two-component films of (a) DP-API and (b) CP-API. Region 1 is the location of electrografted film and region 2 is the location of photografted API.

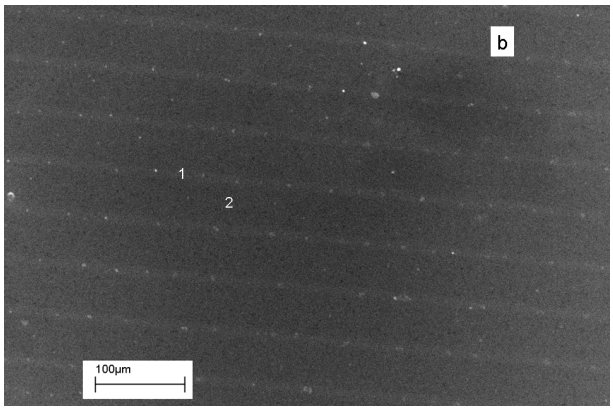

Figure 7.20. SEM micrograph of a PPF surface patterned with two-component films of NP(BA/ACN)-API. Region 1 is the location of electrografted NP(BA/ACN) film and region 2 is the location of photografted API.

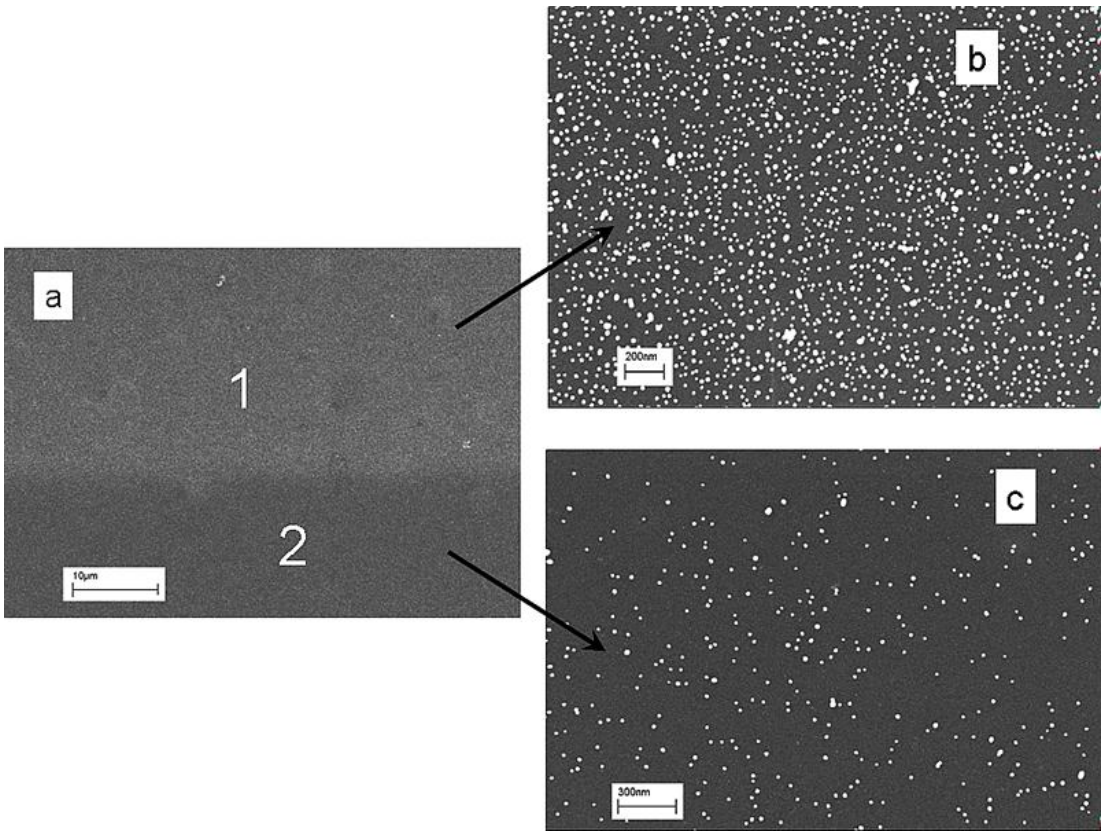

Figure 7.21. (a) SEM micrograph of edge boundary of patterned NP(BA/ACN)-API film-modified PPF after incubation in gold nanoparticle solution for 30 min. Region 1 is the location of electrografted NP(BA/ACN) film and region 2 is the location of photografted API. Closer SEM micrographs inside (b) region 1 and (c) region 2.

Reaction of a NP(BA/ACN)-API patterned surface with NAAB was also explored. The patterned surfaces were incubated with an acetonitrile solution containing 4 mM NAAB for 3 h with stirring. After reaction, the patterned surfaces were rinsed with acetonitrile and dried with N_2. Figure 7.22a shows a SEM micrograph of the patterned surface after reaction with NAAB. The patterned features are clearly visible in the micrograph. The patterned surface was rinsed in acetonitrile again before isolating a part of the surface with an O-ring and a glass cell for electrochemical analysis. Figure 7.23 shows the voltammogram of NP(BA/ACN)-API-NAAB patterned surface recorded in PBS solution. The voltammogram shows a broad reductive feature with $E_{p,c}$ ~ -1.1 V and an oxidative process centered near $E_{1/2}$ ~ 0.2 V, as expected for the electroreduction of surface-attached nitroaryl groups (Chapter 4) on the patterned surface. A large area of the NAAB-coupled patterned surface was included in the electrochemical cell in order to obtain a measurable response from NAAB groups that have coupled to photografted API modifiers however the absolute surface area occupied by the API is unknown. In contrast to this sample, a NP(BA/ACN) surface that

had been photolyzed for 30 min in the absence of API and incubated with NAAB did not show the voltammetric response from nitroaryl products. This further confirms that NAAB had reacted with photo-patterned API modifiers and that –NCS groups are available for coupling and are not significantly buried within the underlying BA/ACN-reduced film. Figure 7.22b shows the SEM micrograph for NP(BA/ACN)-API-NAAB patterned surface after electroreduction in H_2SO_4. The patterned features remain clearly visible after electroreduction of the NAAB-coupled patterned NP(BA/ACN)-API surface, which also demonstrates the stability of the patterned film in aqueous acidic conditions. As mentioned earlier, the grafting mechanism of photolyzed azide species to reduced NP films is unknown and may possible insert to the C-H bonds at the outer layer of the underlying film. However, for reduced NP films, insertion of nitrene species into N-H bonds is also possible.

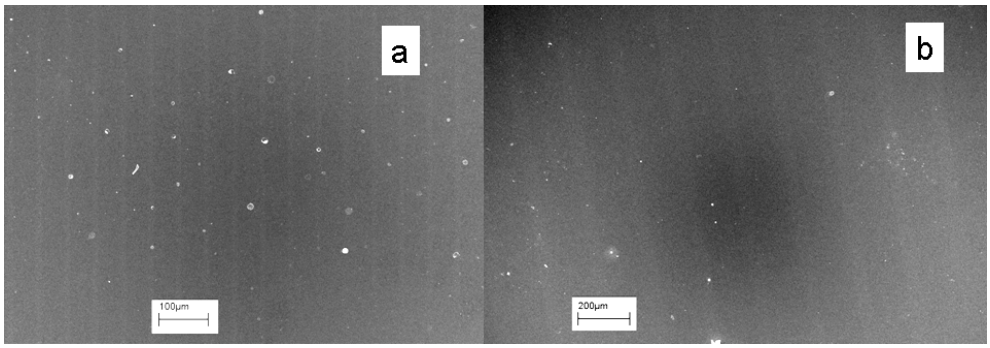

Figure 7.22. SEM micrograph for PPF surface patterned with NP(BA/ACN)-API-NAAB (a) before and (b) after electroreduction in PBS solution.

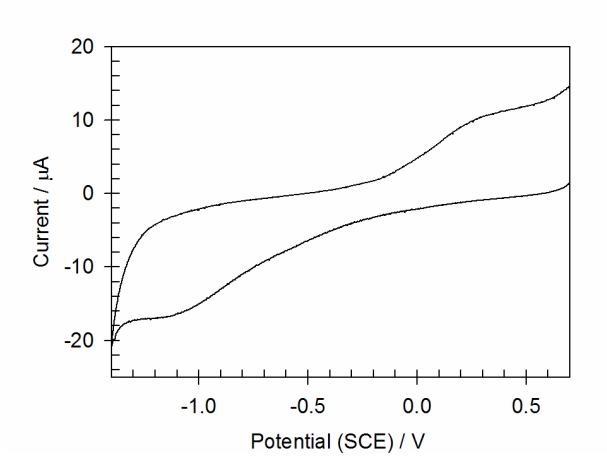

Figure 7.23. Cyclic voltammogram recorded in PBS solution of a PPF surface with NAAB coupled to patterned NP(BA/ACN)-API.

7.4 Conclusion

A simple procedure involving photolysis of azide modifiers for surface grafting was demonstrated on both GC and PPF. Contact angle measurements, voltammetric and AFM analysis established that the films are covalently grafted loosely packed monolayers with film thickness between 0.6 and 0.8 nm. Amine- and isothiocynate-terminated photografted surfaces were prepared by photolysis of azides and used as tether layers for further coupling. Reaction with gold nanoparticles and amine; carboxylic acid and acid chloride derivatives were demonstrated and the immobilization capacity of these loosely packed films was found to be substantial. In particular, API-derived films were found to have the same coupling capacity for amines as alkene-films photoactivated with oxalyl chloride. The modification procedure was expanded by combining electro- and photochemical methods to prepare patterned two-component films, which also utilized photolithographical techniques in the photochemical step. Azides were photolithographically patterned on continuous diazonium ion-derived films, which created patterns with inter-digitated lines of hundreds of micrometers and line-arrays with a minimum line width of 10 μm. When used as the second modifier, azides did not appear to nonspecifically add to the first modifier film. Alternate strategy of photo- then electro- 'fill-in' patterning undoubtedly leads to electrografted modifiers within photografted areas. The strategy described in this work avoids unwanted mixing of modifiers. Patterns were reproducible, which demonstrated that it is a reliable method for patterning. The minimum feature size achievable by this photochemical method was not explored but is expected to be limited by the resolution of the UV technique (i.e. source, delivery and wavelength of UV light) and photosensitivity of azides. The clarity of the pattern can be affected if the chosen azide cannot graft efficiently and produce homogenous layers. A potential limitation of the patterning method is the efficiency of the photografting reaction of azide. Based on AFM and electrochemical analysis, the layers photografted from azide-modifiers have a film density slightly higher than aryldiazonium-derived films however the clump-like morphology of the layers may be undesirable for the production of high definition patterns. Diarizines offer an alternative choice to azides as the photosensitive modifier. In summary, the photochemical procedure with azides has been demonstrated to be a simple and useful method for producing useful tether layers on carbon surfaces, which can be integrated with other patterning techniques involving UV irradiation for large scale utilization.

7.5 References

1. Urano, T.; Takahama, K.; Yamaoka, T., *Imaging Science Journal* **1999,** 47, 133.
2. Roy, D.; Basu, P. K.; Raghunathan, P.; Eswaran, S. V., *Magnetic Resonance in Chemistry* **2003,** 41, 671.
3. Shimizu, S.; Bird, G. R., *Journal of the Electrochemical Society* **1977,** 124, C102.
4. Han, C. C.; Corelli, J. C., *Journal of Vacuum Science & Technology B* **1988,** 6, 219.
5. Evans, R. A., *Australian Journal of Chemistry* **2007,** 60, 384.
6. Collman, J. P.; Devaraj, N. K.; Chidsey, C. E. D., *Langmuir* **2004,** 20, 1051.
7. Collman, J. P.; Devaraj, N. K.; Eberspacher, T. P. A.; Chidsey, C. E. D., *Langmuir* **2006,** 22, 2457.
8. Devaraj, N. K.; Miller, G. P.; Ebina, W.; Kakaradov, B.; Collman, J. P.; Kool, E. T.; Chidsey, C. E. D., *Journal of the American Chemical Society* **2005,** 127, 8600.
9. Hiramatsu, T.; Guo, Y.; Hosoya, T., *Organic & Biomolecular Chemistry* **2007,** 5, 2916.
10. Ziani-Cherif, H.; Imachi, K.; Matsuda, T., *Macromolecules* **1999,** 32, 3488.
11. Tirrell, D.; Zhang, K.; Diehl, M., *Journal of American Chemical Society* **2005,** 127.
12. Brase, S.; Zimmermann, V.; Gil, C.; Knepper, K., *Angewandte Chemie International Edition* **2005,** 44, 5188.
13. Dontha, N.; Nowall, W. B.; Kuhr, W. G., *Analytical Chemistry* **1997,** 69, 2619.
14. Nowall, W. B.; Dontha, N.; Kuhr, W. G., *Biosensors & Bioelectronics* **1998,** 13, 1237.
15. Brooks, S. A.; Ambrose, W. P.; Kuhr, W. G., *Analytical Chemistry* **1999,** 71, 2558.
16. Brooks, S. A.; Dontha, N.; Davis, C. B.; Stuart, J. K.; O'Neill, G.; Kuhr, W. G., *Analytical Chemistry* **2000,** 72, 3253.
17. Scriven, E.; Turnbull, K., *Chemical Reviews* **1988,** 88, 297.
18. Gritsan, N.; Platz, M., *Chemical Reviews* **2006,** 106, 3844.
19. Bowden, W.; Giritsan, N.; Hadad, C.; Karney, W.; Kemnitz, C.; Platz, M., *Accounts of Chemical Research* **2000,** 33, 765.
20. Platz, M.; Munoz, D.; Leyva, E., *Journal of Organic Chemistry* **1989,** 54, 5938.
21. Mayer, T.; Maier, M. E., *European Journal of Organic Chemistry* **2007**, 4711.
22. Clayden, J.; Greeves, N.; Warren, S.; Wothers, P., *Organic Chemistry*. Oxford University Press: 2001.
23. Moss, R. A.; Tian, J. Z.; Chu, G. S.; Sauers, R. R.; Krogh-Jespersen, K., *Pure and Applied Chemistry* **2007,** 79, 993.

24. Platz, M. S.; Huang, H. Y.; Ford, F.; Toscano, J., *Pure and Applied Chemistry* **1997,** 69, 803.

25. Downard, A. J.; Garrett, D. J.; Tan, E. S. Q., *Langmuir* **2006,** 22, 10739

26. Andersson, H.; Jonsson, C.; Moberg, C.; Stemme, G., *Sensors and Actuators, B: Chemical* **2001,** B79, 78.

27. Ober, C.; Andruzzi, L.; Senarantne, W., *Biomacromolecules* **2005,** 6, 2427.

28. Downard, A.; Garrett, D.; Lehr, J.; Miskelly, G., *Journal of American Chemical Society* **2007,** 129, 15456.

29. Preece, J.; Mendes, P., *Current Opinion in Colloid & Interface Science* **2004,** 9, 236.

30. Michel, B.; Bernard, A.; Bietsch, A.; Delamarche, E.; Geissler, M.; Juncker, D.; Kind, H.; Renault, J. P.; Rothuizen, H.; Schmid, H.; Schmidt-Winkel, P.; Stutz, R.; Wolf, H., *Chimia* **2002,** 56, 527.

31. Zhang, H.; Li, Z.; Mirkin, C. A., *Advanced Materials* **2002,** 14, 1472.

32. Demers, L. M.; Ginger, D. S.; Park, S. J.; Li, Z.; Chung, S. W.; Mirkin, C. A., *Science* **2002,** 296, 1836.

33. Brooksby, P. A.; Downard, A. J., *Langmuir* **2005,** 21, 1672.

34. Mendes, P.; Belloni, M.; Ashworth, M.; Hardy, C.; Nikitin, K.; Fitzmaurice, D.; Critchley, K.; Evans, S.; Preece, J., *Chemphyschem* **2003,** 4, 884.

35. Mendes, P. M.; Jacke, S.; Critchley, K.; Plaza, J.; Chen, Y.; Nikitin, K.; Palmer, R. E.; Preece, J. A.; Evans, S. D.; Fitzmaurice, D., *Langmuir* **2004,** 20, 3766.

36. Kim, K.; Lee, I., *Langmuir* **2004,** 20, 7351.

37. Tan, E. S. Q., Assembly of Organic Layers onto Carbon Surfaces. University of Canterbury, 2006.

38. McDonald, J. C.; Duffy, D. C.; Anderson, J. R.; Chiu, D. T.; Wu, H. K.; Schueller, O. J. A.; Whitesides, G. M., *Electrophoresis* **2000,** 21, 27.

39. Lee, S. W.; Lee, S. S., *Microsystem Technologies-Micro-and Nanosystems-Information Storage and Processing Systems* **2008,** 14, 205.

40. Fleet, G. W. J.; Knowles, J. R.; Porter, R. R., *Biochemical Journal* **1972,** 128, 499.

41. Bein, T.; Hoekstra, K., *Chemistry of Materials* **1996,** 8, 1865.

42. Ranganathan, S.; McCreery, R. L., *Analytical Chemistry* **2001,** 73, 893.

43. Brooksby, P. A.; Downard, A. J., *Langmuir* **2004,** 20, 5038.

44. Hermanson, G., *Bioconjugate Techniques*. Academic Press 1996.

45. Mukerjee, M.; Ashare, R., *Chemical Reviews* **1991,** 91, 1.

46. Downard, A. J.; Tan, E. S. Q.; Yu, S. S. C., *New Journal of Chemistry* **2006,** 30, 1283.

47. Wang, J.; Zhu, T.; Song, J.; Liu, Z., *Thin Solid Films* **1998,** 327-329, 591.

48. Raj, C. R.; Ohsaka, T., *Electroanalysis* **2002,** 14, 679.

49. Roy, P. R.; Saha, M. S.; Okajima, T.; Park, S. G.; Fujishima, A.; Ohsaka, T., *Electroanalysis* **2004,** 16, 1777.

50. Maldonado, S.; Morin, S.; Stevenson, K. J., *Analyst* **2006,** 131, 262.

51. Bard, A. J.; Faulkner, L. R., *Electrochemical Methods: Fundamentals and Applications*.3rd ed.; John Wiley: 2001.

52. Lopez, G. P.; Biebuyck, H. A.; Whitesides, G. M., *Langmuir* **1993,** 9, 1513.

53. Wollman, E. W.; Frisbie, C. D.; Wrighton, M. S., *Langmuir* **1993,** 9, 1517.

54. Lopez, G. P.; Biebuyck, H. A.; Frisbie, C. D.; Whitesides, G. M., *Science* **1993,** 260, 647.

55. Xia, Y. N.; Mrksich, M.; Kim, E.; Whitesides, G. M., *Journal of the American Chemical Society* **1995,** 117, 9576.

Chapter 8. Conclusion

Molecular films have been grafted to GC and PPF surfaces by a range of approaches, which utilized electrochemical and/or photochemical modification methods. Films prepared by electrochemical reduction of aryldiazonium ion, electrochemical oxidation of arylacetate and photolysis of alkene, alkyne and azide derivatives were examined in detail using a combination of water contact angle measurements, cyclic voltammetry, X-ray electron spectroscopy (XPS), optical microscopy, scanning electron microscopy (SEM) and atomic force microscopy (AFM).

Films grafted to GC and PPF *via* the electrochemical reduction of aryldiazonium salt were found to have very similar properties, exhibiting similar self-passivating film formation behaviour, blocking properties in redox probe voltammetry and voltammetric response of surface-bound nitrophenyl (NP) groups. The NP moiety was a useful reporting group for film analysis however, limitations with electrochemically determined surface concentration with NP groups and its electroinactivity in the film environment were highlighted. Studies with other reporting groups (for example, using a chemically and electrochemically reversible system) may offer additional insight into characterization of grafted films in future work.

NP films were shown to contain low concentrations of electroinactive azo and other reduced N moieties incorporated in the film structure *via* reactions of aryldiazonium ions or radicals with the grafted film. Characterization of these species with other nonelectrochemical analysis techniques (e.g. time-of-flight secondary ion mass spectrometry) may give further information on film composition and properties. Preparation using a relatively low aryldiazonium salt concentration formed layers with film density of approximately 4.4 x 10^{-10} mol cm^{-2} per monolayer-equivalent. NP films were reduced chemically in Na_2S and electrochemically in three different media. Aminophenyl groups were found to be the major product for all reduction methods with reduction in Na_2S giving the cleanest and most complete conversion to AP groups, with < 5 % unreacted residual NP groups while reduction in acetonitrile-electrolyte solution containing benzoic acid, gave the largest amount of residue. Films decreased in thickness after electroreduction in H_2SO_4 by up to 53 % and remained intact. The change was reversible, which was attributed to film swelling and shrinking effects. Films grafted by aryldiazonium ions formed loosely packed multilayers with an estimated free volume of ~ 25 % and have typical film

thicknesses < 4 nm.

Reaction of reduced NP films with carboxylic acid derivative in aqueous conditions revealed that coupling occurs at the outer part of the film and was independent of the reduction conditions. This may be attributed to steric constraints. However, reaction with acid chloride derivatives in nonaqueous conditions revealed that the highest coupling yield was obtained at H_2SO_4-reduced films and consistent with coupling occurring within the film. Furthermore, reaction with citrate-capped gold nanoparticles revealed that it only electrostatically assembled on BA/ACN-reduced NP films and did not form assemblies at other reduced films. Further studies are needed to gain further insight on how film structure and environment can affect the reactivity and chemical reactions of surface films.

Loosely packed multilayered films were grafted to GC and PPF surfaces by electrooxidation of arylacetate-modifiers. Films prepared by this method had typical thicknesses < 5 nm. However, thicker films of up to ~ 22 nm were formed using an increased overpotential of > 500 mV, which showed that film height is influenced by applied potential. Films grafted on GC and PPF exhibited similar properties, however electrooxidation with 4-nitrophenylacetate exhibited different surface grafting properties at the two carbon surfaces possibly related to adsorption effects. The arylacetate-derived films were electrochemically oxidized after positive polarization to ≤ 2.0 V (*vs* Ag wire) in acetonitrile solution however the films remained intact after treatment. In contrast, polarizations to potentials ≤ -1.8 V revealed significant changes to film properties. Electron-transfer inhibition of the film became lower and approached that observed for a bare electrode, which was attributed to desorption of physisorbed material from the films. Grafted films also exhibited reversible film swelling and shrinking behaviour as a result of applied potential. Negative potential excursions caused film thickness to decrease and it was reversed with an applied positive potential. Further studies on the film formation process of this process can offer insight for broadening the scope of the possible uses for this reaction.

Photochemical modification of carbon surfaces using alkene, alkyne and azide derivatives was carried out in air and was an experimentally simple approach. Photolysis of alkenes on GC and PPF surfaces formed, in general, stable loosely packed monlayers with film thickness of < 1 nm. In contrast, for a fluorinated alkene derivative and an alkyne, loosely packed multilayers of approximately 2-3 nm were formed. Alkyl-terminated

surface films were activated by a photochemical method utilizing oxalyl chloride, which converted the films to become amine-reactive tethers. Amines were coupled to these photochemically prepared surfaces and compared with other typical amine-reactive surfaces. In general, higher concentrations of amines were coupled to photoactivated films; in particular photografted alkyl-terminated films that were photoactivated with oxalyl chloride had the highest amine-coupling yield. Mixed films that contained aromatic and aliphatic modifiers were prepared on carbon surfaces by first photografting a loosely packed film from an alkene modifier followed by aryldiazonium ion-modifiers that were electrochemically grafted to the surface. The addition of each modifier component can be managed during each individual grafting step, which provided a simple approach that gave stable mixed layers. Future work in unraveling mechanistic details of grafting reactions and further optimization of the photochemical step can widen the scope of these reactions and develop them for potential use in chemical patterning methods.

Photolysis of azide modifiers on GC and PPF generated stable loosely packed monolayers with film thicknesses approximately ≤ 1 nm. By choosing different R-groups on the azide-modifier, the photografted films were demonstrated to be useful reactive tether layers, which immobilized a range of species such as gold nanoparticles, amine, carboxylic acid and acid chloride derivatives. The photochemically induced reaction of azides allowed the opportunity for chemical patterning. Patterning incorporated photolithography in the photochemical step to graft azides to specific regions on a continuous film electrochemically prepared from aryldiazonium ions. The method offered a simple approach to generate stable patterned layers that consisted of two different modifiers on the carbon surface. Inter-digitated lines of hundreds of micrometers and line-arrays with widths of tens of micrometers were prepared. A line width of 10 μm was the smallest prepared. Future work to further develop this patterning method for integration with other patterning techniques can open up opportunities for potentially large scale utilization for industry. Future work in optimization and method-refinement can address the possibility to generate smaller features, which will depend largely on the resolution of the patterning technique and the choice of azide-modifier. This photochemical patterning procedure has great potential in fabricating multiple sensing arrays on a surface in which arrays of functional components can be photografted and positioned on a background (or underlying) film that resist nonspecific adsorption of undesired contaminants.

The attractive feature of modification of carbon surfaces is the formation of stable covalently attached layers. The electrochemical and photochemical methods described in this thesis are experimentally simple, rapid and utilize basic and commonly available equipment. With the choice of aryldiazonium salt, arylacetate, alkene, alkyne and azide, a great variety of layers can be grafted to carbon surfaces from commercially available and inexpensive reagents. The wide range of functionalities that can be used for modification of carbon is of practical advantage compared with modification of gold for example, which is largely limited to thiol-based modifiers used in self-assembly.

The reproducibility for the formation of surface layers and the control of the amount of grafted material to the surface are advantages of the methods investigated in this work. For electrochemically assisted methods utilizing aryldiazonium salts and arylacetates, parameters such as the concentration of modifying solution, applied potential and electrolysis time can be varied to control the amount of modifiers grafted to the surface. However, the limitation of electrochemical grafting is that they are prone to multilayer formation due to radicals coupling to already grafted layers. However, careful choice of applied conditions may permit monolayers to be formed by electrochemical methods. For photochemical procedures, similar control in the amount of grafted modifier can be achieved by varying the concentration of modifying solution, photolysis time and photolysis condition (i.e. in solution or spin-coated). A key difference of photochemically assisted methods using alkene and azide are that in general loosely packed monolayers are formed. Aliphatic modifiers can be used for photochemical modification and hence permit the formation of aliphatic layers on carbon surfaces. Aliphatic alkene-based tether layers have in general relatively higher reactivity for subsequent chemical reactions than aryl-based tether layers, which is useful for immobilization applications.

Although the films produced by electrochemical and photochemical methods are not closely packed, the loosely packed structures of these layers enables them to exhibit dynamic film properties such as dynamic changes in film thickness and blocking properties to redox probe. The ability of these grafted films to change between two different states upon an applied stimulus (e.g. applied potential) may be exploited and potentially find application in the fabrication of functional chemical switches.

9. Appendix

- Calculation of the amount of surface grafted NP groups.

Using the H_2SO_4-reduction example from Table 4.1 and cyclic voltammogram Figure 3.2:

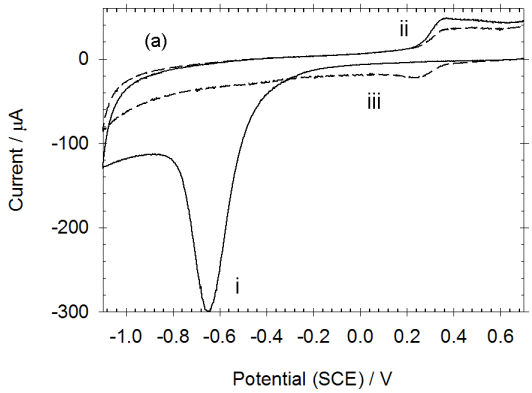

Figure 3.2. First two cycles of cyclic voltammograms recorded in 0.25 M H_2SO_4 for a NP film (t = 600 s) grafted to GC (geometric area of electrode 0.26 cm^2, v = 200 mV s^{-1}).

$$\text{Carbon-Ph-}NO_2 + 6H^+ + 6e^- \rightarrow \text{Carbon-Ph-}NH_2 + H_2O \quad (3.1a)$$

$$\text{Carbon-Ph-}NO_2 + 4H^+ + 4e^- \rightarrow \text{Carbon-Ph-NHOH} + H_2O \quad (3.1b)$$

$$\text{Carbon-Ph-NHOH} \leftrightarrow \text{Carbon-Ph-NO} + 2H^+ + 2e^- \quad (3.1c)$$

Process (i) : Equations 3.1a and 3.1b

Process (ii and iii) : Equation 3.1c

Surface concentrations (Γ, mol cm^{-2}) was calculated according to **Equation 2.1**, $\Gamma = Q / nFA$, where n is the number of electrons involved in the redox process, F is Faraday's constant (96485 C mol^{-1}) and A is the geometric area of the electrode (cm^2).

Charge associated with redox process:

Charge (Q) = Curve-fitted area in cyclic voltammogram *(A.V)* / scan rate *(v, V s^{-1})*

Charge (Q) per geometric area = (C cm^{-2})

From curve-fitting for H_2SO_4-reduced sample:

Curve-fitted area for peak i = 1.0 x 10^{-3} C cm^{-2} (Table 4.1)

Curve-fitted area for peak ii = 1.3 x 10^{-4} C cm^{-2} (Table 4.1)

Calculation example.

Surface coverage of surface-grafted NP groups

The total amount of surface-grafted NP groups is converted into either AP groups (equation 3.1a) or APOH (equation 3.1b), hence

$$\Gamma \text{ (NP groups)} = Q \text{ (peak i)} + Q \text{ (peak ii)} / n.\ F$$

$$\Gamma \text{ (NP groups)} = 1.0 \times 10^{-3} \text{ C cm}^{-2} + 1.3 \times 10^{-4} \text{ C cm}^{-2} / 6 \times 96485 \text{ C mol}^{-1}$$

$$\Gamma \text{ (NP groups)} = 2 \times 10^{-9} \text{ mol cm}^{-2}$$